INFORMATION TO USERS

This manuscript has been reproduced from the microfilm master. UMI films the text directly from the original or copy submitted. Thus, some thesis and dissertation copies are in typewriter face, while others may be from any type of computer printer.

The quality of this reproduction is dependent upon the quality of the copy submitted. Broken or indistinct print, colored or poor quality illustrations and photographs, print bleedthrough, substandard margins, and improper alignment can adversely affect reproduction.

In the unlikely event that the author did not send UMI a complete manuscript and there are missing pages, these will be noted. Also, if unauthorized copyright material had to be removed, a note will indicate the deletion.

Oversize materials (e.g., maps, drawings, charts) are reproduced by sectioning the original, beginning at the upper left-hand corner and continuing from left to right in equal sections with small overlaps.

Photographs included in the original manuscript have been reproduced xerographically in this copy. Higher quality 6" x 9" black and white photographic prints are available for any photographs or illustrations appearing in this copy for an additional charge. Contact UMI directly to order.

University of Alberta

Ethylene Polymerization

over Morphology-Controlled Ziegler-Natta Catalysts

by

Long Wu   ©

A thesis submitted to the Faculty of Graduate Studies and Research

in partial fulfillment of the requirements for the degree of

Doctor of Philosophy in Chemical Engineering

Department of Chemical and Materials Engineering

Edmonton, Alberta

Fall 1999

The author has granted a non-exclusive licence allowing the National Library of Canada to reproduce, loan, distribute or sell copies of this thesis in microform, paper or electronic formats.

L'auteur a accordé une licence non exclusive permettant à la Bibliothèque nationale du Canada de reproduire, prêter, distribuer ou vendre des copies de cette thèse sous la forme de microfiche/film, de reproduction sur papier ou sur format électronique.

The author retains ownership of the copyright in this thesis. Neither the thesis nor substantial extracts from it may be printed or otherwise reproduced without the author's permission.

L'auteur conserve la propriété du droit d'auteur qui protège cette thèse. Ni la thèse ni des extraits substantiels de celle-ci ne doivent être imprimés ou autrement reproduits sans son autorisation.

0-612-46947-6

Canadä

University of Alberta

Library Release Form

Name of Author: Long Wu

Title of Thesis: Ethylene Polymerization over Morphology-Controlled

Ziegler-Natta Catalysts

Degree: Doctor of Philosophy

Year this Degree Granted: 1999

Permission is hereby granted to the University of Alberta Library to reproduce single copies of this thesis and to lend or sell such copies for private, scholarly or scientific research purposes only.

The author reserves all other publication and other rights in association with the copyright in the thesis, and except as herein before provided, neither the thesis nor any substantial portion thereof may be printed or otherwise reproduced in any material form whatever without the author's prior written permission.

(signature)

11147-82 Avenue, #901

Edmonton, Alberta

Canada T6G 0T5

Date: *September 15, 1999*

University of Alberta

Faculty of Graduate Studies and Research

The undersigned certify that they have read, and recommend to the Faculty of Graduate Studies and Research for acceptance, a thesis entitled **Ethylene Polymerization over Morphology-Controlled Ziegler-Natta Catalysts** submitted by **Long Wu** in partial fulfillment of the requirements for the degree of **Doctor of Philosophy** in **Chemical Engineering**.
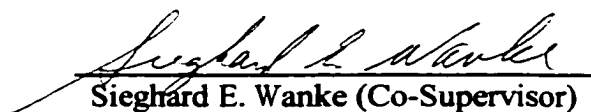
Sieghard E. Wanke (Co-Supervisor)
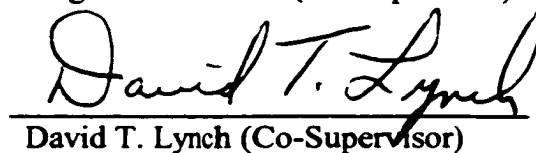
David T. Lynch (Co-Supervisor)

Michael C. Williams
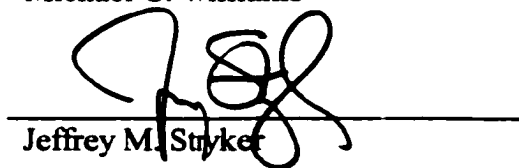
Jeffrey M. Stryker

Kimberley B. McAuley

Date: Sept 10, 1999

To my family: Parents, Sisters, Wife, and Son

even now and more than ever

Abstract

Ethylene polymerization were studied systematically with morphology-controlled prepolymer as a catalyst at temperatures of 30 to 70°C and ethylene concentrations of 120 to 850 mol/m^3. The prepolymer was obtained by polymerizing ethylene in heptane slurry at mild conditions using a morphology-controlled Ziegler-Natta catalyst, in which TiCl$_4$ was supported on spherical MgCl$_2$ particles. The spherical MgCl$_2$ particles were prepared by melt quenching of an MgCl$_2$-ethanol complex. Triethylaluminum was used as the cocatalyst for all the polymerization runs. The catalyst was highly active and produced up to 20 kg of polyethylene per gram of catalyst per hour in gas-phase operation. The nascent prepolymer and polymer, characterized by scanning electron microscopy, showed an excellent shape replication; and the bulk density of the nascent polymer granules was as high as 0.45 g/cm^3.

For ethylene polymerization, mass transfer limitations were probably present in slurry operation, but were negligible for gas-phase operation; these conclusions are based on the results of rate profiles and prepolymer and polymer properties obtained by size exclusion chromatography and scanning electron microscopy. At constant polymerization temperature and ethylene concentration, the overall rate changed markedly with time; one maximum in the rate profiles was observed for slurry operation while two maxima were observed for gas-phase operation. These results suggest that rates of ethylene polymerization in slurry reactors cannot be used directly for predicting gas-phase operation.

For catalysts with time-varying activities, a new experimental method was proposed to determine the power-law order of gas-phase ethylene polymerization. The reaction orders

with respect to ethylene concentration, obtained according to this new method, varied with temperature and were a strong function of reaction time-on-stream from about 1.5 initially to about 1.0 after about 4 hours.

The kinetic results strongly indicated the presence of at least two different types of catalytic sites having different activation and deactivation behavior in this heterogeneous Ziegler-Natta catalyst. The presence of two different types of catalytic sites was also suggested by the two different structures observed by scanning electron microscopy on the fractured surface of nascent polyethylene granules. A reaction-kinetic model with two different types of catalytic sites was proposed for the gas-phase ethylene polymerization; the model predictions were generally in agreement with the experimental observations.

Acknoledgements

I would like to thank my supervisors, Professor Sieghard E. Wanke, Chairman of the Department of Chemical and Materials Engineering, and Professor David T. Lynch, Dean of Engineering, for their generosity in providing guidance and sharing their ideas on the interesting work which I loved doing, and for their academic and personal influence on me which I will benefit lifetime long.

I wish to thank the departmental staff: Mrs. Christina Barker for performing scanning electron microscopy, Mr. Walter Boddez and Mr. Richard Cooper for setting up some of the instrument, Mr. Keith Faulder and Mr. Bob Scott for fabricating the cold bath. I also thank Mrs. Naiyu Bu for measuring the molar masses of polyethylene.

Members of examining committee including Professor Michael C. Williams, Professor Jeffrey M. Stryker of Department of Chemistry, and Professor Kimberley B. McAuley of Department of Chemical Engineering at the Queen's University are acknowledged for their spending time in reviewing my thesis, and for their criticism and advice on my work.

I am also very appreciative of my parents, my sisters, my wife, Zhan, and my son, Michael, for giving me strength by their unending love.

Table of Contents

List of Tables

List of Figures

List of Nomenclature and Abbreviations

Nomenclature

a_{HA}	parameter depending on adsorption of both hydrogen and cocatalyst on the active site
$[A]$	concentration of cocatalyst
b_A	parameter depending on the adsorption of cocatalyst only
c_p	heat capacity of polymer (J/g·K)
$C_{p1}(x)$	active chains or propagation sites for Site 1 (monomer-complexed) with a polymerization degree of x
$C_{p2}(x)$	active chains or propagation sites for Site 2 with a polymerization degree of x
C^*	active site
$[C^*]$	concentration of active sites in the catalyst
$[C^*]_0$	concentration of total concentration of active sites ($[C^*]_0 = [C^*] + [C^*]_p + [C^*]_H$)
$[C^*]_H$	concentration of active sites temporarily deactivated by hydrogen
$[C^*]_p$	concentration of polymerization centre
$[C^*(t_i)]$	active site concentrations at time t
d_{30}	volume-number average diameter
d_c	diameter of the initial catalyst
d_i,	individual granule diameter
d_p	diameter of the polymer granule at time t
D	diffusivity of monomer in polymer
D_l	effective diffusivity of monomer in macroparticle
D_s	effective diffusivity of monomer in microparticle
$f(\theta_2, p)$	functional form of the rate equation determined by $F(x)$
$F(x)$	nature of the deactivation kinetics from the deactivation profile function (DPF) of experimental polymerization kinetics
h	external film heat transfer coefficient

$[H_2]$	concentration of hydrogen
$I.I.$	isotactic index (weight percentage of insoluble polypropylene in boiling heptane)
I_A	$I.I.$ values of polypropylene produced by nonstereospecific sites (stable sites)
I_S	$I.I.$ values of polypropylene produced by stereospecific sites (unstable sites)
k	power-law rate constant of overall polymerization rate
k'	apparent rate constant of overall polymerization rate, including active site concentration
$k_{1d.r}$	first order deactivation constant
$k_{2d.c}$	rate constant for the second order deactivation of active sites
$k_{2d.r}$	second order rate decay constant
k_{ai}	adsorption rate constants for each active site i
k_{d1}	rate constants of spontaneous deactivation for Site 1
k_{d2}	rate constants of spontaneous deactivation for Site 2
k_{dm1}	rate constant for monomer-assisted deactivation of propagation Site 1
k_{di}	desorption rate constants for each active site i
k_e	effective thermal conductivity in polymer particle
k_{eff}	effective rate constant
k_f	rate constant of the formation of active centre
k_{f1}	rate constant for formation of active site for Site 1
k_{f2}	rate constant for formation of active site for Site 2
k_H	Henry's constant
k_i	initiation rate constant with the first monomer
k_{i1}	initiation rate constant with the first monomer for Site 1
k_{p1}	rate constant of chain propagation for Site 1
k_{p2}	rate constant of chain propagation for Site 1
k_p	propagation rate constant

k_s	external film mass coefficient
$k_{tr,M}$	rate constant for chain transfer to monomer
$k_{tr,\beta}$	rate constant for β-hydrogen elimination
$k_{tr,A}$	rate constant for chain transfer to alkyl aluminum
$k_{tr,H}$	rate constant for chain transfer to hydrogen
K	constant
K'	constant
K_1	equilibrium constant ($K_1 = k_1/k_{-1}$)
K_2	equilibrium constant ($K_2 = k_2/k_{-2}$)
K_A	equilibrium adsorption constants for monomer
K_M	equilibrium adsorption constants for cocatalyst (AlR_3)
m	power-law reaction order for chain transfer to alkyl aluminum
M	monomer
M_0	molar mass of monomer
M_n	number average molar mass of polymer
M_w	weight average molar mass of polymer
$[M]$	monomer concentration
$[M]_0$	initial monomer concentration in bulk fluid
$[M]_b$	monomer concentration in the fluid medium
$[M]_l$	monomer concentration in pores of macroparticle
$[M]_s$	monomer concentration in the microparticle
n	power-law reaction order with respect to monomer concentration for overall polymerization rate
n'	apparent reaction order with respect to monomer concentration for overall polymerization rate
n_A	power-law reaction order for chain transfer to cocatalyst
n_H	power-law reaction order for chain transfer to hydrogen
n_t	total number of granules in each set for analysis
p	a set of uncommon parameters
P	pressure

Q	polymer polydispersity
r	radius of particle
r_c	radius of the catalyst particle
r_{cat}	radius of initial catalyst particle
r_{crys}	radius of catalyst primary crystallite
r_l	radial coordinate of macroparticle
r_p	polymer particle radius increasing with the generation of polymer
r_s	radial coordinate of microparticle
R_0	initial overall polymerization rate
R_∞	stationary rate when $t \rightarrow \infty$
R_l	radius of macroparticle
R_p	total polymerization rate
$R_{p.1}(t_i)$	overall polymerization rate at time t_i before the pressure change
$R_{p.2}(t_i)$	overall polymerization rate at time t_i after the pressure change
R_{p1}	polymerization rate for Site 1
R_{p2}	polymerization rate for Site 2
$R_{p.t}$	overall polymerization rate as a function of time, t
R_p^0	polymerization rate in the absence of hydrogen
R_p^H	stationary (or average) polymerization rates in the presence of hydrogen
R_s	radius of microparticle
R_v	volumetric reaction rate in macroparticle
S	surface site
S_1	potential active sites of Site 1 for polymerization
S_2	potential active sites of Site 2 for polymerization
$S_2 M_x$	active chains or propagation sites for Site 2 with a polymerization degree of x
S_{a1}	active site for Site 1
$S_{a1}M\text{-}M_{x-1}$	active chains or propagation sites for Site 1 (monomer-complexed) with a polymerization degree of x

S_{d1}	catalytic inactive sites for Site 1
S_{d2}	catalytic inactive sites for Site 2
$S*$	active site
$[S]_0$	total concentration of potential active centre
$[S_{1.0}]$	initial concentrations of potential active sites for Site 1
$[S_{2.0}]$	initial concentrations of potential active sites for Site 2
t	time
T	polymerization temperature
T_0	initial temperature of particle
T_b	initial temperature in bulk fluid
T_c	critical temperature of ethylene
T_l	temperature in macroparticle
t_{max}	reaction time for the first peak in the rate profile to reach maximum
T_s	temperature in microparticle
u	velocity of sites (length/time)
V_t	volume of a bed of all the granules in a run including porosities of the granules and the inter-granule voids
W	total mass of granules in each set
W_t	mass of a bed of all the granules in a run
x	polymerization degree, *i.e.*, number of monomer units in a polymer chain

Greek Letters

$1/\alpha$	$\equiv Var(k_p{}^2)/E(k_p{}^2)^2$
ϕ	Thiele modulus $(=r_c(k_p C*/D)^{0.5})$
γ	power-law order with respect to active site concentration
ΔH_p	heat of polymerization
η	extent of the relationship between active site species and the ratio of deactivation and propagation rate constants.

$\eta*$	sorption factor of monomer in polymer.
θ_1	initial activity of the catalyst
θ_2	weighted average of the reciprocal of the deactivation half-life, a common deactivation parameter
θ_3	$=1+(\eta+1)/\alpha$
ρ_b,	bulk density of a bed of all the granules in a run
ρ_c	catalyst density (g/cm^3)
ρ_g	granule density
ρ_p	polymer density $(g/cm^3$ or mole of monomer/volume)

Abbreviations

ATREF	analytical temperature rising elution fractionation
DSC	differential scanning calorimetry
GPC	gel permeation chromatography
HDPE	high density polyethylene
HP-LDPE	high pressure - low density polyethylene
LDPE	low density polyethylene
LLDPE	linear low density polyethylene
MMD	molar mass distribution
NIST	National Institute of Standards and Technology
PS	polystyrene
PTREF	preparative temperature rising elution fractionation
SEC	size exclusion chromatography
SEM	scanning electron microscopy
TEAL	triethylaluminum
TEM	transmission electron microscopy
THF	tetrahydrofuran
TREF	temperature rising elution fractionation

1. Introduction

Polyolefins comprise about 60% of the total thermoplastics market of the world. Heterogeneous Ziegler-Natta catalysis has proven to be a remarkably versatile technology for polymerizing α-olefins, and the use of Ziegler-Natta catalysts is increasing even with the advent of homogeneous metallocene catalysts for polyolefin production. Among the thermoplastics, polyethylene accounts for the largest volume; its worldwide production in 1999, including low density polyethylene (LDPE), high density polyethylene (HDPE) and linear-low density polyethylene (LLDPE), will be over 55 million tons (*Modern Plastics*, p.114, July 1999).

Karl Ziegler (Ziegler *et al.*, 1953) discovered a catalyst for ethylene polymerization under mild conditions, and Giulio Natta (Natta *et al.*, 1955) adapted this catalyst for propylene polymerization. With this so-called Ziegler-Natta catalyst, ethylene can be polymerized at low pressure (< 2 MPa) and low temperature ($60\text{-}110^{\circ}C$), compared with free-radical ethylene polymerization at high pressure (~ 300 MPa) and high temperature (~$300^{\circ}C$). The first-generation Ziegler-Natta catalyst consisted of a transition metal compound, as an active component, and an alkyl or hydride of a main group element, as a cocatalyst. The most often used active component was $TiCl_3$, and the most common cocatalyst was triethylaluminum ($AlEt_3$). The development of new generations of Ziegler-Natta catalysts is based on these two components.

The first-generation Ziegler-Natta catalysts have been improved through generations of catalysts since Ziegler's discovery. Initially, the improvements of catalysts (second-

1

generation) were to increase their activity for producing HDPE (to increase both their activity and stereoregularity for producing polypropylene) by introducing a third component, *i.e.*, an electron donor (Lewis base). Since the 1970's, the improvement of Ziegler-Natta catalysts (third-generation) has been extended to the copolymerization ability and morphology, in addition to increasing catalyst activity, by fixing catalytic sites on catalyst supports. The most commonly used supports are $MgCl_2$ and silica. With these supported catalysts, a large fraction of titanium is available to take part in the polymerization reaction compared to the unsupported catalysts, *i.e.*, less titanium is needed. The yield of polymer per gram of titanium with these catalysts is sufficiently high so that no extraction for the removal of catalyst residues from the polymer is required. This resulted in a 20% of reduction in the capital investment cost, and significant reductions in maintenance, labor, raw materials and utility consumption, as well as reduction in potential pollution problems associated with the extracting solvent.

The copolymerization ability of the third-generation Ziegler-Natta catalysts made the production of LLDPE possible. The supported Ziegler-Natta catalysts with controlled morphology can make spherical polymer granules with a controlled morphology, *i.e.*, controlled particle size distribution and high bulk density so that the melting and extrusion of pelletization step can be eliminated in the commercial production. However, the third-generation catalysts limit the production of random polyolefin copolymers to relatively low levels of the second monomer.

Based on the third-generation Ziegler-Natta catalysts, the fourth-generation catalysts were developed to produce polyolefins with improved properties, such as heterophasic

2

olefin copolymers, reactor blends, multiphase polyolefin alloys, and non-olefin grafted polyolefin alloys in a production process. Each particle of the fourth-generation Ziegler-Natta catalysts becomes a single polymer granule which acts as a polymerization reactor, so called "Reactor Granule Technology" (Galli, 1994). The polymerization of an olefin monomer on each catalyst particle is first controlled to give a growing, spherical granule with a porous reaction bed (a prepolymerization step). Within the porous reaction bed, the same or other desirable monomers can then be introduced and polymerized to form polyolefin or polyolefin alloys. The introduction of other monomers to the internal active sites during the polymerization process can produce a second or third different polymer within the original polymer granule. Different polymers are intimately dispersed among the various pre-existing shells or lattice of the initially generated polymer structure.

With the fourth generation Ziegler-Natta catalysts, homogeneous metallocenes can also be introduced into porous polyolefin granules (Galli, 1996). The blends of polyolefins made by Ti-based catalysts and by metallocene catalysts can be obtained directly in the process of "Reactor Granule Technology". The intimate mixing of the two specifically different tailored polyolefins in terms of molecular structure and molar masses was achieved as they grew in the same granule.

With the development of generations of Ziegler-Natta catalysts, the process for polyolefin production has also evolved. The first commercial process was diluent slurry polymerization because of its low investment costs and operational stability. Other industrial processes such as solution and gas phase polymerization were also studied, but were initially limited by low catalyst activity, which reduced advantages of these processes.

3

The success of supported Ziegler-Natta catalysts with controlled morphology increased the complexity of catalysts, but provided versatility in process development and made various industrial processes viable, especially the gas phase processes.

From the viewpoint of polymer properties, diluent slurry processes produce polyolefins with a wide range of molar masses, but only limited range of density. Low-density copolymers like LLDPE and ethylene-propylene rubber (EPR) with their density below 0.93 g/cm^3 cannot be made in slurry processes because polymer solubility increases in the diluent as its density decreases. Solution processes can produce polyolefins with a wide rage of density, but only limited range of molar masses because high molar mass polyolefins with high viscosity in solution limit process operation. The first commercial solution process, the SCLAIRTECH technology, was developed by Du Pont Canada in early 1960 to produce LLDPE in Sarnia, Ontario, Canada (the SCLAIRTECH technology was acquired by NOVA Chemicals Ltd. in 1994) (Dyer *et al.*, 1997). Gas-phase processes have advantages over other processes, and are not limited by viscosity and solubility of polymer. Among the gas-phase processes, the UNIPOL process developed by Union Carbide Corporation (joint-ventured with Exxon to form Univation Technologies in 1996) is one of the most successful gas-phase process for producing polyethylene in fluidized-bed reactor. The UNIPOL process accounts for over 50% of worldwide polyethylene licenses, and Univation has access to more than 100 polyethylene reactors (Morse, 1998).

To further exploit polymerization processes, as well as the catalyst activity and morphology, a two-stage hybrid process was developed, *e.g.*, SPHERILENE, SPHERIPOL, CATALLOY, and HIVALLOY processes developed by Himont Incorporated/Montecatini

4

S.p.A. (merged with the majority of the polyolefin interests of the Royal Dutch/Shell Group to create Montell Polyolefins in April 1995) for producing various polyethylene, polypropylene, and polypropylene alloys (Galli, 1994; Covezzi, 1995). In these processes, the first stage (*i.e.*, the prepolymerization step) is a diluent slurry polymerization, and the second stage is gas phase polymerization for producing homopolymer or copolymer.

Advances of Ziegler-Natta polymerization in industrial catalysts and processes have inspired academic interest and activity, and generated an "acceleration" period and several "maxima" in the number of scientific papers and patents after the initial discoveries by Ziegler and Natta (Kissin, 1985). The scientific papers and patents in Ziegler-Natta polymerizations are reviewed in Chapter 2 with the emphasis on morphology of nascent polymer, preparation of morphology-controlled catalyst support, and polymerization kinetics. Reviews on the published literature provide information for current understanding and future studies.

The objective of this work was to prepare morphology-controlled $MgCl_2$-supported $TiCl_4$ catalysts, to study the kinetics of gas-phase ethylene homopolymerization, and to characterize the resulting polyethylene. Prior to the gas-phase ethylene homopolymerization, a prepolymerization step, in which the prepolymerized catalyst is obtained by slurry polymerization of ethylene over morphology-controlled $MgCl_2$-supported $TiCl_4$ catalyst under mild conditions, is carried out to prevent the breakup of catalyst particles.

Kinetic studies are important for process design and optimization in industry, but the kinetics of Ziegler-Natta polymerization are not well understood. Very little kinetic data are

5

available for gas-phase ethylene polymerization over morphology-controlled catalysts and the possible presence of transport resistance and multiple catalytic sites should be explored. Homopolymerization is easier in experimental operation, simpler in chemical reaction, and more reproducible in experimental results than copolymerization. The insight gained into the kinetics of ethylene homopolymerization can provide the basis for the more complicated copolymerization studies of ethylene and α-olefins.

In this work, the experimental procedures for preparing a morphology-controlled $MgCl_2$-supported $TiCl_4$ catalyst and for performing ethylene prepolymerization and homopolymerization, as well as the equipment for characterizing catalyst and polymer are described in Chapter 3.

In Chapter 4, effects of prepolymerization conditions on prepolymer properties, such as bulk density and morphology, are reported, with the purpose of identifying the optimal prepolymerization conditions; for prepolymer produced under the optimal prepolymerization conditions, effects of mass transfer limitations on molar masses and morphology of nascent prepolymer particles are presented.

Kinetics of ethylene homopolymerization were studied with the prepolymerized catalyst produced under the optimal conditions. The initial results of kinetic studies of ethylene homopolymerization are presented in Chapter 5 with emphasis on the reproducibility of the rate profiles. Experimental results are compared qualitatively with predictions by the multigrain model. The effects of polymerization conditions on rate profiles are discussed with an attempt to determine if kinetic results indicate the presence of

6

multiple active sites and if effects of mass and heat transfers are present in the current Ziegler-Natta catalyst.

In Chapter 6, additional results on the kinetics of ethylene homopolymerization are presented. Effects of mass and heat transfers are examined for various reaction conditions and the resulting polymer properties. A new method for estimating power-law reaction orders is presented. More evidence is reported in resolving the dispute between multiplicity of active sites and effects of mass and heat transfer limitations, and more information is reported on the kinetics of activation and deactivation during ethylene homopolymerization.

The characterization results, including the morphologies of nascent polyethylene and the effect of polymerization conditions on molar masses and polydispersity of polyethylene granules as a function of granule size, are reported in Chapter 7 for polyethylene produced in the gas-phase and slurry reactors. The differences of rate profiles in the gas-phase and slurry polymerization of ethylene are stressed.

On the basis of the observations and discussions on the experiments presented in Chapter 5, a kinetic model is proposed in Chapter 8; the model predictions are compared with the experimental results. The discrepancies between model predictions and experimental results are analyzed, and modifications of the model are also suggested. A summary of this work and recommendations for future work are presented in Chapter 9.

2. Literature Survey: Ziegler-Natta Olefin Polymerization

Since Ziegler's discovery of low pressure polymerization of ethylene over heterogeneous Ti catalyst (Ziegler *et al.*, 1953) thousands of scientific papers and patents have been published on aspects of catalyst preparation, olefin polymerization kinetics and mechanism, and polyolefin characterization. With the development of the technology of catalyst synthesis and olefin polymerization, heterogeneous Ziegler-Natta catalysts have evolved to the so-called fourth generation with very high activity and controlled morphology, and polyolefins with a wide range of properties can be produced in relatively simple processes. However, the mechanism of Ziegler-Natta polymerization is still not understood completely. Reviews on the published literature are helpful in assessing the current understanding of the polymerization mechanism and provide information to guide future studies of Ziegler-Natta polymerization.

In this chapter, the Ziegler-Natta olefin polymerization will be reviewed in areas closely related to the present study. Therefore, the emphasis will be on the morphology of nascent polymer, preparation of morphology-controlled catalyst support, and kinetics of Ziegler-Natta polymerization. The kinetics includes the effects of mass transfer resistances, polymerization kinetics, and deactivation kinetics.

2.1 Nascent Polyolefin Morphologies in Ziegler-Natta Polymerization

The morphological studies of the Ziegler-Natta catalyst and nascent polymer particles are of importance academically and industrially (Boor, 1979). The morphologies of nascent polyolefin particles have been extensively investigated by optical microscopy

8

(OM), scanning electron microscopy (SEM), and transmission electron microscopy (TEM). Various explanations have been proposed based on the qualitative microscopy observation, but little evidence is available in the cause of the observed morphologies.

2.1.1 Morphology and Growth Mechanism of Nascent Polymer

It is widely accepted that the detailed morphology of nascent polyolefins made by heterogeneous Ziegler-Natta polymerizations is of a ternary structure (*e.g.*, Kakugo *et al.*, 1989a; 1989b). The ternary structure consists of the morphologies of the polymer particles, the secondary polymer particles, and the primary polymer particles. Polymer particles are basically made up by various types of secondary polymer particles; secondary polymer particles are aggregations of some tens of primary polymer particles. Polymer particles and secondary polymer particles have been observed by optical microscopy and SEM in most of the studies of nascent polyolefin morphologies; primary polymer particles can only be observed by TEM after careful sample preparations (Kakugo *et al.*, 1989a; 1989b).

2.1.1.1 Polymer Particles

Polymer particles appeared to be globular, ribbon-like, worm-like, shish-kebab, or cobweb type depending on catalyst preparations and polymerization conditions (Wristers, 1973a; Muñoz-Escalona *et al.*, 1983). Among polymerization conditions, polymerization temperature had more influence in the formation of different types of morphologies than other polymerization conditions such as ethylene pressure and stirring speed in the reactor (Muñoz-Escalona and Parada, 1980). The globular morphology can usually be found in polypropylene or polyethylene at a low polymerization rate, *i.e.*, low monomer pressure and

9

low polymerization temperature (Wristers, 1973a; Muñoz-Escalona and Parada, 1980). For polymerization at higher rates, the polymer globules can have worm-like or "shish-kebab" morphologies. The worm-like morphology consisted of a complex aggregation of ribbonlike crystals and platelets (Muñoz-Escalona and Parada, 1980). The "shish-kebab" morphology was found mostly in nascent polyethylene, rarely in nascent polypropylene (Blais and St. John Manley, 1968), made at a high polymerization temperature of about 115 - 120°C under vigorous stirring conditions (Muñoz-Escalona and Parada, 1980). The "shish-kebab" morphology indicated that a certain amount of polymer stayed in solution at high temperature, and it crystallized only when the growing crystals were subject to the shear stress (Muñoz-Escalona and Parada, 1980; Nagasawa and Shimomura, 1974).

The fibrillar cobweb morphology, mainly observed in polyethylene, resulted from a secondary mechanical effect due to stretching or cold-drawing of the growing polymer mass (Graff *et al.*, 1970; Muñoz-Escalona and Parada, 1980). According to Graff *et al.* (1970), the rate of ethylene polymerization at the surface of a catalyst particle was initially much higher than that in the interior due to mass transfer resistance of monomer; whereas in a later stage, the polymerization rate became higher in the interior of the particle. Accordingly, the crust would be formed initially at or near the catalyst surface where the greater amount of the polymer was produced; the crust broke and remained interconnected by cold-drawn threads of polymer as polymerization proceeded and polymer grew in the interior of the particle. The cold-drawn threads are considered to be the fibrils of the secondary morphology.

10

2.1.1.2 Secondary Polymer Particles

Secondary polymer particles were reported to be platelets, lamella, globules and fibrils; their morphologies also varied with polymerization rate and yield (Wristers, 1973a; Muñoz-Escalona *et al.*, 1983). The platelet morphology was more likely to develop around the angular areas of large catalyst particles during the initial stage of polymer formation (Blais and St. John Manley, 1968; Baker *et al.*, 1973).

At a low rate of ethylene polymerization with a Stauffer AA Ziegler-Natta catalyst, polymer growing on the catalyst surface appeared to be lamella or globule (Muñoz-Escalona and Parada, 1980). The lamellae had irregular width of 40 to 200 nm, and thickness of 21.5 nm. The globules had a relatively uniform diameter between 20-500 nm depending on the polymerization conditions and the activity of catalytic sites (Muñoz-Escalona and Parada, 1980).

Secondary polymer particles of polypropylene, produced by either δ-TiCl$_3$, or Stauffer AA Type, or MgCl$_2$-supported Ziegler-Natta catalyst, had similar globular structure (Kakugo *et al.*, 1989a and 1989b). The secondary globules showed a relatively broad size distribution ranging from 0.4 μm to 1.1 μm at a low yield. At a high yield, secondary globules became round with uniform sizes about 1 μm in diameter. The uniform sizes of secondary polypropylene globules at a high yield was also observed by Noristi *et al.* (1994) when they polymerized propylene using the spherical MgCl$_2$-supported catalyst with uniformly distributed active sites. Noristi *et al.* (1994) found that polymer particles exhibited a flat lamellae about 1 - 5 μm wide and 0.5 μm thick in the cross section

11

area of particles at a low yield. As the yield of polymerization increases, lamellae seemed to get progressively replaced by more rounded, almost globular structures with uniform sizes.

The relative uniformity of secondary polymer globules was explained by coalescence theory (Fisa *et al.*, 1974). The coalescence theory was based on successive polymerization and crystallization. According to this theory, at the very beginning of polymerization, the catalyst was not a nucleating agent, and the polymer was amorphous and tended to coalesce in the liquid state until the liquid polymer droplets reached a critical size. Once the polymer liquid droplets reached the critical size, they nucleated and the coalescence was interrupted due to rapid crystallization.

As reaction rate increased, secondary polymer globules and platelets grew and might cover the catalyst surface, and mechanical effects from the growing polymer caused the fragmentation of catalyst particles (Muñoz-Escalona and Parada, 1980). The fragmentation of catalyst particles mainly took place at pre-existing faults. The number of such pre-existing faults appeared to be enhanced by cocatalyst in polymerization (Baker *et al.*, 1973).

2.1.1.3 Primary Polymer Particles

Primary polymer particles were first observed convincingly by Kakugo *et al.* (1989a), and later confirmed by Noristi *et al.* (1994). Kakugo *et al.* (1989a) compared their TEM results of nascent polypropylene morphology with SEM observations published previously by other investigators, and found that the secondary polymer particle consisted of primary polymer particles. Based on calculations of catalyst crystal sizes obtained by X-ray diffraction and observations of nascent polypropylene morphologies by SEM and

12

TEM, Kakugo *et al.* (1989a) described a tertiary particle structure existing in the nascent polymer particle. In the tertiary particle structure, polymer particle consisted of secondary polymer globules while secondary polymer globules were aggregations of some tens of primary polymer particles, no matter if the Ziegler-Natta catalyst used was conventional or $MgCl_2$-supported. Primary polymer particle was produced by one or a few primary catalyst crystallites which remained embedded within the core of individual primary polymer particles (Graff *et al.*, 1970; Kakugo *et al.*, 1989a). Primary polymer particles grew as polymerization proceeded, with the catalyst crystallites dispersed uniformly within the primary polymer particles and retained their initial size and shape even at higher yields (Kakugo *et al.*, 1989b).

Primary polymer particles observed by Noristi *et al.* (1994) were similar to those reported by Kakugo *et al.* (1989b). However, Noristi *et al.* (1994) proposed a different fragmentation process during propylene polymerization. In the fragmentation process described by Noristi *et al.* (1994), catalysts broke up into fragments very early; these fragments became smaller and smaller as polymerization proceeded under very mild reaction conditions from 0.1 to 1000 g of polypropylene per g of spherical $MgCl_2$-supported catalyst. In addition, catalyst particle underwent an even and progressive fragmentation into very fine units, which were homogeneously dispersed in the polymer matrix; the polymer grew uniformly throughout the catalyst particle from the onset of polymerization.

2.1.2 Morphology Replication from Catalyst to Polymer

Despite the differences in detailed polymer morphologies and catalyst fragmentation processes reported in the literature as discussed above, it has been commonly observed that

13

Ti-based Ziegler-Natta catalysts are capable of replicating their overall morphology into the morphology of polymer particles, *i.e.*, polymer granules, under proper polymerization conditions (*e.g.*, Boor, 1979). Catalyst particles with an open structure, observed by SEM, yielded polymer particles with a low particle density, high particle porosity and high particle surface area, measured by mercury porosimetry (Wristers, 1973b). The initial catalyst particles act as templates for growth of polymer particles. The morphology of particles refers to their size, shape, density, and texture (Boor, 1979).

In Ziegler-Natta olefin polymerization, olefin monomers reach active sites on the catalyst where polymerization occurs. When enough polymer is produced, the stress from the growing polymer molecules breaks the catalyst structure; this is referred to as fragmentation of the catalyst (Boor, 1979). The fragmentation of the catalyst particles mainly takes place at the porous walls and at pre-existing faults in the catalyst crystal matrix. The polymer molecules grow from various active sites within the catalyst, and have a great chance to be entangled at the time of fragmentation. The entanglement of polymer molecules attached to different primary polymer particles may keep primary polymer particles from separating physically from one another under certain reaction conditions. The same situation applies to secondary polymer particles. Polymer granules consisting of secondary polymer particles retain the morphology of the catalyst particles, which is observed macroscopically as the replication phenomenon.

2.1.3 Factors Affecting Polymer Morphology

The replication phenomenon is affected by catalyst morphology and polymerization conditions. The catalyst morphology must be in balance with polymerization conditions in

14

order to provide good replication of catalyst morphology into polymer morphology (Galli and Haylock, 1991).

2.1.3.1 Effect of Catalyst

To obtain the desirable replication, it is necessary for a catalyst to have a porous structure consisting of a proper size of crystals and primary particles evenly dispersed in each catalyst particle so that the monomer will have equal access to the active sites (Galli and Haylock, 1991). If catalyst is too porous, or if the breaking stress is stronger than the resistance of polymer entanglements under polymerization conditions, complete separation of secondary polymer particles will occur and lead to fine polymer powders. When active sites are not evenly distributed in the catalyst particle and the catalyst particle has a loose structure, the polymer produced will be brittle and easily broken into irregular pieces. If the catalyst particle has a compact structure (low porosity), the activity will be low inside the particle because monomer will have difficulty in reaching the internal active sites. With such catalysts, the polymer granules produced tend to be hollow, and they also have the tendency to break into irregular shapes instead of replicating the shape of catalysts (Galli and Haylock, 1991; Galli, 1994). Without a proper replication, nascent polymer granules are likely to break into irregular fine particles with "flake-type" morphology. The fine polymer powders have lower flowability and bulk density than polymer granules with regular shapes.

2.1.3.2 Effect of Cocatalyst

The cocatalyst appears to enhance the number of pre-existing faults during polymerization (Baker et al., 1973) (see also Section 2.1.1.2). The increase of the Al/Ti

15

ratio in a certain range will increase the density, smoothness and regularity of polymer granules produced (Boor, 1979).

2.1.3.3 Effect of Polymerization Conditions

The catalyst-polymer replication occurs when polymer chain begins to grow, not only on the external surface, but also on the internal surface of a catalyst particle, progressively causing the particle to expand (Galli and Haylock, 1991). Under reaction conditions with mass transfer limitations, the morphology of final polymer granules will be affected; polymer grows faster in the outer layer than in the inner core, which will also lead to a low granule density. If polymerization can be kinetically controlled and polymer granules can replicate the shape of catalyst particles, the polymer granule size will only depend on catalyst particle size and reaction rate. For spherical catalyst particles, polymer granule size as a function of time was described by Equation 2.1 (Putanov *et al.*, 1989):

$$d_p = d_c \sqrt[3]{(1 + \frac{\rho_c}{\rho_p} \int_0^t R_p dt)} \qquad (2.1)$$

where: d_p is a diameter of polymer granule at time t; d_c is a diameter of initial catalyst; ρ_p is polymer density (g/cm^3) under polymerization conditions; ρ_c is catalyst density (g/cm^3); R_p is total polymerization rate (grams of polymer per gram of catalyst per unit time).

According to mathematical simulations of mass and heat transfer effects on either ethylene or propylene polymerizations, transport limitations are most likely to occur in the initial period of polymerization (Floyd *et al.*, 1986a; 1986b). A high rate in the early stage of polymerization will cause the complete fragmentation of secondary polymer particles to

16

occur before entangled polymer is formed. Prepolymerization at mild conditions prior to polymerization is essential at the initial stage for the proper performances of MgCl$_2$-supported catalyst especially in terms of morphology (Covezzi, 1995), because very fast initial growth can cause catalyst particles to explode physically, and mechanical forces generated by growing polymer chain will fracture the particle into fine polymer powders.

2.1.4 Advantages of Nascent Polyolefins with Controlled Morphology

Nascent polymer granules with controlled morphology are polymer granules that have spherical shape, high flowability (*i.e.*, pourability) and high bulk density (see ASTM D 1895-67), and controlled size with a narrow particle size distribution. Efforts have been made to prepare spherical Ziegler-Natta catalyst particles simply because spherical Ziegler-Natta catalysts can produce spherical nascent polymer granules according to the morphology replication phenomenon reviewed above. It is important to control the size, shape and internal structures of the nascent polymer (Revol *et. al.*, 1980).

Production of nascent polymer granules with controlled morphology eliminates the energy-consuming pelletization (Galli, 1993). Since no seed resin is required at the start-up phase, the changes of product grades do not involve any extra cost. These will lead to substantial reductions in the capital investment and production costs.

Spherical polyolefin granules with a high bulk density, obtained directly from the polymerization reactor, have less entangled morphology and are softer than the melt-crystallized pellets (Smith *et al.*, 1987), which have a thermal history due to a pelletization step. During extrusion of the softer granules, friction-burning and cross-linking phenomena

17

can be reduced, damaging thermomechanical stresses can be avoided due to the lower

plastification temperature, and better end-use performance can be obtained, particularly for

the more viscous polymers such as LLDPE. The deformation of the spheres in extrusion

devices is easier, and melt shear starts earlier with the combination of heat and pressure, *i.e.*,

better processability (Galli, 1993). Due to these physical and morphological properties, the

granules of spherical shape can easily be compacted in the solid-conveying section of the

extrusion devices under the same pressure conditions as the pelletized resins.

The direct use of the polymer granules without a thermal history can protect the

additive package at a certain level against degradation that cannot be avoided during

pelletization (Galli and Haylock, 1991). Consequently, it is possible to reduce the quantity

of additives and enhance product purity. Polymer with high purity is easier to be tailored for

the processing and application requirements.

Since morphology-controlled polymer granules have advantages and can only be

made from morphology-controlled catalysts, it is essential to prepare catalyst supports that

can enhance activity and control morphology of the Ziegler-Natta catalysts. The preparative

methods of morphology-controlled catalyst supports will be reviewed in the next section.

2.2 Preparation of Morphology Controlled Catalyst Support

It has been shown in the last section that one of the important features of the

Ziegler-Natta polymerization is the capability of catalysts to replicate their morphology into

the morphology of polymer granules (Boor, 1979). This feature suggests that the

modification of polymer morphology begins with the catalyst preparation. It was also found

18

that only a small fraction of Ti locating on the lateral faces and edges of the crystal lattice and along the crystal defects were active for $MgCl_2$ support (Galli *et al.*, 1984). In order to improve catalyst activity and morphology, extensive interests have arisen in the modification of catalyst supports.

Many methods have been applied and many materials have been used as catalyst supports to improve the catalyst efficiency and morphology. For example, ball-milling of $MgCl_2$ and $TiCl_4$ with other components was widely used to increase catalyst activities (Kissin, 1985), but it is difficult to control catalyst morphology. In recent years, many effective methods have been developed for preparing catalyst supports with both a controlled morphology and a high activity for α-olefin polymerization catalysts. These supports are magnesium-compounds (*e.g.*, $MgCl_2$), and others, such as silica and some polymers. Since most of these preparations have only been discussed in the patent literature, the preparative methods reviewed in this section will largely be descriptive.

2.2.1 Magnesium-Based Supports

Among magnesium-based materials, anhydrous, activated $MgCl_2$ is most often used as a support for Ziegler-Natta catalysts. $MgCl_2$ can be activated by many methods, such as chemical reaction precipitation, drying recrystallization, spray drying, spray crystallization, and melt quenching.

2.2.1.1 Chemical Reaction Precipitation of Mg Compounds

Spheroidal particles of magnesium compound can be made by chemical reaction. For example, $MgCl_2$ was precipitated by a reaction between dibutyl magnesium and *tert-*

19

butyl chloride in heptane which is inert to $MgCl_2$ (Bailly and Behue, 1990 and 1991; Bailly, 1991). For this method, dibutyl ether was often present to increase the activity of catalyst. The reaction should take place slowly to make sure that the ether is dispersed uniformly from the core to the periphery of $MgCl_2$ support. The solid $MgCl_2$ support can be reacted with trialkylaluminum and titanium compounds to form a catalyst. Other magnesium compounds, such as alkyl magnesium halide *etc.*, can also be prepared by this method as catalyst supports (Standke *et al.*, 1991; Horns *et al.*, 1992; Lee and Karayannis, 1992).

2.2.1.2 Drying Recrystallization of MgCl₂ Complexes

Spherical $MgCl_2$ particles can be made by recrystallization of $MgCl_2$-ethanol complex in an inert medium, such as *n*-decane. When $MgCl_2$ is complexed with ethanol, its melting point decreases with increasing ethanol/$MgCl_2$ ratio. In this method (*e.g.*, Kang *et al.*, 1990; Park and Lee, 1992), $MgCl_2$ was first dissolved in ethanol to form $MgCl_2$-ethanol complex in *n*-decane medium. Then, ethanol was eliminated from $MgCl_2$-ethanol complex by vacuum drying due to the difference in boiling points between ethanol and *n*-decane. As ethanol was eliminated, spherical $MgCl_2$ particles were crystallized in *n*-decane.

2.2.1.3 Spray Drying of MgCl₂ Complexes

Similar to drying recrystallization, ethanol is partially removed from the $MgCl_2$-ethanol complex in the spray process by evaporation at high temperature instead of vacuum. In a patent described by Masi *et al.* (1991), $MgCl_2$-ethanol complex was dispersed in a hydrocarbon liquid with stirring to obtain a uniform emulsion at a high temperature (*e.g.*, 130°C, for a ratio of ethanol/$MgCl_2$ of about 3). The emulsion was then fed into an

20

evaporation chamber of a spray dryer by pressurizing. In this evaporation chamber, the emulsion contacted with a nitrogen stream at a higher temperature (*e.g.*, 250°C of inlet nitrogen) so that ethanol was evaporated.

Hamer and Karol (1981) included $TiCl_4$, tetrahydrofuran (THF) and silica in addition to $MgCl_2$ in a spray drying suspension. According to their description, the spray drying suspension was formed by the mixture of a solution and a slurry. The solution was a partial or total dissolution of $TiCl_4$ and an excess of $MgCl_2$ in THF. The slurry was the dispersion of fumed silica and/or $MgCl_2$ in the THF. The solution was slowly added to the slurry at room temperature to form a suspension. The suspension with a high temperature was spray-dried in a nitrogen atmosphere. The inlet nitrogen temperature should be higher than the boiling point of THF. The catalyst precursor obtained above could be activated by trialkyl aluminum either through a total activation in the polymerization reactor or through two stages of activation outside and inside the reactor.

2.2.1.4 Spray Crystallization of $MgCl_2$ Complexes

In contrast to drying recrystallization and spray drying, ethanol is kept in spherical $MgCl_2$-ethanol complex in the spray crystallization process. A melt $MgCl_2$-ethanol complex is crystallized in a cooled gas chamber. As described by Iikolan and Koshinen (1987), Miya *et al.* (1990), and Pentti and Leskinen (1993), the melt $MgCl_2$-ethanol complex was sprayed from a nozzle to the spraying area, and then to the cooled crystallization area of a chamber to solidify the melt. The complex of $MgCl_2$ and water can also be used in this method (Galli *et al.*, 1974). The spherical support was activated by $TiCl_4$ to form the catalyst.

21

The recrystallization process in the spray crystallization method occurs in a gas-cooling column. Due to the low thermal capacity of gas, the column needs to be sufficiently high for the molten adduct to solidify. Thus, this method needs large investment for the high column and is not suitable for making a small amount of catalyst for research in the laboratory scale.

2.2.1.5 Melt Quenching of MgCl$_2$-ethanol Complexes

A cold inert liquid is used in the melt quenching method to solify the melt of MgCl$_2$-ethanol complex. Two different ways of quenching have been used to obtain spherical supports. In the first process, an emulsion of a molten MgCl$_2$-ethanol adduct, with or without oil-soluble surfactant(s) in an inert liquid (*e.g.* Vaseline), is passed through a small-diameter pipe under turbulent conditions; the emulsion at the outlet of the pipe is quenched in heptane at -30°C to solidify the adduct immediately (Ushida *et al.*, 1980; Ferraris *et al.*, 1981). This process was used in the current studies. The size of the emulsion droplet depends on the inner diameter of the pipe which is usually at least 3 - 4 times the maximum diameter of the support particle. In another method (Ferraris *et al.*, 1981; Sacchetti *et al.*, 1992), the emulsion of a MgCl$_2$-ethanol adduct under vigorous stirring at 2,000 - 10,000 rpm was quenched directly into an inert liquid under stirring at a temperature below 0°C. The solidified MgCl$_2$-ethanol adduct was then partially dealcoholated by heating to obtain the desired ratio of ethanol/MgCl$_2$, and finally treated by TiCl$_4$ and electron donor(s) to obtain an active catalyst.

22

2.2.2 Other Supports

Other supports (*e.g.*, silica and polymers) are used mainly to reduce the chlorine content in the final polymer product without losing desired morphology such as shape and flowability of catalyst particles. Bulk density of polymers made by these silica and polymer supported catalysts can be greater than 0.4 g/cm^3.

2.2.2.1 Silica Supports

Silica can be used as a support for olefin polymerization catalyst to achieve outstanding morphology and flowability of the polyolefins. Silica acts not only as a template for polymer growth, but also as a reagent to produce a highly active catalyst (Luciani *et al.*, 1992; Luciani *et al.*, 1995). According to Luciani *et al.* (1992), silica containing hydroxyls and water interacted with *n*-butyl *n*-octyl magnesium so that the magnesium compound was deposited on the silica to give an activated support for the α-olefin polymerization catalyst. The activated silica was chlorinated in heptane by SiCl$_4$, and then treated with TiCl$_4$ and an electron donor to form a catalyst. The polypropylene obtained with this catalyst was claimed to have bulk density of 0.38 - 0.48 g/cm^3 and a low chlorine content. Polypropylene granules had an average diameter of about 1 mm and the flowability (ASTM D 1895-67) of less than 20 seconds.

2.2.2.2 Polymer Supports

Polymer-supported Ziegler-Natta catalysts for α-olefin polymerization have been developed since it was found that aluminum chloride can be introduced into the structure of polystyrene-divinylbenzene (Nekers *et al.*, 1972). Functionalized polystyrenes can be used

23

as supports by taking advantage of the polystyrene morphology with a spherical shape from the catalyst-polymer replication point of view. It was reported that a polystyrene-supported catalyst for the polymerization of isoprene had a greater storability and can be reused and regenerated (Ran, 1993), but the low activity compared to $MgCl_2$-supported catalyst seems to limit their use in industry for the time being. Little has been reported on the morphology of the polyolefins made with these polystyrene-supported catalysts. Polyvinyl chloride and some chlorinated polymers, such as atactic polypropylene and natural rubber, can be used as catalyst supports for ethylene polymerization (Jericó *et al.*, 1995). However, these catalysts deactivated quickly and polyethylene produced had relatively low molar masses.

Commercial poly(ethylene-*co*-acrylic acid) was also used as a support after it was subjected to the reprecipitation and wet-grinding (Sun *et al.*, 1994a; 1994b). The catalyst made with $TiCl_4/MgR_2/$poly(ethylene-*co*-acrylic acid) polymerized ethylene, and copolymerized ethylene and 1-hexene with relatively high activity. A functionalized step was not needed since poly(ethylene-*co*-acrylic acid) used has its own function group (*i.e.*, -COOH) which leads to its reactions with the metal compound. No details were reported on the polyethylene morphology.

2.3 Transport Resistance Models of Ziegler-Natta Polymerization

Mass transfer limitations are an important aspect in the polymerization kinetics. Mass transfer limitations can affect polymerization rate profiles, and final properties of polymer produced since monomer diffusion leads to the establishment of monomer concentration gradients in the polymer particles. Resistance to monomer diffusion toward the surface of the catalyst particles, caused by progressive polymer encapsulation, was first

24

proposed by Pasquon *et al.* (1959) to explain the activity decay with time in the TiCl$_3$-Al(C$_2$H$_5$)$_3$ catalytic system. Many models have since associated such a concept to the broadening of MMD (Zucchini and Cecchin, 1983). In most of these models, catalyst and polymer particles are assumed to be spherical, and simple chemical kinetics with single type of active site are considered. Among various models with a single type of active site in catalyst, the simplest forms are core models including the solid core model and the polymeric core model. The more realistic models are expansion models including the polymeric flow model and the multigrain model. Variations of the models above, which predict similar trends, are not discussed in detail. Further improvement of the multigrain model, the double grain model (Mei and Cecchin, 1996), is only available theoretically and is not reviewed.

By reviewing different transprot resistance models, it can be seen whether the results predicted by these models can consistently match experimental results most commonly observed in the Ziegler-Natta olefin polymerization systems.

2.3.1 Core Models

Core models, including the solid core and polymeric core models, are the earliest models considered for polymer growth in Ziegler-Natta polymerization. Solid core model and polymeric core model predict qualitatively similar rate behavior. However, the molar mass distribution predicted by these two models are quite different depending on the value of Thiele modulus (ϕ), the ratio of the characteristic diffusion time to the characteristic reaction time.

25

2.3.1.1 Solid Core Model

In the solid core model, polymerization occurs at the surface of an inner core and polymer is assumed to accumulate around a catalyst sphere. Monomer diffuses through the growing polymeric coat (Schmeal and Street, 1971). The conservation of mass for the outer polymeric coat is:

$$\frac{1}{r^2}\frac{\partial}{\partial r}(r^2\frac{\partial[M]}{\partial r}) = 0 \qquad \text{outer polymer} \qquad (2.2)$$

boundary conditions: $\quad @\ r{=}r_c\ , \qquad 4\pi r_c^2 D\frac{\partial[M]}{\partial r} = \frac{4}{3}\pi r_c^3 R_p$

$\qquad\qquad\qquad\quad @\ r{=}r_p\ , \qquad [M]{=}[M]_b$

where: r is radius; r_c is radius of the catalyst particle; r_p is entire polymer particle radius which increases with the generation of polymer; $[M]$ is the monomer concentration; $[M]_b$ is the monomer concentration in the fluid medium; D is diffusivity of monomer in polymer; R_p is polymerization rate $R_p{=}k_p[C^*][M]$ (where: k_p is polymerization rate constant, and $[C^*]$ is concentration of catalytic sites).

For reaction control conditions, *i.e.*, small Thiele modulus defined as ϕ $=r_c(k_pC^*/D)^{0.5}$, the apparent polymerization rate depends only on the reaction parameters. For reaction conditions with diffusion control, *i.e.*, large values of the Thiele modulus, the reaction rate declines from its initial value to a final asymptotic value as the relative radius of the polymer coat increases. The initial rate is the same as that for reaction control case, but the asymptotic final rate is dependent only on the diffusion parameters. However, the predicted polydispersity of the polymer was always equal to unity.

26

2.3.1.2 Polymeric Core Model

In the polymeric core model, the polymerization occurred at active sites in the catalyst. The active sites were distributed evenly through a stationary inner polymer sphere and could move indefinitely slowly (Schmeal and Street, 1971). The equations of conservation of mass are:

$$D \frac{1}{r^2} \frac{\partial}{\partial r} (r^2 \frac{\partial [M]}{\partial r}) - R_p = 0 \qquad \text{inner sphere} \qquad (2.3)$$

$$\frac{1}{r^2} \frac{\partial}{\partial r} (r^2 \frac{\partial [M]}{\partial r}) = 0 \qquad \text{outer sphere} \qquad (2.4)$$

boundary conditions: @ $r=0$, $\frac{\partial [M]}{\partial r} = 0$

@ $r=r_p$, $[M] = [M]_b$

This model predicted polymerization rate identical to the solid core model. However, polydispersity of polymer (Q) predicted was equal to 1 under the reaction control, while it increased with increasing Thiele modulus by $Q=\phi/6$ in case of diffusion control.

For the above core models, the unity polydispersity, which is not possible, arises from the absence of termination kinetics in the models. In addition, none of the core models take into consideration the generally accepted phenomenon that the catalyst particles break up after the initial polymerization. The more realistic models are the following expansion models: polymeric flow model and multigrain model.

2.3.2 Expansion Models

For the expansion models, catalyst microparticles exist in a polymer macroparticle (*i.e.*, polymer granule) because the catalyst particle breaks up right after the initial

27

polymerization while the particle as a whole is held together by the polymer formed. One level of monomer diffusion is considered for the polymeric flow model while three levels of monomer mass and heat transfers are considered for the multigrain model in a growing polymer granule at the external boundary layer into the pores of granules, on the macroscale in the interstices between microparticles, and on the microscale within the microparticles.

2.3.2.1 Polymeric Flow Model

In the polymeric flow model, the catalyst microparticles are dispersed in a polymer continuum and are free to move outward with the polymer in proportion to the volumetric expansion due to polymerization. Therefore, the active site concentration is a function of radius and time. The growing polymer granules are assumed to be nonporous and only one value of diffusivity is considered (Schmeal and Street, 1971; Singh and Merrill, 1971). The equations describing the model are:

$$\frac{\partial [M]}{\partial t} = D \frac{1}{r^2} \frac{\partial}{\partial r} (r^2 \frac{\partial [M]}{\partial r}) - R_p \qquad \text{monomer} \qquad (2.5)$$

$$\rho_p \frac{1}{r^2} \frac{\partial}{\partial r} (r^2 u) - R_p = 0 \qquad \text{polymer} \qquad (2.6)$$

$$\frac{\partial [C^*]}{\partial t} = -\frac{1}{r^2} \frac{\partial}{\partial r} (r^2 [C^*] u) \qquad \text{catalytic sites} \qquad (2.7)$$

initial condition: @ $t=0$, $[M]=[M]_b=u=0$

boundary conditions: @ $r=0$, $\frac{\partial [M]}{\partial r} = \frac{\partial [C^*]}{\partial r} = u = 0$

           @ $r=r_p$, $[M]=[M]_b$

where: t is time; $[C^*]$ is concentration of catalyst sites (number of sites/volume); ρ_p is density of incompressible polymer (mole of monomer/volume); u is velocity sites of (length/time).

28

The polymeric flow model predicts qualitatively similar polymerization rate behavior and molar mass distribution as core models for the conditions of reaction control. In case of diffusion control, the asymptotic rate predicted was almost an order of magnitude larger than the polymeric core model, while a broader molar mass distribution was predicted according to $Q=\phi$ (Schmeal and Street, 1971). If termination reaction was assumed to be chain transfer to monomer in the reaction kinetics, the polydispersity could be even larger (Singh and Merrill, 1971).

Galvan and Tirrell (1986) modified the polymeric flow model with two different active site types and catalyst deactivation in the heterogeneous Ziegler-Natta polymerization. They found that the increase of polydispersity mainly depended on the presence of two types of active sites and the changes in molar mass and polydispersity were either minor or negligible when diffusion limitations were present. Incorporating a first order deactivation rate into the rate equation eliminated the possible diffusion limitations without appreciably changing molar mass and polydispersity of polymer.

2.3.2.2 Multigrain Model

The multigrain model is based on the microscopic observation that in the early stage of heterogeneous Ziegler-Natta polymerization, the original catalyst particles quickly break up into many small fragments which are uniformly dispersed throughout the porous polymer granule produced. The porous polymer granule (macroparticle) is comprised of many small polymer particles (microparticles) which encapsulate those catalyst fragments. The multigrain model considered three levels of monomer mass and heat transfer; these are: transfer at the external boundary layer into the pores of granules, transfer at the macroscale

in the interstices between microparticles, and transfer at the microscale within the microparticles.

Since transport resistance can be made negligible at the boundary layer level (Laurence and Chiovetta, 1983; Floyd *et al.*, 1986a), material and energy balances for the growing polymer particle in macroparticle and microparticle level are as following:

macroparticle ($0 < r_l < R_l$):

$$\frac{\partial [M]_l}{\partial t} = \frac{1}{r_l^2} \frac{\partial}{\partial r_l} (D_l r_l^2 \frac{\partial [M]_l}{\partial r_l}) - R_v \qquad (2.8)$$

$$\frac{\partial T_l}{\partial t} = \frac{1}{r_l^2} \frac{\partial}{\partial r_l} ((\frac{k_e}{\rho_p C_p}) r_l^2 \frac{\partial T_l}{\partial r_l}) - \frac{(-DH_p)}{r_{pol} Cp} R_v \qquad (2.9)$$

initial condition: @ $t=0$, $[M]_l=[M]_0$; $T_l=T_0$; $R_l=r_{cat}$

boundary conditions: @ $r_l=0$, $\frac{\partial [M]_l}{\partial r_l} = \frac{\partial T_l}{\partial r_l} = 0$

                        @ $r_l=R_l$, $D_l \frac{\partial [M]_l}{\partial r_l} = k_s ([M]_b - [M]_l)$

                                            $k_e \frac{\partial T_l}{\partial r_l} = h(T_b - T_l)$

microparticle ($r_{crys} < r_s < R_s$):

$$\frac{\partial [M]_s}{\partial t} = \frac{1}{r_s^2} \frac{\partial}{\partial r_s} (D_s r_s^2 \frac{\partial [M]_s}{\partial r_s}) \qquad (2.10)$$

$$\frac{\partial T_s}{\partial t} = \frac{1}{r_s^2} \frac{\partial}{\partial r_s} ((\frac{k_e}{\rho_{pol} C_p}) r_s^2 \frac{\partial T_s}{\partial r_s}) \qquad (2.11)$$

initial condition: @ $t=0$, $[M]_s=[M]_0$; $T_s=T_0$; $R_s=r_{crys}$
boundary conditions: @ $r_s=R_s$, $[M]_s=\eta^*[M]_l$; $T_s=T_l$

                        @ $r_s=r_{crys}$, $4\pi(r_{crys})^2 D_s \frac{\partial [M]_s}{\partial r_s} = \frac{4\pi}{3} (r_{crys})^3 R_p$

                                            $-4\pi(r_{crys})^2 k_e \frac{\partial T_s}{\partial r_s} = \frac{4\pi}{3}(r_{crys})^3 (-\Delta H_p) R_p$

30

where: subscripts l and s denote macroparticle and microparticle; $[M]_l$ and $[M]_s$ are monomer concentration in pores of macroparticle and in the microparticle, respectively; r_l and r_s are radial coordinate of macroparticle and microparticle, respectively; R_l and R_s are radius of macroparticle and microparticle, respectively; r_{crys} and r_{cat} are radius of catalyst primary crystallite and initial catalyst particle, respectively; D_l and D_s are effective diffusivity of monomer in macroparticle and microparticle, respectively; T_l and T_s are temperature in macroparticle and in microparticle, respectively; $[M]_0$ and $[M]_b$ are initial monomer concentration and monomer concentration in bulk fluid, respectively; T_0 and T_b are initial temperature of particle and temperature in bulk fluid, respectively; R_v is volumetric reaction rate in macroparticle; R_p is reaction rate at catalyst particle surface; ρ_p is polymer density; c_p is heat capacity of polymer; k_e is effective thermal conductivity in polymer particle; k_s and h are external film mass and heat transfer coefficient, respectively; ΔH_p is heat of polymerization; η^* is sorption factor of monomer in polymer.

Assuming the steady state is applied to the microparticle diffusion, simulation results of the multigrain model indicated that effects of mass and heat transfers on the polymerization were different for different levels of transport resistances (Floyd *et al.*, 1986a; 1986b). Under most reaction conditions, intraparticle temperature gradients should be negligible for both microparticles and macroparticles in gas-phase and slurry polymerization except for high activity catalyst particles of large size early in the life of the polymer particles during gas-phase operations. Intraparticle concentration gradients in microparticles could be significant for highly active catalyst systems having large primary crystallites of catalyst, especially in gas-phase polymerization, while concentration gradients

31

in macroparticles would normally be negligible except for high activity catalysts of large size in gas-phase polymerization especially early in the life time of polymer particles, but were expected to be significant in many slurry systems, even for relatively low activity catalysts. Mass transfer resistance appeared to be of more general significance in the pores of macroparticles than at microparticle level. As polymer particles grew, macroparticle diffusion resistance decreased while microparticle diffusion resistance increased slightly. The overall mass transfer resistance decreased because the surface area for mass transfer increased and the catalyst concentration decreased with time, which leads to a lower volumetric monomer consumption rate. This means that rate decay cannot be due to an increase in the resistance to monomer transfer as polymer particles grow.

The simulation results of Floyd *et al.* (1987) showed that macroparticle diffusion effects on polymerization rate profile would result in an acceleration-type profile, not a decay-type profile. It is possible that microparticle diffusion resistance can lead to decay type behavior for relatively large catalyst sizes and very high catalyst activities. For deactivating catalysts, the decay is offset by diffusions so that both the observed maximum activity and the time needed to reach the maximum activity would increase, and the rate would appear to decay slower than the actual decay kinetics in the presence of microparticle and macroparticle diffusion resistances. For nondeactivating catalysts in the presence of severe diffusion resistance, the reaction rate would be nonlinear with respect to monomer concentration, and the apparent activation energy would be lower than the true value, and a curvature in the Arrhenius plot would appear. However, it should be noted that catalyst deactivation can also lead to curvature in the Arrhenius plot. In addition, polymerizations at

32

a high temperature, or at a low monomer concentration, or with large catalyst particle sizes of high activity were likely to display characteristics of diffusion-controlled kinetics.

Molar masses and molar mass distribution of polymer produced are also affected by diffusion resistances during polymerization (Nagel *et al.*, 1980; Floyd *et al.*, 1987). The effects of diffusion limitations on polymer properties were less evident than the effect on the polymerization rate and observed activation energies. In the presence of diffusion limitations, polymer molar mass increases and its polydispersity (Q) decreases initially, then both values level off with reaction time. With increasing diffusion resistances, polymer molar mass decreases while Q increases. For polymerization kinetics with a single type of active site, the multigrain model can predict Q up to 7 for polyethylene, which is still lower than some experimental values which are as high as 30. However, when the multigrain model is combined with reaction kinetics having multiple types of active sites, it can predict polydispersities high enough to match those obtained experimentally (Floyd *et al.*, 1987).

In summary, none of the transport resistance models with single type of active site can predict the broad MMD of polyolefins (*i.e.*, large Q) produced by heterogeneous Ziegler-Natta catalysts. However, the well-known phenomenon of replication from catalyst particle to polymer granule agrees with the postulates of the multigrain model.

2.4 Kinetic Models of Ziegler-Natta Polymerization

A kinetic rate model is an attempt to describe the observed rate behavior. The time dependence of catalytic polymerization, *i.e.*, the rate profiles, are affected by many factors, such as types of catalyst, methods of preparing catalyst, and reaction conditions (*e.g.*, Keii,

33

1972). The rate profiles of Ziegler-Natta olefin polymerizations can be generalized by three types: acceleration type, decay type, and hybrid type (*e.g.*, Kissin, 1985). An acceleration type always shows a gradual increase of the polymerization rate until a stationary state is reached. The polymerization rate of a decay type goes directly from the maximum followed by a rate decay to a stationary state. The hybrid-type rate profiles show that the polymerization rate goes through an acceleration period up to a maximum followed by a rate decay to a stationary state.

2.4.1 Acceleration Period

The acceleration period observed experimentally has been explained by transport resistance, equilibrium reaction for formation of active sites, and polymerization reaction kinetics. There is no general criterion to determine which of these is more important.

The presence of mass transfer limitations has been proposed and modeled for Ziegler-Natta olefin polymerization. Most of the proposed models have been reviewed in more detail in Section 2.3. According to the multigrain model, a realistic model, Floyd *et al.* (1986b) attributed the acceleration period to the diffusion control during the polymerization. The multigrain model also predicted that intraparticle mass transfer effects might be significant at both macroparticle and microparticle level for slurry polymerizations, while, for gas phase polymerizations, mass transfer effects appeared more likely to be important in high activity catalyst systems for large primary crystallites in catalyst at the microparticle scale, and for large particle size at the macroparticle scale, especially early in the life time of the polymer particle.

34

Experimentally with ball milling MgCl$_2$/ethyl benzoate/TiCl$_4$+TEAL catalyst, Dusseault and Hsu (1993b) reported that the polymerization rate curve changed from straight decay to initial acceleration followed by the normal decay behavior when the Al/Ti ratio was greater than 130; this was attributed to the mass transfer diffusion by monomer sorption (macroparticle diffusion) in gas phase ethylene polymerizations.

Keii (1972) proposed that for the acceleration period in conventional Ziegler-Natta catalyst systems, polymerization centres were formed in two steps of reactions after the adsorption of alkylaluminum and monomer on the catalyst surface. The first step was the formation of an active site S^* from a surface site S and Al_2Et_6, and the second step was the formation of a polymerization center C^* (initiation) by an active site S^* and a monomer M. These two steps of reactions are shown in Equations 2.12 and 2.13.

$$S + Al_2Et_6 \xrightleftharpoons[k_{-1}]{k_1} S^*$$ (2.12)

$$S^* + M \xrightarrow{k_i} C^*$$ (2.13)

Assuming that the polymerization rate R_p is proportional to the concentration of monomer and polymerization centres C^*, the polymerization rate during the acceleration period in the hybrid type is given by:

$$R_p = k_p [M][S_0] \frac{K_1[A]}{1 + K_1[A]} (1 - e^{-k_i [M] t})$$ (2.14)

where: R_p is polymerization rate; k_p is propagation rate constant, which is independent of polymerization time; $[S_0]$ is the concentration of total surface sites available for active site formation; $[A]$ and $[M]$ are the concentration of alkylaluminum and monomer, respectively, and K_1 is the equilibrium constant for the formation of active site by Equation 2.12, and k_i is the rate constant of initiation in the second step; and t is the polymerization time.

35

With TiCl$_4$/Al/TIBAL catalyst system prepared by fixation of TiCl$_4$ on the surface of nonporous and annealed aluminum powder with an average particle size of 30 μm and a specific surface area of 0.4 m^2/g, Schnauß and Reichert (1990) assumed catalyst formation by an equilibrium reaction of alkylation and dealkylation of supported Ti species with alkylaluminum species without changing Ti valence state in order to model the kinetics of slurry ethylene polymerization. This equilibrium reaction is similar to first stage reaction of Equation 2.12 proposed by Keii (1972), and was reported to be responsible for the acceleration period in acceleration type and hybrid type of polymerization rate profiles.

Kissin (1985) pointed out that an initiation reaction, like Equation 2.13, can describe some acceleration rates, but Equation 2.13 alone cannot describe the characteristic S-shape of the rate curve frequently observed at low temperatures. Kissin suggested the existence of two consecutive reactions in the acceleration period: a reaction generating active centres without monomer participation (Equation 2.15) prior to an initiation Equation 2.13, *i.e.*:

$$PotentialCentres \xrightarrow{k_f} S*$$ (2.15)

$$S*+M \xrightarrow{k_i} C*$$ (2.13)

With the two-step initiation, the rate function becomes:

$$R_p = k_p[M][S]_0(1 - \frac{k_i[M]e^{-k_f t} - k_f e^{-k_i[M]t}}{k_i[M] - k_f})$$ (2.16)

where: *[S]*$_0$ is the total concentration of potential active centre, *k$_f$* is the rate constant of the formation of active centre, *k$_i$* is the rate constant of the initiation with the first

36

monomer. Kissin (1985) demonstrated that Equation 2.16 can describe the experimental results with S-shaped rate curves very well.

2.4.2 Rate Dependence on Concentration of Monomer and Alkylaluminum

In modeling polymerization kinetics, a power-law rate function is usually used as the first step to obtain the reaction order with respect to a specific reactant. Based on the results of power-law rate functions, possible kinetic models can be proposed to describe the kinetic behavior. The rate dependence on monomer concentration appears to be more complicated than that on alkylaluminum concentration, although alkylaluminum, used not only as cocatalyst but also as scavenger in the reaction system, could cause various reactions with active species $TiCl_4$ and electron donors due to the reducing ability of alkylaluminum.

2.4.2.1 Power-Law Model for Monomer Concentration

Most of the early literature reported that the overall rate of olefin polymerization R_p, as defined by a power-law rate function in Equation 2.17, was simply a zero order ($n=0$), first order ($n = 1$), or second order ($n = 2$) with respect to olefin monomer concentration.

$$R_p = k_{eff} [M]^n \tag{2.17}$$

where: k_{eff} is the effective rate constant, and n is the apparent reaction order.

For ethylene polymerization, the apparent order of rate law has been reported from zero to two ($n = 0 - 2$), while for propylene polymerization, the first order rate law was often reported, as well as second order rate law (e.g., Singh and Merrill, 1971; Kissin, 1989; Bu et al., 1995). By mathematical simulation using a simple mass transfer model, called the

37

uniform site concentration model, Singh and Merrill (1971) showed that the apparent reaction order with respect to ethylene concentration can be greater than unity even if the intrinsic rate was assumed to be first order. It should be noted that the first order rate function has been reported most often, and is widely used in modeling kinetics of catalytic olefin polymerization.

2.4.2.2 Adsorption Theory

In classical heterogeneous catalytic systems, adsorption has been shown to be an important process. Schindler (1963) applied adsorption theory to describe the kinetic behavior of slurry ethylene polymerization for $TiCl_4$/di-*iso*-butylaluminum hydride catalyst by Equation 2.18:

$$R_p = \frac{K[M]^2}{1 + K'[M]} \tag{2.18}$$

where: K and K' are constants. According to Equation 2.18, the rate is second order at low ethylene concentration, while the rate approaches first order at high ethylene concentration.

Keii (1972) and Keii *et al.* (1982) also applied the adsorption theory with competitive adsorption process between monomer and cocatalyst to describe kinetic behavior in the stationary period of ethylene and propylene homopolymerizations. Keii (1972) showed that Langmuir-Hinshelwood rate law, Equation 2.19, was applicable for the polymerization rate at a fixed time for a wide range of TEAL and propylene concentrations with both conventional and $MgCl_2$-supported catalysts.

$$R_p = k_p[M]\frac{K_A[A]}{(1 + K_A[A] + K_M[M])^2} \tag{2.19}$$

38

where: K_A and K_M are the equilibrium adsorption constants for monomer and cocatalyst (AlR_3), respectively. The value of the exponent of the denominator in Equation 2.19 could increase from 2 to higher value as time increases. Equation 2.19 can be simplified to Equation 2.20 under the condition of: $K_M[M] \ll K_A[A] < 1$,

$$R_p = k_p[M] \frac{K_A[A]}{(1 + K_A[A])^2}$$
(2.20)

The dependence of polymerization rate on the concentration of $Al(C_2H_5)_3$ was also found to follow Equation 2.20 for the ethylene polymerization with a rate profile of rapid decay over a high-activity $MgCl_2$-supported $TiCl_4$ catalyst (Marques, *et al.*, 1993).

A Rideal type rate law, as defined in Equation 2.21, was only valid for low concentration of TEAL with conventional Ziegler-Natta catalysts, under which condition it can be approximated by a Langmuir-Hinshelwood type of Equation 2.20 (Keii, 1972).

$$R_p = k_p[M] \frac{K_A[A]}{1 + K_A[A]}$$
(2.21)

The first order rate law, *i.e. n = 1* in Equation 2.17, could also be a special case of Equation 2.19, 2.20 or 2.21.

Burfield *et al.* (1972) presented a general kinetic scheme for Ziegler-Natta catalysis and proposed equilibriums due to the adsorption and desorption of monomer and cocatalyst by the Hinshelwood mechanism with a polymerization rate as Equation 2.22.

$$R_p = k_p[C^*] \frac{K_A[M]}{1 + K_A[A] + K_M[M]}$$
(2.22)

39

Chien and Bres (1986) found that the rate of polymerization for propylene and ethylene by the CW catalyst, a ball-milled $MgCl_2$-supported $TiCl_4$ catalyst, can be represented by Equation 2.23:

$$R_p = k_p [M] [C^*]$$ (2.23)

For higher α-olefins such as 1-decene, a Langmuir-Hinshelwood rate law, as defined by Equation 2.24, was necessary:

$$R_p = k_p [C^*] \frac{K_M [M]}{1 + K_M [M]}$$ (2.24)

In the kinetic study of gas-phase ethylene homopolymerization over SiO_2/$MgCl_2$-supported $TiCl_4$ catalysts with a tri-n-octylaluminum as cocatalyst, Bu *et al.* (1995) observed reaction orders with respect to ethylene from less than unity to about 1.5 depending strongly on the reaction temperature. A combination of at least two Langmuir-Hinshelwood rate functions, Equation 2.25, with different ethylene concentration dependencies was found to be the only explanation for the observed rate behavior.

$$R_p = \frac{A_1 e^{-E_1/RT} [M]^2}{1 + B_1 e^{Q_1/RT} [M]} + \frac{A_2 e^{-E_2/RT} [M]}{1 + B_2 e^{Q_2/RT} [M]}$$ (2.25)

The rate behavior also strongly suggested that at least two catalytic sites, having rates with different ethylene concentration dependencies, were present in these catalysts and the propagation rates for the sites had different concentration and temperature dependencies. Equation 2.25 can predict order of rate with respect of monomer concentration from 0 to 2. There is no deactivation part in Equation 2.25 since catalytic activity was fairly constant and no deactivation was observed during the polymerization runs.

2.4.2.3 Equilibrium Kinetic Models

Böhm (1978b) pointed out that rate constants for adsorption and desorption of monomer must be very high compared to propagation rate constant; hence, he formulated a comprehensive kinetic scheme including equilibrium state for complexation or adsorption for homogeneous and heterogeneous Ziegler-Natta polymerization processes under certain conditions. For heterogeneous catalytic processes, his model was a special case of Rideal mechanism. The rate of polymerization derived from his model can be used with either single site catalyst or multiple active sites of catalysts as shown in Equation 2.26:

$$R_p = [M] \sum_{i=1}^{k} \frac{k_{p,i} k_{a,i}}{k_{p,i} + k_{d,i} + k_{a,i} [M]} \frac{[C^*]_i}{1 + \frac{b_i}{a_i} + \frac{c_i}{a_i}} \qquad (2.26)$$

where: k_{ai} and k_{di} are adsorption and desorption rate constants for each active site i, respectively; k is the number of active site type; and value $1/[1+(b_i/a_i)+(c_i/a_i)]$ describes the extent of inhibition of the polymerization process by organoaluminum compound for each active site i. Although complicated with many parameters, Equation 2.26 with single active site type ($k=1$) was confirmed by kinetic study (Böhm, 1978c) and molar mass regulation (Böhm, 1978d) in slurry ethylene polymerization with $Mg(OC_2H_5)_2$-$TiCl_4$ catalyst.

Kissin (1989) observed that the empirical value of n in Equation 2.17 was 1.5 -1.7, and the effect of ethylene pressure on the polymerization rate was completely reversible in the kinetic study of gas phase ethylene homopolymerization at the temperature range of 80 - 90°C using a typical $TiCl_4$/$MgCl_2$-silica Ziegler-Natta catalyst system. On the basis of these observations, assuming that the polymer chain propagation rate followed Equation 2.23 except that C^* was also a function of ethylene concentration, he proposed a reversible

41

monomer activation process to convert potential polymerization centers C^*_p into active polymerization centers C^* in these catalysts as Equation 2.27:

$$C^*_p + M \underset{k_{-1}}{\overset{k_1}{\rightleftarrows}} C^*$$ (2.27)

Kissin (1989) obtained the following equation for the polymerization rate in the absence of hydrogen:

$$R^0_p = k_p [C^*]_0 \frac{K_1 [M]^2}{1 + K_1 [M]}$$ (2.28)

where: R_p^0 is the polymerization rate in the absence of hydrogen; $[C^*]_0$ is the concentration of total active sites ($[C^*]_0 = [C^*]_p + [C^*]$); and K_1 is the equilibrium constant in Equation 2.27 ($K_1 = k_1/k_{-1}$). Equation 2.28 was validated experimentally by the linear relationship between $[M]/R_p^0$ and $1/[M]$. Kissin (1989) pointed out that experimental evidence showed that ethylene polymerization rates were often lower than the polymerization rates of other olefins such as propylene, even though the intrinsic ethylene reactivity was 3 to 10 times higher than that of propylene from the studies of copolymerization reactions. Similarly, ethylene-olefin copolymerization reactions often proceeded at higher rates than ethylene homopolymerizations, although the higher olefins had much lower intrinsic reactivities and their addition to the polymerization medium should bring about rate reduction. Kissin (1989) attributed the above experimental observations to the slow reaction of Equation 2.27 and high value of k_p in Equation 2.23 in case of ethylene polymerization, rather than the adsorption theory and redox reactions of Ti atoms (potential active sites).

It is interesting to note that Equation 2.28, obtained from equilibrium reaction by Kissin (1989), has the same form as Equation 2.18 obtained from adsorption theory by

42

Schindler (1963). In addition, Equation 2.19 by Keii (1972), Equation 2.22 by Burfield *et al.* (1972), and Equation 2.24 by Chien and Bres (1986), also from adsorption theory, are special cases of Equation 2.26 obtained by Böhm (1978b), although Böhm emphasized that his mechanism was different and independent of adsorption theory. Equation 2.25 by Bu *et al.* (1995) is a combination of Equations 2.18 and 2.24 showing different dependencies of monomer concentration for different sites.

The fact that different mechanisms result in the same rate expression shows that kinetic data alone cannot be used to arrive at a reaction mechanism. The same opinion is expressed by Carberry (1976) when he wrote "no amount of statistical manipulation of kinetic data will yield a mechanism."

2.4.3 Rate Dependence on Hydrogen Concentration

Hydrogen is the principal chain transfer agent for molar mass control in heterogeneous Ziegler-Natta olefin homo- and copolymerization processes, but hydrogen does not change stereospecific properties of active sites (*e.g.*, Chien and Kuo, 1986; Rishina *et al.*, 1994). Hydrogen concentration can strongly affect the polymerization rate. For conventional Ziegler-Natta catalyst system of $TiCl_3/AlEt_3$ or $AlEt_2Cl$, decreases of the polymerization rate have been observed in the presence of hydrogen for both ethylene and propylene polymerization (*e.g.*, Keii, 1972). For $MgCl_2$-supported Ziegler-Natta catalyst systems, hydrogen generally reduces the rate of ethylene polymerization, but enhances the rate of propylene polymerization to a certain limit after which the hydrogen effect is less evident. Qualitative explanations for the hydrogen effect on propylene polymerization include: the revival of "dormant" centers resulting from 2-1 propylene insertion into the

43

polymer chain in the chain transfer reaction with hydrogen (Vizen *et al.*, 1994), and the

hydrogen inhibition of chain transfer by β-hydrogen elimination to some extent (Imaoka *et*

al., 1993). Quantitative models are reviewed in this section, which include slow reinitiation,

adsorption theory, and an equilibrium kinetic model.

2.4.3.1 Slow Reinitiation

Natta (1959) studied propylene polymerization in the presence of hydrogen with

TiCl$_3$/AlEt$_3$ catalysts, and found the stationary polymerization rate decreased upon the

addition of hydrogen. This hydrogen effect was explained as a rapid transfer reaction by

hydrogen (Equation 2.29), and then a slow chain reinitiation (Equation 2.30):

$$C*-(M)_x + H_2 \rightarrow C*-H + Polymer \tag{2.29}$$

$$C*-H + M \rightarrow C*-M \tag{2.30}$$

where: subscript *x* is the number of monomer units in a polymer chain. Equation 2.31 was

reported for the rate of propylene polymerization in the presence of hydrogen (Natta, 1959):

$$R_p^H = R_p - a[H_2]^{0.5} \tag{2.31}$$

where: R_p^H and R_p are the stationary rates in the presence and absence of hydrogen,

respectively, and *a* is a constant. However, rate enhancement of propylene polymerization

cannot be explained by Equation 2.31 with a positive value of *a* (Keii, 1986). In addition,

this explanation assumes that the ethylene insertion reaction into the transition metal-

hydrogen bond proceeds more slowly than the ethylene insertion reaction into the transition

metal-carbon bond. If this assumption is valid, a long polymer chain will not be attained by

the chain propagation in the presence of hydrogen.

44

2.4.3.2 Adsorption Theory

With conventional Ziegler-Natta catalyst system of $TiCl_3/AlEt_3$ or $AlEt_2Cl$, Keii (1972) assumed a pre-established equilibrium for the dissociative adsorption of hydrogen on the $TiCl_3$ catalyst surface in the slurry propylene polymerization, as shown in Equation 2.32:

$$H_2 \rightleftharpoons 2H_{ads} \qquad (2.32)$$

This type of dissociative adsorption results in a Langmuir type rate function of Equation 2.33:

$$R_p^H = \frac{R_p}{1 + b[H_2]^{n_H}} \qquad (2.33)$$

where: b is a constant. The n_H value of 0.5 could best describe the hydrogen effect on the stationary rate of polymerization which seemed to confirm the existence of dissociative adsorption of hydrogen by Equation 2.32. When summarizing the effect of hydrogen on the stationary rate of ethylene polymerization, Keii (1972) concluded that n value in Equation 2.33 was 0.88 with $AlEt_3$ and was 1.0 with $AlEt_2Cl$ as cocatalyst. However, in the gas phase polymerization of ethylene using silica supported Mg-Ti catalyst, Salajka *et al.* (1993) found that the value of n_H in Equation 2.33 was 0.5 without any cocatalyst.

In order to explain the complicated hydrogen effects on the polymerization rate, Keii (1986) proposed another model based on that hydrogen adsorbed dissociatively on two types of active sites and formed active hydrides C^*-H for the insertion of monomer and transfer of growing chain. The initiation reaction (*i.e.*, Equation 2.30) was rapid. The adsorption of hydrogen occurred not only on the site which was occupied by a monomer

45

molecule before its insertion into the growing chain, but also on the site produced after the chain transfer reaction with hydrogen as Equation 2.29. The final rate, given by Equation 2.34, could predict rate increase and decrease in the presence of hydrogen:

$$R_p^H = R_p \frac{1 + a_{HA}[H_2]}{(1 + a_{HA}b_A[H_2])^2}$$ (2.34)

where: a_{HA} is a parameter depending on adsorption of both hydrogen and cocatalyst on the active site, b_A is a parameter depending on the adsorption of cocatalyst only. Equation 2.34 predicts rate decreases and increases upon addition of hydrogen under conditions of $b_A \geq 0.5$ and $b_A < 0.5$, respectively. However, Equation 2.34 predicts a continuous change of rate with increasing hydrogen concentration.

In gas phase copolymerization of ethylene and 1-butene using silica supported $MgCl_2$-$TiCl_4$ catalyst, Huang *et al.* (1997) found that the rate dependence on hydrogen concentration can be best described by Equation 2.35, which is the combination of Equations 2.31 and 2.33:

$$R_p^H = \frac{0.596R_p}{1 + 0.082[H_2]^{0.5}} + 0.404(R_p - 44.3[H_2]^{0.5})$$ (2.35)

where: R_p^H and R_p are the average polymerization rate in the presence and absence of hydrogen, respectively. On the basis of TREF-SEC cross-fractionation, Huang *et al.* (1997) concluded that the hydrogen rate dependence given by Equation 2.35 is the result of responses to hydrogen by the different types of catalytic sites in their catalyst.

For a simple catalyst system of $TiCl_4$/$MgCl_2$/TEAL, Guastalla and Giannini (1983) reported that hydrogen reduced ethylene polymerization rate, but increased propylene polymerization rate asymptotically with increasing hydrogen partial pressure in 30 minutes

46

of runs. No further increase of rate was observed when hydrogen partial pressure was higher than 600 kPa. The hydrogen-activating phenomenon was attributed to the presence of hydrogen adsorbed on the surface of solid catalyst. At low temperature ($17°C$), hydrogen did not increase catalyst activity, but still strongly decreased molar mass of polymer produced. Therefore, the chain regulating ability of hydrogen was not related to its activating influence. No kinetic equation was given regarding the hydrogen effects observed.

In the propylene polymerization with a ball-milled CW catalyst, Chien and Kuo (1986) reported that hydrogen increased the yield of polymer at early stages of polymerization up to 6 minutes but decreased the yield toward the latter stage. The rate decay was faster than that without hydrogen. The yield during the initial stage did not increase further with higher hydrogen pressure. This saturation of hydrogen effect at high pressure was rationalized by the Langmuir-Hinshelwood mechanism shown in Equation 2.36:

$$R_p = k_p [C^*] [M] \frac{K[H_2]^{0.5}}{1 + K[H_2]^{0.5}}$$ (2.36)

It seems that Equation 2.36 cannot justify the propylene polymerization in the absence of hydrogen and the activating effect in the presence of hydrogen on the initial rate of propylene polymerization with same value of K.

2.4.3.3 Equilibrium Kinetic Model

In gas phase ethylene polymerization with typical $TiCl_4/MgCl_2$-silica Ziegler-Natta catalyst, Kissin (1989) reported that the rate decreased in the presence of hydrogen, and the action of hydrogen was reversible. However, progressively higher hydrogen pressures were

47

incapable of halting the polymerization reaction completely but reduced the reaction rate by half. According to the above observations, Kissin (1989) proposed that hydrogen deactivated the polymerization center (C^*) in a reversible manner as shown in Equation 2.37 after the reversible monomer activation process to convert potential polymerization centers C^*_p into active polymerization centers C^* in these catalysts as shown by Equation 2.27:

$$C^*_p + M \xrightleftharpoons[k_{-1}]{k_1} C^* \tag{2.27}$$

$$C^* + H_2 \xrightleftharpoons[k_{-2}]{k_2} C_H^* \tag{2.37}$$

When combining these two reactions, Equations 2.27 and 2.37, and the assumptions therein, Kissin (1989) obtained Equation 2.38 for the polymerization rate in the presence of hydrogen:

$$R_p^H = k_p [C^*]_0 \frac{K_1 [M]^2}{1 + K_1 [M] + K_1 K_2 [M][H_2]} \tag{2.38}$$

where: $[C^*]_0$ is concentration of total concentration of active sites ($[C^*]_0 = [C^*] + [C^*]_p + [C^*]_H$, where $[C^*]_H$ is the concentration of active centres temporarily deactivated by hydrogen); and K_2 is equilibrium constant for Equation 2.37 ($K_2 = k_2/k_{-2}$). The combination of the reciprocals of Equation 2.28 and 2.38 gives:

$$\frac{1}{R_p^H} - \frac{1}{R_p^0} = \frac{K_2 [H_2]}{k_p [C^*]_0 [M]} \tag{2.39}$$

Experimentally, the existence of a linear dependence between ($1/R_p^H - 1/R_p^0$) and $[H_2]/[M]$, shown in Equation 2.39, supported the postulated equilibrium deactivation of the polymerization centers with hydrogen shown in Equation 2.37. The reversibility of the

48

hydrogen effect on polymerization rate shown by Equation 2.37 also excluded the possibility that the redox reactions of Ti in the polymerization were involved.

2.4.4 Rate Dependence on Concentration of Active Sites

The rate dependence on concentration of active sites can be expressed by a power-law rate function if a first-order dependence on the monomer concentration is assumed:

$$R_{p,t} = k_p [M][C^*]_t^\gamma \tag{2.40}$$

where: k_p is the propagation rate constant, $[M]$ is the monomer concentration, $[C^*]_t$ is active site concentrations at time t, γ is the power-law order with respect to active site concentration.

The concentration of active sites cannot be easily obtained directly by physical methods because of very low content of active sites in the Ziegler-Natta catalyst systems. The concentration of active sites in the Ziegler-Natta catalyst systems has been determined by five methods: quenching method, radiolabelling method, inhibition method, kinetic method, and stopped-flow method. Different methods have been discussed by Tait (1979), Zlotnikov *et al.* (1988) and Shiono *et al.* (1993), which are not reviewed in detail here since they are not directly related to the current work.

Various studies have showed that the propagation rate constant (k_p in Equation 2.40) is essentially constant (*e.g.*, Tait, 1979; Doi *et al.*, 1982), and that polymerization rate was in direct proportion to the concentration of active site, *i.e.*, $\gamma = 1$ in Equation 2.40 (*e.g.*, in Equations 2.22 to 2.24, and 2.26). However, γ values other than unity have also been reported.

49

Keii *et al.* (1984) used the CO inhibition method to measure *[C*]* for the gas-phase propylene polymerization, and found that γ in Equation 2.40 was 1.5 for a $TiCl_3/Al(C_2H_5)_2Cl$ catalyst, for which the rate was free from any decay. Using the same CO inhibition method in the gas-phase propylene polymerization with catalyst $TiCl_4/MgCl_2/C_6H_5COOC_2H_5/Al(C_2H_5)_3$, Keii *et al.* (1984) obtained a γ value of 2, and Doi *et al.* (1982) reported that the decrease in concentration of active sites was second order with respect to *[C*]*, *i.e.*, the time dependence of C^* is given by:

$$\frac{1}{[C^*]_t} = \frac{1}{[C^*]_0} + k_{2d.c}t \tag{2.41}$$

where: $k_{2d.c}$ is rate constant for the second order deactivation of active sites; *[C*]_0* and *[C*]_t* are concentrations of active sites at time *0* and *t*, respectively.

With $MgCl_2$-supported $TiCl_4$ catalyst, Giannini (1981) applied radiolabelling of ^{14}CO that reacted with active sites in slurry propylene polymerization at 65°C during rate decay, and found that both polymerization rate and concentration of active sites decreased as polymerization proceeded; the polymerization rate was not linearly proportional to the concentration of active sites. From the experimental data reported by Giannini (1981), the value of γ is about 2.18 if the data of rate versus concentration of active sites are fitted with Equation 2.40, and the data of the active site concentration versus time was described very well by Equation 2.41; the values of r^2 were greater than 0.99 for both fits.

When studying the effect of different alkylaluminums on the kinetic parameters of the initial stage of propylene polymerization with $MgCl_2$-supported $TiCl_4$ catalyst by the stopped-flow method, Mori *et al.* (1997) found that total propagation rate constant (k_p in

Equation 2.40) was linearly proportional to the ratio of the concentration of isospecific active sites to that of the whole of active sites. Since about 90% of polypropylene produced is isospecific, this result implies that the dependence of polymerization rate on the concentration of the isospecific active sites is approximately the second order (*i.e.*, $\gamma \approx 2$ in Equation 2.40).

The result that γ value is equal to 2 is interesting because a combination of Equation 2.40 with Equation 2.41 gives a 1.5 order of the concentration of active sites on the rate of decay, which seems to contradict the common observations on the order of rate decay (see Section 2.5.4 below). As pointed out by Mori *et al.* (1997) and others (*e.g.*, Buzina *et al.*, 1988; Chien *et al.*, 1989; Marques *et al.*, 1998), the reliability of different methods for active site determination is still questionable; thus, it is not surprising that results may differ for different methods of measuring *[C*]*. Although the values of γ have been observed from 1 to 2, almost all of the kinetic models have assumed $\gamma = 1$ in Equation 2.40.

2.5 Rate Decay of Ziegler-Natta Polymerization

The kinetic behavior of ethylene and/or α-olefin polymerization by heterogeneous Ziegler-Natta catalysts, especially advanced supported catalysts, generally shows a very high initial activity followed by a decrease in rate. The order of rate decay kinetics in power-law rate functions has been reported from unity to two, or changes with polymerization time. The origins of polymerization rate decay is largely unknown and is complicated by the existence of multiple catalytic sites. Four different mechanism have been proposed (Chien *et al.*, 1989) to explain the rate decay: 1) a decrease of active sites

51

or chain propagation rate constant due to structural changes in the catalysts; 2) a decrease in the number of active centers by dissolution; 3) mass transfer limitations; 4) chemical deactivation of catalytic active sites. Unfortunately, none of these theories can explain the observed decay rates completely.

2.5.1 Structural Change

By studying slurry polymerization of propylene with a ground α-$TiCl_3$ catalyst, Natta and Pasquon (1959) suggested that catalyst particle size was changed to a common size appropriate for the particular polymerization conditions. The mechanical action of polymer chain formed on the catalyst surfaces caused cleavage and agglomeration of catalyst particles which gave rise to the high initial activity and the following activity decay. Kissin (1969) proposed that metal-carbon bond, which was the weakest chemical bond in a polymer chain, could be broken down by mechanical forces as polyolefin chains grew and crystallized with $TiCl_3$-$Al(C_2H_5)_3$ catalyst. Unfortunately, as pointed out by the author, it is hard to verify his mechanism experimentally because the mechanical termination is kinetically indistinguishable from chain transfer to monomer.

However, there was no appreciable loss of total metal-polymer bond during the period of rapid decay of polymerization rate (Chien *et al.*, 1989), and the mean chain propagation rate constant k_p remained almost constant during polymerization for either conventional or supported Ziegler-Natta catalysts (Keii *et al.*, 1982; Doi *et al.*, 1982; Chien *et al.*, 1989, Rishina *et al.*, 1994). This seems to indicate that the breaking of metal-carbon bonds is not a cause of catalyst deactivation.

52

2.5.2 Dissolution of Active sites

Chien *et al.* (1989) analyzed the amount of solubilized Ti during aging and during slurry propylene polymerization with ball-milling $MgCl_2$-supported Ziegler-Natta catalyst (CW catalyst), and found that maximum amount of Ti species solubilized was about 10% with little variation in 65 minutes of experiments. This was quite small compared to that of deactivation because the CW catalyst was characterized by 3-5 fold rate decays in the course of a batch polymerization (Chien and Hu, 1989). The dissolution mechanism is not applicable to gas-phase operations which also experience significant catalyst deactivation.

2.5.3 Mass Transfer Limitations

The rate decay was first linked to the monomer diffusion toward the surface of the catalyst particle caused by the progressive encapsulation of the polymer formed on the $TiCl_3$-$Al(C_2H_5)_3$ catalyst system (Pasquon *et al.*, 1959). Chien (1979) proposed four criteria to judge if Ziegler-Natta polymerization was diffusion controlled and concluded that olefin polymerizations were not diffusion limited for conventional Ziegler-Natta catalyst systems. Keii (1972) also stated that mass transfer of monomer from gas to liquid phase and from liquid to polymer phase can be eliminated or at least minimized by varying reaction conditions, *e.g.*, stirring speed.

For $MgCl_2$-supported Ziegler-Natta catalysts, experimental results of propylene polymerization demonstrated that the yield was independent of the catalyst concentration in slurry phase (Galli *et al.*, 1981), and the deactivation was independent of catalyst aging and the polymer formed in both slurry (Galli *et al.*, 1981; Keii *et al.*, 1982; Chien *et al.*,

1989) and gas phase (Doi *et al.*, 1982). Chien *et al.* (1989) showed there was a comparable rate decay for slurry propylene and decene homopolymerization with CW catalyst even though polypropylene was insoluble but polydecene was soluble at reaction conditions. McKenna *et al.* (1996) varied reaction conditions and found no evidence of mass transfer resistance when catalyst activity was increased from 9,000 to 40,000 g of polymer per g of catalyst per h in slurry ethylene homo- and copolymerization using $MgCl_2$-supported $TiCl_4$ catalyst. From simulation results of the multigrain model, Floyd *et al.* (1986b) found that rate decay would be offset by diffusions so that rate would appear to decay slower than the actual decay kinetics in the presence of mass transfer resistances.

2.5.4 Chemical Deactivation

Overall rate decay of polymerization due to the chemical deactivation of catalytic sites has been studied by various methods or analysis. Based on experimental observations, the deactivation of the catalytic sites has been related to the change of Ti oxidation state due to the presence of alkyl aluminum as a cocatalyst in the polymerization system. Without the change of Ti valence state, the deactivation has also been reported with the involvement of both monomer and hydrogen assistances.

Since the real chemical nature of catalyst deactivation is not known and the concentration of catalytic sites cannot be measured accurately during Ziegler-Natta polymerization (see Section 2.4.4), the deactivation of catalytic sites is usually studied by fitting the rate decay profiles by the power-law rate functions. This implies that rate of polymerization $R_{p,t}$ is directly proportional to the concentration of active sites in the

54

catalyst system, as shown in Equation 2.42 (*i.e.*, $\gamma = 1$ in Equation 2.40). [Equation 2.42 was implicitly applied for Equations 2.43 and 2.45 in the following analysis.]

$$R_{p,t} \propto [C^*]_t \qquad (2.42)$$

The results of the fitting have shown that the deactivation process can be reasonably described well by a first order reaction with respect to the concentration of catalytic site, as well as a second order or a mixed first and second order reactions depending on the catalyst used (Kissin, 1985). No general agreement has been reached in the literature on the deactivation order of the catalytic sites.

2.5.4.1 First Order

Keii (1972) suggested that there were two types of polymerization sites present for slurry propylene polymerization with ground $TiCl_3/Al(C_2H_5)_3$ catalyst system. One of them was deactivated mainly by the attack of Cl^- from an adjacent lattice point or from the bulk of $TiCl_3$ to a surface defect, and to some extent by monomers or by polymer formation while another type was responsible for the observed stationary reaction rate. Equation 2.43 was claimed to agree with kinetic curve in the decay portion with respect to rate itself for propylene polymerization, which indicated a first-order rate decay:

$$\frac{R_{p,t} - R_\infty}{R_0 - R_\infty} = e^{-k_{1d,r}t} \qquad (2.43)$$

where: R_0 is the initial overall polymerization rate; $R_{p,t}$ is the overall polymerization rate as a function of time, t; R_∞ is the stationary rate when $t \rightarrow \infty$ ($R_\infty = 0$ is the special case); and $k_{1d,r}$ is the first order deactivation constant. Equation 2.43 was also applicable for ethylene polymerization. Since polypropylene can be separated into two parts, *i.e.*, soluble

and insoluble polypropylene in boiling heptane by extraction, the relation of reciprocal isotactic index (*I.I.*) with $R_{p,t}$, according to Equation 2.44, had a linear positive slope from experiments, which seems to have justified his assumption of two types of active sites.

$$I.I. = I_S + \frac{(I_A - I_S)R_\infty}{R_{p,t}}$$ (2.44)

where: *I.I.* is the isotactic index defined as weight percentage of insoluble polypropylene in boiling heptane, I_S and I_A are *I.I.* values of polypropylene produced by stereospecific (unstable) and nonstereospecific (stable) sites, respectively. It is interesting to note that the positive slope indicates that nonstereospecific sites produce more stereospecific polypropylene.

Similarly, the same two types of active centers were supported by Galli *et al.* (1981) for MgCl$_2$ supported TiCl$_4$ catalysts in slurry propylene polymerization under industrial conditions, in which the stereospecific sites deactivated by first-order kinetics and the nonstereospecific sites (or slightly stereospecific) were stable; Equation 2.43 describes this behavior. For MgCl$_2$ supported TiCl$_4$ catalysts, the slope of a *I.I.* versus $1/R_{p,t}$ plot was negative; this indicates that I_S for stable sites is larger than I_A for unstable sites for these catalysts.

When ethylene was polymerized over a high-activity MgCl$_2$-supported TiCl$_4$ catalyst activated by Al(C$_2$H$_5$)$_3$, Marques *et al.* (1993) found that the polymerization rate decreased rapidly with time, and the decay order was represented better by first order than by second order kinetics.

56

2.5.4.2 Second Order and Mixed Orders

Rate decay by other than first order kinetics has also been widely reported. For propylene polymerization in slurry (Keii *et al.*, 1982) and gas phase (Doi *et al.*, 1982) with ball-milled $MgCl_2$-supported $TiCl_4/C_6H_5COOC_2H_5$ catalysts, it was shown that for the temperature range of 1 - 65°C, the rate curves under most of the polymerization conditions could be approximately represented by a second order decay:

$$\frac{1}{R_{p,t}} = \frac{1}{R_0} + k_{2d,r}t \tag{2.45}$$

where: $k_{2d,r}$ is second order rate decay constant. For slurry polymerization under the conditions of monomer concentration of 0.22-0.48 mol/L and triethylaluminum (TEAL) concentration of 1-100 mmol/L, Keii *et al.* (1982) found that a third order decay was initially applicable before 10 minutes, then a second order decay from 0.5 to 3 hours, and finally a first order decay after 3 hours. But the second order decay was not applicable for polymerization at temperature less than 23°C. The second order deactivation during both gas and slurry polymerization was explained by a mechanism that the disproportionation of two alkylated surface active sites (Ti^{3+} species) adsorbed strongly by TEAL results in the reduction of Ti^{3+} to Ti^{2+}. Keii *et al.* (1982) also applied two Langmuir-Hinshelwood rate equations for the average reaction rates for the boiling heptane soluble and insoluble fraction of polypropylene. The results showed that the reaction rate for the heptane insoluble fraction decreased and rate for soluble fraction remain approximate constant.

When studying the effect of hydrogen in slurry propylene polymerization with $MgCl_2$-supported Ziegler-Natta catalyst, Rishina *et al.* (1994) found that at low and

57

moderate concentration of hydrogen ($[H_2]$ < 0.044 mol/L), the termination of active centres followed the bimolecular deactivation law, *i.e.*, second order rate decay up to 60 minutes at propylene concentration of 1.0 mol/L and for only 30-40 minutes at propylene concentration of 0.4 mol/L. At other conditions, the rate decay deviated from second order. Brockmeier and Rogan (1985) analyzed the kinetic data of slurry and bulk polymerization of propylene over $MgCl_2$ supported $TiCl_4$ catalysts mostly from Montedison Laboratories, and found that the first order deactivation model provided the most accurate correlation at reaction time up to 2 hours, and the second order deactivation model provided an accurate correlation from 0.5 to 15 hours while the 1.5 order deactivation model provided an accurate correlation from 2 to 15 hours. Brockmeier and Rogan did not give any explanations for their observation.

Chien and Hu (1987) attributed the activity decay to the simultaneous deactivation of two adjacent catalytic sites in the support surface so that deactivation kinetics were often apparently second order for slurry propylene polymerization with CW catalysts. Sometimes the decay kinetics deviated from second order as polymerization proceeds because there were isolated catalytic sites which deactivated according to first order kinetics. These isolated catalytic sites could be produced either initially or as a result of deactivation of neighboring sites.

Based on calorimetric data in $MgCl_2$-supported $TiCl_4$ catalysts prepared by different methods, Vermel' *et al.* (1980) and Zakharov *et al.* (1986) pointed out the nonuniformity of surface adsorption sites and titanium complexes that were formed on the surface, and found a strong interaction of $TiCl_4$ with $MgCl_2$ so that reaction between

58

two active sites, which will result in second order rate decay, was unlikely. Busico *et al.* (1986) presented structural models of Ti^{3+}-containing catalytic sites on the lateral faces of $MgCl_2$ crystals that the reduction of Ti^{3+} species to Ti^{2+} by trialkylaluminum would imply clustering, which agreed with the observed kinetics of second order deactivation of active sites. To be consistent with second order deactivation, Chien *et al.* (1989) also proposed reactions between two adjacent active Ti-polymer bonds to form nonactive cyclic compounds. These reactions could happen with or without the participation of monomer and hydrogen while Ti valence can remain unchanged.

2.5.4.3 Effect of Alkylaluminums - Origin of Deactivation?

Trialkylaluminums (AlR_3) play an important role in the deactivation, in addition to other roles as a scavenger and cocatalyst in the olefin polymerization process. Among the most commonly used AlR_3 is TEAL, a very aggressive reducing agent. It was reported that overreduction of Ti^{3+} species to Ti^{2+} by AlR_3 was responsible for the decay of propylene polymerization rate (Keii *et al.*, 1982; Doi *et al.*, 1982; Kashiwa *et al.*, 1984) because Ti^{3+} species were active for both ethylene and propylene while Ti^{2+} species were active only for ethylene polymerization (Soga *et al.*, 1982; Busico *et al.* 1985, Chien *et al.*, 1989). However, Soga *et al.* (1982) also found that very little Ti^{3+} was reduced in the presence of TEAL during propylene polymerization for a SiO_2-supported $MgCl_2/TiCl_3$ catalyst. While studying the change of Ti valence states in either aging or homopolymerization of propylene and decene with CW catalyst, Chien *et al.* (1989) showed that the distribution of different valence states of Ti by reduction depended on the type of cocatalysts used, and there was no change of Ti^{3+} concentration from 1.5 to 65

minutes. Busico *et al.* (1986) copolymerized ethylene and propylene using ball-milled MgCl$_2$-supported TiCl$_4$ catalyst and argued that if rate decay was caused by overreduction of Ti^{3+} to Ti^{2+}, the product of reactivity ratios, r_1r_2 (subscript 1: ethylene, subscript 2: propylene), would decrease to zero since the propagation rate constant, k_{22}, decreased tending to zero with polymerization time. However, they found that r_1r_2 was substantially independent of polymerization time. Therefore, it seems that rate decay cannot be explained solely by overreduction of Ti^{3+} to Ti^{2+} during polymerization.

The molar ratio of Al to Ti (Al/Ti ratio) in Ziegler-Natta catalyst systems is also an important factor in the deactivation process of olefin polymerization. Murachev *et al.* (1989), using electron spin resonance (ESR) to study the Al/Ti ratio effect on the activity of butadiene polymerization on the catalytic TiI$_2$Cl$_2$- tri-*iso*-butylaluminum (TIBAL) system, found that the concentration of active centres (ESR observable Ti^{3+}) remained virtually unchanged at a low Al/Ti ratio, while the concentration of the active centres dropped rapidly at higher Al/Ti ratios. The rapid drop in the concentration of the active centres was postulated to be responsible for the rapid deactivation which was related to the overreduction of Ti^{3+} to Ti^{2+} at high Al/Ti ratios. They also observed that at the very start of the polymerization the concentration of the active centres depended only weakly on the Al/Ti ratio although the initial rate of polymerization dropped markedly with increasing Al/Ti ratio. Therefore, they proposed that the drop in the initial rate was due to the reversible competitive adsorption of TIBAL at the active centre which may proceed the further overreduction.

60

The effect of Al/Ti ratio on the deactivation process was also examined in olefin polymerization. Chien and Kuo (1986) and Chien and Bres (1986) found that first order deactivation was applicable at low Al/Ti ratio and second order at high Al/Ti ratios for propylene homopolymerization and ethylene homopolymerization in the slurry phase. Dumas and Hsu (1989) proposed, then Dusseault and Hsu (1993) generalized, a multisite kinetic model to describe the deactivation kinetics of slurry propylene and gas-phase ethylene polymerizations using ball milling $MgCl_2$/ethyl benzoate/$TiCl_4$+TEAL catalyst on the basis of gamma distribution of multiple active sites. Their proposed rate expression including deactivation is:

$$R_p = \theta_1 [M] f(\theta_2, p) \tag{2.46}$$

where: θ_1 is the initial activity of the catalyst; $f(\theta_2, p)$ is the functional form of the rate equation determined by the nature of the deactivation kinetics from the deactivation profile function (DPF), $F(x)$, of experimental polymerization kinetics; θ_2 is the weighted average of the reciprocal of the deactivation half-life, a common deactivation parameter; and p is a set of uncommon parameters. Finally, by substituting the gamma distribution of multiple active sites into $F(x)$, Equation 2.47 can be derived from Equation 2.46:

$$R_p = \frac{\theta_1 [M]}{(1 + \theta_2 \theta_3 t)^{1/\theta_3}} \tag{2.47}$$

where: $\theta_3 = 1 + (\eta + 1)/\alpha$ in which $1/\alpha \cong Var(k_p^2)/E(k_p^2)^2$, and η describes the extent of the relationship between active site species and the ratio of deactivation and propagation rate constants. By fitting Equation 2.47 to their kinetic data, Dusseault and Hsu (1993) found that at least two types of first order deactivation processes, one fast and one slow, seemed to occur at low Al/Ti ratio. As the Al/Ti ratio increased, a gradual transition from first

61

order to second order deactivation was observed. At high Al/Ti ratio, deactivation was predominantly second order with what seemed to be underlying slow first order deactivation. Their explanation was that at lower Al/Ti ratios the first order deactivation seemed to indicate that only partial activation of Ti resulted in mostly isolated active sites; while at higher Al/Ti ratios, more Ti atoms were activated with more adjacent sites, which were responsible for the second order deactivation. Note in Equation 2.47, θ_1, θ_2 and θ_3 are all independent of monomer concentration and polymerization time, t. Therefore, Equation 2.49 is essentially a first-order rate function with respect to monomer, but the coefficient is rather complicated in order to model deactivation kinetics.

Alkylaluminums activate Ti species as an alkylating agent (*e.g.*, Buzina *et al.*, 1988; Murachev *et al.*, 1989). The disproportionation of two alkylated surface active sites (Ti^{3+} species) with strongly adsorbed TEAL was also proposed to result in the reduction of Ti^{3+} to Ti^{2+} and this was proposed as the cause for the second-order rate decay in propylene polymerization (Keii *et al.*, 1982; Doi *et al.*, 1982).

Based on the alkylating ability of alkylaluminums, Schnauß and Reichert (1990) proposed a kinetic model of slurry ethylene polymerization, and assumed catalytic site formation and deactivation by two reaction schemes using $TiCl_4$/Al/TIBAL catalyst system prepared by fixation of $TiCl_4$ on the surface of nonporous and annealed aluminum powder with an average particle size of 30 μm and a specific surface area of 0.4 m^2/g. The first reaction was an equilibrium reaction of alkylation and dealkylation of supported Ti species with alkylaluminum species without changing the valence state of Ti, and the second reaction was reduction of vicinal active Ti species to a lower valence state by

62

dealkylation. Polymerization rate profiles with acceleration type and build-up period in the decay type can be explained by the first reaction, while the second reaction can be responsible for decay period in the decay type profile. The equilibrium in the first reaction in connection with a second-order deactivation can lead to a dependence of polymerization on the alkylaluminum concentration described by Rideal or Langmuir-Hinshelwood rate laws. Alkylated Ti species in the oxidation states of IV, III and II are all active for ethylene polymerization with different propagation rate constants.

2.5.5 Heterogeneity of Catalytic Sites

The above review showed that the order of rate decay kinetics can change during a reaction run. This seem to imply the existence of multiple active sites in the Ziegler-Natta catalyst systems. Pino *et al.* (1985) hypothesized the existence of two types of stereospecific catalytic centres in addition to nonstereospecific one. They reported that the catalytic centres disappeared according to a pseudo second-order rate law and deactivation had a half-order dependence on TIBAL concentration for propylene polymerization with a catalyst prepared by ball-milled $MgCl_2/TiCl_4$/Lewis base in the presence of a large excess of TIBAL. They found that two types of stereospecific catalytic centres were insufficient, and proposed that at least three type of stereospecific catalytic centres are present. While studying the role of internal and external donors systematically in propylene polymerization with ball-milled $MgCl_2$-supported $TiCl_4$ catalyst systems, Busico *et al.* (1985) found that the decrease of the overall polymerization rate following the addition of the external donor to the cocatalyst was mainly due to the deactivation of

63

the non-stereospecific sites and suggested that there are more than one type of non-stereospecific centres differing in Lewis acidity.

Based on electron paramagnetic resonance (EPR) studies of Ti oxidation state, Chien and Kuo (1986) grouped titanium ions into two classes. One of them was situated adjacent to one or more Ti ions; its deactivation could occur involving two or more Ti ions, *i.e.*, deactivation is the second or higher order. Another had either inactive Ti ions or none adjacent to Ti ion, and deactivation was the first order. The two classes of Ti ions were indistinguishable because the kinetic order was obtained from the change in rate $R_{p,t}$, but not on the actual concentration of Ti ions.

Due to different catalyst preparations and reaction conditions in the Ziegler-Natta polymerization of olefins, complicated behavior of the decay rate kinetics and the possible existence of multiple active sites have been observed. Since multiple catalytic sites have not been distinguished in the catalyst preparations, most of the studies in catalyst deactivation were based on the overall polymerization rate. Simple first-order or second-order deactivation kinetics may not be able to well describe the deactivation of multiple catalytic sites with different characteristics such as stability, chain propagation (reactivity) and termination rates, copolymerization abilities and stereospecificities. Hence, work remains to be done to understand the processes involved in deactivation of Ziegler-Natta catalysts.

3. Experimental Methods

Experimental work in this study consisted of preparations of morphology-controlled Ziegler-Natta catalysts, polymerization of ethylene, and characterization of catalysts and polyethylenes. Catalyst preparation included construction of equipment and development of preparation procedures. The catalyst prepared had to be active for polymerizing ethylene, and its morphology must be replicated into the morphology of polyethylene. In order to achieve this desired replication, two stages of ethylene polymerization were carried out, *i.e.*, prepolymerization and polymerization. Prepolymerization is a term used to describe ethylene polymerization under mild conditions with a fresh $MgCl_2$-supported $TiCl_4$ catalyst and the polymer produced in the prepolymerization stage, which contains the active catalyst, is referred to as prepolymer. In the polymerization stage, prepolymer is used as catalyst for further polymerization to produce polymer. Polyethylenes produced in both prepolymerization and polymerization stages were characterized by size exclusion chromatography to measure their molar masses. The morphologies of catalyst and polyethylenes were examined by scanning electron microscopy.

3.1 Materials

Anhydrous magnesium chloride (98%), ethyl alcohol (anhydrous, denatured with methyl alcohol), anhydrous heptane (99%), anhydrous hexanes, titanium tetrachloride (99.9%), and neat triethylaluminum (93%) were obtained from Aldrich and used without further purification. Vaseline and dibutyl phthalate (>98%) were obtained from Fluka and

used without further purification. Sodium chloride (NaCl) with an average particle size of about 0.5 mm and 1,2,4-trichlorobenzene (HPLC-grade) were obtained from Fisher Scientific. Rulon LR sheet was made by Furon Company. Polymer-grade ethylene was obtained from Matheson. Prepurified nitrogen and ultrahigh-purity hydrogen were obtained from Praxair. Ethylene, nitrogen, and hydrogen were each passed through a series of Alltech high-pressure gas purifiers containing BASF R3-11 catalyst, Ascarite, and 3A molecular sieves for the removal of oxygen, carbon dioxide, and moisture, respectively. Complete details of the feed purification, monitoring, and control equipment were previously described by Lynch and Wanke (1991).

Polystyrene, linear paraffins and polyethylene were used for calibration of SEC. TSK standard polystyrene samples of known molar masses ranging from 870 to 8,420,000 were obtained from Tosoh Corporation and Toyo Soda Manufacturing Co., Ltd. Linear paraffins $C_{20}H_{42}$, $C_{40}H_{82}$, and $C_{60}H_{122}$ were obtained from Fluka. Polyethylene standard reference materials 1475, 1482, 1483, and 1484 were obtained from National Institute of Standards and Technology (NIST).

3.2 Preparation of Morphology-Controlled MgCl$_2$-Supported TiCl$_4$ Catalysts

In Section 2.2, the many methods, which can be used to make catalyst supports for morphology-controlled catalyst, were reviewed. Much of the reviewed literature is in the patent literature, and information provided in patents is usually vague with insufficient details to reproduce claims and results. This may cause, in part, that "scientific knowledge has lagged behind the huge amount of technological developments in the field of Ziegler-Natta polymerizations" (Keii, 1972). Catalyst preparation method reported in

66

this thesis should assist in narrowing the gaps between scientific knowledge and technological know-how in the area of morphology-controlled Ziegler-Natta catalysts.

Two methods were examined for preparing spherical $MgCl_2$ supports: one, chemical reaction precipitation of $MgCl_2$ and two, melt quenching of a $MgCl_2$-ethanol complex. Both methods have been used widely in industry. Detailed work on chemical reaction precipitation, which can only produce a limited size range of catalyst (Butts, 1999), is provided in Appendix A. The method of melt quenching of $MgCl_2$-ethanol complexes was employed in the current study to prepare catalyst for subsequent activity studies. The quenching method is similar to that described by Ferraris *et al.* (1983). No information on this preparation technique was found in the open literature; hence, detailed descriptions of experimental equipment and preparation procedures are presented.

3.2.1 Experimental Equipment for Support Preparation

A schematic diagram of the equipment used for preparation of spherical $MgCl_2$ particles is shown in Figure 3.1. The system was designed and constructed by the author at the beginning of this study. The apparatus consists of three parts: mixing vessel, transfer tubing and cooling vessel.

The mixing vessel (Laboratory autoclave BEP 280, 9202e, Type I, from Büchi) was a one-litre, jacketed Pyrex vessel equipped with a variable-speed, magnetically driven stirrer. The magnetic drive was mounted on the cover flange by means of a thread and a seal. The cover flange was bolted to the Pyrex vessel and sealed with a Viton O- ring. The emulsion, in which droplets of $MgCl_2$-ethanol complex were dispersed in the

67
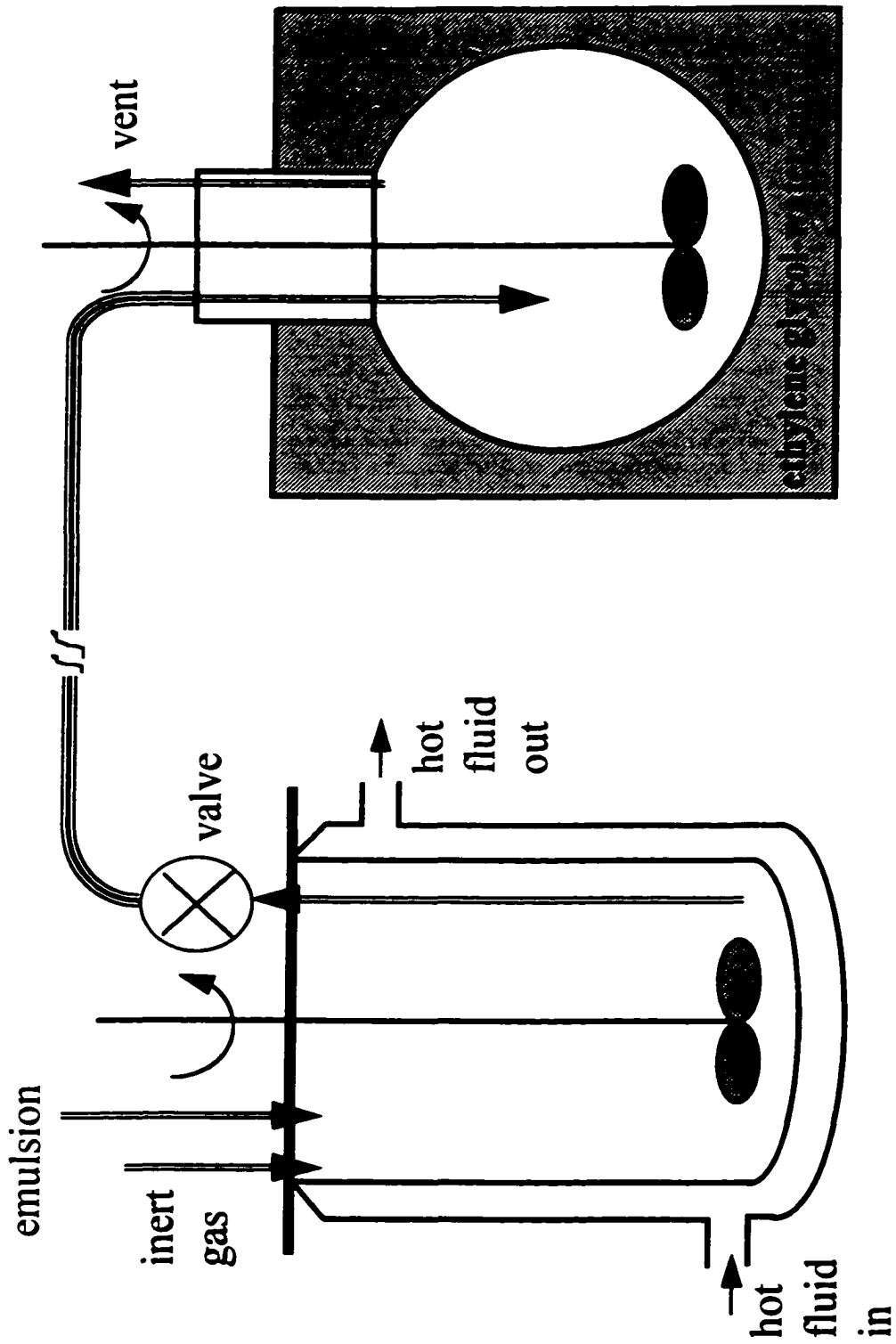
Figure 3.1 Schematic diagram of equipment for melt quenching.

68

continuous Vaseline phase, was prepared in the mixing vessel. Vaseline was chosen as the continuous phase because it is immiscible with the $MgCl_2$-ethanol complex and has a higher viscosity than other inert organic materials such as heptane and octane. The Pyrex vessel was cylindrical in shape with a round bottom. The inside diameter of the Pyrex vessel was about 82 mm and its depth is about 185 mm. The maximum operating pressure of the Pyrex vessel was 12 bar, and its maximum operating temperature was 200°C. The temperature in the glass vessel, measured by a sheathed thermocouple (Type J), was adjusted by circulating oil (50 cSt of Dow Corning 200 Fluid®, from Dow Chemical Corporation) from a high temperature bath (EX-251HT, from Neslab) through the heating jacket on the Pyrex vessel.

At the center of the Pyrex vessel, a Rushton turbine impeller with six blades was employed for mechanical agitation of the emulsion. Mechanical agitation was used to generate and maintain a droplet dispersion of the dispersed phase in the continuous phase. After stirring at 1000 rpm for 2 hours, a dynamic equilibrium was established between breakup and coalescence of droplets of the dispersed phase. The droplets of the dispersed phase are spherical because they tend to contract into as little volume as possible (Davies and Rideal, 1961). The Rushton turbine impeller was selected because this type of impeller transforms more of the input energy into turbulent kinetic energy and produce narrower droplet size distributions than other types of impellers (Zhou, 1997). The impeller was in its standard configuration. The diameter of the impeller was about one-third of the diameter of the Pyrex vessel. The blade width and length of the impeller are one-fifth and a quarter of its diameter, respectively. The impeller was placed where the distance between the bottom of

69

the Pyrex vessel and the centre line of the impeller blades is approximately equal to the diameter of the impeller.

The Pyrex vessel was connected to a vacuum pump (RV5, from Edwards) and a nitrogen cylinder (Prepurified, from Praxair). The vacuum pump was used to evacuate the Pyrex vessel before any chemicals were introduced into the glass vessel. The nitrogen cylinder was used to adjust the pressure in the Pyrex vessel; the pressure due to the nitrogen was used to force the high-temperature emulsion out of the mixing vessel.

The emulsion from the Pyrex vessel flowed into a cooling vessel through a transfer tubing. The transfer tubing was made of Teflon (from Chromatographic Specialties Inc.) with an inside diameter of 1.57 mm and a length of 3 m. The transfer tubing outside of the Pyrex vessel was located inside a stainless steel tubing with an inside diameter of 10.5 mm, and high temperature oil form the circulating bath (EX-251HT, from Neslab) was passed through the annular region of this double-pipe heat exchanger. The large ratio of length to diameter of the transfer tubing was used to keep the emulsion transferred under fully-developed turbulent flow. This narrows the droplet size distribution and prevents the coalescence of the droplets during the transfer process.

The outlet of the transfer tubing was dipped into a cooling medium inside the cooling vessel. Heptane was used as a cooling medium since heptane is inert to the $MgCl_2$-ethanol complex and the freezing point of heptane is low (-90.5°C). The cooling vessel was a 3-litre glass flask equipped with a stirrer and filled with 1 litre of heptane. The 3-litre flask was immersed in a bath containing a 50-50 mixture of ethylene glycol and water. The ethylene glycol-water mixture was precooled by adding liquid nitrogen into it in order to

70

cool heptane inside the flask down to a low temperature. The spherical droplets of $MgCl_2$-ethanol complex in the high-temperature emulsion was solidified rapidly when they entered the heptane from the Teflon transfer tubing.

3.2.2 Catalyst Preparation Procedure

The overall preparation procedure consisted of two main steps. The first step was to prepare spherical $MgCl_2$-ethanol complex by melt quenching, and the second step consisted of treating the $MgCl_2$ support with $TiCl_4$ and an electron donor to obtain a very active, spherical catalyst.

The specific steps of melt quenching consisted of charging 220 g of Vaseline, 20 g of $MgCl_2$ and 40 mL of ethanol into the one-liter jacketed Pyrex vessel described in Section 3.2.1. In the one-liter Pyrex vessel, an emulsion of $MgCl_2$-ethanol complex in Vaseline was formed at 120°C by stirring at 1000 rpm. The emulsion was kept stirring at 120°C for 2 hours and then was forced out of the one-litre Pyrex vessel by pressurizing the vessel with nitrogen to 600 kPa. The emulsion flowed through the small diameter Teflon tubing and then into the cold heptane at about -30°C where it solidified rapidly. The emptying of the Vaseline/$MgCl_2$-ethanol emulsion took about 40 seconds. After the Vaseline was washed away with heptane at about 50°C, the $MgCl_2$-ethanol complex particles were transferred into a glass tube, having a fritted disk at the bottom, for a thermal treatment. The thermal treatment partially dealcoholated the $MgCl_2$-ethanol complex. The temperature for the thermal treatment were increased steadily from room temperature to 120°C in four hours. After the thermal treatment, about 50% of ethanol was eliminated and the molar ratio of ethanol to $MgCl_2$ was about 1.5 in the partially dealcoholated $MgCl_2$-ethanol complex.

71

The second step of the preparation of the catalyst consisted of treating the partially dealcoholated $MgCl_2$-ethanol complex with $TiCl_4$ and an electron donor. The temperature history and chemical addition times for the second step is schematically illustrated in Figure 3.2.

Special precautions, such as operating environment and purity of other chemicals used, are required for handling toxic and air-sensitive chemicals like $TiCl_4$. About 5 g of the partially dealcoholated $MgCl_2$-ethanol complex, suspended in 150 mL of heptane, was introduced into a 500-mL glass flask equipped with a mechanical agitator. About 150 mL of $TiCl_4$ was added into the flask slowly to remove ethanol in the $MgCl_2$-ethanol complex by reaction with $TiCl_4$ and to fix additional $TiCl_4$ on the $MgCl_2$-support. The temperature of the flask was increased slowly from -20°C to 50°C in 7 hours while stirring slowly at 15 rpm. It is crucial that the stirring be gentle and addition of $TiCl_4$ be slow; rapid stirring resulted in breakup of the $MgCl_2$-ethanol particles and fast addition of $TiCl_4$ can possibly reduce the mechanical strength of $MgCl_2$. When the temperature reached 50°C, 0.6 mL of dibutyl phthalate, an electron donor, was added into the flask. The mixture was then heated from 50 to 110°C in 3 hours and kept at 110°C for 1 hour. After the liquid was removed, an additional 150 mL of $TiCl_4$ was added into the flask and the temperature was kept at 110°C for another 1 hour. The resuspension of catalyst in a large excess of $TiCl_4$ at a high temperature can result in further decrease of Ti content in the catalyst (Hu and Chien, 1988) because Ti species that are loosely bound to $MgCl_2$ support are soluble in $TiCl_4$ at high temperature. After the soluble Ti species are removed by the further treatment of $TiCl_4$, the specific activity of the catalyst prepared, *i.e.*, catalyst activity per mole of Ti is

72
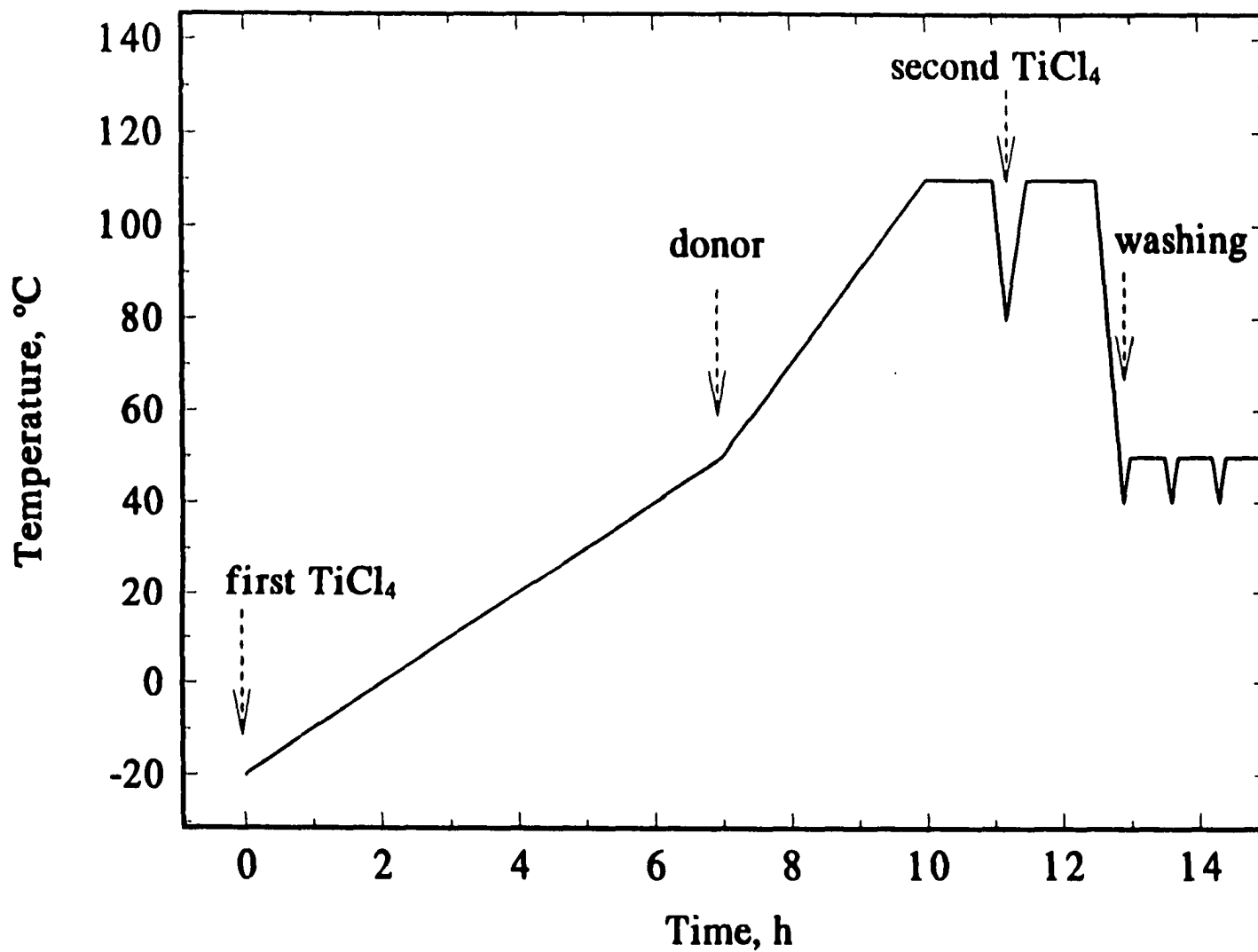
Figure 3.2 Schematic illustration of procedure for the second step of catalyst preparation.

is higher since soluble Ti species have low activity for olefin polymerization (Hu and Chien, 1988; Vizzini *et al.*, 1993).

The catalyst particles in the flask were then cooled to 50°C and washed with 100 mL of heptane. The wash was repeated 10 times; hexane was used for the last wash. The particles thus obtained were dried in vacuum at room temperature for 30 minutes. The dry solid catalyst contained 3.7 wt % Ti as determined by a colorimetric analysis method (Vogel, 1961). Examination of the catalyst particles with scanning electron microscopy showed that the dry solid catalysts were mostly in spherical form with diameter in the range of 30 to 150 μm; sample micrographs are shown in Figure 3.3.

3.3 Equipment and Procedure for Prepolymerization and Polymerization

A semibatch reactor system, which is shown schematically in Figure 3.4, was used for ethylene prepolymerization and polymerization at various reaction conditions, such as temperatures, hydrogen and ethylene pressures, and reactor modes (*i.e.*, gas-phase or slurry). The reactor system and polymerization procedure have been well described by Lynch and Wanke (1991), Shanbhag (1992), and Huang (1995), in which the one-litre stainless steel reactor was used for high-pressure slurry operations and for all the gas-phase operations. Further modification of the reactor system was made in the current study by using a one-litre jacketed Pyrex reactor for the low-pressure ethylene prepolymerization in slurry.

Before each run, the reactor was leak-tested with nitrogen and then evacuated overnight at 90°C by a circulating jacket for the Pyrex reactor or by an outside oil bath for the stainless steel reactor. For all the slurry runs, 300 mL of heptane was used as a reaction
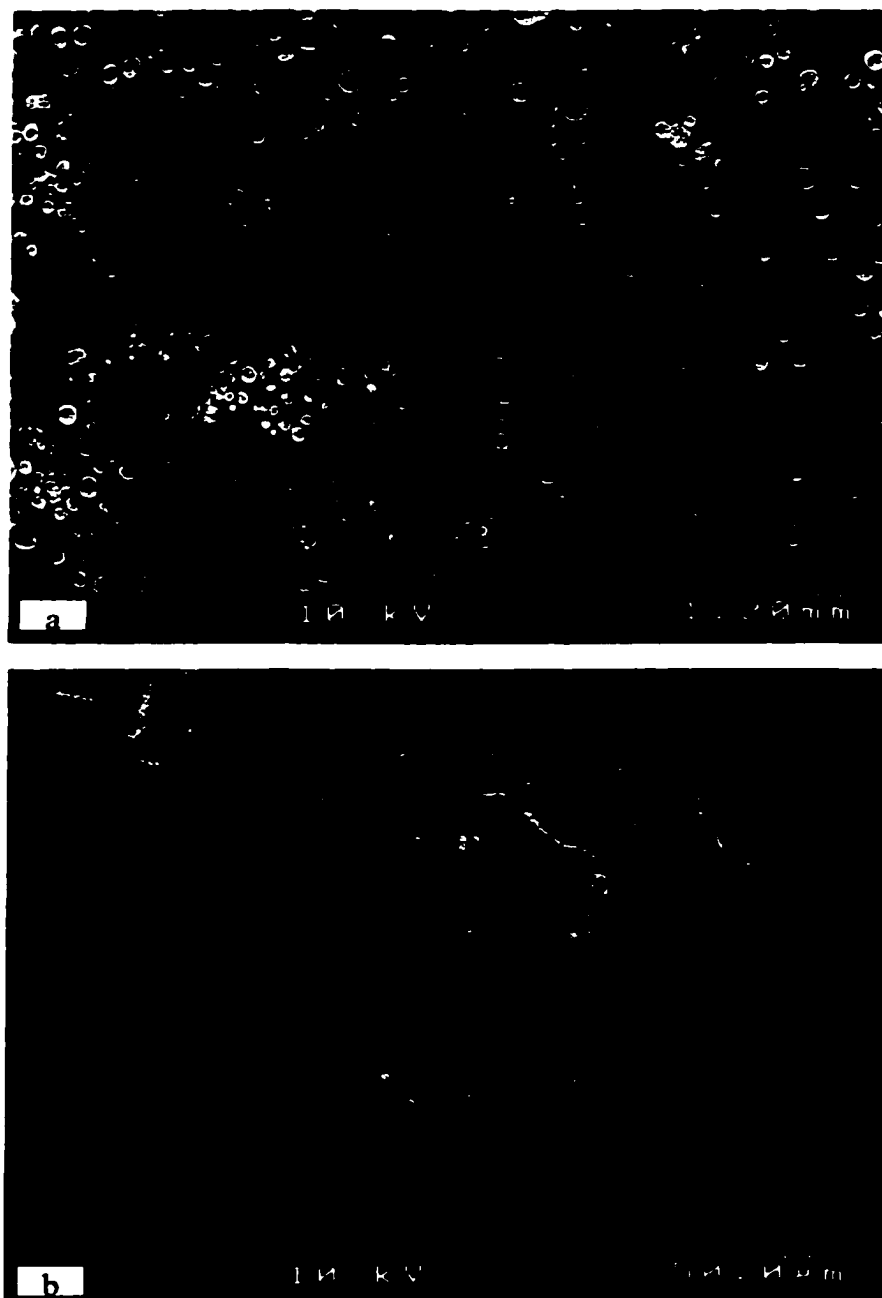
Figure 3.3   SEM micrographs of morphology-controlled MgCl$_2$-supported TiCl$_4$ catalyst (MgCl$_2$ support was prepared by melt quenching).
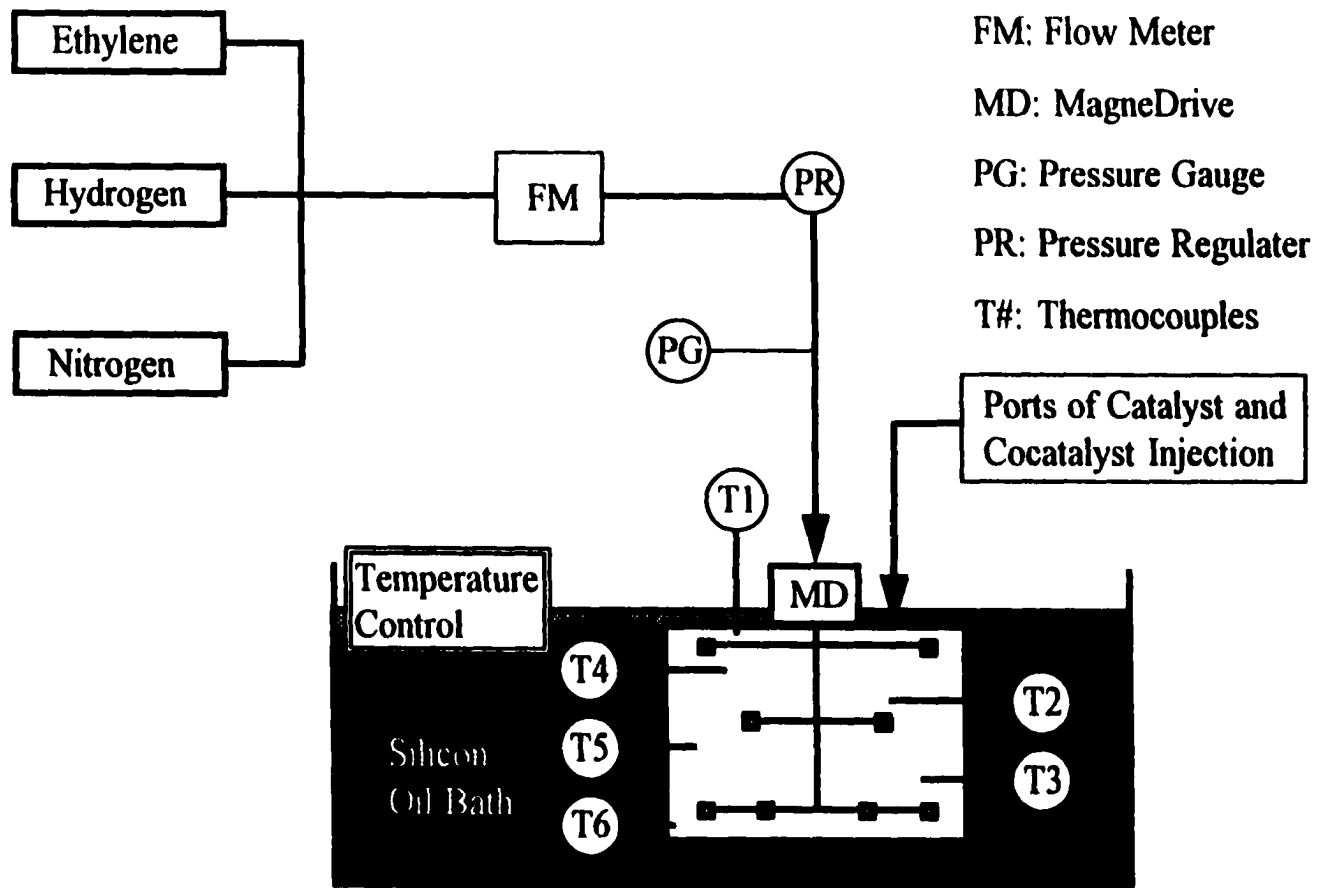
Figure 3.4 Schematic diagram of the semi-batch reactor system (stainless-steel reactor).

medium. For all the gas-phase reactions, NaCl or Rulon particles were used as a seed bed. Rulon particles were obtained by cuting a Rulon LR sheet into ~ 2×2×2 in length (Rulon LR is the tradename of Furon Company for a very stable engineered polymer consisting mostly of polytetrafluoroethylene). After the cocatalyst and catalyst were injected into the reactor, hydrogen, if used, was added into the reactor and reaction was started by feeding ethylene continuously. For all the runs, temperature inside the reactor was kept constant by adjusting the temperature of the oil bath for the stainless steel reactor or the circulating jacket for the Pyrex reactor. The pressure in the reactor was controlled by the pressure regulator which allowed ethylene to be fed on demand to maintain the set pressure. Ethylene feed rates were monitored by Matheson mass flow transducers and reported at the conditions of STP, *i.e.*, standard temperature (0°C) and pressure (101325 Pa). The values of flow rate, temperatures, and total pressure in the reactor were recorded as a function of time at 10 s intervals by a data acquisition system, which was described previously by Lynch and Wanke (1991).

For the polymerization conditions reported in this study (including prepolymerization and homopolymerization runs reported in all the figures and tables), the temperature is the average temperature of the thermocouples T2, T3, T4, T5, and T6 (see Figure 3.4) because the temperature difference between these thermocouple was typically less than 1°C, the pressure is the ethylene pressure in the reactor, and the polymerization rate is calculated from the flow rate of ethylene into the reactor.

3.4 Prepolymerization of Ethylene

The Pyrex reactor was used as a slurry reactor, and the stainless steel reactor was used as a gas-phase reactor for the prepolymerization of ethylene in the semibatch reactor

system described in Section 3.3. Neat triethylaluminum, as a cocatalyst, and the $MgCl_2$-supported $TiCl_4$ catalyst, prepared by the procedure described in Section 3.2, were injected into the reactor prior to the prepolymerization. Ethylene prepolymerization was carried out at a constant temperature and constant ethylene pressure in the presence of hydrogen. The run conditions and the rate profiles of ethylene prepolymerization are given in detail in Appendix B. After the prepolymerization, prepolymer particles were dried in vacuum at room temperature for 30 minutes. The dry prepolymer particles are used as a catalyst for the next step of polymerization. The prepolymerization run numbers start with a prefix of Pre, *e.g.*, Pre-5 stands for ethylene prepolymerization experiment Run Number 5.

3.5 Homopolymerization of Ethylene

Ethylene homopolymerization was carried out using the stainless steel reactor in a gas-phase or slurry mode. For all the gas-phase polymerizations, the reactor was charged with neat triethylaluminum, as a cocatalyst, and prepolymerized catalyst. Three types of operating procedures in the gas-phase reactor were used, *i.e.*, Types A, B, and C. For both Types A and B operations, the reactor pressure was kept constant throughout the run. For Type A operations, a desired amount of hydrogen was fed to the reactor at the beginning of the experiment followed by continuous addition of ethylene; ethylene was fed at a rate which kept the pressure constant at the desired set value. Type B operation was similar to Type A except that no hydrogen was fed to the reactor. Type A and B experiments were done to define the dependencies of the activity profiles and polymer properties on operating conditions. Type C experiments were also carried out in the absence of hydrogen, but the ethylene pressure was varied during a given experiment. Step-wise increases in ethylene

78

pressure were followed by a period of no ethylene feed (reactor pressure decreased); then, another set of step increases in ethylene pressures followed. Type C experiments were done in an attempt to separate polymerization kinetics from deactivation kinetics.

The experiments carried out in the slurry mode were designated as Type D operations. The slurry Type D operations are similar to the gas-phase Type A operations, in which a desired amount of hydrogen was fed to the reactor at the beginning of the experiment followed by continuous addition of ethylene; ethylene was fed at a rate which kept the pressure constant at the desired set value. Type D experiments were done to compare the properties of polyethylene particles made in the slurry reactor with that in the gas-phase reactor.

The detailed polymerization conditions for all the runs are listed in Appendix C. The run numbers of ethylene polymerization start with their type as a prefix, *e.g.*, A5 stands for Run Number 5 of a Type A experiment for ethylene polymerization in the gas phase.

3.6 Size Exclusion Chromatography

The molar masses and polydispersity of polyethylene were measured by size exclusion chromatography (SEC) with a Waters 150C GPC equipped with a differential refractometer and a series of four Shodex GPC/UT-800M columns. The columns and the detector were maintained at 140°C. The solvent, HPLC-grade 1,2,4-trichlorobenzene, was pumped through the columns at 1.0 cm^3/min. The 1,2,4-trichlorobenzene contained approximately 0.25g/L of 2,6-*tert*-butyl-4-methylphenol as an antioxidant. The molar masses were calibrated by polymer samples of known molar masses. These polymer

79

samples included: TSK standard polystyrene samples with molar masses from 870 to 8,420,000, linear paraffins $C_{20}H_{42}$, $C_{40}H_{82}$, and $C_{60}H_{122}$, and NIST polyethylene standard reference materials 1475, 1482, 1483, and 1484. The universal calibration approach, *i.e.*, $M[\eta]$ as a universal parameter, was assumed for the range of molar masses measured. The universal calibration data, *i.e.*, molar masses as a function of retention times measured, were generated by applying Mark-Houwink Equation $[\eta]=KM^{\alpha}$ for polystyrene ($K=1.90\times10^{-4}$ dL/g, $\alpha=0.655$) and polyethylene ($K=3.95\times10^{-4}$ dL/g, $\alpha=0.726$), and fitted with a third or fifth order polynomial function.

For each sample measured, a solution of polyethylene concentrations of 0.035 to 0.07 mass % in 1,2,4-trichlorobenzene was prepared, and each solution was injected at least twice. The molar masses were reported as the averages of at least two measurements.

3.7 Scanning Electron Microscopy

The morphology of catalysts and polymers was examined by scanning electron microscopy (SEM) with a Hitachi S-2700 SEM equipped with a camera and a Polaroid film (Type 55). The specimens were subsequently coated with a thin layer of carbon (under vacuum by high-temperature evaporation) and gold (by sputter coating) before they were placed in the specimen chamber of the SEM. The accelerating voltage of electron beam used was low at 10 kV in most of the SEM examinations. Application of specimen coating and low accelerating voltage operation can reduce the accumulation of electrons on the surface of the specimen. The accumulation of electrons will lead to severe distortions of the images (charging artifacts) for insulating materials, such as polyethylene.

Special care should be given for the preparation of catalyst specimens since the catalyst is moisture-sensitive and transferring catalyst will expose the catalyst to the air. It is desirable that the air-exposure time during the process of transferring catalyst be as short as possible so that the catalyst morphology will not be affected by absorbing significant amount of moisture. In this study, the time that the catalyst specimen was exposed to the air was typically less than 10 seconds when the catalyst was transferred from the glove box to the carbon-coating device.

81

4. Prepolymerization of Ethylene

It is known that morphology-controlled $MgCl_2$-supported $TiCl_4$ Ziegler-Natta catalysts have a porous structure and are very active for ethylene polymerization. The porous $MgCl_2$ structure of the catalyst is fragile; and fragile catalysts with high activity are easily fragmented, and polymer product consists mainly of fines with uncontrolled morphology. Prepolymerization to a certain yield under mild conditions, *i.e.*, low temperature and low ethylene concentration, can control the catalyst morphology to be replicated into nascent polymer morphology. The catalyst particle acts as a template for the growth of a polymer particle. The controlled morphology of nascent polymer particles refers to their size, shape, density, and texture (Boor, 1979). In addition, prepolymerization enhances the overall activity of catalysts, and increases the bulk density of final polymer particles (Tang, 1986). Final polymer particles with high bulk density can be directly processed without the energy-consuming pelletizing step.

In this chapter, the effects of prepolymerization conditions on prepolymer properties will be presented in Section 4.1. Based mostly on a prepolymer made under optimum prepolymerization conditions, mass transfer effects on the molar masses, the particle growth mechanism, and the globule size distribution on the surface of nascent prepolymer particles will be discussed in Sections 4.2, 4.3, and 4.4, respectively. The morphology of prepolymer was examined by scanning electron microscopy, and molar masses of prepolymer were measured by size exclusion chromatography. The reaction conditions and rate profiles of prepolymerization runs are provided in Appendix B.

82

4.1 Prepolymerization Conditions

Prepolymerization conditions affect prepolymer properties such as morphology and bulk density (Tang, 1986). The morphology and bulk density of nascent polymer particles are important properties, and they are difficult to control and reproduce in Ziegler-Natta polymerization. The prepolymerization conditions used in this study are listed in Table 4.1.

Table 4.1   Prepolymerization Conditions[1] and Bulk Density of Prepolymer

Run No.	Reactor Type	T, °C	P_{H_2}, kPa	$P_{C_2H_4}$, kPa	Time, h	Yield, g PE/g Cat	Bulk Density, g/cm^3
Pre-1	Gas phase	30.0	89.8	36.2	2.43	75	N/M^2
Pre-2	Gas phase	91.6	351.7	1,387.9	0.24	1,167	N/M
Pre-3	Slurry	29.6	86.2	61.6	2.64	73	0.34
Pre-4	Slurry	30.6	83.6	342.2	1.11	110	0.31
Pre-5	Slurry	72.6	85.4	342.9	0.33	160	0.29
Pre-6	Slurry	78.4	356.8	1,411.0	0.30	1,046	0.29

Notes:

1. For all the prepolymerization runs, catalyst used was as shown in Figure 3.1, cocatalyst used was 0.25 mL of triethylaluminum; 300 mL of heptane was used as a diluent in slurry reactor while 35 g of Rulon LR particles were used as seed beds in gas phase reactor.

2. N/M = Not measured

The typical morphologies of nascent prepolymer particles are shown in Figure 4.1. For gas-phase prepolymerization, prepolymer particles were totally broken into fine powders and flakes, even under mild polymerization conditions as shown in Figure 4.1a for

Figure 4.1 Typical morphologies of nascent prepolymer particles at different polymerization conditions (a: Run Pre-1; b: Run Pre-3; c: Run Pre-6).

84

Run Pre-1. The bulk densities of broken prepolymer particles from gas-phase prepolymerization were not measured for Runs Pre-1 and Pre-2. The total fragmentation of particles in gas-phase prepolymerization was possibly due to the absence of mass transfer and the presence of heat transfer limitations, which are discussed in Section 4.3.

In slurry prepolymerization, the spherical shape of catalysts was basically replicated into the shape of prepolymer particles under various conditions, *e.g.*, for Run Pre-3 shown in Figure 4.1b and for Run Pre-6 in Figure 4.1c. This indicates that slurry prepolymerization is a very important first step in terms of particle replication in commercial production of polyolefins using Ziegler-Natta catalysts in the multistage reactors.

The bulk density is affected by the prepolymerization conditions in the slurry phase as can be seen from the results in Table 4.1, which show that the bulk density of prepolymer is generally higher at lower polymerization temperature, *cf.* Runs Pre-3 and Pre-4 with Runs Pre-5 and Pre-6. This is reasonable because lower polymerization temperature decreases the intrinsic polymerization rate, thus decreasing possible mass transfer limitations (Floyd *et al.*, 1986a and 1986b; Tang, 1986; Hutchinson and Ray, 1991). The bulk density of prepolymer is higher under lower ethylene pressure, *cf.* Runs Pre-3 and Pre-4. With the same ratio of hydrogen and ethylene concentration, the bulk densities of prepolymer are the same as can be seen from Run Pre-5 and Run Pre-6, irrespective of ethylene pressure and polymerization yield. This implies that prepolymerization conditions in slurry reactors are crucial to make prepolymer with high bulk density, which will provide the basis for producing polymer with high bulk density in the subsequent polymerization.

85

It is worth noting that the highest bulk density of prepolymer particles for the Run Pre-3 may also be due to the longest polymerization time as shown in Table 4.1. Past experimental results and mathematical simulations have indicated that the bulk density of nascent polymer particles increases with polymerization time for Ziegler-Natta olefin polymerization. For example, Tang (1986) showed experimentally that the increase of polymerization time increases bulk density of nascent polyethylene and nascent polypropylene. The continuous electron microscopic observation of polymer formation by Baker *et al.* (1973) showed that polymer is filling the void as ethylene polymerization progresses in the gas-phase using a $TiCl_3$ catalyst. For propylene polymerization using $MgCl_2$-supported $TiCl_3$ catalysts in the slurry phase, Conner *et al.* (1993) measured the total pore volume and surface area of nascent polymer particles with polymerization yield and found both properties decrease with yield. It is speculated that polymer is filling pores as well as blocking the surface as polymer accumulates (Conner *et. al.*, 1993) after the initial fragmentation of catalyst particle.

The filling of voids by polymer is also reflected by the increase of bulk density from prepolymer to polymer, which will be presented in Section 7.2, where results for further polymerizations using prepolymer from Run Pre-3 as the catalyst are presented. The increase of bulk density with polymerization time indicates that mass transfer limitations are most severe during initial stages of particle growth (Hutchinson and Ray, 1991). Mass transfer limitations of monomer decrease with increasing time so that monomer molecules have better access to the interior of particles.

86

The nascent prepolymer particles from Run Pre-3 have the highest bulk density; hence, this prepolymer was used as a catalyst for subsequent polymerizations. Most of the following discussions are based on this prepolymer.

4.2 Mass Transfer Effects on Molar Masses of Prepolymer

Using a morphology-controlled catalyst, the properties of polyethylene particles, such as molar masses and surface morphology, can be analyzed as a function of their particle size. Shown in Figure 4.2 are molar masses, measured by SEC, of nascent prepolymer particles from Run Pre-3 as a function of their sizes. It is seen from Figure 4.2 that molar masses decrease with prepolymer particle sizes. This indicates that the growth of polyethylene around catalyst particle depends on individual size of initial catalyst particles. Assuming that initial catalyst particles are equally porous and active, large catalyst particle will produce large polyethylene particles (Boor, 1979). The dependence of molar masses on sizes of nascent prepolymer particles can be caused by the size dependence of mass transfer.

Polymerization process can be mainly under kinetic control or mass transfer limitations (Mkrtchyan *et al.*, 1986; Tang, 1986; Floyd *et al.*, 1986a and 1986b; Galli and Haylock, 1991). For kinetically controlled polymerization, all catalytic sites are equally accessible to reactants, and polymer particles grow uniformly regardless of sizes of catalyst particles. Polymerization under mass transfer limitations leads to a nonuniform growth and tends to affect properties of nascent polymer particle because concentrations of monomer or other components inside particle would be lower than those at the particle surface. Any properties that are affected by concentrations of components in the reactor would be affected by mass transfer limitations.

87
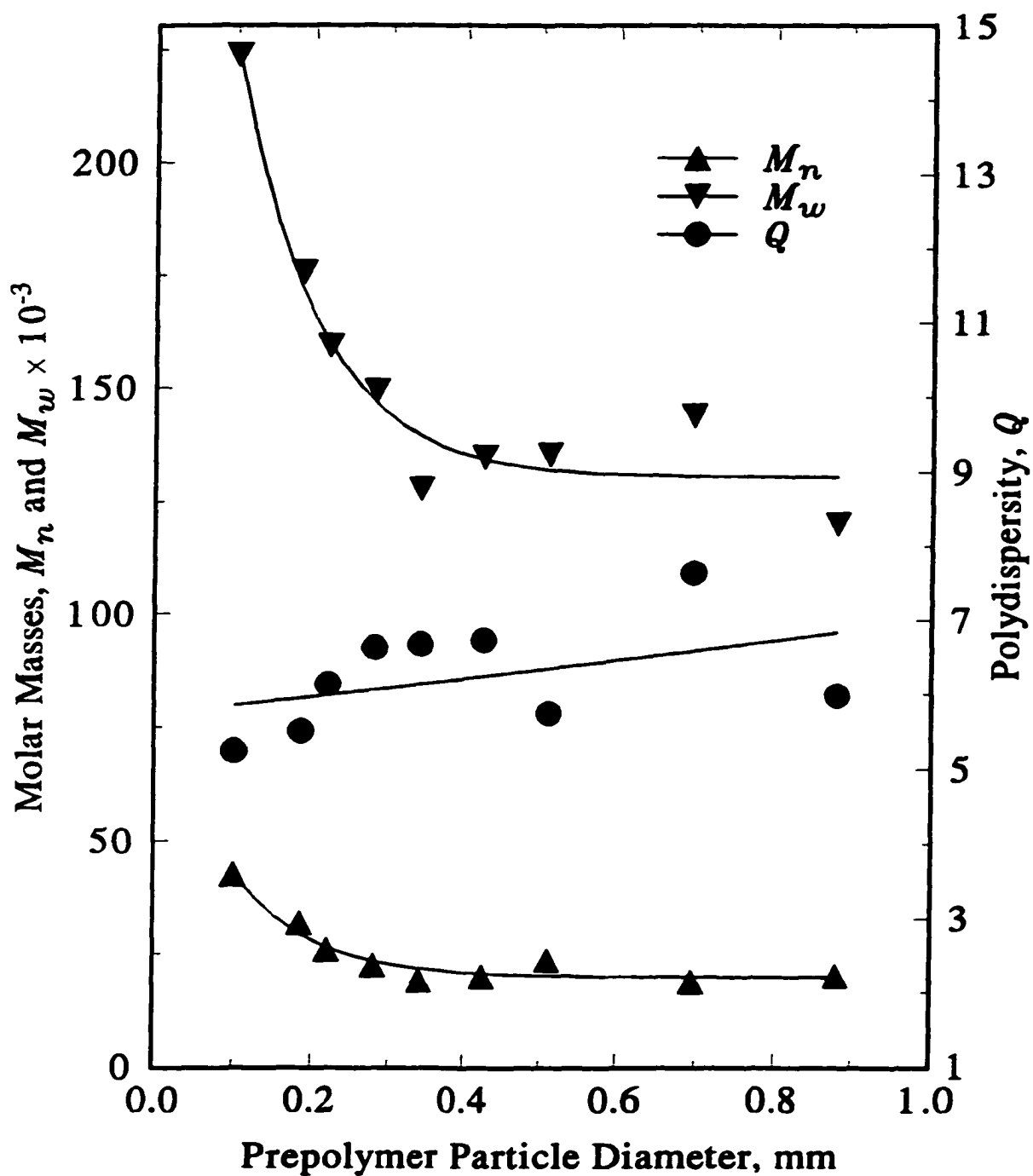
Figure 4.2   Effects of prepolymer size on M_n, M_w, and Q (Run Pre-3).

Molar masses are affected by mass transfer limitations because molar masses are dependent on concentration of specific components participating in chain transfer processes. Equation 4.1 defines the dependence of number-average molar mass of polyethylene on concentrations of components in possible chain transfer processes assuming that simplified first-order kinetics with ethylene concentration is applied to ethylene polymerization in the presence of hydrogen.

$$\frac{M_n}{M_0} = \frac{k_p[M]}{k_{tr.M}[M] + k_{tr.\beta} + k_{tr.A}[A]^{n_A} + k_{tr.H}[H_2]^{n_H}}$$ (4.1)

where: M_n is the number average molar mass of polyethylene; M_0 is molar mass of ethylene monomer; k_p is the propagation rate constant; $k_{tr.M}$ is the rate constant for chain transfer to monomer, $k_{tr.\beta}$ is the rate constant for β-hydrogen elimination; $k_{tr.A}$ is the rate constant for chain transfer to alkyl aluminum; $k_{tr.H}$ is the rate constant for chain transfer to hydrogen; $[M]$, $[A]$, and $[H_2]$ are concentration of monomer, alkyl aluminum, and hydrogen, respectively; superscript n_A and n_H are power-law reaction orders for chain transfer to alkyl aluminum and hydrogen, respectively.

The effect of mass transfer limitations will possibly decrease the concentrations of monomer, alkyl aluminum, or hydrogen at the active sites in the slurry operation. According to Equation 4.1, only the decrease of monomer concentration, due to the increase of mass transfer limitations, will lead to the decrease of the number-average molar mass. The decrease of molar masses with increasing the size of nascent prepolymer particles is clearly seen in Figure 4.2. This suggests that the average concentration of ethylene in large particles is lower than that in small particles. This lead to the conclusion that mass transfer resistance

of ethylene was present during ethylene prepolymerization conditions in the slurry reactor for Run Pre-3 and the mass transfer resistances increased with increasing catalyst particle size.

Shown also in Figure 4.2 is the increase of polydispersity with the size of nascent prepolymer particles for Run Pre-3. The above observations from Figure 4.2 are in agreement with the predictions of the multigrain model, which have been discussed in Section 2.3, that the molar masses will decrease and polydispersity will increase with the size of catalyst particles in the presence of mass transfer limitations.

4.3 Surface Morphology and Growth Mechanism of Prepolymer

Figure 4.3 shows typical surface structures, observed by SEM, of nascent prepolymer particles as a function of their sizes from Run Pre-3. It is seen from Figure 4.3 that small prepolymer particles are denser and show globular structure while larger prepolymer particles are more porous and show cobweb structure which is more evident at the surface. Similar observation were also made for prepolymer form Runs Pre-4 and Pre-5. The cobweb structure on the surface of nascent polyethylene particles was attributed to mass transfer limitations of ethylene (Graff *et al.*, 1970). Due to mass transfer resistance of monomer, the rate of ethylene polymerization at the surface of a catalyst particle is initially much higher than that in the interior. Accordingly, the crust (or skin) consisting of globules will be formed initially at or near the catalyst surface where the greater amount of the polymer is produced. Whereas in a later stage of slurry prepolymerization when mass transfer limitations decrease, the polymerization rate becomes higher in the interior of the particle. As the polymer particles start to grow from the interior of the particle, the polymer

90
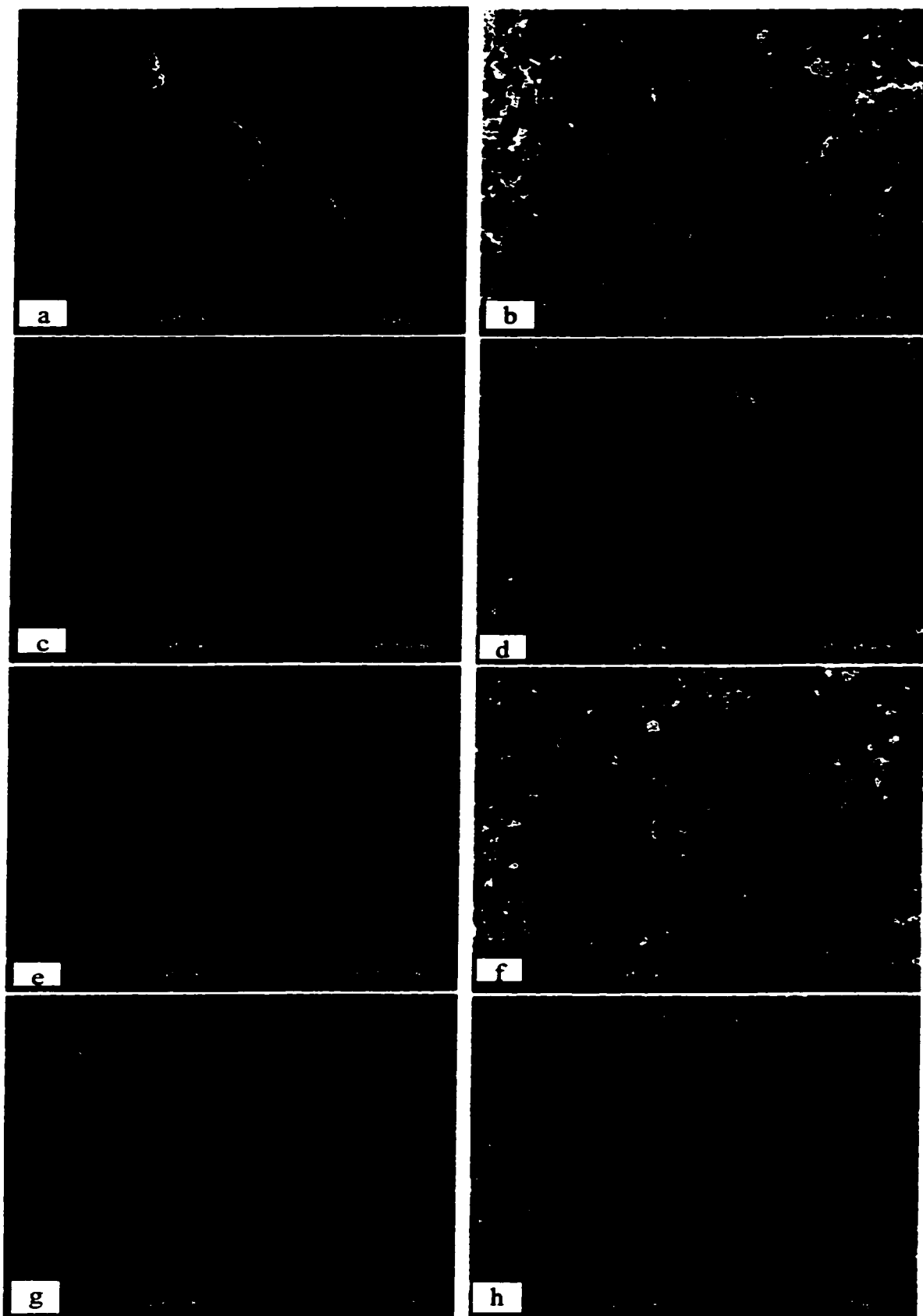
Figure 4.3 Surface structures of nascent prepolymer particles as a function of size (Run Pre-3).

91

crust may partially break and the globules remain interconnected by cold-drawn threads to form the cobweb structure on the surface of nascent polyethylene particles.

The initial formation of the polymer crust at the surface due to mass transfer limitations of ethylene is very important for slurry prepolymerization because the polymer crust is stronger than $MgCl_2$, which acts as catalyst support and has the spherical shape of initial catalyst particle. This polymer crust can prevent particles from breaking apart totally as polymerization proceeds. The absence of mass transfer limitations in gas-phase prepolymerization leads to the total fragmentation of catalyst particle because $MgCl_2$ particles are very fragile. This possibly explains fine powders and flakes of prepolymer, *e.g.*, from Run Pre-1 shown in Figure 4.1a, produced during gas-phase operation.

By comparing ethylene polymerization with propylene polymerization, Graff *et al.* (1970) proposed ethylene polymerization to be under mass transfer limitations and propylene polymerization to be under kinetic control since intrinsic rate of propylene polymerization was much lower than that of ethylene polymerization. Polypropylene initially grows inside and outside of the catalyst particle at the same rate. This is in agreement with the morphology studies by Kakugo *et al.* (1989b), who found polymer globules appear both on the surface and in the interior of nascent polypropylene particles. If the particle growth mechanism for polypropylene is considered as the limiting case for the growth of polyethylene under kinetic control, then the observation in Figure 4.3 would provide additional evidence that mass transfer limitations are more severe in larger particles; this is in agreement with molar mass analysis in Section 4.2, based on the results from Figure 4.2.

92

Surface area measurements of prepolymer particles as a function of prepolymer particles size show that surface area increases with increasing particles size (see Table 4.2). Larger surface areas mean higher porosity if the pore size remain the same. Hence, increased surface areas suggest increased porosity. The variations in porosity of the prepolymer particles will be mirrored in the polymer made using prepolymer from Run Pre-3 as the catalyst. This effect will be discussed in detail in Section 7.2.

Table 4.2   Effect of Particle Size on BET Surface Area[1] for Prepolymer Produced from Run Pre-3

Prepolymer Particle Diameter, mm	0.15	0.24	0.35	0.60
BET Surface Area, m^2/g	N/D[2]	1.9	2.3	3.8

NOTE:

1. BET measurements were done using an OMNISORP 360 (Pieters and Venero, 1984) with nitrogen as the adsorbate.

2. N/D = Not detectable.

The two different surface morphologies of nascent prepolymer particles from Runs Pre-5 and Pre-6 are shown in Figure 4.4. The major difference between polymerization conditions of Run Pre-5 and Run Pre-6 is the ethylene pressure (see Table 4.1). The cobweb morphology is seen in Figure 4.4b for Run Pre-5 at lower ethylene pressure; the globular morphology is seen in Figure 4.4d for Run Pre-6 at higher ethylene pressure. If the presence of mass transfer limitations during particle growth as described above is used to explain the different morphologies between Figure 4.4b and Figure 4.4d, the conclusion will be that the mass transfer limitations are more severe under low ethylene pressure. This is in agreement with the mathematical simulations of Floyd *et al.* (1986a; 1986b) which showed that mass transfer limitations decreased as monomer concentration increased.

93
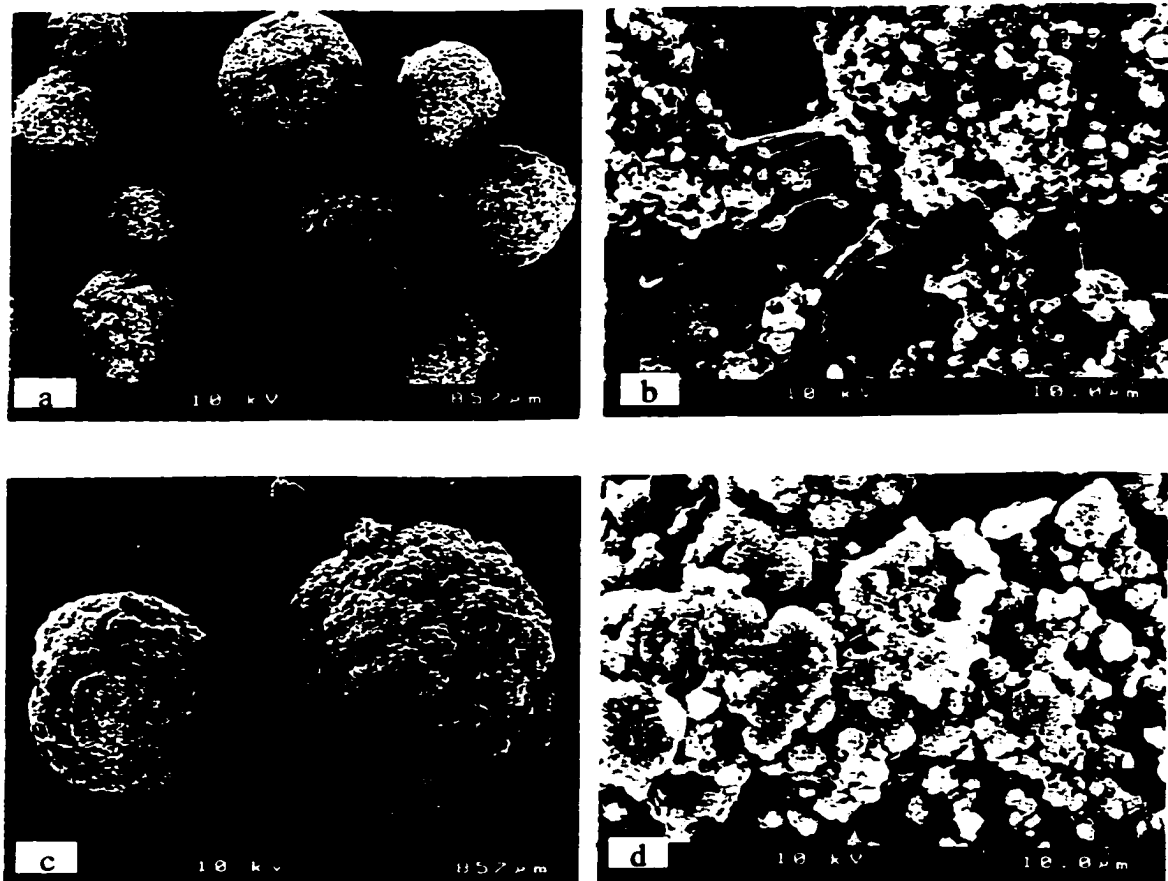
Figure 4.4 Effects of ethylene pressure on surface structures of nascent prepolymer particles (a & b: Run Pre-5; c & d : Run Pre-6).

94

4.4 Globule Size Distribution

Despite of two different surface structures, *i.e.*, globule and cobweb, observed by SEM in Figure 4.3 and Figure 4.4, both structures basically consist of globules. These globules are believed to be secondary polymer particles, whose size distributions are dependent on polymerization yields, *i.e.*, the higher the polymerization yield, the more uniform globule size will be formed, irrespective of types of Ziegler-Natta catalysts (Kakugo *et al.*, 1989a and 1989b; Noristi *et al.*, 1994). Polymerization yield is defined as the amount of polyethylene produced per unit of mass of catalyst. [The structure of nascent polyolefins produced by Ziegler-Natta catalysts has been reviewed in Section 2.1.]

Comparing SEM micrographs of nascent polyethylene at a higher magnification in this study, the globule sizes shown in Figure 4.4 for Runs Pre-5 and Pre-6, produced at high polymerization temperature with a high yield, are generally more uniform than those shown in Figure 4.3 for Run Pre-3, produced at low polymerization temperature with a low yield (see Table 4.1 for prepolymerization conditions and yields). The globule sizes are even more uniform when polyethylene was produced by further polymerization using prepolymerized polyethylene from Run Pre-3 as a catalyst, which will be presented in Section 7.2.

The relative uniformity of polymer globules was explained by coalescence theory (Fisa *et al.*, 1974). The coalescence theory is based on a successive polymerization and crystallization. According to this theory, the catalyst is not a nucleating agent and the polymer is amorphous in the liquid state at the very beginning of polymerization until the liquid polymer droplets reach a critical size. Once the polymer liquid droplets reach a

critical size, they nucleate and coalesce; the coalescence is interrupted due to rapid crystallization. As pointed out by Fisa *et al.* (1974), the coalescence theory explains the observation that relatively uniform globule size distribution is, more or less, independent of catalyst and polymerization conditions in slurry or gas phase. However, it has been observed on polymer particle surface that globule size distribution is dependent on the polymerization yield for polypropylene (*e.g.*, Kakugo *et al.*, 1989a and 1989b; Noristi *et al.*, 1994); for polyethylene in this study, globule size distribution and morphology on the particle surface depend on polymerization conditions and polymerization yield.

The most likely explanation for the dependence of surface morphology on polymerization conditions and yield is the presence of at least two different types of catalytic sites with different activities and deactivating behaviors. Catalytic sites with high activity deactivate faster than catalytic sites with low activity, especially when polymerization temperature increases. At constant polymerization temperature, catalytic sites with high activity will produce more polymer (higher yield) than catalytic sites with low activity during a short time period of polymerization. Different types of catalytic sites having different activities will produce different yields of polymer around catalytic sites, which will lead to nonuniform globule sizes since polymer globules grow with polymerization yield (Kakugo *et al.*, 1989a and 1989b). Furthermore, catalytic sites at the surface are more likely to be attacked by poisonous materials, such as residual moisture and oxygen in the reactor. Poisonous materials deactivate catalytic sites, and will cause different polymerization yields and different globule sizes even for the same type of catalytic site. When polymerization proceeds with a higher yield or at a higher temperature,

the site with low activity and slow deactivation is dominating in the polymerization because catalytic sites with high activity deactivate faster than catalytic sites with low activity. Eventually, the two different types of catalytic sites have chance to reach comparable range of polymerization yield, and relatively uniform globule sizes are formed.

5. Rate Profiles of Gas-Phase Ethylene Homopolymerization*

With supported Ziegler-Natta catalysts, polymerization rates have been observed to change with time under conditions of constant temperature and constant monomer pressure. The rate profile usually exhibits a maximum followed by a rate decay to, more or less, a steady-state level of activity; however, more complicated activity profiles, for example, profiles with two maxima, have been reported (Han-Adebekun *et al.*, 1997). The maximum rate could appear at the start of the polymerization or after a few hours, *i.e.* the acceleration period could be very short or quite long. The rate profiles can also be affected by monomer diffusion in such a way that monomer concentration gradients would be established around active sites, and these concentration gradients may be a function of time.

In this chapter, results are presented for the polymerization of ethylene is in the gas phase over the prepolymerized Ziegler-Natta catalyst, obtained from Run Pre-3 (see Chapter 4), at a constant ethylene pressure and temperature (*i.e.*, Type B experiments). No hydrogen was used to simply the procedure and increase the reproducibility of experiments. The reproducibility in the rate profiles, which is discussed in Section 5.1, is always a problem, especially for gas-phase operation (Bu *et al.*, 1995). The effects of various polymerization conditions on rate profiles are presented in Sections 5.2 to 5.4. The effects of relative amount of catalyst and cocatalyst on the polymerization rates are usually examined by Al/Ti ratio. Since the cocatalyst also acts as a scavenger in the reactor, the amount of cocatalyst interacting with the catalyst is not known. Thus, the effects of the prepolymerized catalyst amount on the rate profiles are reported in this study (Section 5.2). The effects of

---

* A version of this chapter has been accepted for publication in *Macromolecules*.

temperature and ethylene pressure on the rate profiles, as well as qualitative comparison of the rate profiles with predictions of a well-defined transport resistance model, the multigrain model (reviewed in Chapter 2), are presented in Sections 5.3 and 5.4. In Section 5.5, explanations of the rate profiles other than the mass transfer interpretation are presented. Additional experimental results of polymerization kinetics will be reported in Chapter 6.

5.1 Reproducibility in Rate Profiles

The reproducibility of rate profiles is one of the most controversial areas of Ziegler-Natta olefin polymerization ever since Ziegler's discovery because Ziegler-Natta catalysts are very sensitive to impurities which cause catalytic deactivation and frequently prevent the collection of unequivocal data. The irreproducibility in rate profiles can have many causes starting form the catalyst preparation to the polymerization process. The catalyst properties can vary from batch to batch even when the same preparation steps are used with the same sources of raw materials (McKenna *et al.*, 1995). In this study, the use of a single batch of catalyst and a single prepolymerized catalyst for subsequent gas-phase polymerization reduced irreproducibility associated with the catalyst preparation.

The reproducibility of experiments are examined by comparing the rate profiles of two individual runs (Type B) done with the same start-up procedure, polymerization conditions, and well-controlled ethylene pressure and temperature in the gas-phase reactor. For each run, ethylene pressure was kept constant by presetting the pressure regulator, and temperature in the reactor were controlled at a constant level by adjusting the temperature of the outside oil bath during polymerization. The polymerization conditions for this

99

comparison at polymerization temperature of 30°C are listed in Table 5.1. Similar comparisons at temperatures of 40, 50, 60 and 70°C are reported in Section 5.2, except that the prepolymerized catalyst amounts were different for two runs. The repeat experiments (Type B) were not done sequentially but were done in random order in a 4-month period.

Table 5.1   Run Conditions[1] for the Reproducibility of Rate Profiles at 30°C

Run No.	Amount of TEAL, mL	Prepolymerized Catalyst, mg	T, °C	$P_{C_2H_4}$, MPa	Time, h	Activity, kg PE/g Cat·h (kg PE/mol Ti·h·MPa)
B3	0.30	51	30.1	2.06	8.17	1.97 (1,244)
B4	0.30	48	30.0	2.09	8.18	3.17 (1,971)

Note:
1. The stirring speed of the reactor was 204 rpm, the seed bed was 100 g of NaCl, and no hydrogen was added in the reactor for the two runs.

The "same" polymerization conditions for the comparison of two individual runs were not completely achieved, with a small variation in the prepolymerized catalyst amounts and ethylene pressure as can be seen in Table 5.1. Small variations in operation conditions, *e.g.*, small differences in temperature or ethylene pressure, should have a small effect on the absolute rate if heat transfer effects are negligible during polymerization. The presence of heat transfer effects could lead to the temperature of polymerizing particles significantly higher than the gas-phase temperature measured by the thermocouples in the reactor (see Chapter 7). The effects of polymerization temperature on the rate profiles are further discussed in Sections 5.2 and 5.3.

The results of experiments listed in Table 5.1 are illustrated in Figure 5.1, which shows the ethylene pressure, gas-phase temperature in the reactor and polymerization rate as

100
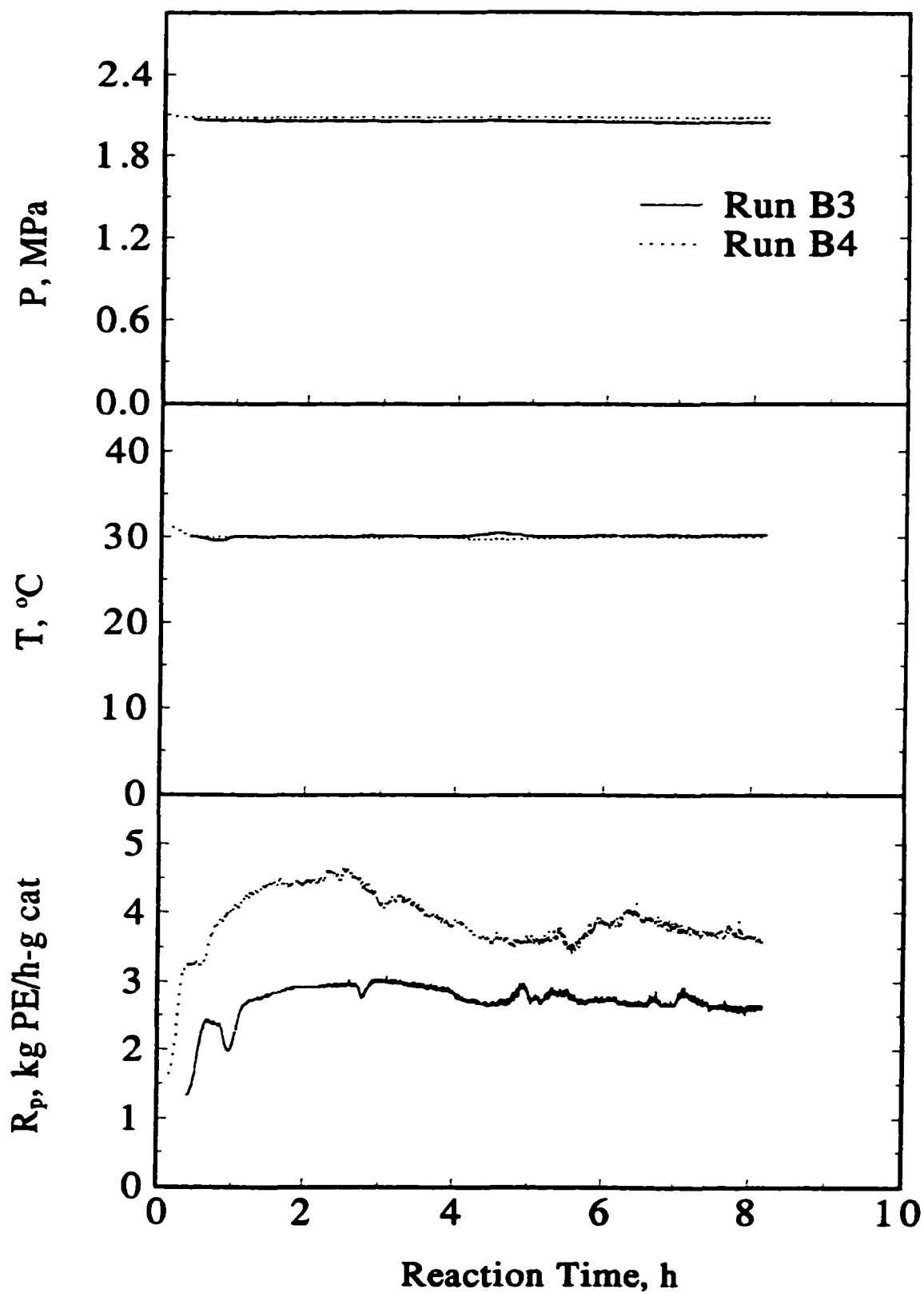
Figure 5.1 Profiles of ethylene pressure, temperature and rate at 30°C (Runs B3 and B4).

101

a function of time. The polymerization rate was calculated from the rate of ethylene addition to the reactor. No agglomeration of polymer particles was observed even after 8 h of reaction time, but most of the polymer granules are broken into smaller pieces after 8 h due to the grinding by the salt seed bed and attrition by stirrer blades.

Ethylene pressure and polymerization temperature, as can be seen in Figure 5.1, were controlled very well during both runs. The results of rate profiles in Figures 5.1 show that the rate profiles are more reproducible in shape than in absolute rate (the irreproducibility in the absolute rate can also be seen from Table 5.1, in which the activity for Run B3 is only 62% of that for Run B4). The variations in the absolute rate of the gas-phase ethylene polymerization, which were previously analyzed by Bu *et al.* (1995), are probably caused by variation of actual amount of catalyst. Errors in the amount of active catalyst in the reactors can be due to uncertainties in the measured amount of catalyst, trapping of small amount of injected catalyst in only partially accessible places, such as inlet and exit ports and reactor internals, in the reactor, and catalyst deactivation due to oxygen and moisture during catalyst handling prior to injection and by residual poisons in the reactor.

5.2 Effects of Prepolymerized Catalyst Amount on Rate Profiles

The effects of the amount of prepolymerized catalyst were studied by comparing two polymerization rate profiles with different amounts of prepolymerized catalyst at approximately same polymerization conditions (*e.g.*, ethylene pressure and gas-phase temperature, *etc.*). The comparison of the two rate profiles are made at same temperature. The polymerization conditions for the effects of prepolymerized catalyst amount on rate

profiles are listed in Table 5.2. Rate profiles for the runs listed in Table 5.2 at temperatures

of 40, 50, 60 and 70°C are shown in Figures 5.2 to 5.5, respectively.

Table 5.2   Run Conditions[1] for Effects of Prepolymerized Catalyst Amount on Rate
Profiles

Run No.	Amount of TEAL, mL	Prepolymerized Catalyst, mg	T, °C	$P_{C_2H_4}$, MPa	Time, h	Activity, kg PE/g Cat·h (kg PE/mol Ti·h·MPa)
B5	0.30	85	40.5	0.67	8.46	2.39 (4,616)
B6	0.30	30	41.9	0.68	8.20	2.38 (4,563)
B11[2]	0.30	85	52.1	2.07	7.29	19.21 (12,047)
B12	0.30	50	50.0	2.05	8.20	17.66 (11,195)
B15	0.25	47	60.1	2.07	7.21	16.46 (10,324)
B16	0.30	40	59.9	2.09	8.22	17.40 (10,811)
B19	0.30	50	69.8	2.06	7.52	16.28 (10,240)
B20	0.30	40	69.8	2.08	8.19	13.88 (8,652)

Notes:
1. The stirring speed of the reactor was 204 rpm, the seed bed was 100 g of NaCl, and no hydrogen was added in the reactor for all the runs.

2. The temperature in this run was increased by 4°C at the end of the run.

The rate profiles in Figures 5.2 and 5.3 share a common feature that the rate profiles

are of the hybrid type with an initial acceleration period followed by a slow decay. The

results in Figures 5.2 and 5.3 show that the rate profiles at 40 and 50°C are independent of

the amount of prepolymerized catalyst and are very reproducible in shape and absolute rate

(the deviation at the end of the rate profiles at 50°C in Figure 5.3 is likely due to the

temperature increase after 90 min of polymerization during Run B11).

103
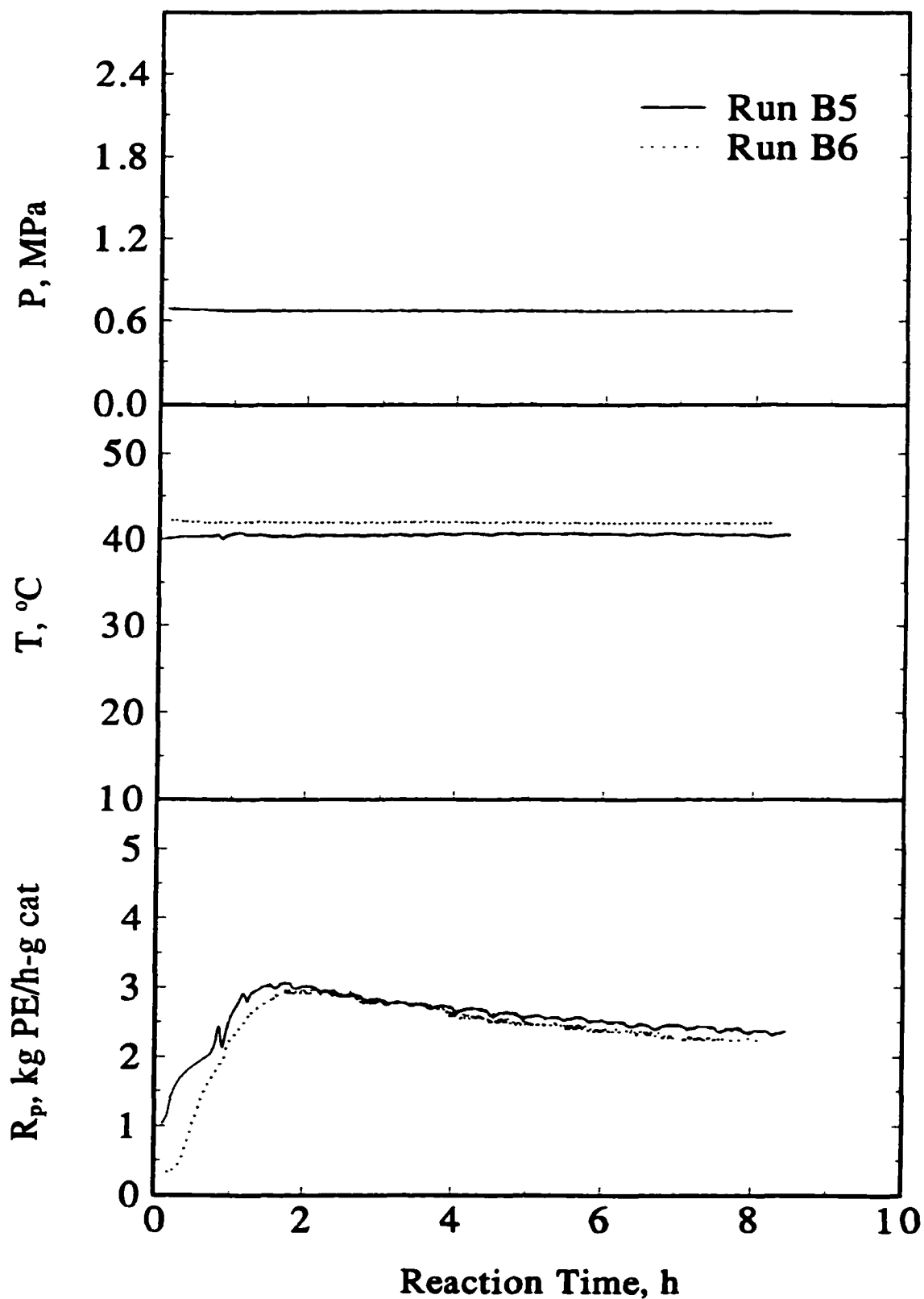
Figure 5.2 Profiles of ethylene pressure, temperature and rate at 40°C (Runs B5 and B6).
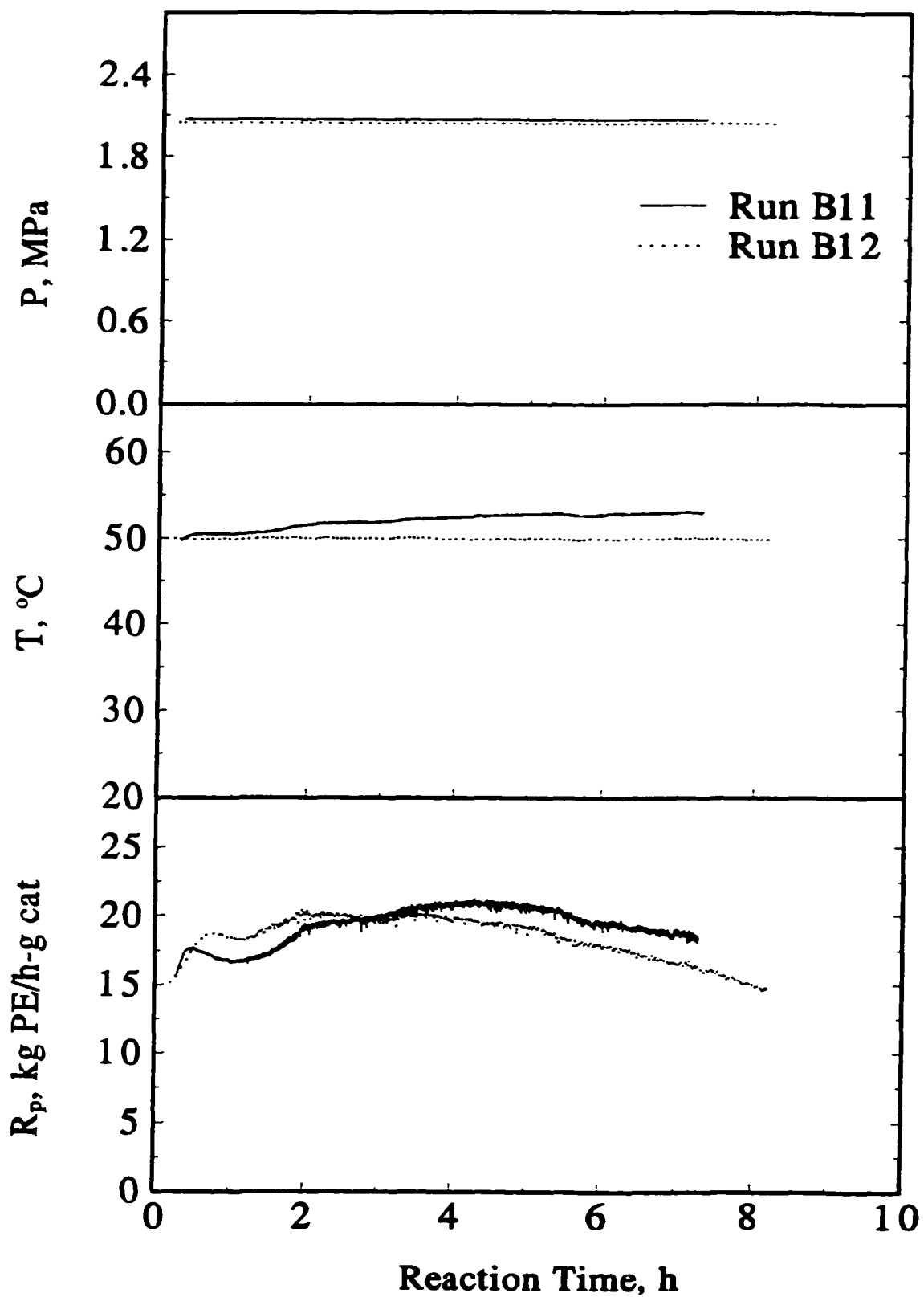
Figure 5.3 Profiles of ethylene pressure, temperature and rate at 50°C (Runs B11 and B12).

105
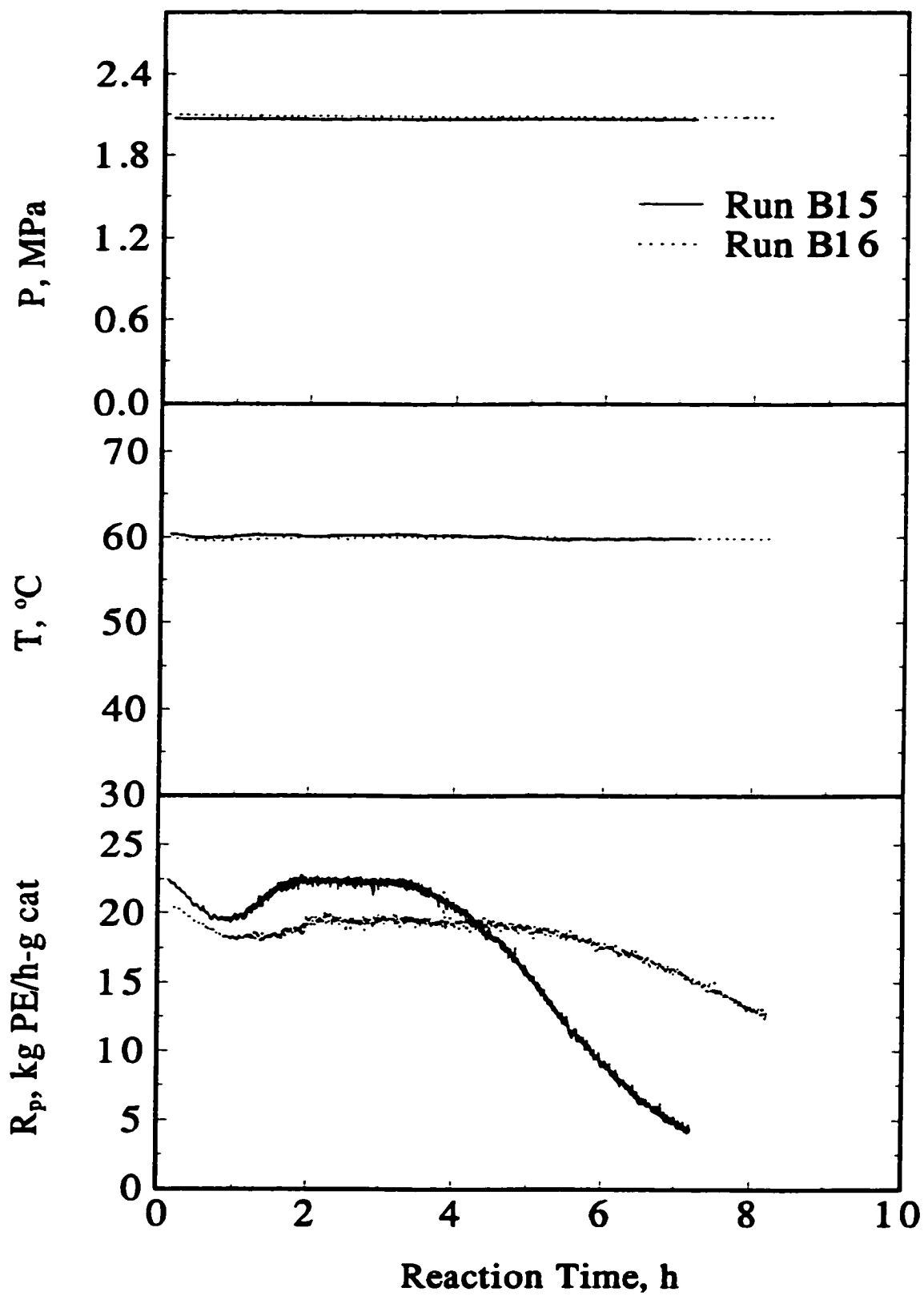
Figure 5.4 Profiles of ethylene pressure, temperature and rate at 60°C (Runs B15 and B16).
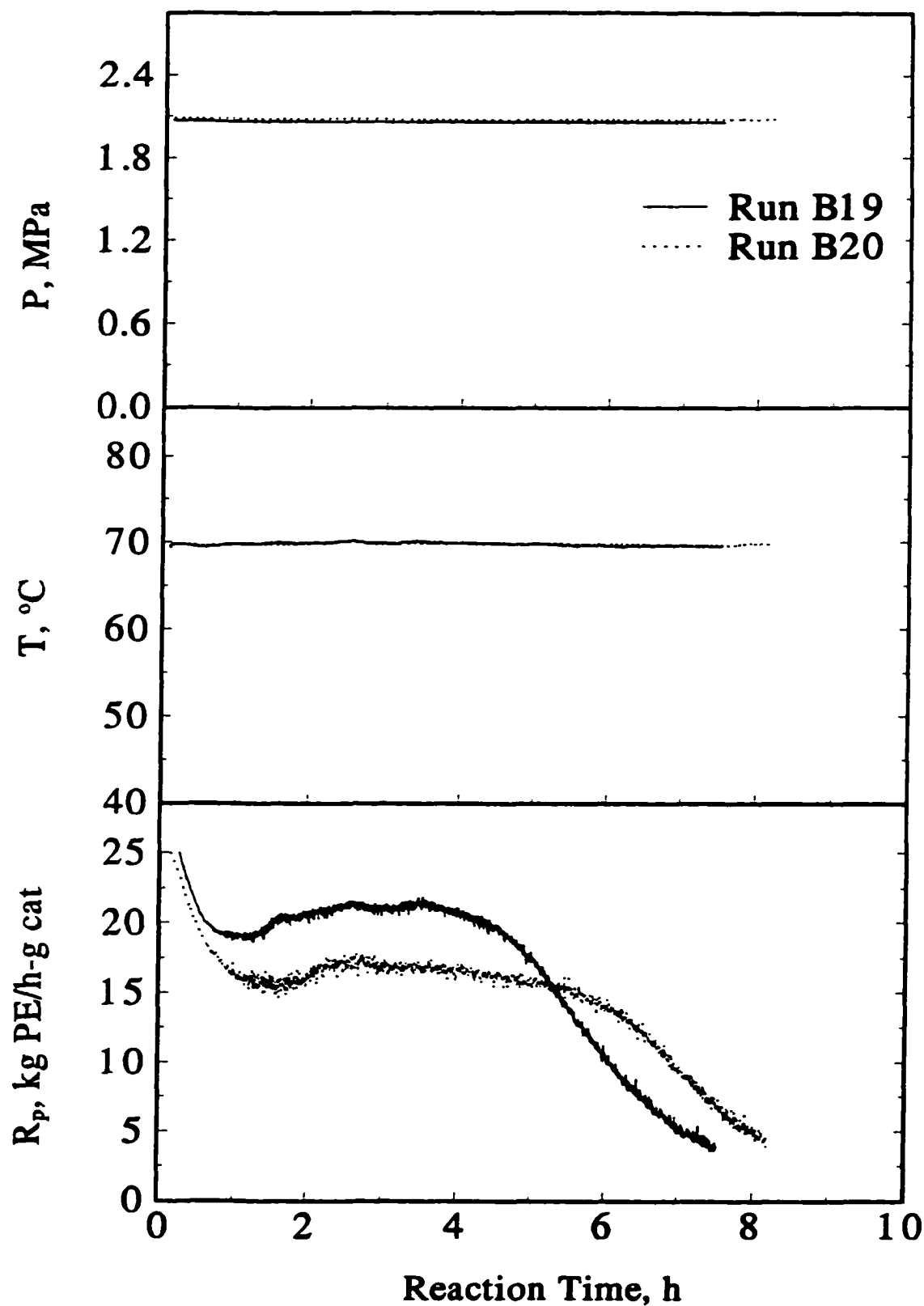
Figure 5.5 Profiles of ethylene pressure, temperature and rate at 70°C (Runs B19 and B20).

107

The results from Figures 5.4 and 5.5 indicate that the rate profiles at 60 and 70°C are not as reproducible as those at lower temperatures, especially the shape at the end of the polymerization rate profiles. The rate profiles in Figures 5.4 and 5.5 show that the initial activities are very high and the noticeable second peaks are developed after about 2 hours of polymerization; the higher initial rate appears to cause more rapid rate decay after the maximum of the second peak. High initial rate can lead to heat transfer limitations in the gas phase polymerization (Floyd *et al.*, 1987), and high polymerization temperature can cause rapid deactivation of Ziegler-Natta catalysts (Jejelowo *et al.*, 1991). Temperature effects on initial rate and catalyst deactivation will be quantitatively discussed in Chapter 8 by modeling the polymerization process.

It should be mentioned that the polymerization rates, as seen in Figures 5.1 to 5.5, changed significantly with time and polymerization conditions, such as ethylene pressure and polymerization temperature. Thus, if temperature in the outside oil bath was kept constant during a run, the temperature inside the reactor will change in response to the rate change since ethylene polymerization is exothermic. This temperature change can also cause irreproducibility of rate profiles (*e.g.*, Run B11 in Figure 5.3) because the rate profiles are temperature-dependent. For all the runs, except Run B11, reported in this chapter, the gas-phase temperature in the reactor during a run was well controlled with variations ± 0.5°C by frequent adjustment of the oil bath temperature.

5.3 Effects of Temperature on Rate Profiles

The polymerization conditions used to investigate the effects of temperature on rate

profiles are shown in Table 5.3. Only one of the repeat runs listed in Tables 5.1 and 5.2, the

one which had better temperature control is included in Table 5.3.

Table 5.3   Effects of Polymerization Conditions[1] on the Rate Profiles

Run No.	Amount of TEAL, mL	Prepolymerized Catalyst, mg	T, °C	$P_{C_2H_4}$, MPa	Time, h	Activity, kg PE/g Cat·h, (kg PE/mol Ti·h·MPa)
B1	0.30	95	30.1	0.68	8.08	1.02 (1,956)
B2	0.30	98	32.0	1.34	8.22	2.72 (2,635)
B4	0.30	48	30.0	2.09	8.18	3.17 (1,971)
B6	0.30	30	41.9	0.68	8.20	2.38 (4,563)
B7	0.30	99	41.6	1.34	8.18	6.36 (6,173)
B8	0.30	97	42.2	2.04	8.24	9.14 (5,809)
B9	0.30	85	50.1	0.67	8.23	3.20 (6,191)
B10	0.30	90	49.5	1.33	8.22	9.38 (9,124)
B12	0.30	50	50.0	2.05	8.20	17.66 (11,195)
B13	0.30	88	59.9	0.68	8.14	3.75 (7,199)
B14	0.30	46	59.2	1.34	8.16	10.63 (10,285)
B16	0.25	40	59.9	2.09	8.22	17.41 (10,811)
B17	0.30	63	68.7	0.67	8.07	2.99 (5,775)
B18	0.30	50	69.7	1.34	8.19	10.16 (9,810)
B19	0.30	50	69.8	2.06	7.52	16.28 (10,240)

Note:
1. The stirring speed of the reactor was 204 rpm, the seed bed was 100 g of NaCl, and no hydrogen was added in the reactor for all the runs.

109

The polymerization rate profiles, as a function of temperature, are shown in Figure 5.6 to 5.8 at a constant ethylene pressures of about 0.68, 1.34, and 2.07 MPa, respectively. The following observations are made from the results presented in Figures 5.6 to 5.8:

1. All the rate profiles show deactivation at longer times.

2. At temperatures $\leq 60°C$, the initial acceleration periods can be easily observed; at temperatures $\geq 60°C$, the initial rates decrease from the beginning of the runs.

3. At low temperatures and low ethylene pressures, the initial acceleration periods appear to be S-shaped.

4. At temperatures $\leq 40°C$, there is a single maximum in the rate profiles; at temperatures $\geq 40°C$, the rate profiles have two maxima (the two peaks will be referred to as the first peak and the second peak, respectively).

5. The first peaks shift from longer to shorter times and the second peaks become more pronounced with increasing temperature.

6. The second peaks are broader than the first peaks, and the second peak would not be observed if the polymerization run had been stopped at less than 2 hours.

7. The overall polymerization rate increased with increasing temperature up to 50 or 60°C and then decreased at higher temperatures.

An Arrhenius plot is frequently used to determine the temperature dependence of a reaction rate, *i.e.*, the activation energy of the reaction. The major sources of error in the results of the Arrhenius plot are the concentration measurements (Hill, 1977). The gas-phase ethylene concentration in the reactor, *[M]*, is calculated using the Peng-Robinson equation of state (Peng and Robinson, 1976). The Peng-Robinson equation was modified following the method by Bu *et al.* (1995): the constants in the definitions of $a(T_c)$ and $b(T_c)$ were changed from 0.45724 and 0.07780 to 0.408 and 0.070, respectively, so that the

110
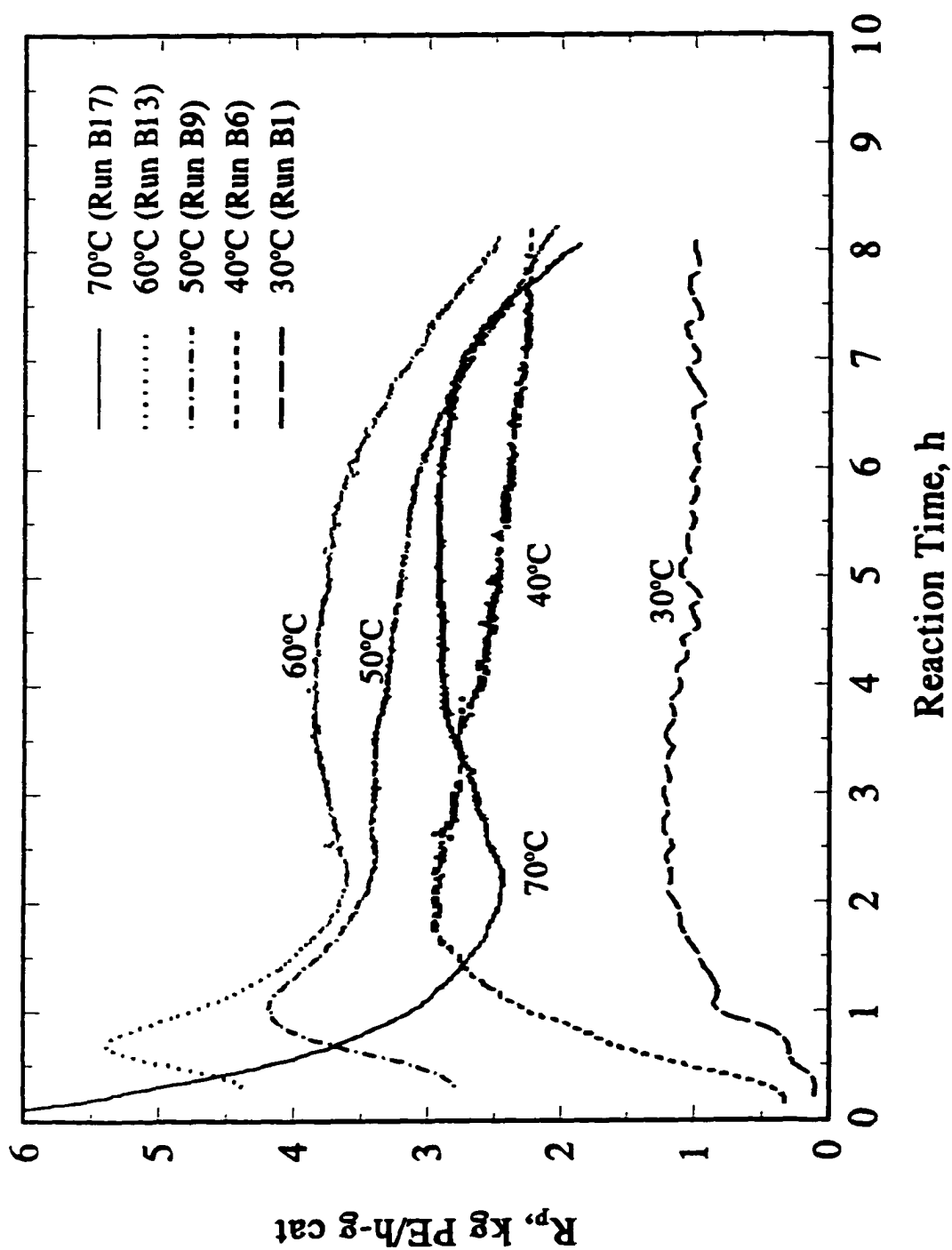
Figure 5.6 Temperature effects on rate profiles at $P_{C_3H_6}=0.68$ MPa.

111
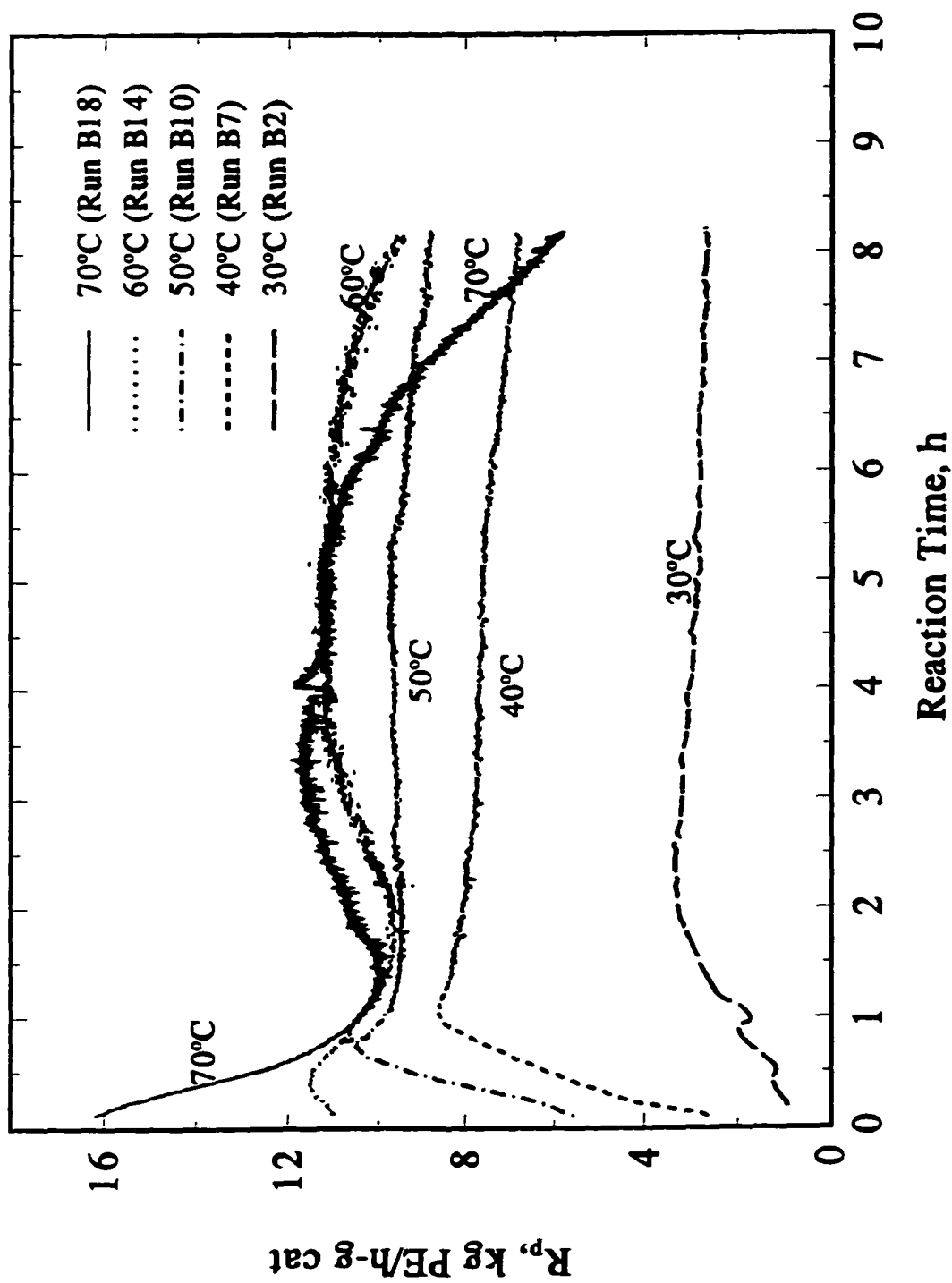
Figure 5.7 Temperature effects on rate profiles at $P_{C_2H_4}=1.34$ MPa.
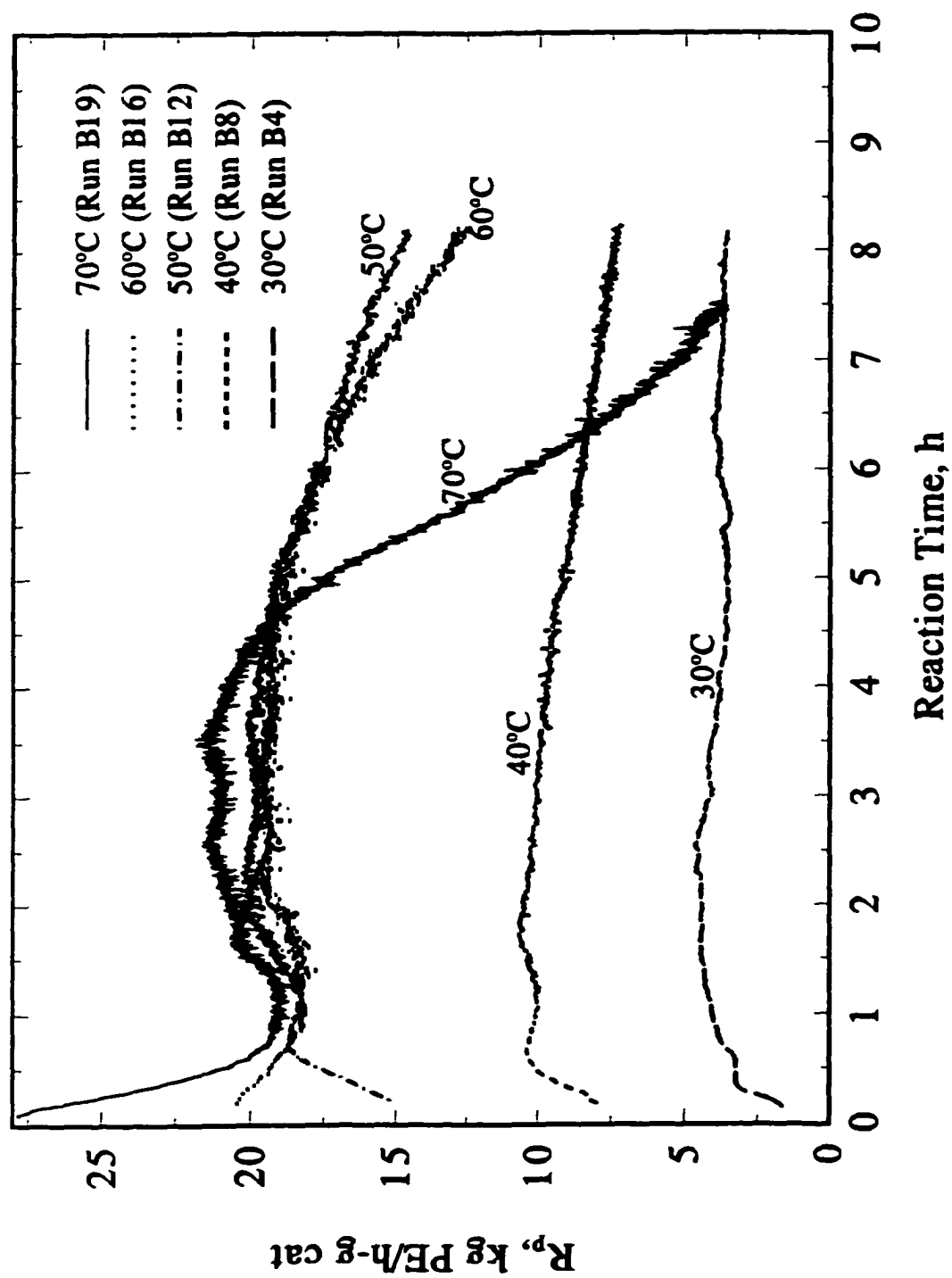
Figure 5.8 Temperature effects on rate profiles at $P_{C_2H_4}$=2.07 MPa.

predicted specific volumes of ethylene, at the conditions used in the experiments, were in better agreement (within 0.1%) with the values tabulated in the IUPAC ethylene tables (Jacobsen *et al.*, 1988).

The Arrhenius plot of the experimental results shown in Figure 5.6 is shown in Figure 5.9 by the solid circles and a solid line, in which the polymerization rate, R_p, is the average rate over the 8 hours of each run. It is seen from Figure 5.9 that the Arrhenius plot, with the rate normalized with respect to *[M]*, is not linear; but it has a maximum at 60°C. Similar temperature effects were reported by Dusseault and Hsu (1993), who observed a maximum in productivity at 55°C for gas-phase polymerization of ethylene using $MgCl_2$/ethylbenzoate/$TiCl_4$ + triethylaluminum catalyst at high Al/Ti ratio.

The appearance of a maximum in the Arrhenius plot (solid symbols in Figure 5.9) has been explained by the deactivation of catalytic sites at higher temperatures or by the sorption theory (Hutchinson and Ray, 1990). In the sorption theory, the polymerization rate is assumed to be proportional to the monomer concentration in the amorphous polymer around the surface of catalytic sites, not the bulk monomer concentration in the reactor. With increasing temperature, the extent of sorption decreases, which will lead to a decrease in the polymerization rate. The concentration of sorbed ethylene can be approximated by Henry's law according to Equation 5.1:

$$[M^*] = k_H P \tag{5.1}$$

where *[M*]* is ethylene concentration in the amorphous polymer; k_H is a Henry's law constant; and *P* is ethylene pressure in the reactor. The temperature effect on the Henry's

114
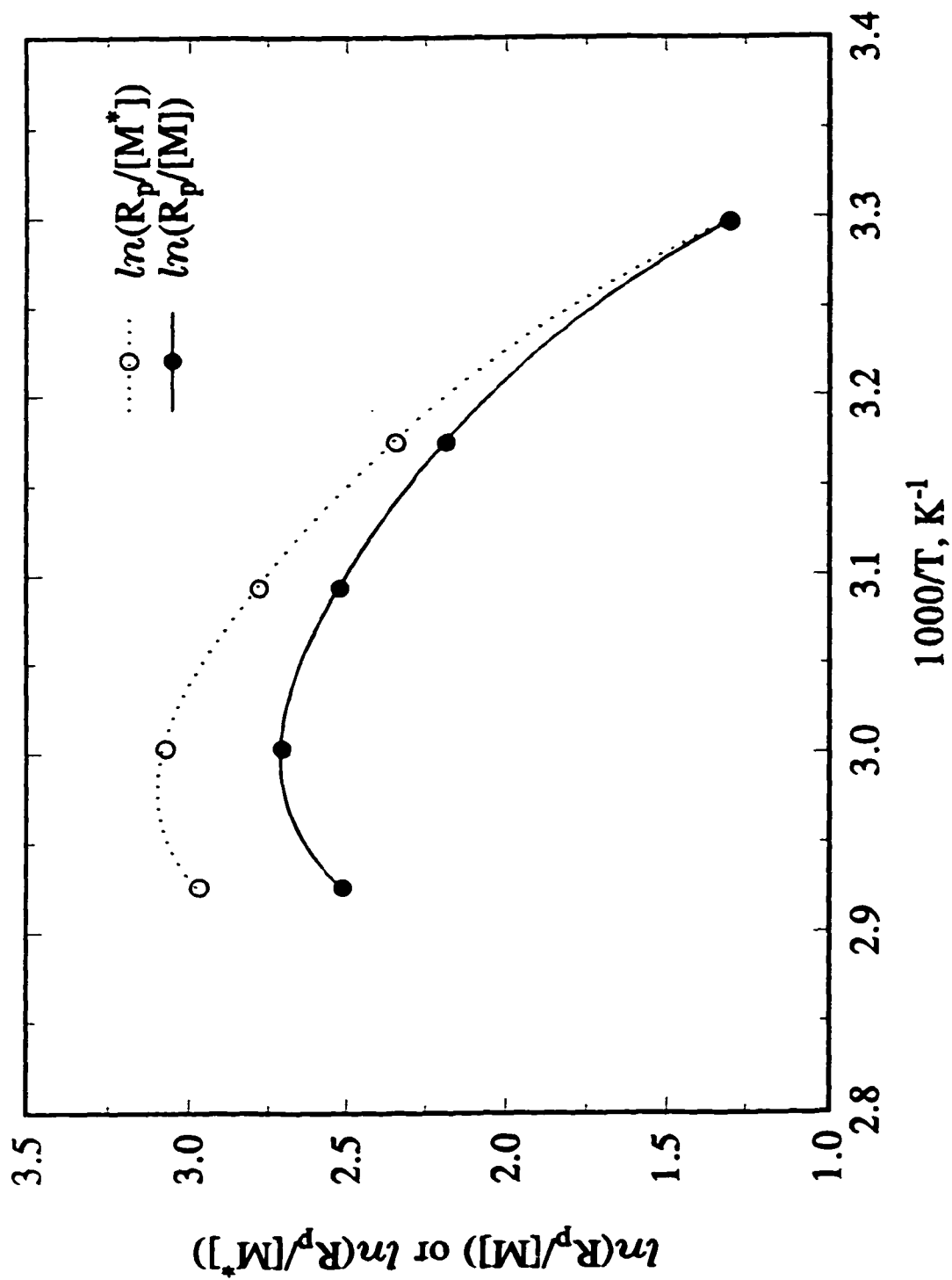
Figure 5.9 Arrhenius plot of average polymerization rate at $P_{C_3H_6}$=0.68 MPa.

law constant, k_H, for the sorption of ethylene in the polyethylene, has been correlated by Stern *et al.* (1969) to the following equation:

$$log(k_H) = -2.38 + 1.08(T_c / T)^2 \qquad (5.2)$$

where T_c is the critical temperature of ethylene. The Arrhenius plot, based on Equation 5.1 using relative ethylene concentration sorbed in polyethylene predicted by Equation 5.2 and normalized to 30°C, is also shown in Figure 5.9 by the open circles and a dotted line. It is seen in Figure 5.9 that sorption effects alone do not remove the maximum in the average polymerization rate as a function of temperature. Therefore, the low polymerization rate at high temperatures was mainly caused by catalyst deactivation (discussed in Section 5.2). The Arrhenius plots of the experimental results shown in Figures 5.7 and 5.8 lead to the same conclusions as those from Figure 5.9.

For the temperature effect on the rate profiles, the simulation results of the multigrain model (Floyd *et. al.*, 1987) predicts that the hybrid-type rate profile (*i.e.*, an initial accelerating period followed by deactivation) is the first telltale sign of the existence of mass transfer resistance; and if mass transfer is controlling, the first maximum in the rate will shift to the longer times with increasing polymerization temperatures. This is not the case seen in Figures 5.6 to 5.8, which shows that the rate profiles at low temperatures had a hybrid-type activity profile, and the maximum of the first peaks shit to lower times with increasing temperature. It is therefore concluded that mass transfer resistances were not responsible for the observed rate profiles and it is likely that mass transfer effects were negligible during gas-phase ethylene polymerization at the experimental conditions used.

116

It is worth noting that the shift of the first peaks from the right hand to the left hand side (or from longer to shorter time) with increasing temperature cannot be predicted by the multigrain model with a simple rate function. The shift of the peaks on the rate profiles, as well as other observations made in this section, is analyzed in Section 5.5.

5.4 Effects of Ethylene Pressure on Rate Profiles

In this section, rate profiles in Figures 5.6 to 5.8 of Section 5.3 shown for the temperature effect are rearranged to show the effects of ethylene pressure. The purpose of rearranging the same data by different sequences is to examine if the predictions of the multigrain model (Floyd *et al.*, 1987; Hutchinson *et al.*, 1992) are sufficient to determine the presence of mass transfer limitations in Ziegler-Natta olefin polymerizations.

Figures 5.10 shows the typical effect of ethylene pressure on rate profiles at a constant temperature of 60°C (the effects of ethylene pressure on rate profiles at temperatures of 30, 40, 50, and 70°C will be shown in Chapter 8 for the comparison of experimental results and modeling). In addition to the observations made from Figures 5.6 to 5.8 of Section 5.3, observations from the result of Figures 5.10 include: the first peaks shift from longer to shorter times, and the second peak becomes more pronounced with increasing ethylene pressure. The behavior of the rate profiles at temperatures of 30, 40, 50, and 70°C are similar.

The times needed for the first peaks to reach maximum, t_{max}, at different temperatures are summarized in Table 5.4 as a function of ethylene pressure. The values of t_{max} at 70°C are not listed in Table 5.4 because the maxima of the first peak at 70°C are close

117
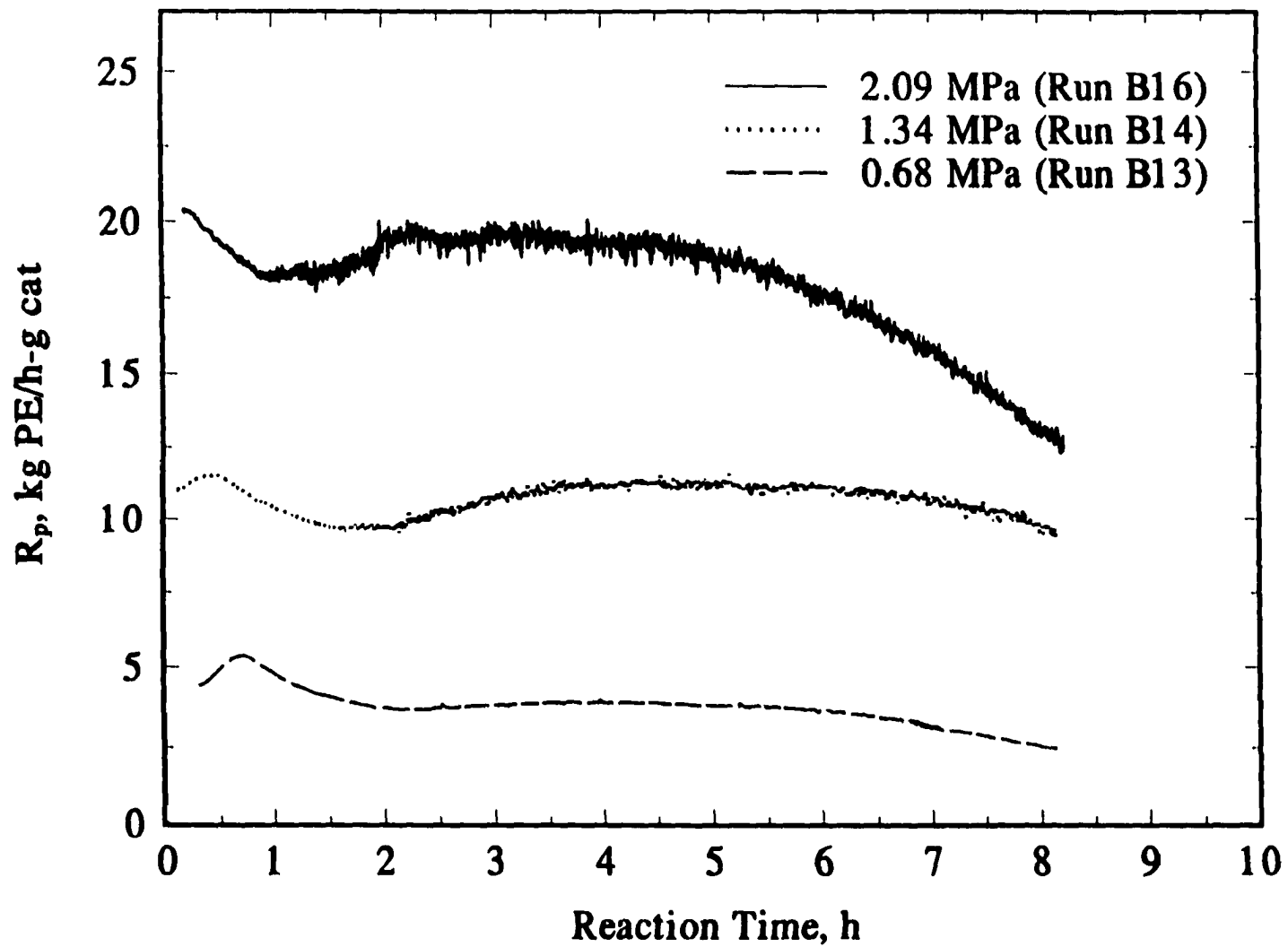
Figure 5.10   Effects of ethylene pressure on rate profiles at 60°C.

to the beginning of rate profiles (*i.e.*, $t_{max} \approx 0$) and cannot be clearly located due to the initial addition of ethylene into the reactor.

Table 5.4   Effect of Ethylene Pressure on the Maximum Position of the First Peak as a Function of Polymerization Temperature[1]

Ethylene Pressure, MPa	t_{max}, h			
	30°C	40°C	50°C	60°C
2.06	1.59	0.65	0.66	0.23
1.34	2.42	1.12	0.74	0.49
0.68	2.73	1.59	1.09	0.73

Note:
1. See Table 5.3 for polymerization conditions.

The observation that increases in ethylene pressure result in decreases in times required to achieve a maximum rate is in agreement with the predictions by the multigrain model (Hutchinson *et al.*, 1992) in the presence of mass transfer limitations. However, it should be recalled that the conclusion based on the effects of reaction temperature on the rate profiles with the same experimental data in Section 5.3 shows that the mass transfer limitations are not the cause of the observed rate profiles; *i.e.*, the multigrain model based on the first order kinetics and mass transfer limitations cannot be used to model the gas-phase polymerization of ethylene in the present study. The shift of the first-peak maximum observed in the rate profiles as a function of temperature and ethylene pressure will be accounted for by a reaction rate model proposed in Chapter 8. This proposed model is based on the reaction-kinetic interpretations of the rate profiles observed in this chapter and further discussions presented in Section 5.5.

119

5.5 Kinetic Interpretations of Rate Profiles

The shift of the first peak maximum from longer to shorter times in the polymerization rate profiles with increasing temperature can be explained by the requirement of an initiation step of catalytic sites by ethylene before chain propagation can occur. If the initiation step is activated, then the initiation rate constant would increase with an increase in polymerization temperature. At low temperature, the low initiation rate constant would result in a long accelerating period and at high temperature, the accelerating period would be short. In addidtion, the S-shaped initial acceleration period requires a two-step initiation reaction prior to chain propagation, as reviewed in Chapter 2.

The appearance of the second peaks implies the presence of the second type of catalytic site in this prepolymerized catalyst (Site 1 for the first peaks and Site 2 for the second peaks). The nature of these sites is not known, but it is unlikely that the different sites are due to Ti in different oxidation states since Chien *et al.* (1989) reported that the distribution of oxidation states of various active Ti does not change with time after 30 minutes of polymerization. As shown in Figures 5.6 to 5.8, the second peak appears much later than 30 minutes; hence, the change of oxidation states of Ti during polymerization was probably not the reason for the appearance of the second peak.

The observations on the relative broadness of the first and second peaks and the more pronounced second peaks with polymerization temperature and ethylene pressure have not been reported in the literature. The detailed information on catalyst deactivarion is not known. A kinetic model is need to determine if these observations are related to the

120

activation and deactivation steps for Site 1 and Site 2 in the polymerization. Such a kinetic

model will be presented in Chapter 8.

121

6. Kinetics of Gas-Phase Ethylene Homopolymerization[*]

Ethylene polymerization over heterogeneous Ziegler-Natta catalysts involves at least three simultaneous processes: mass transfer, activation-deactivation, and polymerization; these processes are not easily separated from each other. To study the kinetics of polymerization, it is desirable to eliminate mass transfer and activation-deactivation effects. Mass transfer effects can be minimized by appropriate catalyst preparation (*e.g.*, catalyst particle size and active site concentration) and reactor operating conditions. However, the activation-deactivation processes cannot be avoided for highly active, $MgCl_2$-supported $TiCl_4$ catalysts since they are an integral part of behavior of the catalysts.

In this chapter, the effects of mass and heat transfers on polymerization kinetics are examined, in Section 6.1, by changing the reactor conditions, and are further checked by measuring the polymer properties such as molar masses and polydispersity. In Section 6.2, a new experimental method is presented which allows the determination of the order of power-law rate function with respect to monomer concentration independently of activation-deactivation kinetics. The reproducibility of the experimental results in this chapter is addressed where applicable since Ziegler-Natta catalysis is one of the scientific areas where the reproduction of some experimental observation are very important (Kissin, 1985).

---

[*] A version of this chapter has been accepted for publication in *Macromolecules*.

122

6.1 Mass Transfer and Heat Transfer

The kinetic behavior can be affected by mass transfer resistances in such a way that monomer concentration gradients would be established around active sites as a function of time and position. The establishment of monomer concentration gradients around active sites would affect the shape of polymerization rate profiles and the properties of the polymer formed because the rate profiles (*e.g.*, see Section 5.3) and polymer properties (*e.g.*, see Section 7.4) are dependent on the monomer concentration, *i.e.*, ethylene pressure.

A well-defined transport resistance model, the multigrain model (Floyd *et. al.*, 1986 and 1987), described that mass transfer can occur at microparticle and macroparticle levels, and at the particle external boundary layer. This model predicts that reaction temperature, monomer pressure and catalyst particle size affect mass transfer resistance of monomer during polymerization. Increase in catalyst particle size and reaction temperature, and decreases in monomer pressure are predicted to increase mass transfer resistance. As mass transfer resistance increases, the molar masses of the polymer produced will decrease, and its polydispersity will increase. The heat transfer effects, predicted by the multigrain model, can be significant with increasing catalyst particle sizes.

In the current study, the effect of external mass transfer and heat transfer from the reactor was examined by changing reaction conditions, such as stirring speed and catalyst amount. The temperature in the reactor was well controlled for all the experiments. The results in Figure 6.1 shows that changing stirring speed from 204 to 500 rpm during a run did not increase the polymerization rate. Shown in Table 6.1 are the polymerization yields and bulk densities of polyethylene made at different amounts of prepolymerized catalyst.

123
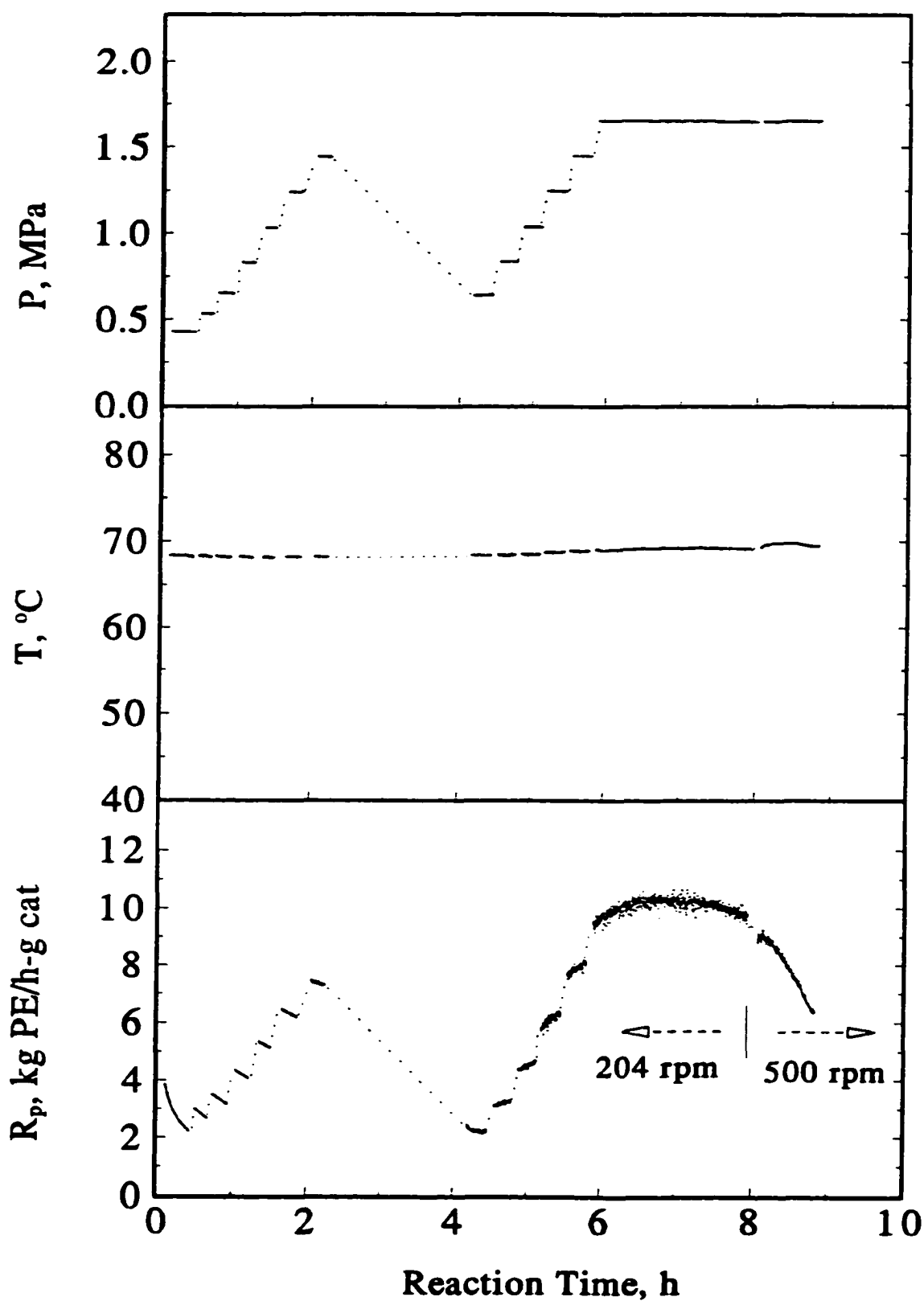
Figure 6.1   Effects of stirring speed on the rate profile   (Type C experiment).

124

and different seed beds It can be seen in Table 6.1 that the yield in Runs A1 and A2 does

not change with changes in the amount of prepolymerized catalysts from 45 (Run A1) to

200 mg (Run A2); this also indicates good reproducibility of experiments. Therefore, it can

be concluded that external mass and heat transfer resistances are negligible during

polymerization at the above conditions.

Table 6.1   Effect of the Amount of the Prepolymerized Catalyst on the Yield of Gas-
Phase Ethylene Homopolymerization[1]

Run No.	Seed Bed	Prepolymerized Catalyst, mg	P_{H_2}, MPa	$P_{C_2H_4}$, MPa	T, °C	Activity, kg PE/g Cat·h	Bulk density, g/cm^3
A1	NaCl 100 g	45	0.36	1.39	68.1	4.59	0.45
A2	Rulon[2] 35 g	200	0.31	1.37	70.5	4.96	0.45
A3	NaCl 100 g	63	0.35	0.69	67.9	1.19	0.42

Notes:

1. For the three runs, the stirring speed in the reactor was 204 rpm, 0.25 mL of
TEAL was used as a cocatalyst, and the polymerizations were carried out for 2
hours. The rate profiles of Runs A1 and A2 are shown in Appendix C.

2. The Rulon LR particles used in this run were about 2×2×2 mm by length.

Using morphology-controlled catalyst, the properties of polyethylene, such as molar

masses, can be measured as a function of polymer granule size. In a single polymerization

run, larger catalyst particles should grow to larger polymer granules if all the catalyst

particles have equal specific activity. Large polymer granules are more likely subjected to

internal mass and heat transfer resistances during polymerization than small particles,

especially under conditions of high temperature and low ethylene pressure. Internal mass

and heat transfer resistances should affect average molar masses as well as polydispersity.

125

Large polymer granules are also more likely subjected to internal heat transfer resistances during polymerization than the small granules (Floyd *et al.*, 1986b). Under the effects of heat transfer resistances, the temperature of large granules will be higher than that of small granules. The effect of polymerization temperature on molar masses and polydispersity of polyethylene produced in the gas phase of this study showed that increases in temperature caused decreases in the molar masses and an increase in polydispersity in the presence of hydrogen (see Chapter 7). Similar observation was made by Jejelowo *et al.* (1991) for gas-phase operation with decay-type rate profiles in the absence of hydrogen.

In this study, molar masses were measured by SEC as a function of polyethylene granule size. The polymer granules from a single run (Run A3 in Table 6.1) were manually sorted into seven sets of sizes as shown in Figure 6.2 (this procedure is described in Section 7.3). To make the SEC measurement of molar masses more reliable, hydrogen was added into the reactor to lower molar masses of polyethylene, and each sample was measured twice. The dependencies of number-average molar mass (M_n), weight-average molar mass (M_w), and polydispersity (Q) on the sizes of polyethylene granules shown in Figure 6.2 are plotted in Figure 6.3. The solid symbols were the average values of two measurements and the lines are linear regression lines. The results in Figure 6.3 show that molar masses and polydispersity are essentially independent of polymer granule sizes; this implies that internal mass transfer and heat transfer resistances are not significant at the experimental conditions used. Thus, it can be inferred that there are negligible effects of mass transfer and heat transfer in ethylene homopolymerization using the prepolymerized catalyst at any ethylene pressure above 0.69 MPa and at any polymerization temperature below 70°C.

126
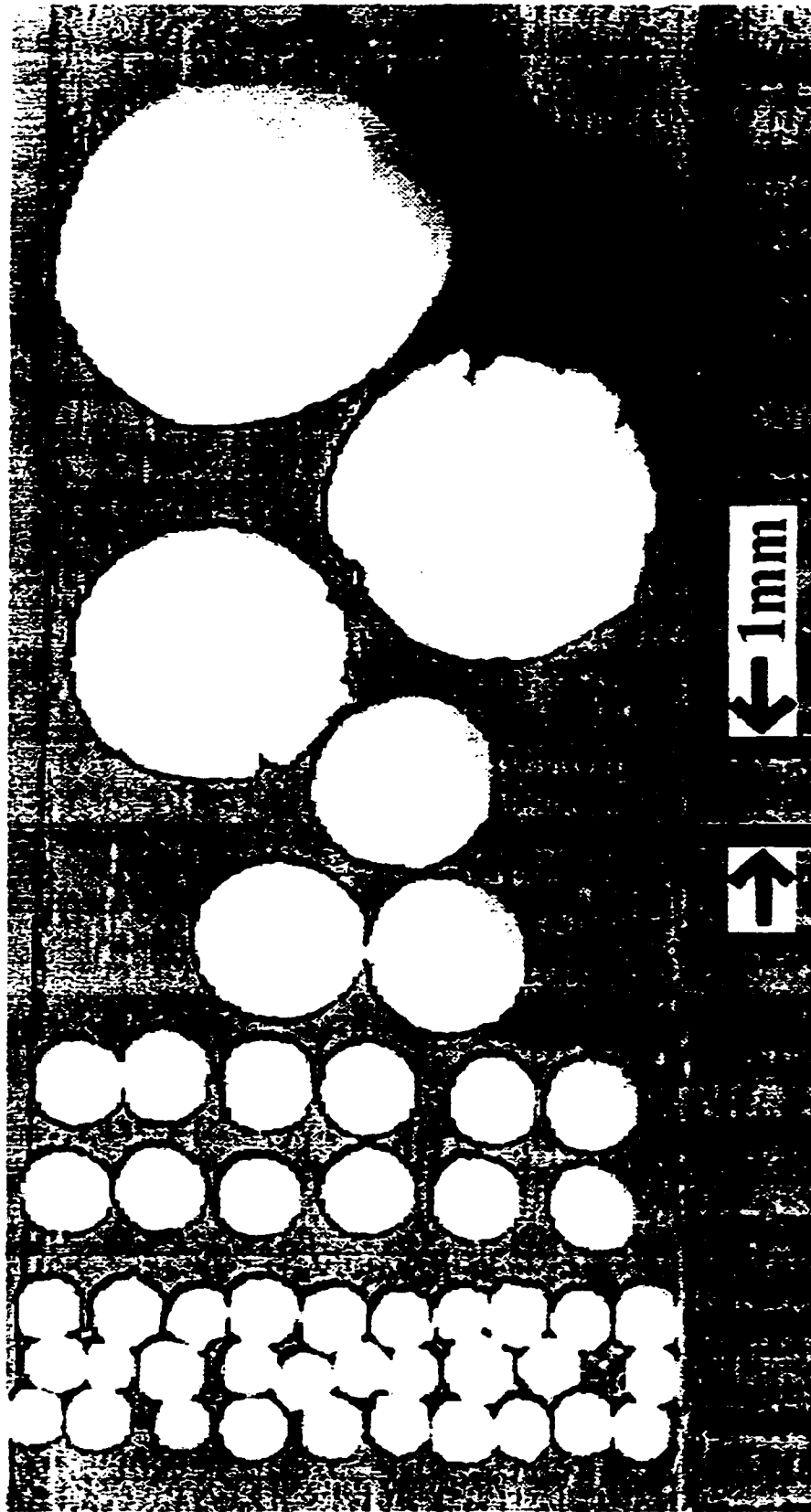
Figure 6.2 Optical micrograph of different sizes of polyethylene granules used for molar mass measurement.

127
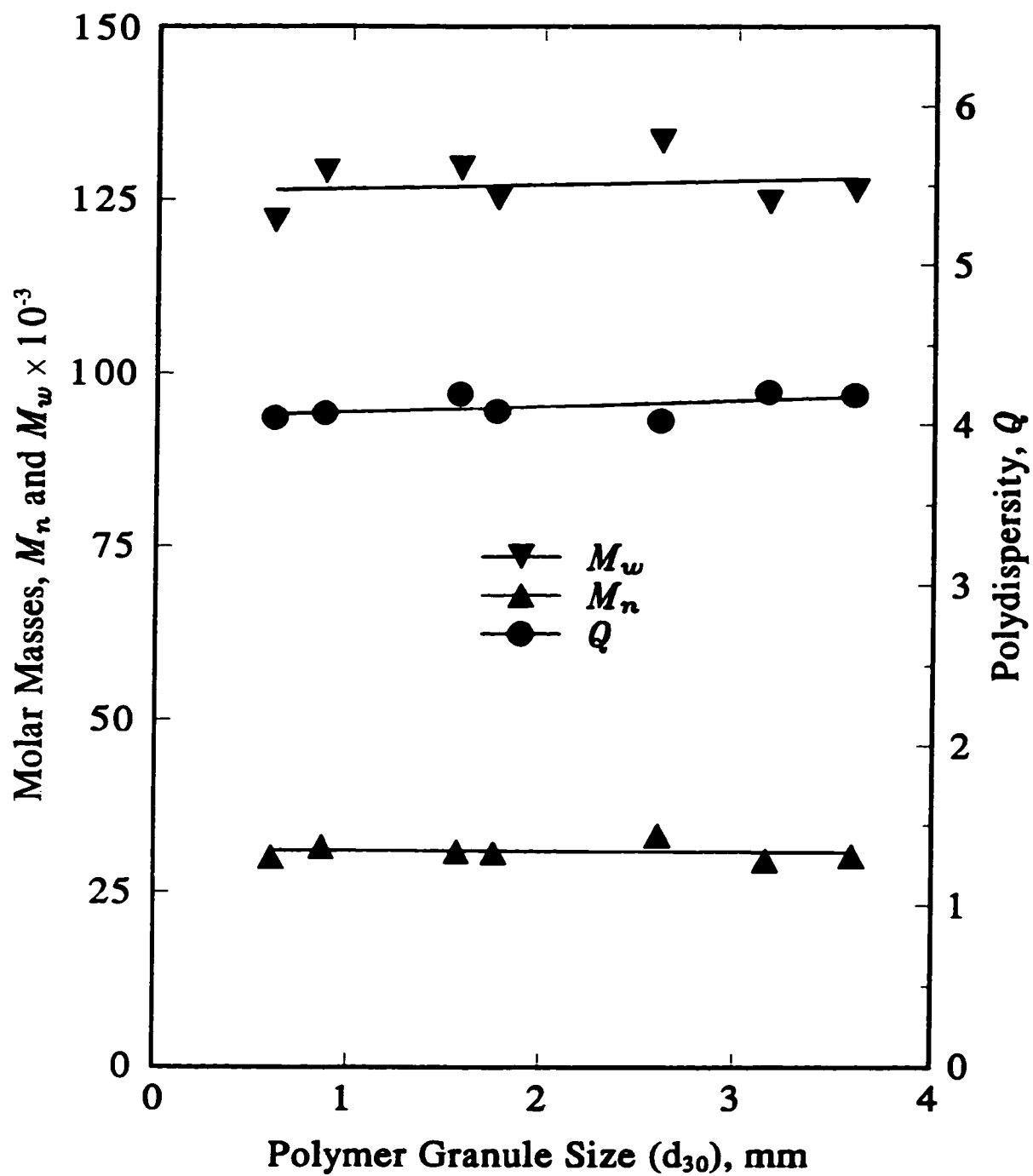
Figure 6.3   Dependence of molar masses and polydispersity on the size of polyethylene granules (Run A3).

6.2 Power-Law Order with respect to Ethylene Concentration

Fitting the overall rate of polymerization R_p on ethylene concentration *[M]* at a constant temperature for Ziegler-Natta ethylene homopolymerization by a power-law rate function has yielded a range of power-law orders with respect to ethylene concentration. For a $SiO_2/MgCl_2$ supported $TiCl_4$ catalyst with constant polymerization rate, power-law orders have been reported from less than unity to 1.5 at temperature range of 30 to 70°C (Bu *et al.*, 1995) and from 1.5 to 1.6 at temperature range of 80 to 90°C (Kissin, 1989).

Kinetic analysis of most ethylene polymerization is complicated by catalyst deactivation and the possible presence of mass and heat transfer effects. It has been shown in Section 6.1 that mass transfer and heat transfer effects were not significant in the current study. Hence, the rates of polymerization measured in this study are intrinsic rates; however, the concentration of active sites, *[C*]*, is a function of time due to catalyst activation and deactivation. A simple power-law rate expression, as a function of ethylene concentration (*[M]*) and active site concentration (*[C*]*), for this case is given by Equation 6.1

$$R_p = k[M]^n [C * (t)] \tag{6.1}$$

The usual method of estimating values of the power-law order *n* for deactivating systems is to decouple the polymerization kinetics from the deactivation kinetics by assuming a functional dependence for *[C*]* (*e.g.*, Doi *et al.*, 1982) and then fitting the measured rates to the combined polymerization activation-deactivation model. At times a simple power-law rate function is used to fit polymerization rate data without separating polymerization and activation-deactivation kinetics (Han-Adebekun and Ray, 1997). In an

129

attempt to experimentally decouple the polymerization kinetics from the activation-deactivation kinetics, the rates of polymerization were measured at two different ethylene concentrations at approximately the same time. This was done by changing the ethylene pressure in the reactor rapidly (Type C experiments), and then extrapolating the rate of polymerization at the new ethylene pressure to the time at which the pressure change was made. This procedure is illustrated in Figure 6.4 (the data in Figure 6.4 is the same as the bottom panel of Figure 6.1; the pressure and temperature histories for the rate shown in Figure 6.4 are given in Figure 6.1).

Applying Equation 6.1 at a time, t_i, at which the ethylene concentration was changed from $[M]_1$ to $[M]_2$, yields

$$R_{p,1}(t_i) = k[M]_1^n [C * (t_i)]$$ (6.2)

$$R_{p,2}(t_i) = k[M]_2^n [C * (t_i)]$$ (6.3)

Taking the ratio of Equation 6.3 to Equation 6.2 and solving for n yields

$$n = \frac{ln(R_{p,2}/R_{p,1})}{ln([M]_2/[M]_1)}$$ (6.4)

The power-law reaction order, n, can be calculated directly from Equation 6.4 without making any assumption about the activation-deactivation kinetics.

The same procedure was applied to polymerization runs at different temperatures from 30 to 69°C. At each temperature of 30, 40, 50, 60, and 69°C, two runs were done so
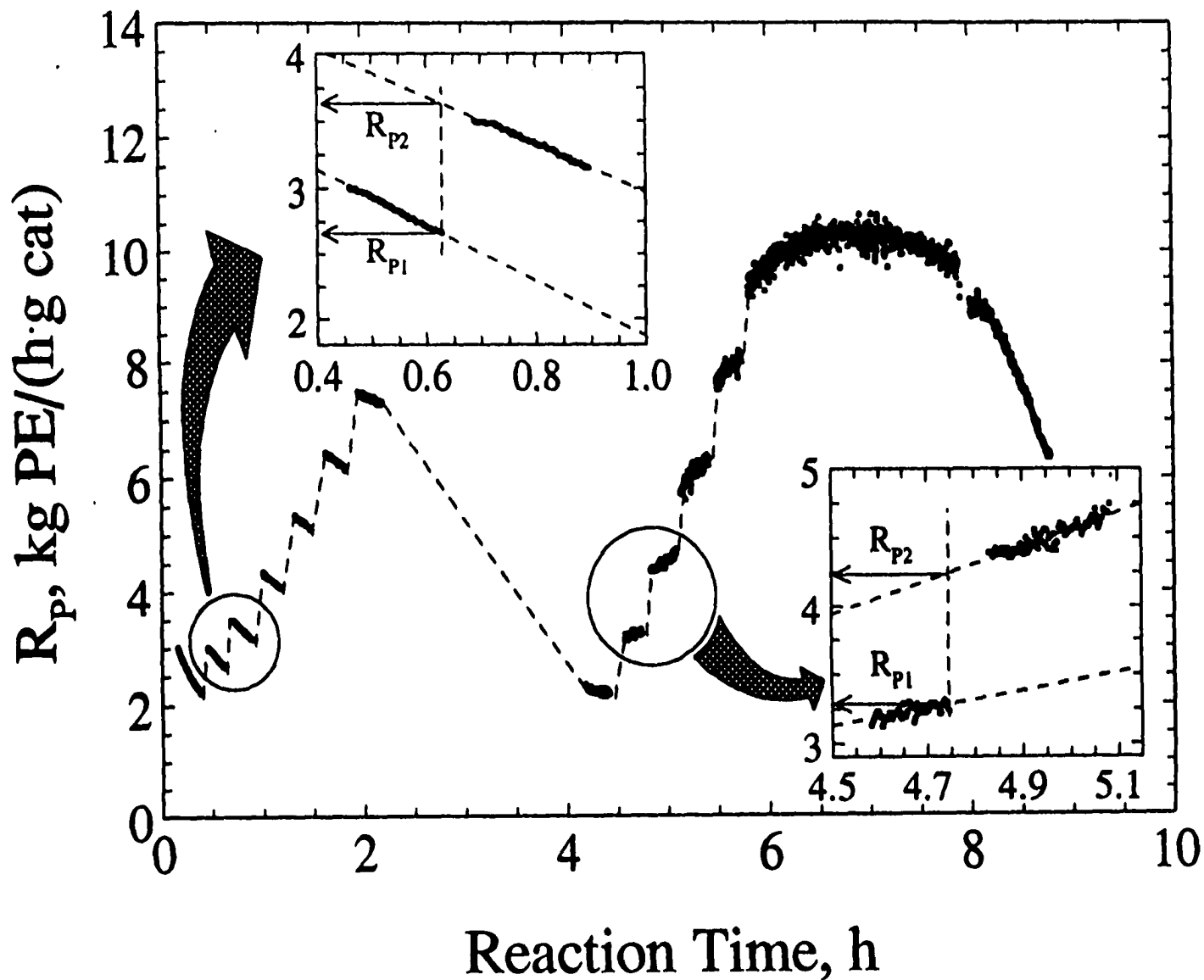
Figure 6.4 Illustration of obtaining $R_{p,1}(t_i)$ and $R_{p,2}(t_i)$ at a specific time t_i for Equation 6.4 with the change of ethylene pressure by extrapolation of polymerization rate profiles in a typical Type C experiment.

that the reproducibility of the experiments can be examined. Table 6.2 shows polymerization conditions of these runs.

Table 6.2   Run Conditions[1] for the Kinetics of Gas-Phase Ethylene Homopolymerization

Run No.	T, °C	Seed Bed NaCl, g	Amount of TEAL, mL	Prepolymerized Catalyst, mg	Range of Ethylene Pressure, MPa
C1-a	31.5	100	0.30	94	0.38 - 1.59
C1-b	31.3				0.86 - 1.99
C2-a	29.9	100	0.30	108	0.35 - 1.77
C2-b	30.2				0.97 - 1.98
C3-a	39.2	100	0.30	103	0.53 - 1.39
C3-b	39.6				0.55 - 1.37
C4-a	40.2	100	0.30	90	0.34 - 1.55
C4-b	40.6				0.55 - 1.55
C5-a	49.8	100	0.30	95	0.35 - 1.36
C5-b	50.2				0.37 - 1.35
C6-a	50.0	100	0.30	84	0.34 - 1.35
C6-b	50.4				0.39 - 1.35
C7-a	59.5	100	0.30	96	0.35 - 1.35
C7-b	60.2				0.36 - 1.36
C8-a	59.8	100	0.30	90	0.33 - 1.35
C8-b	60.1				0.34 - 1.35
C9-a	69.3	200	0.35	80	0.34 - 1.27
C9-b	69.6				0.54 - 1.28
C10-a	68.4	100	0.30	94	0.34 - 1.36
C10-b	68.7				0.55 - 1.56

Note:

1. The stirring speed of the reactor was 204 rpm, and no hydrogen was added in the reactor for all the runs.

132

Values of *n*, the power-law reaction orders calculated according to Equation 6.4, were a function of time-on-stream; values of *n* as a function of time-on-stream are shown in Figures 6.5 to 6.9 for temperatures of 30, 40, 50, 60, and 69°C. The ethylene concentrations were calculated by the Peng-Robinson equation, as modified in Section 5.2. At every temperature, the reproducibility for the repeat runs was very good, as shown by the clustering of the different symbols in Figures 6.5 to 6.9 (Runs C1 to C10, Table 6.2).

From Figures 6.5 to 6.9, it is clearly shown that the values of *n*, the power-law orders with respect to ethylene concentration, change with polymerization time, generally from about 1.5 for the first 2 to 3 hours to a constant level after about 2 to 3 hours of polymerization, regardless of the ethylene concentration. Values of the power-law order *n* obtained from Figures 6.5 to 6.9 are summarized in Table 6.3. It is seen from Table 6.3 that the constant values of *n* after 2 to 3 hours of polymerization tend to be slightly less than unity at lower temperatures, and slightly above unity at higher temperatures.

The above method of obtaining apparent orders of reaction with respect to monomer concentration results in significantly different reaction orders than those obtained by direct fitting of rate data by a power-law rate function which ignores the changes in active site concentration with time, *i.e.*,

$$R_p = k' [M]^{n'} \tag{6.5}$$

where k' is the apparent rate constant which includes the active site concentration, and n' is the apparent reaction order. [Note: k in Equation 6.4 does not include the active site concentration.]

133
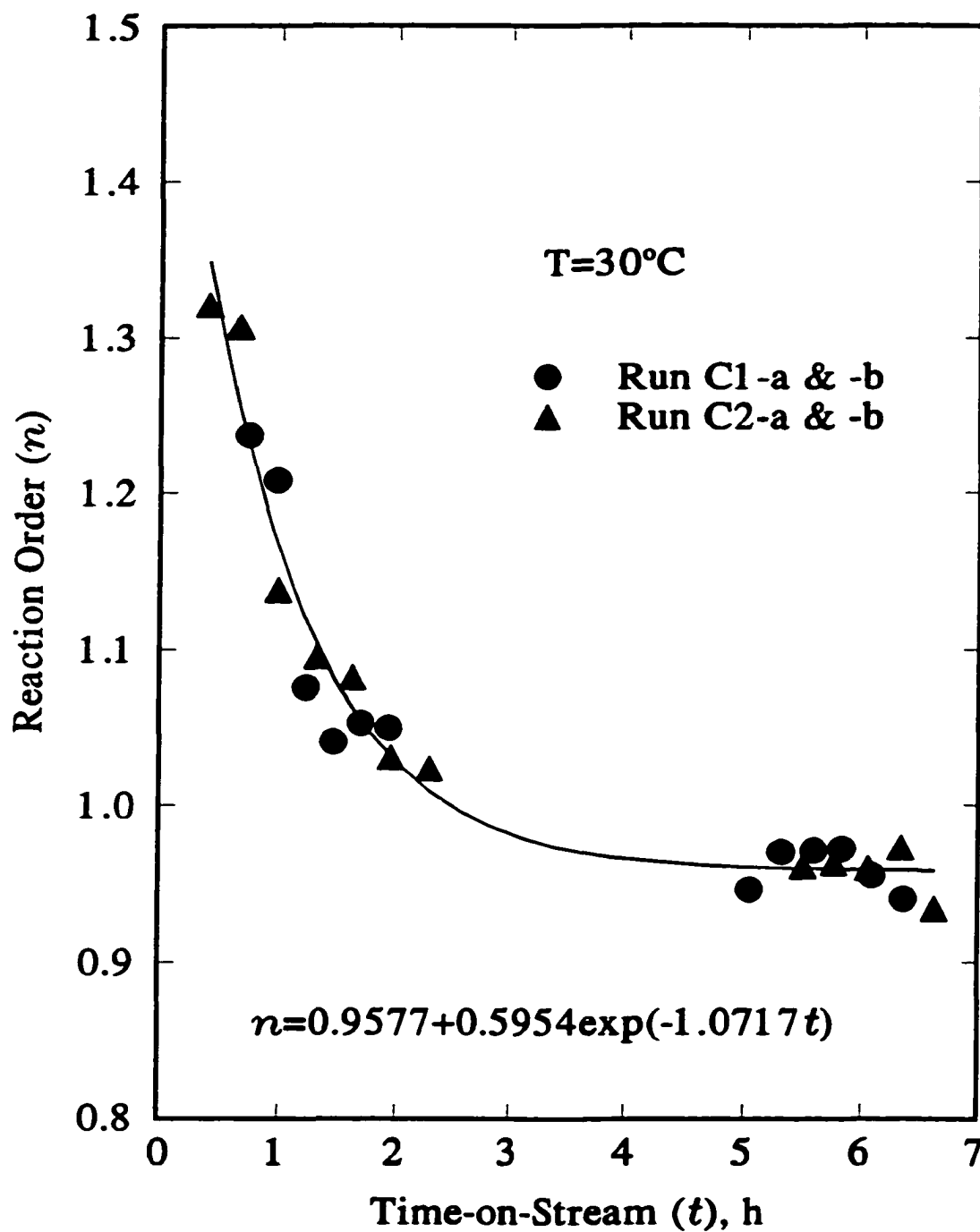
Figure 6.5 Dependence of power-law order n on time at polymerization temperature of 30°C.
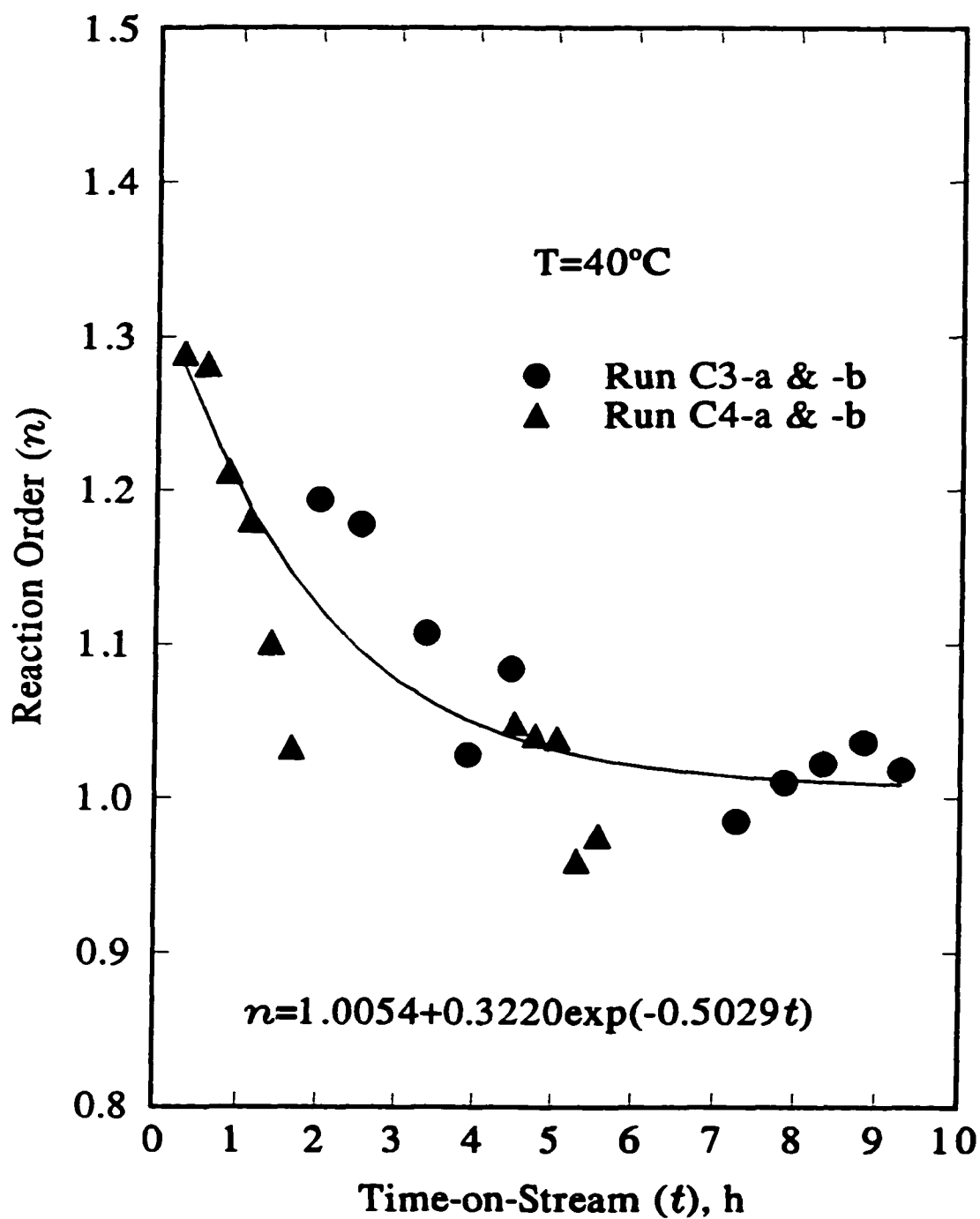
Figure 6.6 Dependence of power-law order n on time at polymerization temperature of 40°C.

135
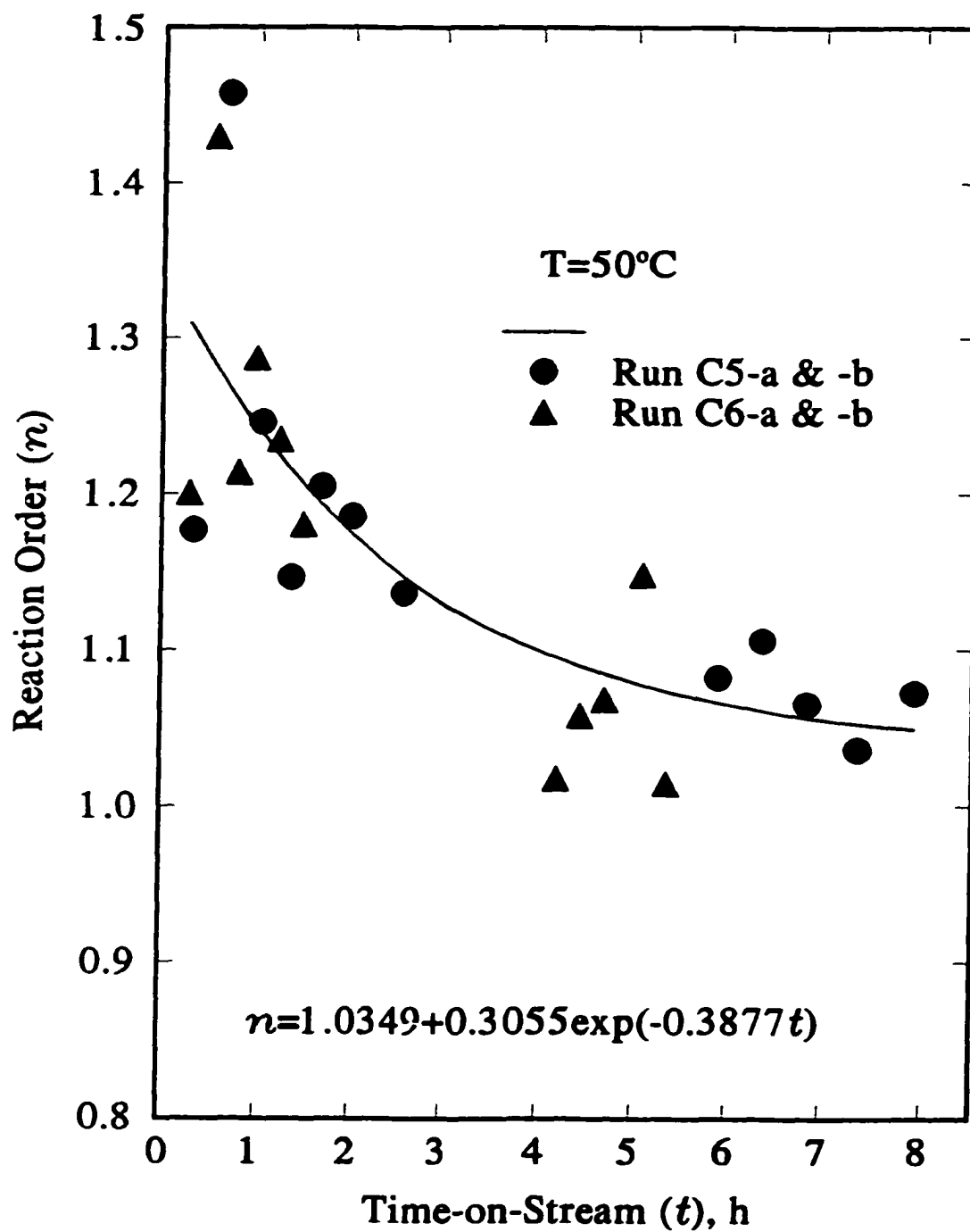
Figure 6.7   Dependence of power-law order n on time at polymerization temperature of 50°C.

136
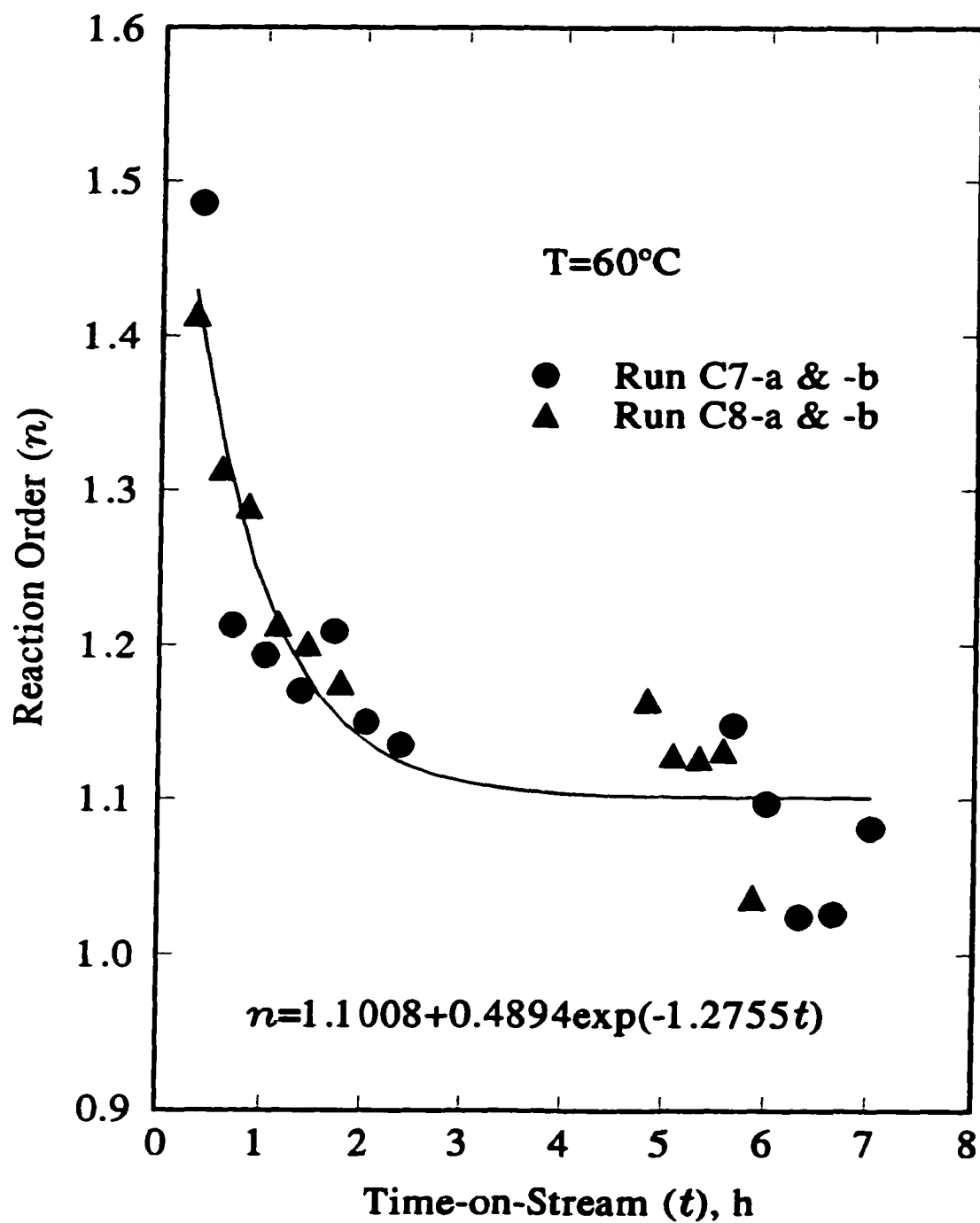
Figure 6.8 Dependence of power-law order n on time at polymerization temperature of 60°C.

137
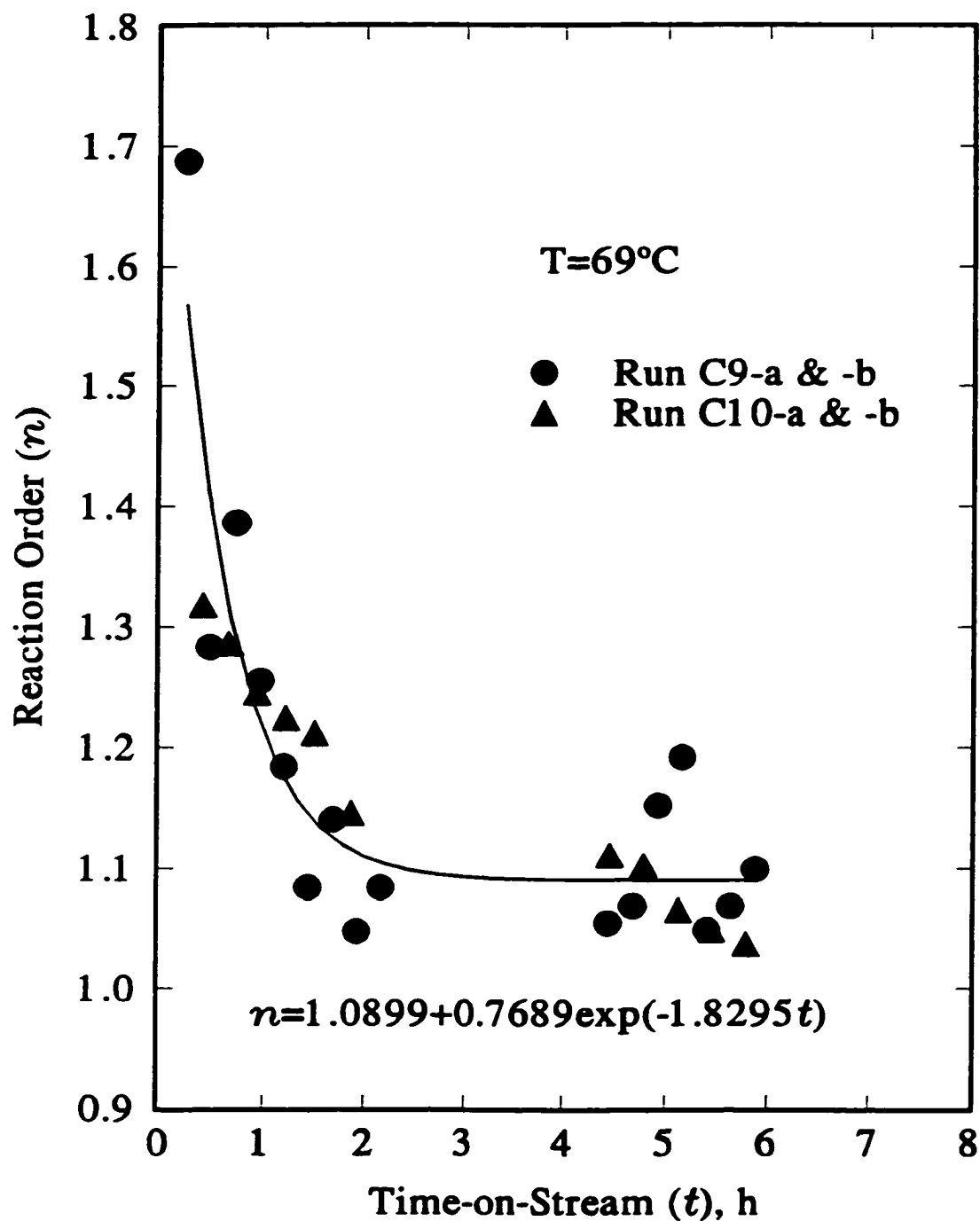
Figure 6.9   Dependence of power-law order n on time at polymerization
temperature of 69°C.

Values of n' can be obtained by fitting the rate dependence on ethylene concentration to Equation 6.5. Figures 6.10 to 6.14 show the fits for all the runs (Runs C1 to C10), in which the data for each run were split into two regions: short time-on-stream region (typically 0 to 2 h) and long time-on-stream region (typically 4 to 7 h). The short and long time-on-stream regions can be readily identified in Figures 6.5 to 6.9. The resulting equations by the fitting are also shown in Figures 6.10 to 6.14 for the two regions.

Reaction orders obtained from Equations 6.4 and 6.5 are compared in Table 6.3. The values of n in Table 6.3 were taken from the regression lines shown in Figures 6.5 to 6.9. These regression lines can provide information on the change of power-law orders with time-on-stream; the regression equations shown in Figures 6.5 to 6.9 do not have to have kinetic meaning as far as the kinetic-reaction model proposed in Chapter 8 is concerned.

Table 6.3   Comparison of Power-Law Orders Obtained by Equations 6.4 and 6.5

Run No.	Temperature, °C	Values of Power-Law Orders			
		n (based on Equation 6.4)		n' (based on Equation 6.5)	
		0 - 2 hours	4 - 7 hours	0 - 2 hours	4 - 7 hours
C1	31.4	1.30 to 1.03	0.96	1.15	0.93
C2	30.0			1.17	0.87
C3	39.4	1.30 to 1.12	1.00	1.07	1.03
C4	40.3			1.24	1.05
C5	50.1	1.45 to 1.14	1.04	1.11	1.20
C6	50.2			1.21	1.21
C7	59.9	1.50 to 1.15	1.10	0.92	1.19
C8	60.0			0.95	1.22
C9	69.5	1.70 to 1.10	1.10	0.65	1.10
C10	68.6			0.86	1.38
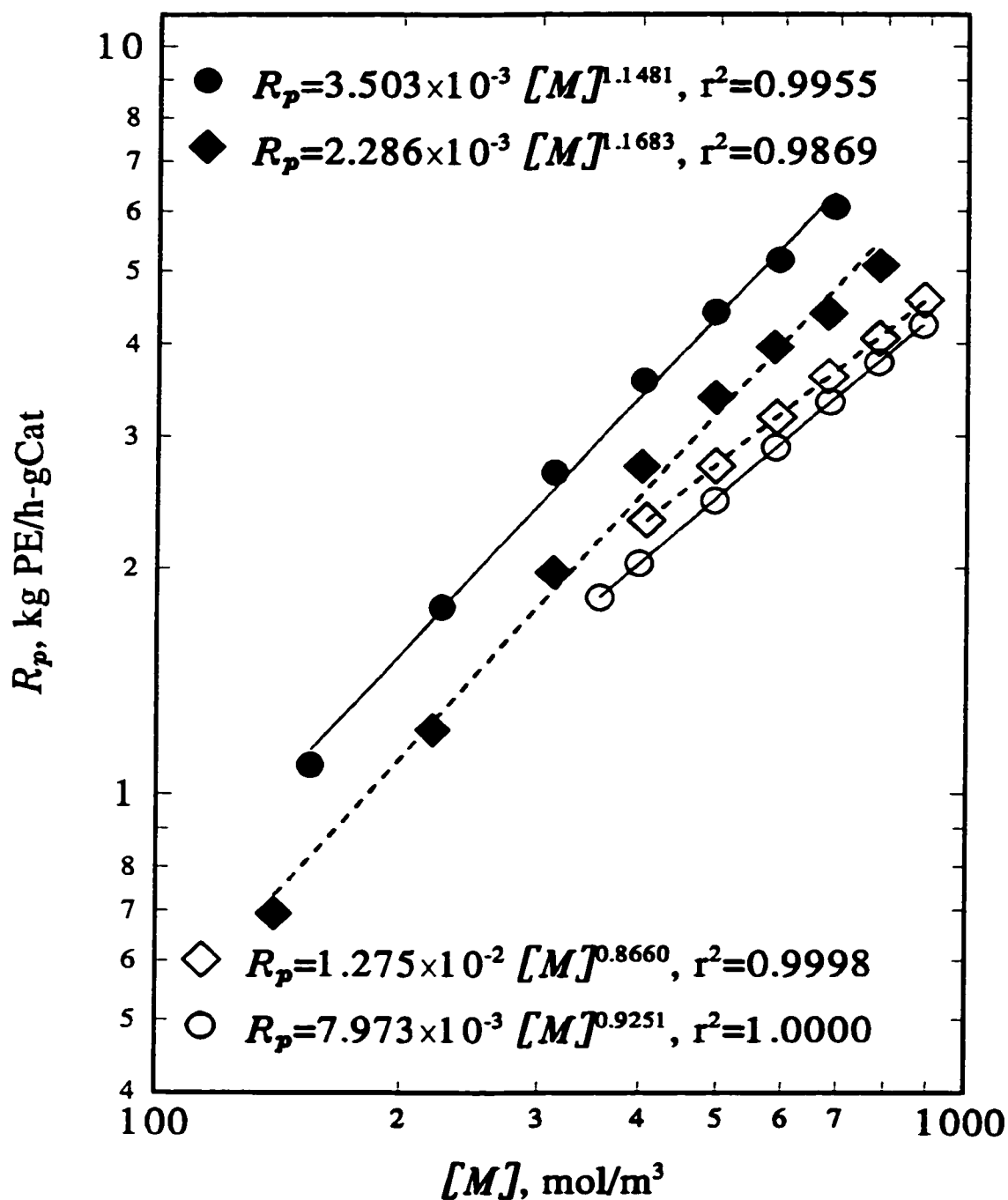
Figure 6.10 Log-log plot of R_p versus [M] by Equation 6.5 for Runs C1 (solid regression lines) and C2 (dash regression lines) at the beginning of run (solid symbols) and the end of run (open symbols) at 30°C.
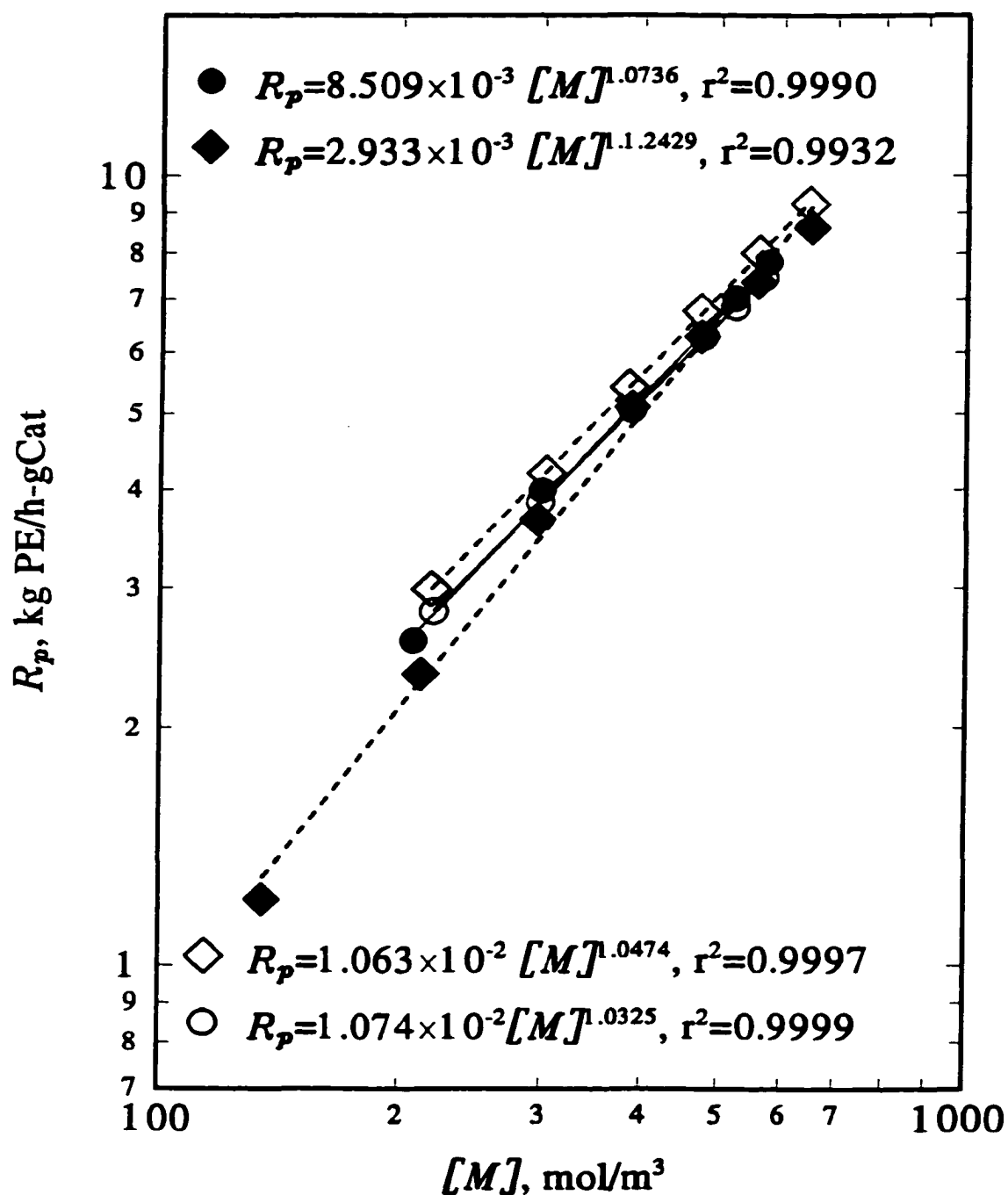
Figure 6.11 Log-log plot of R_p versus [M] by Equation 6.5 for Runs C3 (solid regression lines) and C4 (dash regression lines) at the beginning of run (solid symbols) and the end of run (open symbols) at 40°C.
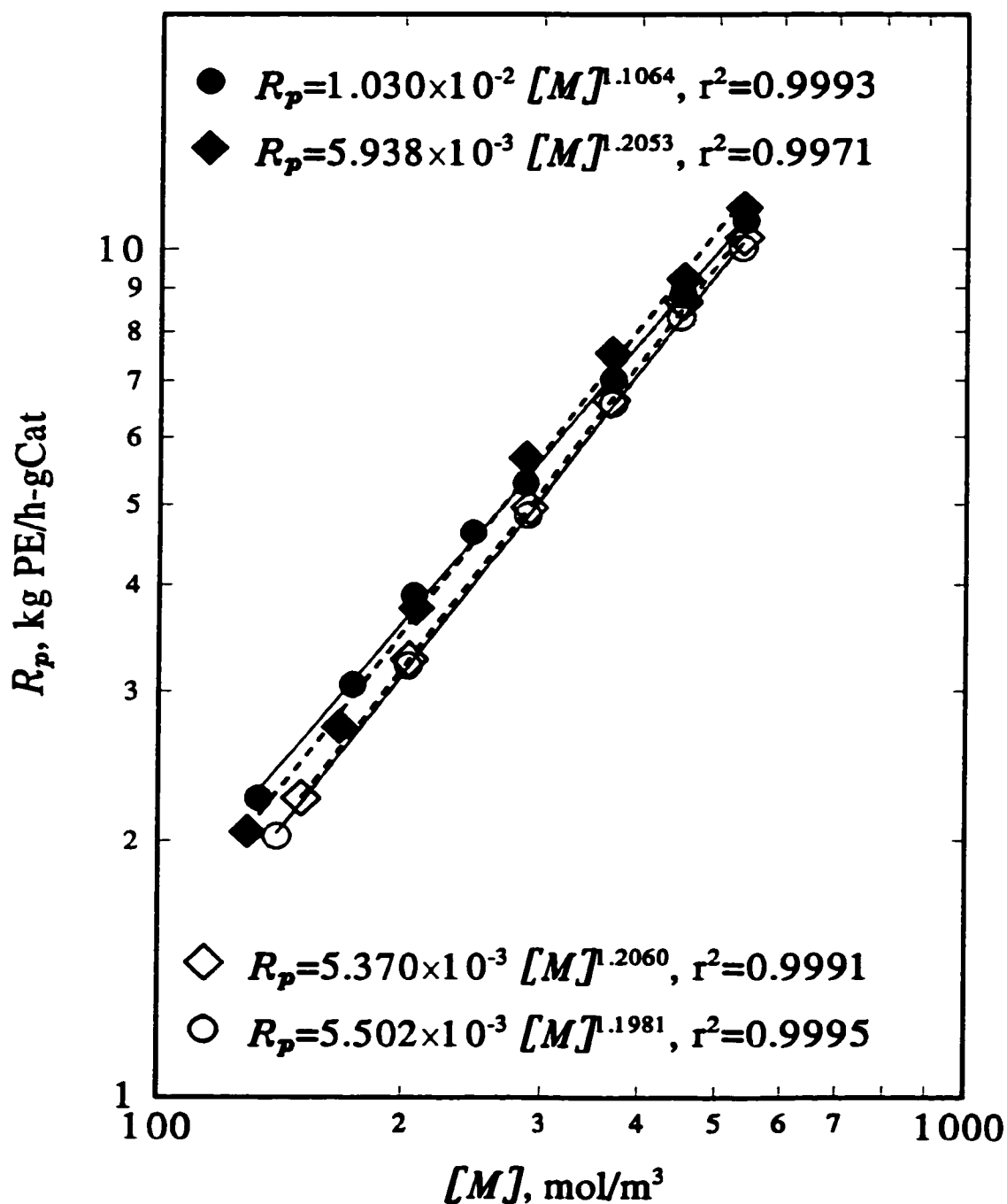
Figure 6.12 **Log-log plot of R_p versus [M] by Equation 6.5 for Runs C5 (solid regression lines) and C6 (dash regression lines) at the beginning of run (solid symbols) and the end of run (open symbols) at 50°C.**
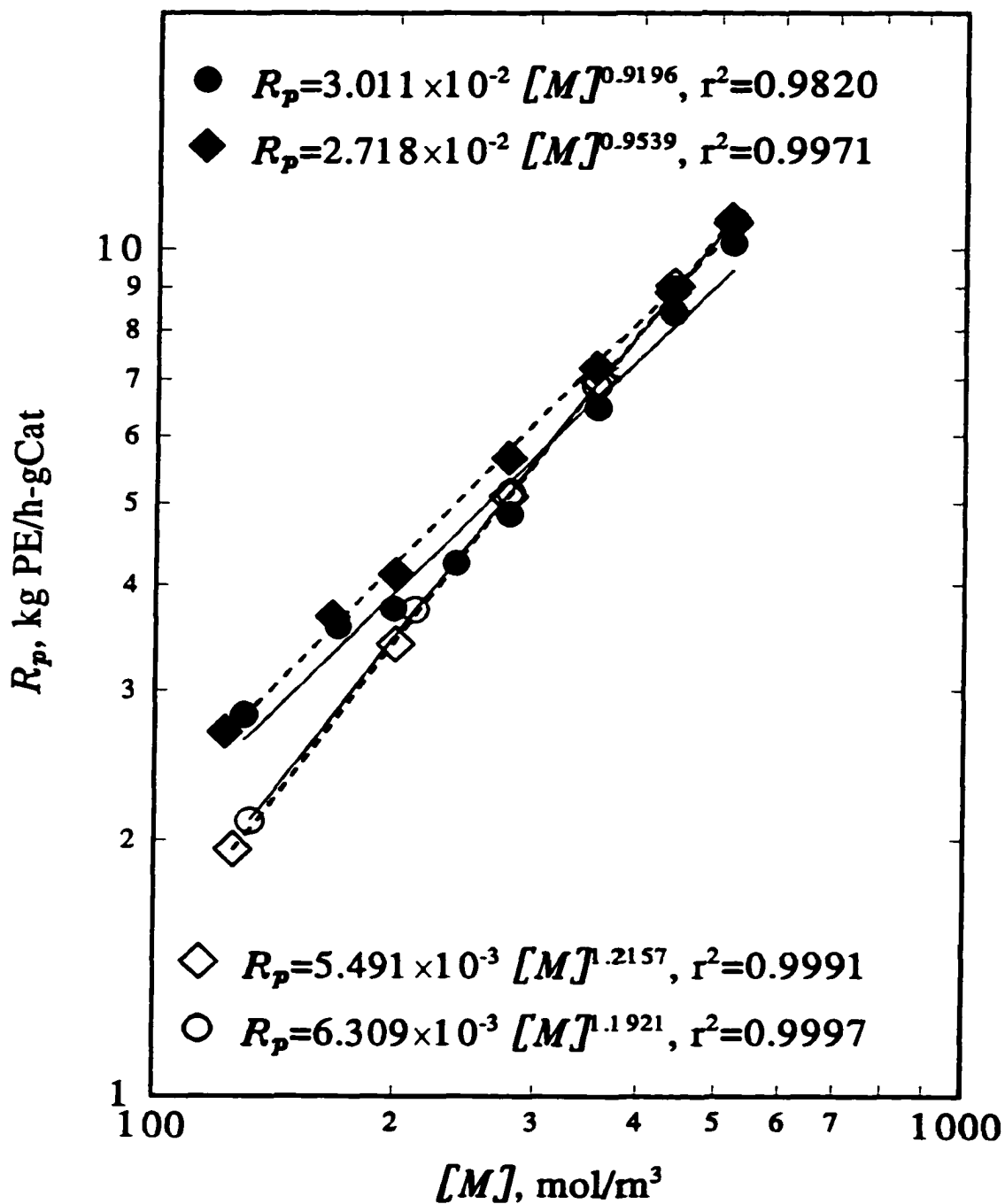
Figure 6.13 Log-log plot of R_p versus [M] by Equation 6.5 for Runs C7 (solid regression lines) and C8 (dash regression lines) at the beginning of run (solid symbols) and the end of run (open symbols) at 60°C.
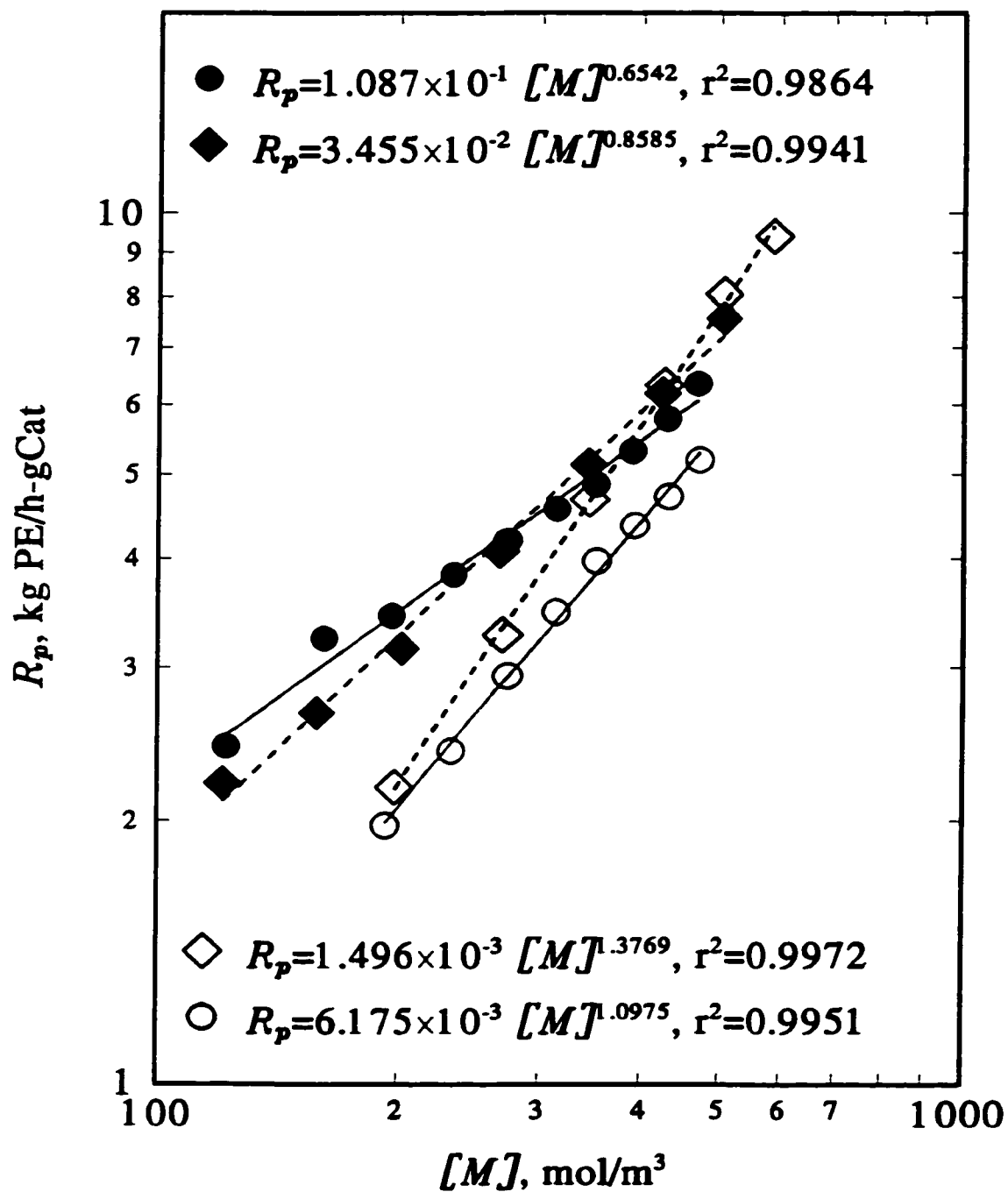
Figure 6.14 Log-log plot of R_p versus [M] by Equation 6.5 for Runs C9 (solid regression lines) and C10 (dash regression lines) at the beginning of run (solid symbols) and the end of run (open symbols) at 69°C.

144

It is not surprising that the values of n' obtained from Equation 6.5 are different from the values of n obtained from Equation 6.4 with the same rate data, as can be seen in Table 6.3, since k' is not constant for polymerization systems with time-varying activities. All correlation coefficients for estimating n' were ≥ 0.98, as shown in Figures 6.10 to 6.14 (The average value of r^2 for all 20 fits was 0.996). This indicates that the fits of the data for all the runs (C1 to C10) by Equation 6.5 were very good for the split data of each run.

It is surprising that the data for time-varying activities are so well correlated by Equation 6.5 which ignores the time dependence of the active site concentration; Han-Adebekun and Ray (1997) also found that Equation 6.5 provided a good correlation for both ethylene and propylene polymerization rate over a deactivating catalyst. However, the values of n' obtained from Equation 6.5 do not provide information on the kinetics of the polymerization (propagation) step, *i.e.*, the monomer dependence of the specific polymerization rate since the n' depend heavily on whether the data used to obtain the value of n' are measured at a time when the activity of the catalysts is increasing or decreasing. During periods of increasing rate (catalyst activation), the n' values from Equation 6.5 are higher than the 'true' power-law orders, and during periods of decreasing rates (catalyst deactivation), the values of n' are lower than the 'true' power-law orders. This dependence on the shape of the activity profiles of the apparent order determined using Equation 6.5 is evident in the temperature dependence of n' shown in Table 6.3. At temperatures of 30 and 40°C and low reaction times, the activity of the catalysts increased; this resulted in high values of n' (see activity profiles in Figures 5.6 to 5.8, Chapter 5). At temperatures of 50 and 60°C and low reaction times, the activity of the catalysts first increased and then decreased;

145

this resulted in intermediate values of n'. At about 70°C and low reaction times, the activity of the catalysts decreased (see also Figure 6.1); this resulted in low values of n'. The changes in catalytic activities for longer times-on-stream are also reflected in the trend in the n' values. For example, at higher reaction temperatures (60 and 70°C) and long reaction times, the n' values are higher because the catalytic activity was increasing at longer times (see also Figure 6.1).

The n values obtained by the use of Equation 6.4 should reflect the intrinsic kinetics of the polymerization process in the absences of activation-deactivation phenomena. The results in Table 6.3 indicate that the order with respect to ethylene at the beginning of the polymerization was 1.3 to 1.7, with higher values at higher reaction temperature. The order decreased to 0.96 to 1.1 for longer times-on-stream; again higher values were observed for higher polymerization temperatures.

This time dependence of n, just like the activity profiles discussed previously in Chapter 5, indicates the presence of at least two catalytic sites which have different activation, propagation and deactivation kinetics. If it is assumed that the catalysts contains two distinctly different sites, Sites 1 and Site 2, then the variation of n with temperature provides information, in addition to that inferred form the activity profiles, about the behavior of the catalytic sites. The order of the overall dependence of polymerization rate with respect to ethylene concentration for Site 1, which has more rapid activation and deactivation than Site 2, varies between one and two while the order for Site 2 appears to be close to unity. Site 1 appears to dominate the polymerization behavior during the initial stages of polymerization while Site 2, which activates and deactivates slowly, appears to

146

govern the behavior after several hours on stream. The values of n, determined by the new method (use of Equation 6.4), do not provide information on the deactivation kinetics, but evidence of at least two types of deactivation behavior has been reported for gas-phase polymerization of ethylene (Dusseault and Hsu, 1993). The deactivation behavior will be discussed with the kinetic modeling in Chapter 8.

7. Characterizations of Nascent Polyethylene

Scanning electron microscopy (SEM) and size exclusion chromatography (SEC), were used to examine the morphology and molar masses of nascent polyethylene granules. The nascent polyethylene granules examined by these characterization techniques were produced with spherical prepolymer from Run Pre-3 as catalyst.

The characterization results are qualitatively compared for polyethylene produced in slurry and gas-phase polymerization. Due to the particle replication, which is discussed in Section 7.1, the properties of nascent polyethylene granules, such as surface morphology, density and molar masses, can be studied as a function of polymer particle size. A variety of morphologies at the surface and in the interior of nascent polyethylene granules are described in Section 7.2. In Section 7.3, the granule density and bulk density are defined, then the effects of polymerization conditions on the granule density and bulk density are reported. The effects of polymerization conditions on molar masses, including number-average molar mass (M_n) and weight-average molar mass (M_w), and polydispersity (Q), are presented in Section 7.4, with a brief discussion on the rate profiles and mass transfer limitations of polymerization.

7.1 Catalyst-Prepolymer-Polymer Morphology Replication

It is widely observed that heterogeneous Ziegler-Natta catalysts can replicate their morphology into the morphology of polymer particles under certain polymerization conditions (Boor, 1979). The replication from catalyst to prepolymer to polymer particles in this study was investigated using SEM. Shown in Figure 7.1 are the typical SEM

148
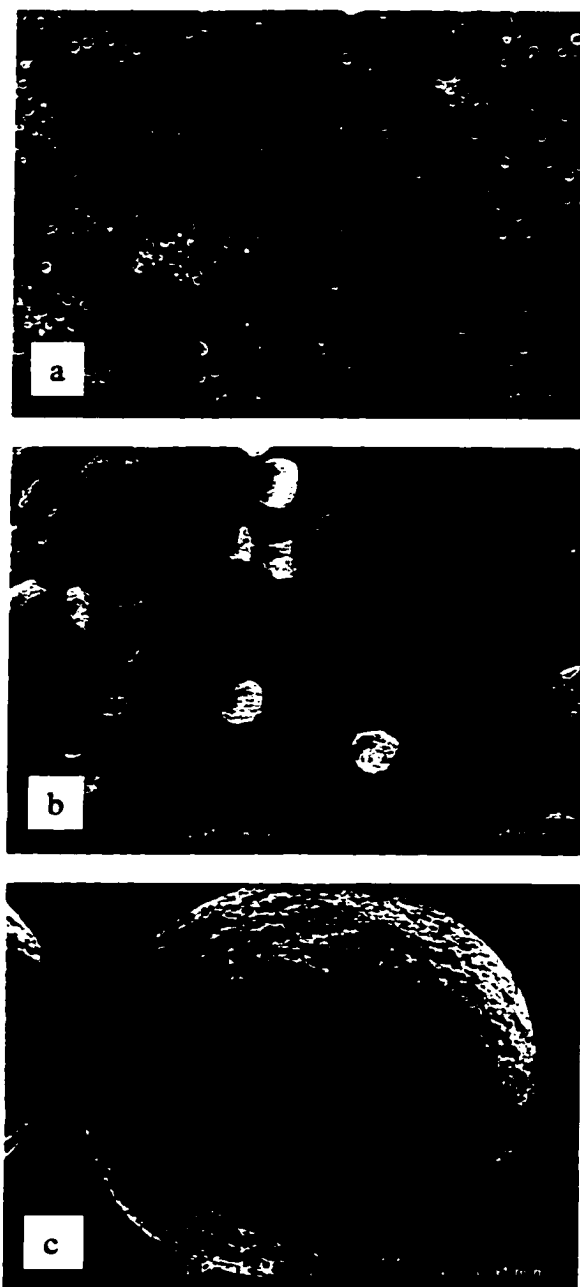
Figure 7.1   Morphology replication from catalyst (a) to prepolymer (b) to polymer (c).

micrographs of the spherical particles of catalyst, prepolymer, and polymer (prepolymer shown in Figure 7.1b are from Run Pre-3, and has been described in Chapter 4). The individual particles in Figure 7.1 are shown at a higher magnification in Figure 7.2. It is obvious from Figure 7.2 that beside the shape replication, there are cracks on the surface of some catalyst particles (see Figure 7.2a). Similar cracks have been reported on the surface of spherical catalyst particles used commercially for propylene polymerization (*e.g.*, Di Drusco and Rinaldi, 1984). In Figure 7.2c, some cracks are also evident on the surface of polymer particle. Numerous prepolymer particles were examined, but no crack was ever found (see Figure 7.2b).

Similar observation that cracks initially existing on the surface of catalyst particles disappear on the surface of prepolymer and reappear on the surface of polymer particles is shown in Figure 7.3 for spheroidal particles. The catalyst shown in the SEM micrograph of Figure 7.3a was a different $MgCl_2$-supported $TiCl_4$ catalyst prepared by the method of chemical reaction precipitation (see Appendix A). The prepolymer in the SEM micrograph of Figure 7.3b was produced by the catalyst shown in Figure 7.3a; the polymer in Figures 7.3c (SEM micrograph) and 7.3d (optical micrograph) were obtained by polymerizing ethylene using the prepolymer shown in Figure 7.3b as the catalyst. Observation directly under optical microscope (see Figure 7.3d) excludes the possibility that the cracks on the polyethylene particles are due to the evacuation during SEM analysis, which was speculated by Soga *et al.* (1989b).

The disappearance of the cracks on the surface of prepolymer particles can be explained by possible presence of mass transfer limitations during polymer particle

150
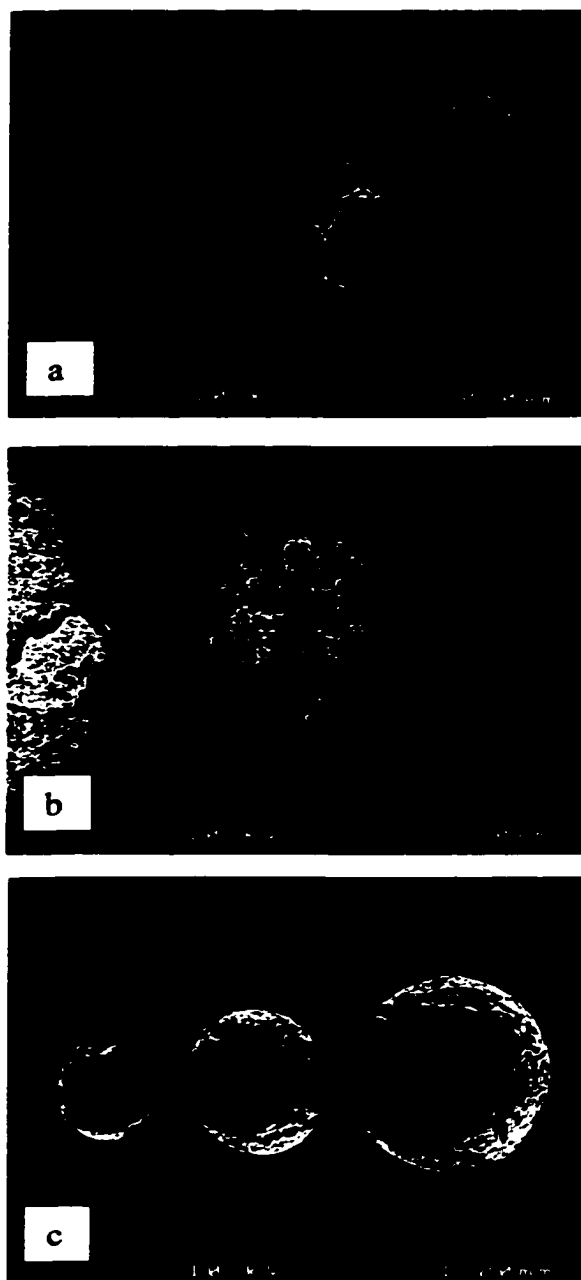
Figure 7.2 SEM micrographs show the cracks on the catalyst (a), no cracks on the prepolymer (b), and the cracks on the polymer (c).

151
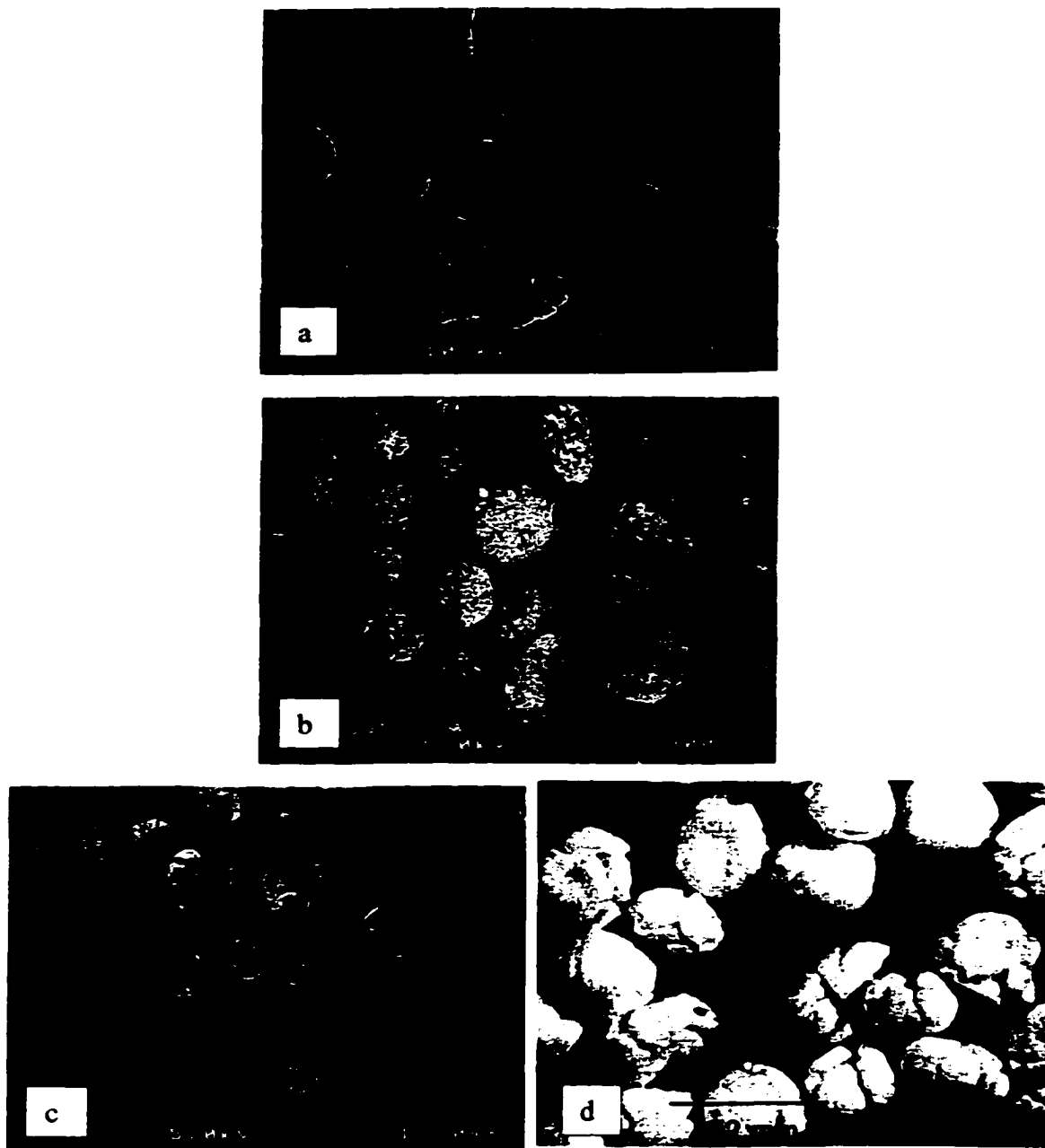
Figure 7.3   SEM and optical micrographs show the cracks on the catalyst (a), no cracks on the prepolymer (b), and the cracks on the polymer (c) and (d).   [the catalyst (a) was prepared by chemical reaction precipitation described in Appendix A,   and the polymer (d) was the micrograph of an optical microscope.]

growth in the prepolymerization stage as discussed in Sections 4.2 and 4.3. Due to mass transfer limitations of ethylene in the prepolymerization stage, the most favored active sites for polymerization are on the surface of catalyst particles and produce polymer at higher polymerization rate. The continuous observation by electron microscopy on polymer formation showed that the pre-existing cracks on catalysts are preferential sites for polymer growth in Ziegler-Natta ethylene polymerization (Baker *et al.*, 1973). Since more polymer is formed initially on the catalyst surface during prepolymerization, the surface of catalyst particles is covered by polymer, which fills up cracks and voids on the surface. The filling of voids and cavities by growing polymer has been observed microscopically by Baker *et al.* (1973) for ethylene polymerization under 10 torr of ethylene pressure and up to 34 minutes of polymerization, and by Hock (1966) for propylene polymerization.

During the polymerization stage, the polymerization rate at catalytic sites in the interior of the particles increases because mass transfer limitations decrease and catalytic sites at the surface are more likely poisoned and deactivated (see also Section 4.4). As polymerization progresses, more polymer will be produced in the interior of particles. Growing polymer in the interior will generate mechanical force to expand the particles, and finally tends to crack, or even break particles. Particles crack or break at the weakest points which probably correspond to the initial cracks in the catalysts particles. The overall particle shape is maintained by secondary and primary polymer particles, which act as a cement.

7.2 Morphology of Nascent Polyethylene Granules

The effects of polymerization conditions on the properties of nascent polyethylene granules, as a function of granule size, are reported in the following sections. All the results reported in this chapter are for polyethylene granules produced at the polymerization conditions listed in Table 7.1.

Table 7.1   Description of Polymerization Conditions[1] for Production of Polymer Used to Investigate Morphology, Granule Density, and Molar Masses

Run No.	Prepolymerized Catalyst[2], mg	T, °C	P_{H_2}, MPa	$P_{C_2H_4}$, MPa	Time, h	Bulk Density, g/cm^3	Yield, gPE/g cat
D1 (slurry)	65	68.9	0.35	0.66	2.03	0.32	2,770
D2 (slurry)	100	68.3	0.33	1.38	5.15	0.40	8,531
A1 (gas-phase)	45	68.1	0.36	1.39	2.00	0.45	9,180
A2 (gas-phase)[3]	200	70.5	0.31	1.37	2.02	0.45	10,030
A3 (gas-phase)	63	67.9	0.35	0.69	2.01	0.42	2,385
A4 (gas-phase)	50	68.4	0.35	1.41	7.79	0.39[4]	12,437
A5 (gas-phase)	36	28.7	0.34	0.71	2.03	0.42	1,487

Notes:

1. For all the runs, 0.25 mL of TEAL was used as a cocatalyst. For runs in the slurry, Runs D1 and D2, 300 mL of heptane was used as reaction medium; for runs in the gas phase, Runs A1 to A5, 100 g of NaCl was used as seed bed unless specified.

2. Prepolymer from Pre-3 was used for all the runs as the catalyst.

3. For this run, 35 g of Rulon LR particles (2×2×2 mm by length) were used as seed bed.

4. For this run, the majority of polyethylene granules were broken in the reactor.

154

The surface and interior morphologies of nascent polyethylene granules were characterized by SEM. The granules produced from two runs were characterized: one from slurry operation of Run D1 and one from gas-phase operation of Run A2 (see Table 7.1 for polymerization conditions of the two runs). For the sample produced at each run, at least two granules were analyzed, and numerous SEM micrographs were taken; micrographs shown in this section are representative of the generally observed features. The granules for the surface characterization were not treated after removal from the reactor; the granules for the characterization of interior morphology were fractured in the liquid nitrogen.

The typical surface morphologies of nascent polyethylene granules are shown in Figure 7.4. Shown in Figure 7.4b is the cobweb morphology for polymer produced in the slurry (Run D1). The cobweb morphology, consisting of globules which are interconnected by the cold-drawn fibrils, has been observed on the surface of nascent polyethylene made by various types of Ziegler-Natta catalysts (reviewed in Section 2.1.1). According to Kakugo *et al.* (1989a; 1989b), these globules are the secondary polymer particles. Similar morphology was observed for polymer produced in the gas phase (Figure 7.4d, Run A2), except that the globule sizes in Figure 7.4d are more uniform than those in Figure 7.4b. This is in agreement with the observation reported in Section 4.4 that the higher the yield, the more uniform the size distribution of the globules (see Table 7.1 for the higher yield of Run A2 compared to Run D1).

Samples for the characterization of interior morphology were obtained by fracturing the nascent polyethylene granules with a hammer when the granules were immersed in liquid nitrogen. The cross-sections of a fractured sample, made from slurry operation of Run

155
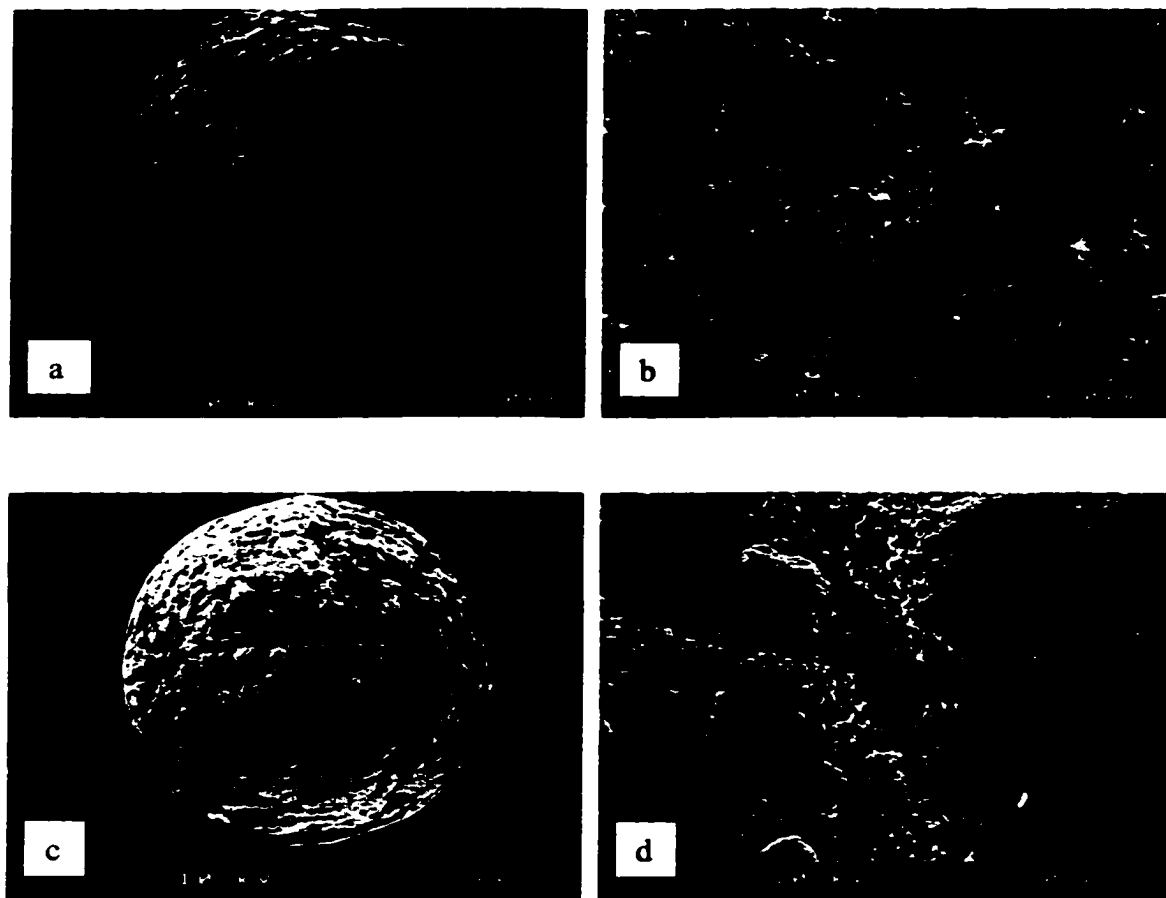
Figure 7.4   Typical surface morphologies of nascent polyethylene granules produced in the slurry (a & b) and gas phase (c & d).

D1, are shown in Figure 7.5a. Shown in Figure 7.5b and 7.5d are areas I and II in Figure 7.5a at a higher magnification, and Figures 7.5c and 7.5e are areas III and IV in Figure 7.5b and 7.5d at higher magnifications, respectively. It can be seen from Figure 7.5 that the cobweb structure, which was commonly observed on the surface (*e.g.*, Figure 7.4), was not dominantly present in the interior. Instead, two different globular structures are observed in Figures 7.5c and 7.5d, respectively. The globules in Figure 7.5c are loosely connected (referred to the loosely connected globules); the globules in Figure 7.5e are tightly bound with each other and only part of an individual globule (like a hemisphere) can be seen (referred to the tightly bound globules). Similar tightly bound globules were observed by Wristers (1973a) for nascent polypropylene made with a compact $TiCl_3$ catalyst.

The two different globules, *i.e.*, the loosely connected and tightly bound globules, on the fractured surface can also be observed for the nascent polymer granules from the gas-phase polymerization of Run A2, as shown in Figure 7.6. The shape and cross section of the fractured samples from the gas-phase polymerization (see Figure 7.6a) are more regular than that obtained from the slurry operation (see Figure 7.5a). This is probably due to the higher bulk density (see Figure 7.1) of the nascent polymer produced in the gas phase than in the slurry (discussed in Section 7.4).

From Figures 7.5 and 7.6, it can be seen that the size of the loosely connected globules are larger than that of the tightly bound globules, and the loosely connected globules seem to be more completely fragmented than the tightly bound globules (see Figures 7.5b and 7.6b for the individuality of loosely connected globules, and Figures 7.5d and 7.6d for the aggregate of the tightly bound globules). The globules with complete
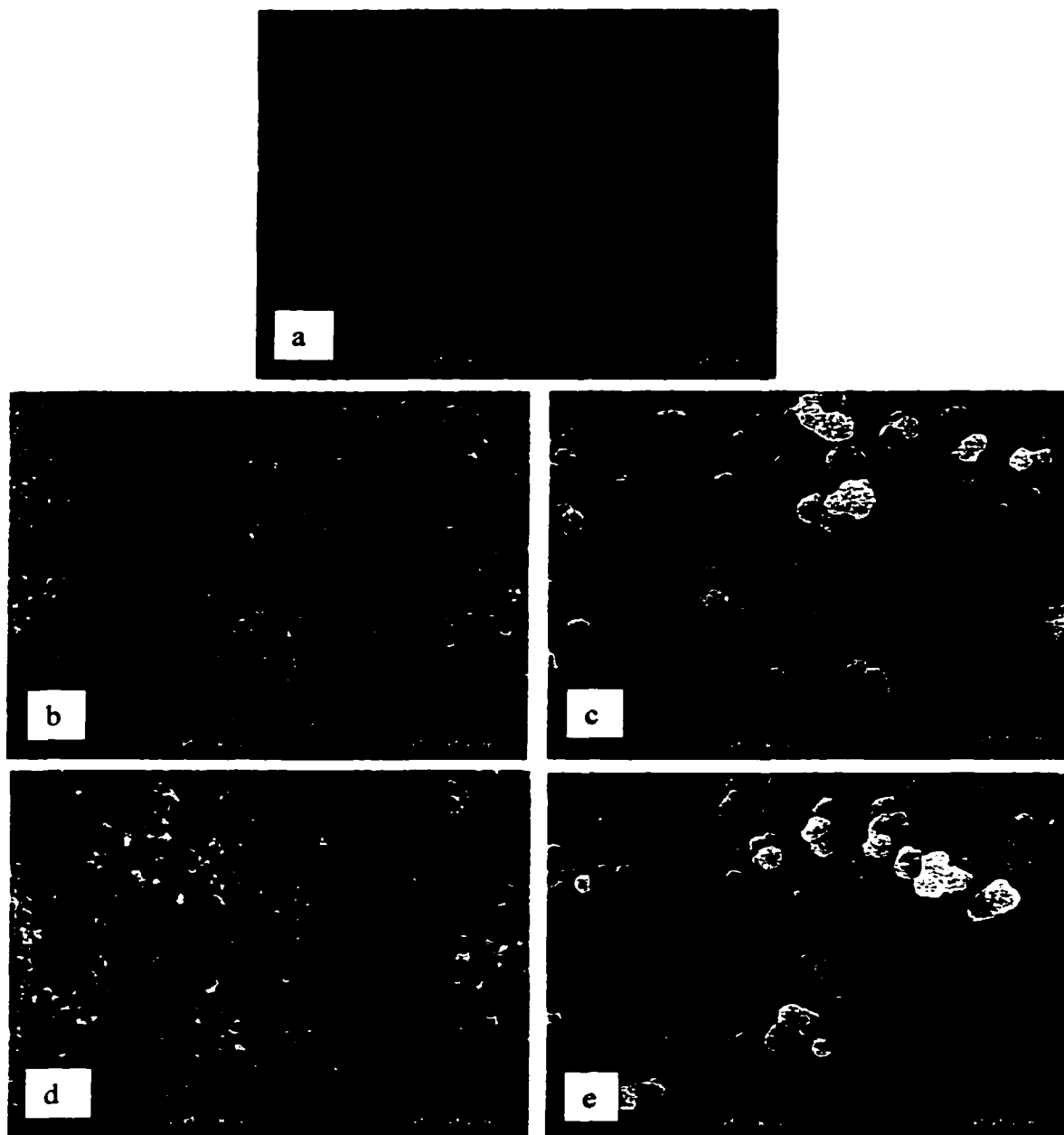
Figure 7.5 Interior morphology of the fractured nascent polyethylene granule produced in the slurry (Figure 7.5b and d are areas (I) and (II), respectively, in Figure 7.5a; Figure 7.5c and e are areas (III) and (IV) in Figure 7.5b and d, respectively).

158
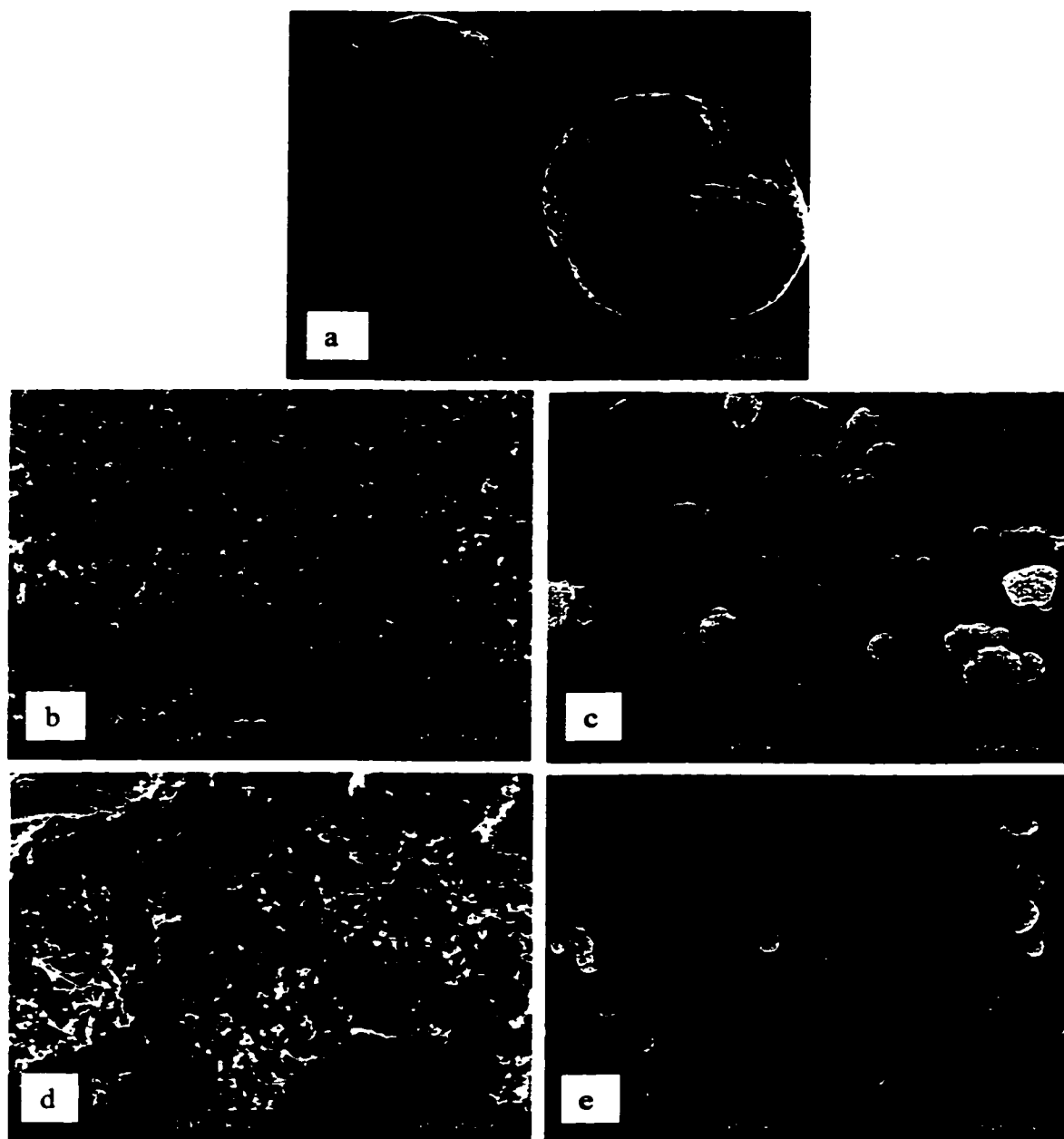
Figure 7.6   Interior morphology of fractured polyethylene granules produced in the gas phase (Figure 7.6b and d are areas (I) and (II), respectively, in Figure 7.6a;   Figure 7.6c and e are areas (III) and (IV) in Figure 7.6b and d, respectively).

159

fragmentation have larger surface area exposed for polymerization. Thus, the catalytic site producing larger loosely connected globules is more active than the site producing smaller tightly bound globules. However, the globule size distribution of each kind is very uniform.

Based on the above observations from Figures 7.5 and 7.6, it seems reasonable to assume that the different sizes and morphologies for the two kinds of globules were caused by the presence of two different catalytic sites, having different activities. This is in agreement with the observation on the prepolymer morphology in Chapter 4 and the analysis of the rate profiles in Chapter 5, *i.e.*, Site 1, the one that produced larger size of the loosely connected globules, is more active than Site 2, the one that produced smaller tightly bound globules.

The tightly bound globules can aggregate into elliptical or spherical shapes as shown in Figures 7.5d and 7.6d, or dispersed in the loosely connected globules as can be seen in Figure 7.7. In addition to the globular structures, worm-like structures were observed for nascent polyethylene granules. Figure 7.8a shows the helicoidal worm-like structure on the surface of polyethylene produced in the slurry reactor; Figures 7.8b and 7.8c show the similar structure on the different areas of the cross section of polyethylene produced in the gas phase reactor. It can also be seen in Figure 7.8 that all the worm-like morphologies are made up of globules in nascent polyethylene granules produced in both slurry and gas-phase reactors. The causes for the formation of the worm-like structures on the fractured surface of nascent polyethylene are not known, but are probably due to the limited space between catalytic sites which prevents three-dimensional fragmentation of the catalyst particles at the early stage of polymerization.

160
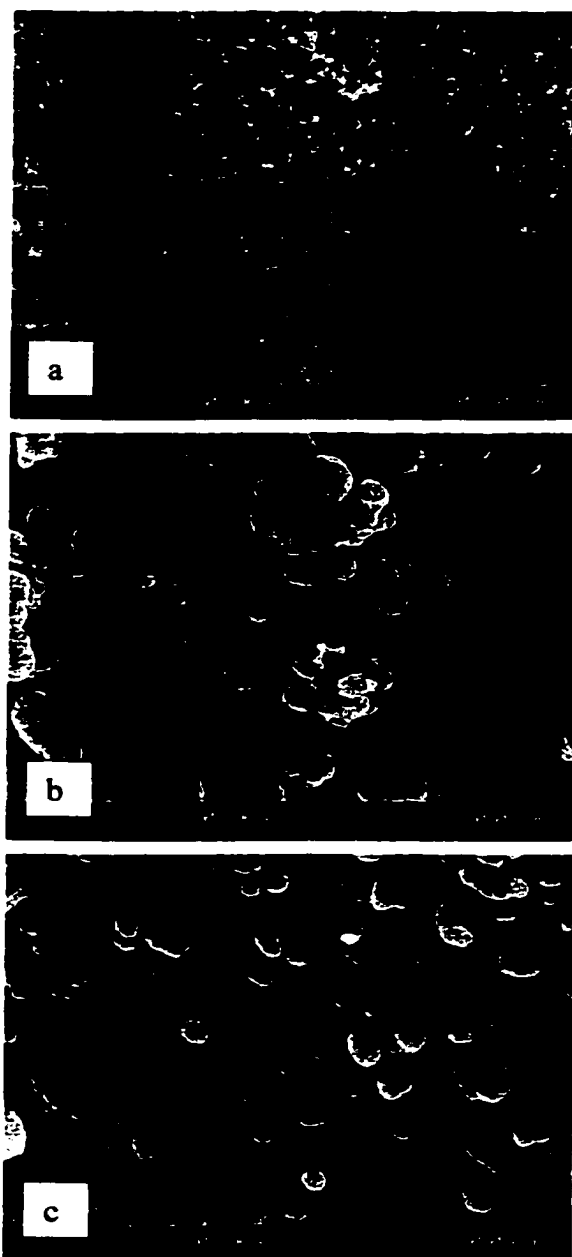
Figure 7.7   The tightly bound globules are dispersed in the loosely connected globules for polyethylene granules produced in the gas phase (Figure 7.7b and c are areas (I) and (II), respectively, in Figure 7.7a).
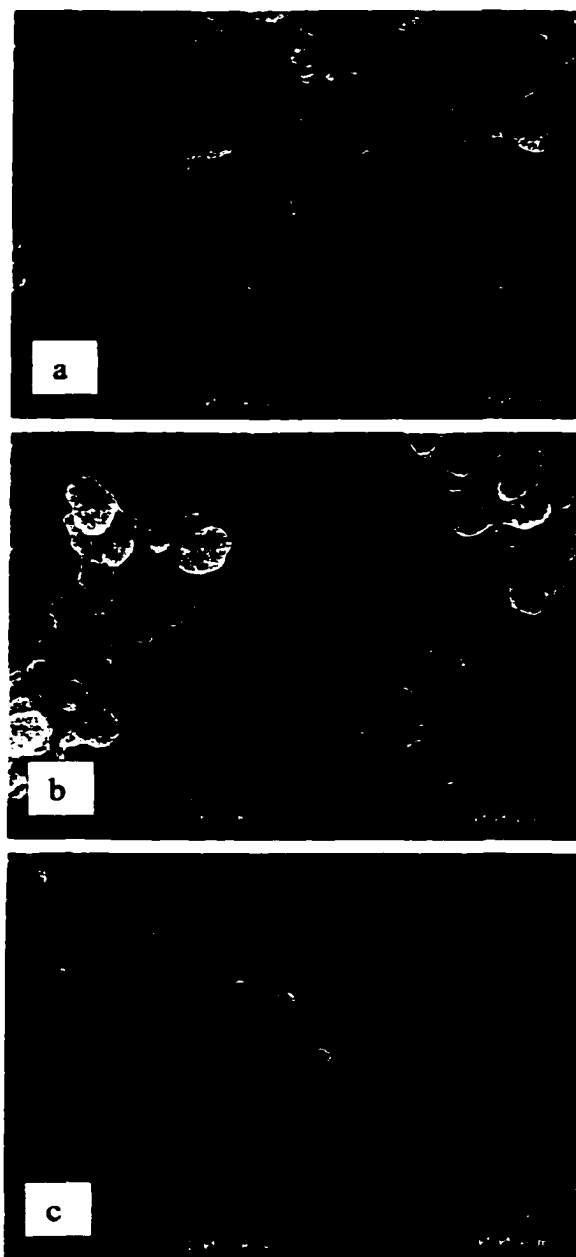
Figure 7.8   The helicoidal worm-like structures on the fractured surface of nascent polyethylene granules produced in the slurry (a) and gas phase (b and c).

7.3 Granule Density and Bulk Density of Nascent Polyethylene

In this section, the effects of polymerization conditions on the granule density and bulk density are discussed for nascent polyethylene granules produced in the slurry and gas-phase experiments. The granule density are also studied as a function of granule size. For this determination, the nascent polyethylene granules were manually sorted into several sets of granules size. The diameter of each individual granule was measured under an optical microscope (a typical micrograph was shown previously in Figure 6.2, Section 6.1). The individual granule diameter, d_i, was taken as the average of the diameters measured at different positions. Since density is related to the volume-number average diameter (d_{30}), the volume-number average diameter of each set was calculated according to Equation 7.1:

$$d_{30} = \left(\frac{\sum_i d_i^3}{n_t} \right)^{1/3}$$

(7.1)

where n_t is the total number of granules in each set. The granule density ρ_g was then obtained by:

$$\rho_g = \frac{6W}{\pi d_{30}^3}$$

(7.2)

where W is the total mass of granules in each set. In contrast, the bulk density, ρ_b, is the mass (W_t) per unit volume of a bed of all the granules (V_t) obtained in a run (see ASTM D1895-67).

$$\rho_b = \frac{W_t}{V_t}$$

(7.3)

163

where V_t includes porosities of the granules and the inter-granule voids. In general, the bulk density increases with increasing the granule density. The bulk density of granules for each run are listed in Table 7.1. The granule densities, as a function of granule size for polyethylene made from all the runs listed in Table 7.1, is shown in Figure 7.9.

The following observations can be made from the results of bulk density (see Table 7.1) and granule density (see Figure 7.9) for nascent polyethylene granules produced in slurry and gas-phase experiments:

1. The granule density tends to decrease with increasing granule size for both slurry and gas-phase operations.

2. The granule density increases with increasing ethylene pressure for both slurry and gas-phase operations.

3. The bulk density is insensitive to the polymerization temperature for both slurry and gas-phase operations.

4. The granule densities and bulk densities of polymer made in slurry are lower than those made in the gas phase.

The general trend shown in Figure 7.9 is the decrease of granule density with increasing granule size for all the runs in the slurry and gas-phase experiments with prepolymer from Pre-3 as catalyst. The studies of prepolymer particles from Run Pre-3 (see Chapter 4), based on surface morphology, molar masses and BET surface area measurements, indicated that mass transfer limitations were present during ethylene prepolymerization Run Pre-3; the mass transfer limitations cause the increase in porosity with increasing prepolymer particle size. Thus, the decrease in polymer granule density with increasing size in Figure 7.9 suggests that the more porous structure of larger prepolymer

164
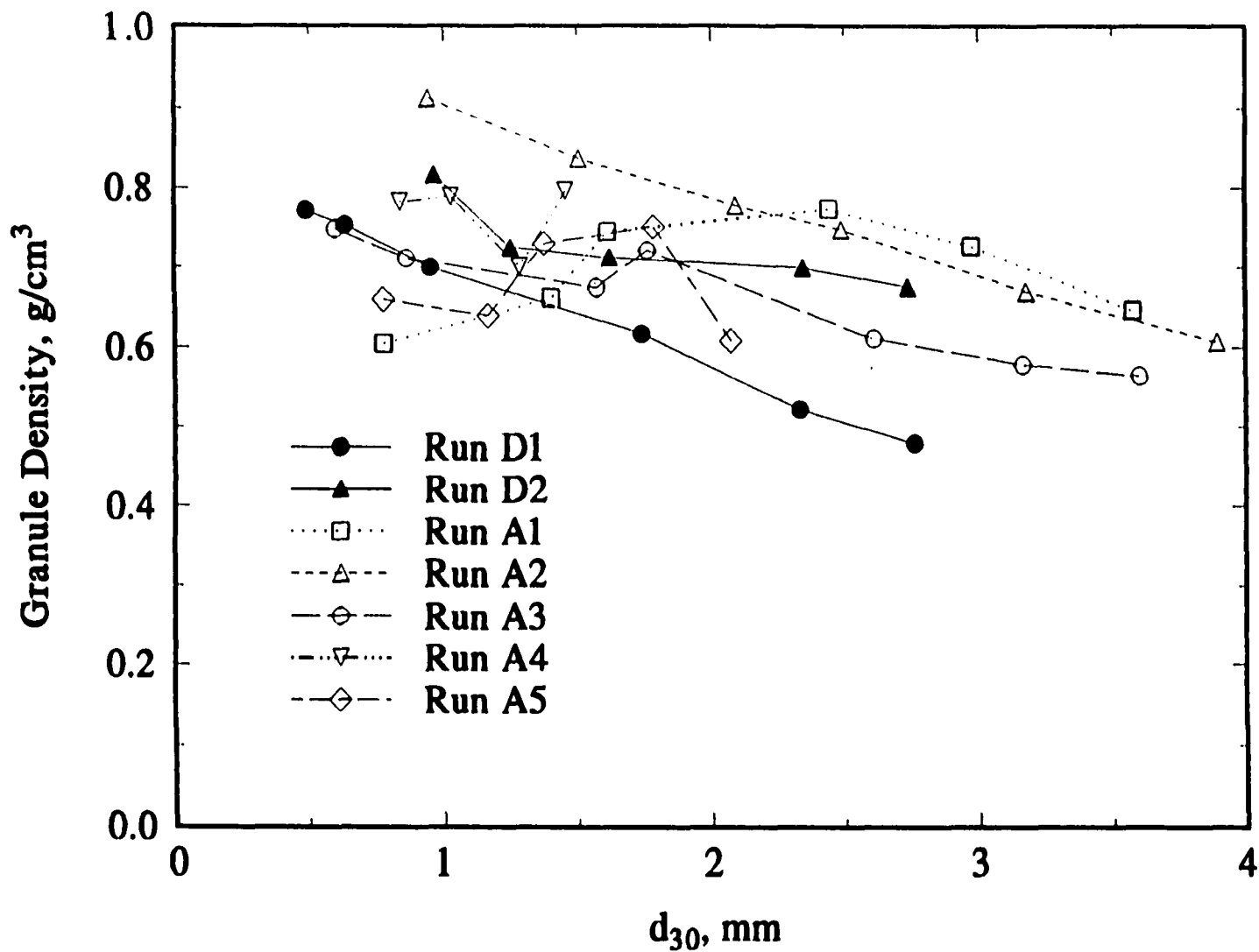
Figure 7.9 Granule density versus volume average diameter, d_{30}, at various polymerization conditions.

particles has been carried over to polymer granules even if mass transfer limitations are absent in the polymerization.

The granule density increases with increasing ethylene pressure for polyethylene produced in both slurry (comparing Run D1 with Run D2) and gas phase (comparing Run A3 with Run A2), as shown in Figure 7.10 (the results in Figure 7.9 were reploted for Runs D1, D2, A2, And A3). At same ethylene pressure, the density of granules produced in the gas phase was higher than for polymer produced in the slurry reactor (comparing Run D1 with Run A3, and Run D2 with Run A2 in Figure 7.10). These results on granule density are consistent with the results on bulk density listed in Table 7.1; this is reasonable since granule density is proportional to the bulk density if the bed void fraction is constant.

The lower granule density observed in the slurry operation is probably due to the fact that polyethylene granules in the slurry reactor were surrounded by liquid reaction medium, *e.g.*, heptane in this study. Heptane, which essentially consists of the same chemical structure ($-CH_2-$) as polyethylene, can swell polyethylene particles during polymerization. Removal of heptane from the granules after polymerization will result in particles with higher porosity than those formed during gas-phase polymerization. The presence of mass transfer limitations in slurry polymerization can also result in hollow granules which have very low granule density (reviewed in Section 2.1.3.3), especially for larger catalyst particles (reviewed in Section 2.3.2.2). Mass transfer limitations in slurry polymerization are further discussed in Section 7.4.

166
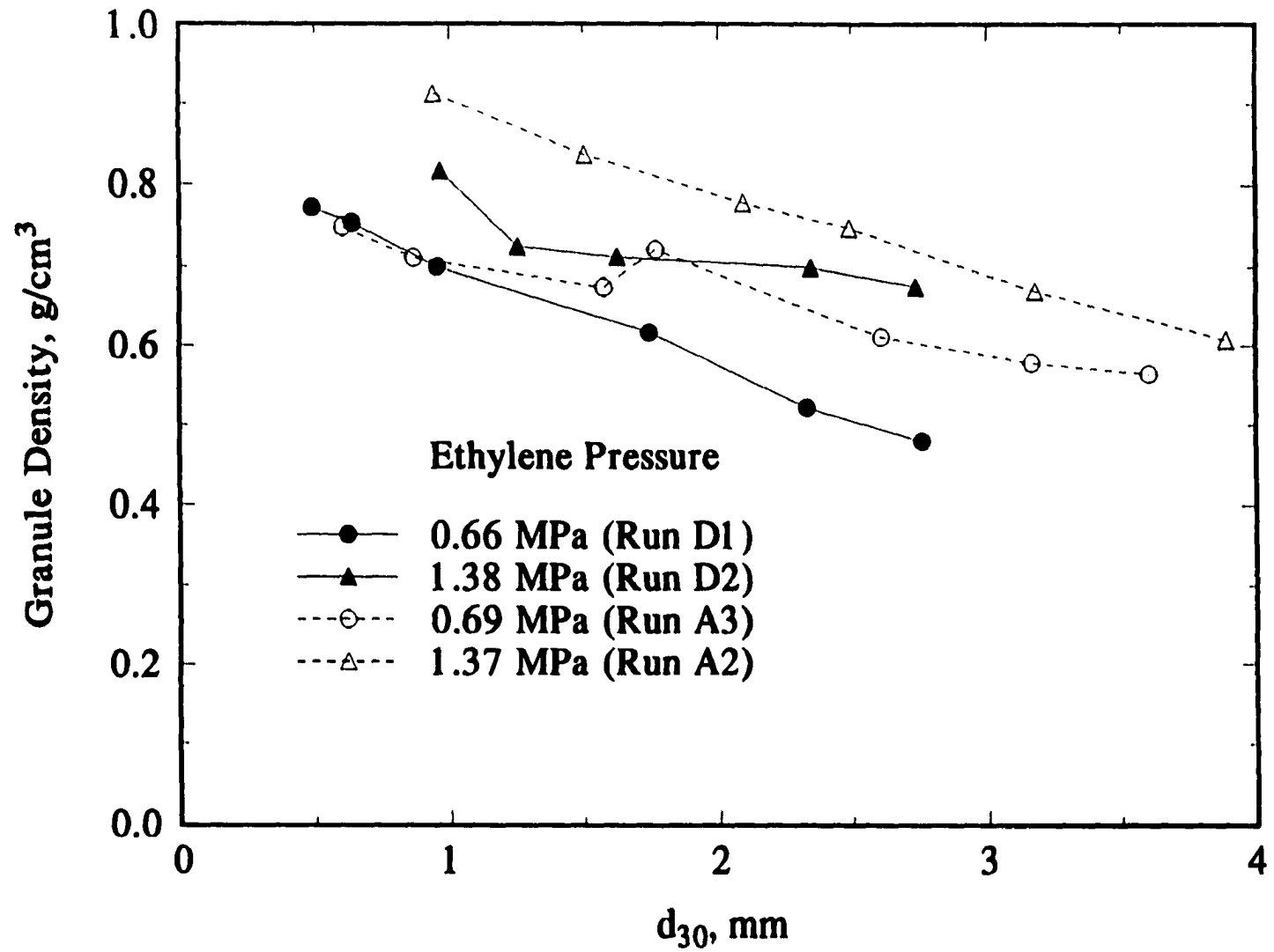
Figure 7.10   Effects of ethylene pressure on granule density: slurry (solid symbols) versus gas-phase (empty symbols).

7.4 Molar Masses and Polydispersity

The molar masses and polydispersity were measured as a function of granule size for nascent polyethylene made in both slurry and gas-phase experiments in the presence of hydrogen. The differences of rate profiles in the slurry and gas-phase reactors are compared in terms of shape. Mass transfer resistances of ethylene are discussed for slurry polymerization. The effects of polymerization conditions on the molar masses and polydispersity of nascent polyethylene granules are presented, with an emphasis on the gas-phase products. The polymerization conditions examined include amount of prepolymerized catalyst, temperature, ethylene pressure, and time of polymerization. The polymerization conditions have been listed in Table 7.1.

7.4.1 Nascent Polyethylene Granules from Slurry Polymerization

The molar masses and molar mass distribution of nascent polyethylene granules produced in the slurry experiments of Runs D1 and D2 are shown in Figure 7.11 as a function of granule size. It is seen from Figure 7.11 that at a polymerization temperature of about 69°C, molar masses, including M_n and M_w, decrease while polydispersity (Q) increases with increasing granule size; at a high ethylene pressure, there is a smaller changes in both molar masses and polydispersity. The decrease of M_n with increasing size of polyethylene particles produced in slurry polymerization was also reported by McKenna *et al.* (1996). These results indicate that the mass transfer limitations are likely present in the slurry experiments according to the predictions by the multigrain model that the mass transfer limitations are more severe at lower ethylene pressure for larger catalyst particles (reviewed in Section 2.3.2.2). In addition, the decrease of molar masses and increase of

168
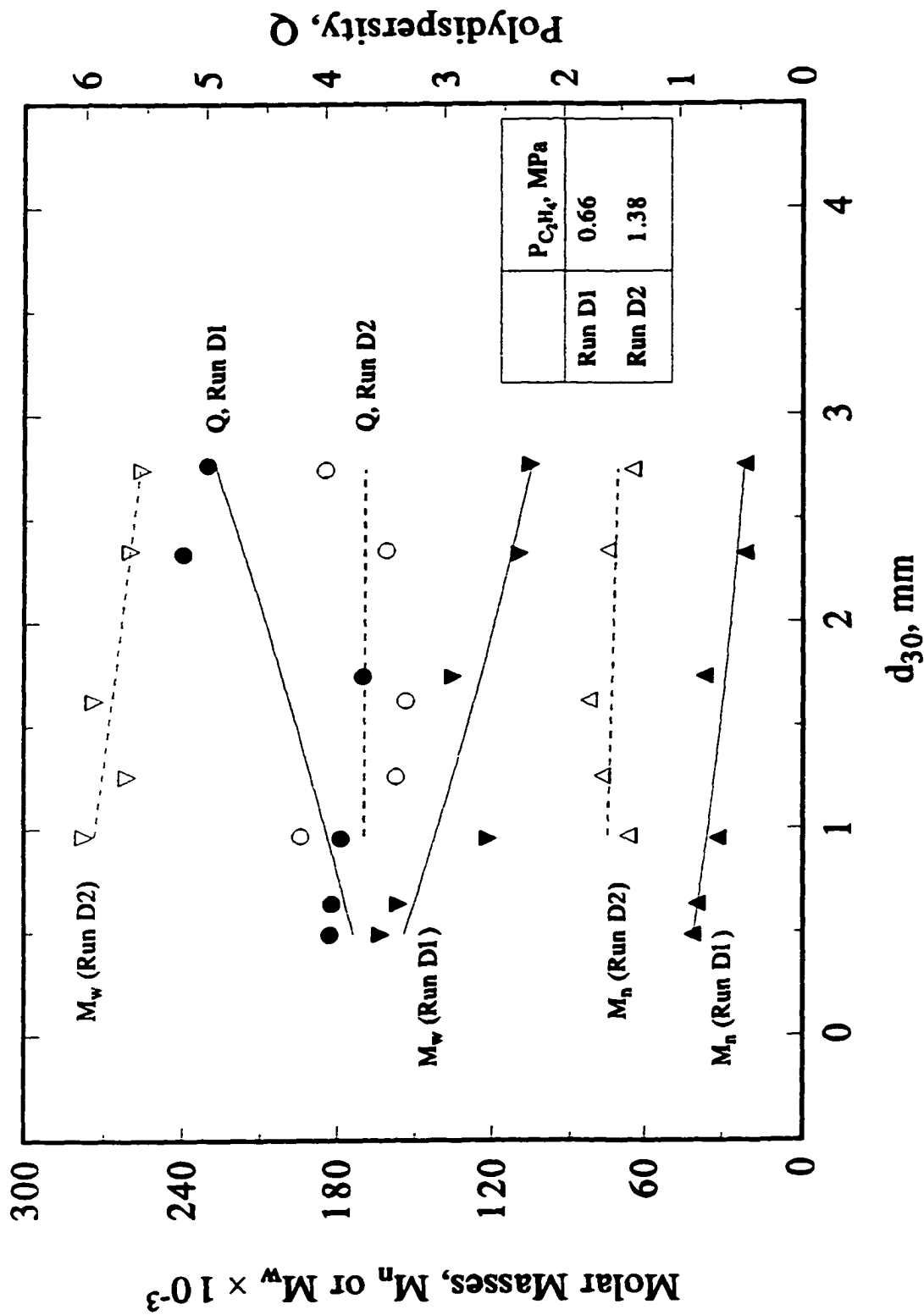
Figure 7.11 Effects of ethylene pressure on M_n, M_w, and Q of slurry polymerization at T=68.5°C and P_{H_2}=0.34 MPa.

169

polydispersity with decreasing ethylene pressure are also shown in Figure 7.11, which is in

agreement with the common observations (Zucchini and Cecchin, 1983). Similar

observation are made in the gas-phase operations (see Section 7.4.2).

The mass transfer limitations are further examined by the effect of ethylene pressure

on the maximum in the rate profiles of slurry polymerization. The rate profiles of Runs D1

and D2 are shown in Figure 7.12. It is seen in Figure 7.12 that the rate maximum shifts from

longer to shorter times with increasing ethylene pressure (similar ethylene pressure effects

were observed for the gas-phase polymerization without hydrogen in Section 5.3). Shown

also in Figure 7.12 is that under similar polymerization conditions, the initial rate decreases

faster in the gas phase than that in the slurry (*cf.*, Runs D1 and A3, Runs D2 and A4).

Similar observation on the rate profiles in the absence of hydrogen was reported by

Jejelowo *et al.* (1991). These results in Figure 7.12 suggest that the mass transfer limitations

of ethylene are present according to the predictions by the multigrain model (see discussion

in Section 5.3). However, as pointed out in Section 5.3, the multigrain model based on the

first-order kinetics and mass transfer limitations cannot model the effects of ethylene

pressure on the rate profiles in this study.

The more pronounced decrease of the initial rates in gas phase operations, as shown

in Figure 7.12, can also be caused by the more rapid deactivation of catalyst in the gas phase

than in the slurry (Jejelowo *et al.*, 1991). It is even more interesting to see in Figure 7.12

that at temperature of 68°C, only one peak in the rate profile of Run D2 can be observed in

up to 5 hours of polymerization in the slurry operation while there are two peaks for the rate

profile of Run A4 in gas-phase polymerization. These differences in the rate profiles
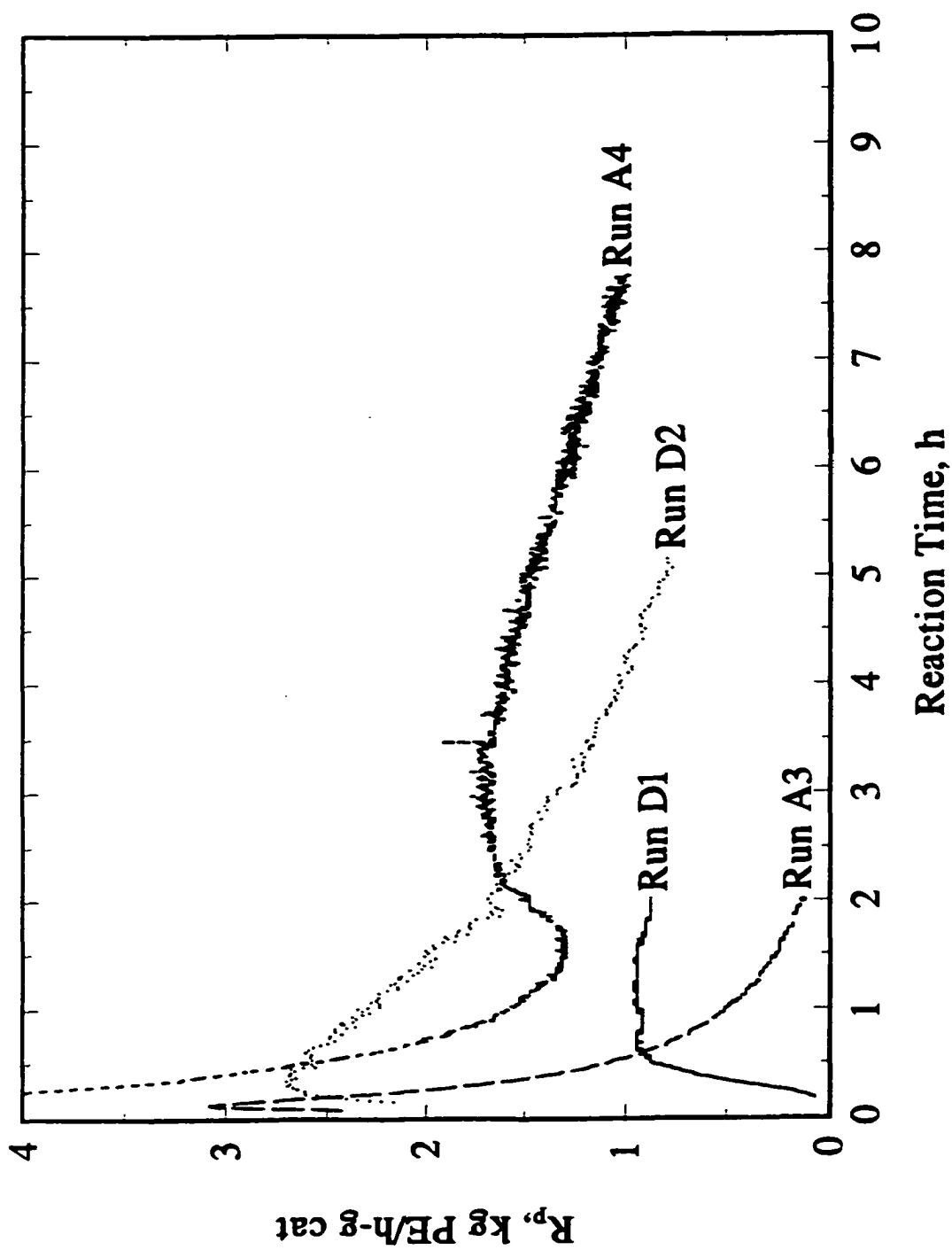
Figure 7.12   Rate profiles of polymerization in the slurry (Runs D1 and D2) and gas phase (Runs A3 and A4).

171

reinforce the statement, made by Jejelowo *et al.* (1991) from the temperature effects on the deactivation rate profiles, that the polymerization rates in slurry reactors cannot be used directly for predicting the rates of gas-phase polymerizations. Systematic experiments are needed to further study the kinetics and mass transfer effects in slurry polymerization.

7.4.2 Nascent Polyethylene Granules from Gas-Phase Polymerization

For nascent polyethylene granules made in gas-phase polymerization, the effects of the amount of prepolymerized catalyst on the molar masses and polydispersity, shown in Figure 7.13, are examined as a function of granule size produced from Runs A1 and A2. It can be seen from Figure 7.13 that the molar masses and polydispersity are essentially independent of the granule size for the amount of prepolymerized catalyst varying from 45 to 200 mg. The slight difference in the molar masses from the two runs is probably due to the slightly higher polymerization temperature of Run A1 compared to Run A2. Thus, it can be concluded that the amount of prepolymerized catalyst has no significant effects on the molar masses and polydispersity at polymerization temperature about 70°C. From the point of view of polymerization yield, this is in agreement with the results on the molar masses of ethylene/1-butene copolymer (Huang *et al.*, 1997) that the absolute rate of polymerization (*i.e.*, yield) does not have significant effect on the molar masses and polydispersity.

The effects of ethylene pressure on the molar masses and polydispersity, as a function of granule size, are shown in Figure 7.14 for polyethylene produced in Runs A1 and A3. It is seen in Figure 7.14 that the molar masses increase with increasing ethylene pressure, but are not proportional to ethylene pressure at polymerization temperature of about 68°C. This indicates that in the presence of hydrogen, chain transfer to monomer is an
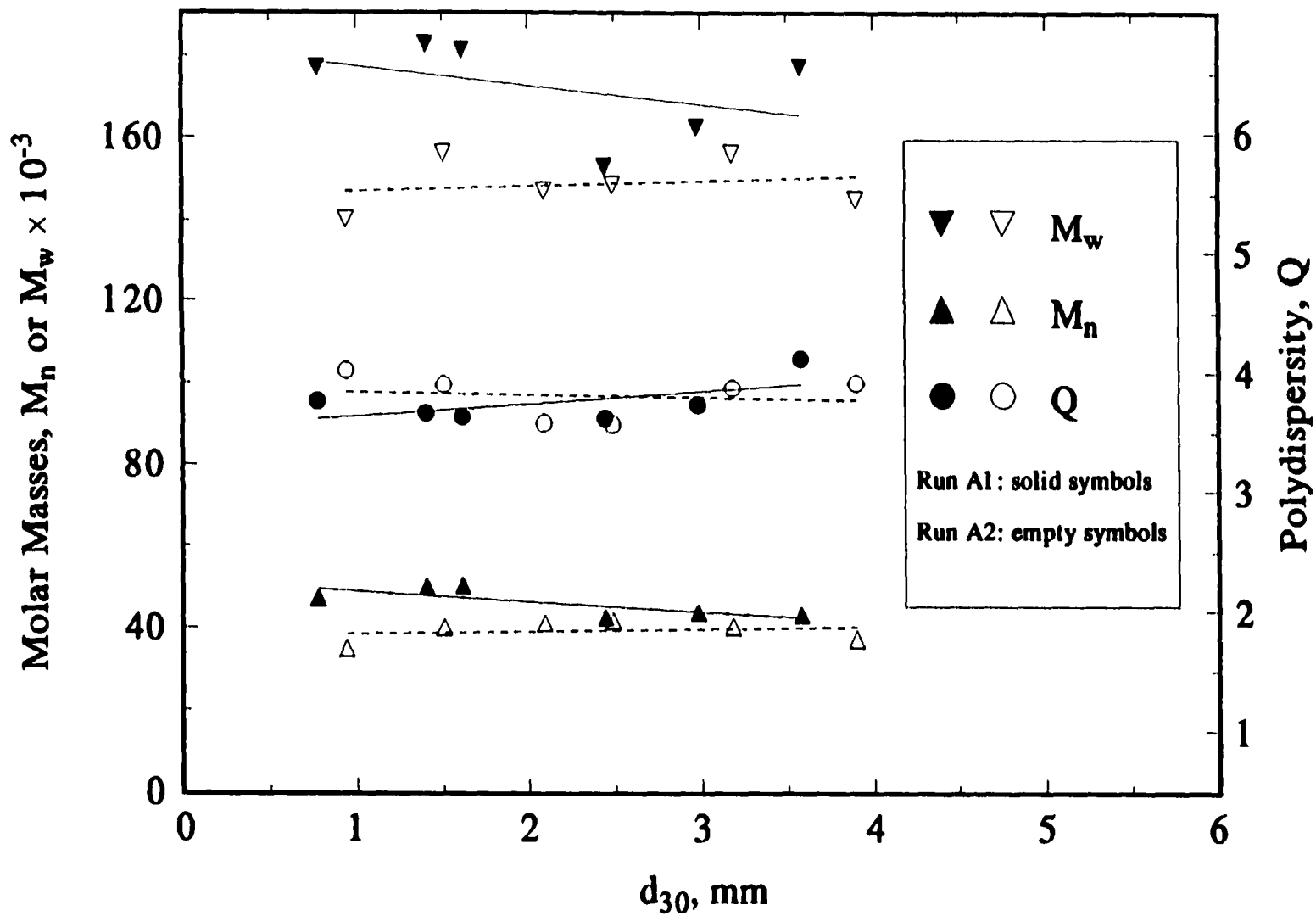
Figure 7.13   Effects of catalyst amount on M_n, M_w, and Q of gas-phase polymerization.
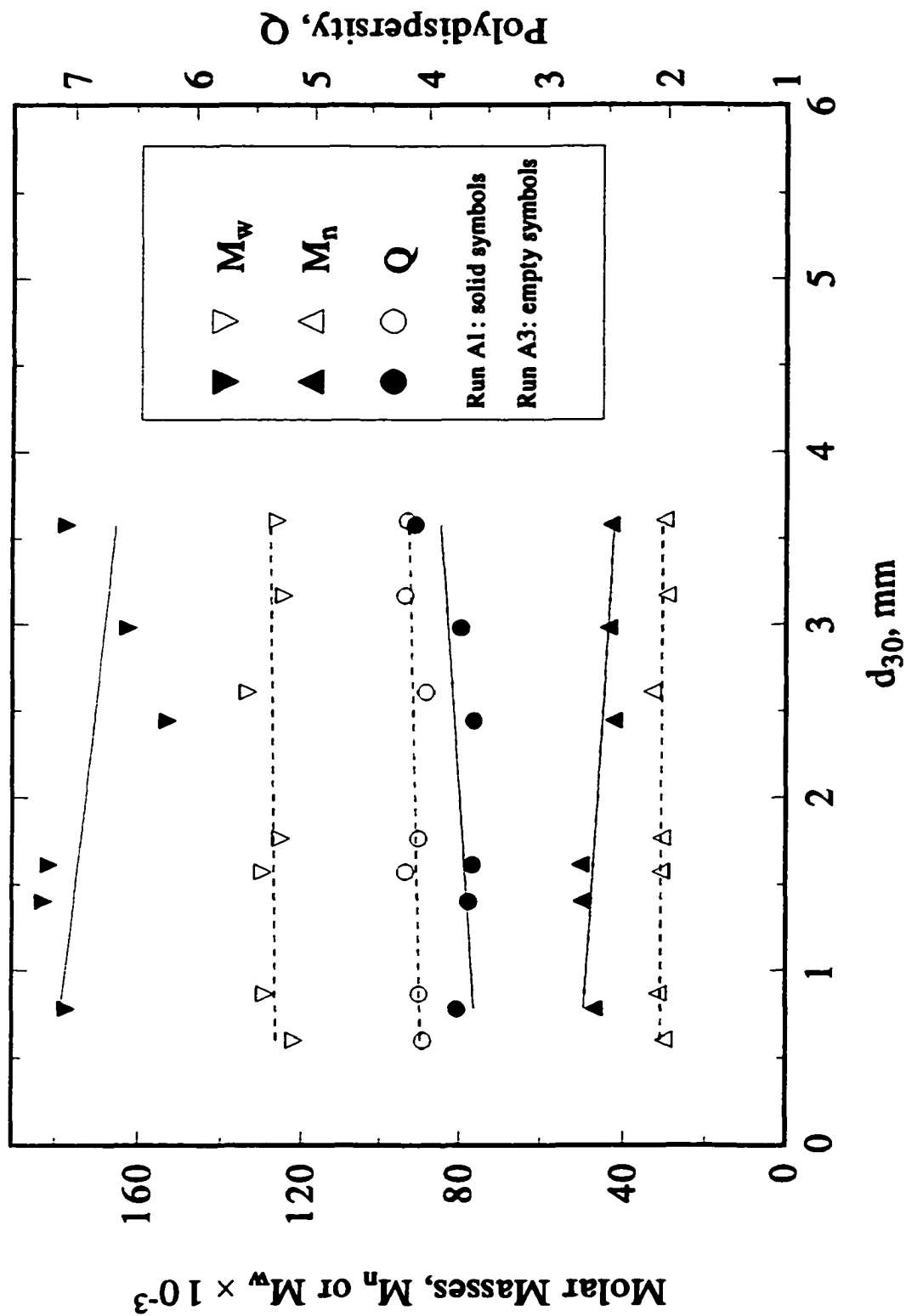
Figure 7.14   Effects of ethylene pressure on M_n, M_w, and Q of gas-phas polymerization at T=68°C and P_{H_2}=0.35 MPa ($P_{C_2H_4}$=1.39 MPa for Run A1, $P_{C_2H_4}$=0.69 MPa for Run A3).

174

important process for the termination of chain propagation during the formation of a macromolecule; which is consistent with the observation that the molar masses are essentially independent of ethylene pressure in the absence of hydrogen (Jejelowo *et al.*, 1991). Polydispersity, shown in Figure 7.14, is essentially independent of granule size, and decreases with increasing ethylene pressure at polymerization temperature of about 68°C (*cf.* explanation for Figure 7.11).

Shown in Figure 7.15 is the effect of polymerization temperature on the molar masses and polydispersity as a function of granule size produced from Runs A3 and A5. It is seen in Figure 7.15 that molar masses and polydispersity are essentially constant for different sizes of granules from each run; but molar masses are significantly higher and polydispersity is slightly lower at 30°C (Run A5) than at 70°C (Run A3). Similar temperature effects on the molar masses and polydispersity were observed for ethylene polymerization over $SiO_2/MgCl_2$-supported Ziegler-Natta catalyst in the absence of hydrogen (Jejelowo *et al.*, 1991). According to Jejelowo *et al.* (1991), the temperature effect on molar masses indicates that the activation energy for chain termination process is higher than that of the chain propagation; the temperature effect on polydispersity seems to support the speculation that the broadening of molar mass distribution (*i.e.*, increase in polydispersity) is related to the more pronounced catalyst deactivation with increasing polymerization temperature, since the more pronounced deactivation of catalyst can result in an increase in the nonuniformity of the activity of the catalytic sites. If different catalytic sites produce polymer with different molar masses, then the greater nonuniformity of the catalytic sites will broaden the molar mass distribution of polymer. The more rapid decay of

175
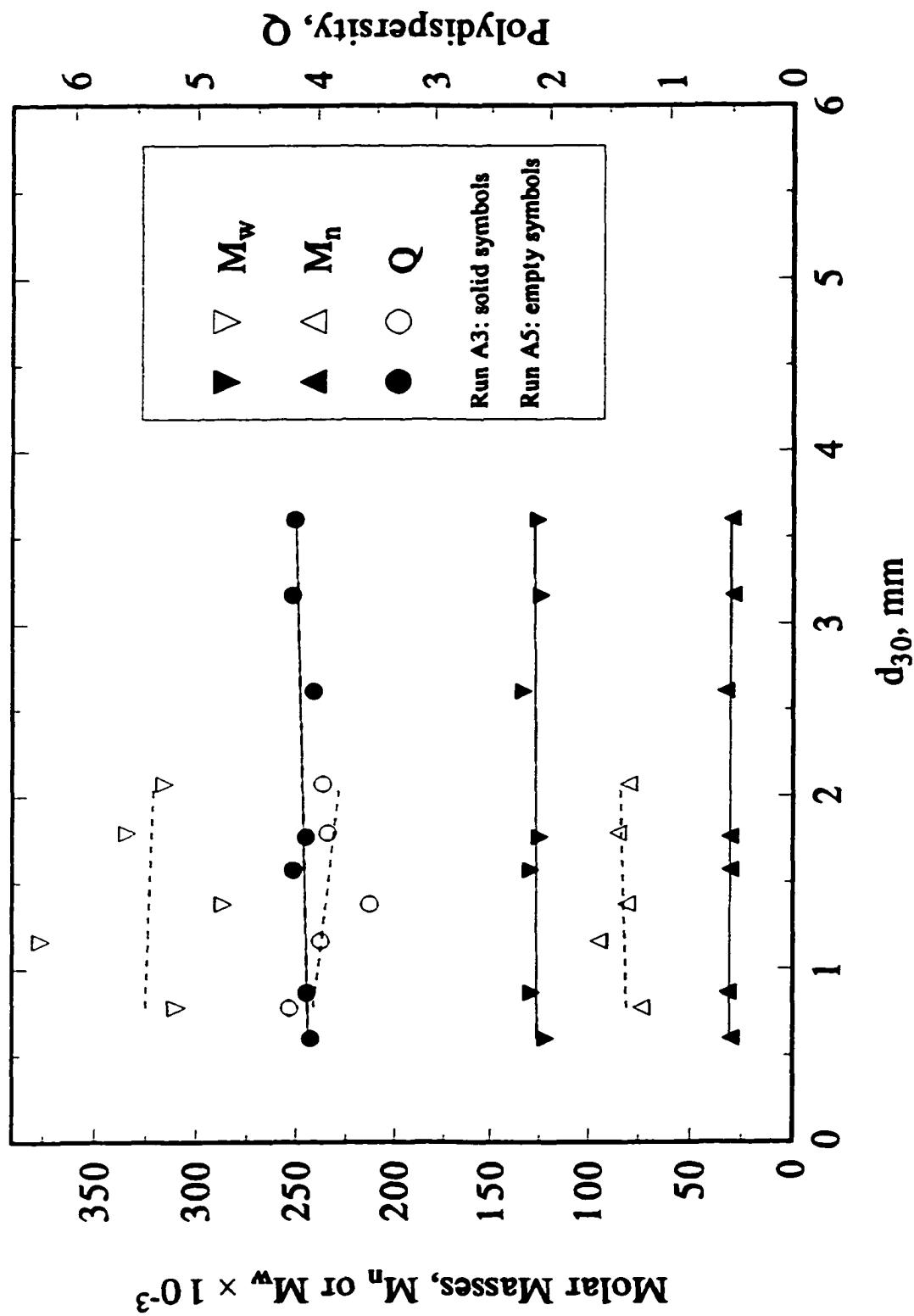
Figure 7.15 Effects of reaction temperature on M_n, M_w, and Q of gas-phase polymerization at $P_{C_3H_6}$=0.7 MPa and P_{H_2}=0.35 MPa (T=68°C for Run A3, T=29°C for Run A5).

176

polymerization rate, which was caused by more pronounced catalyst deactivation at higher temperature, is evidenced by comparing the rate profiles of Runs A3 and A5 in Figure 7.16.

The effects of polymerization time on the molar masses and polydispersity, as a function of granule size produced from Runs A1 and A4, are shown in Figure 7.17. The broken larger granules in Run A4 due to the long time grinding were not characterized. It is seen in Figure 7.17 that molar masses and polydispersity are essentially constant for different sizes of granules for each run; but molar masses and polydispersity increase slightly as polymerization proceeded from 2 (Run A1) to 7.8 hours (Run A4); this is different from the common observation that increasing polymerization time tends to decrease the molar masses and polydispersity (Zucchini and Cecchin, 1983).

The slightly higher molar masses of Run A4 with a longer polymerization time are partly due to the slightly higher ethylene pressure and lower hydrogen pressure of Run A4 than those of Run A1 (see Table 7.1). The slight increase of polydispersity with time can be caused by the presence of multiple catalytic sites. As proposed in Chapters 5 and 6, at least two different catalytic sites, one of which activates and deactivates faster than the other, are present in the catalyst. If each catalytic site can produce polymer with different molar masses, the two sites will produce different amount of polymer at shorter and longer times. The site with slow activation and deactivation will produce less polymer at shorter times, but produce more polymer at longer times than the site with fast activation and deactivation. At shorter times, the majority of the polymer produced are from the site with fast activation and deactivation. Polydispersity will be increased at longer times as more polymer is produced by the site with slow activation and deactivation.

177
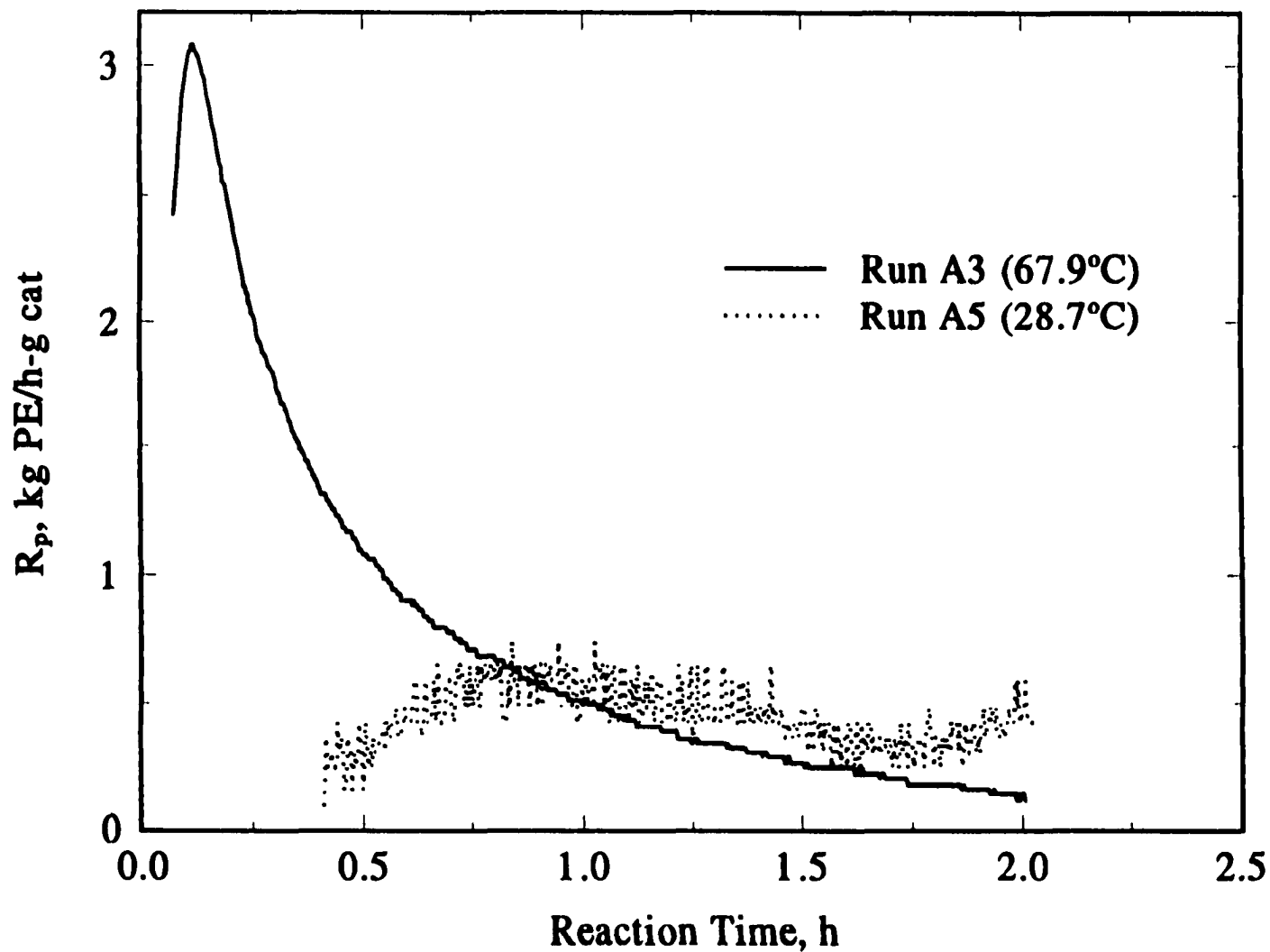
Figure 7.16   Temperature effects on rate profiles in the presence of H_2 (gas-phase polymerization).
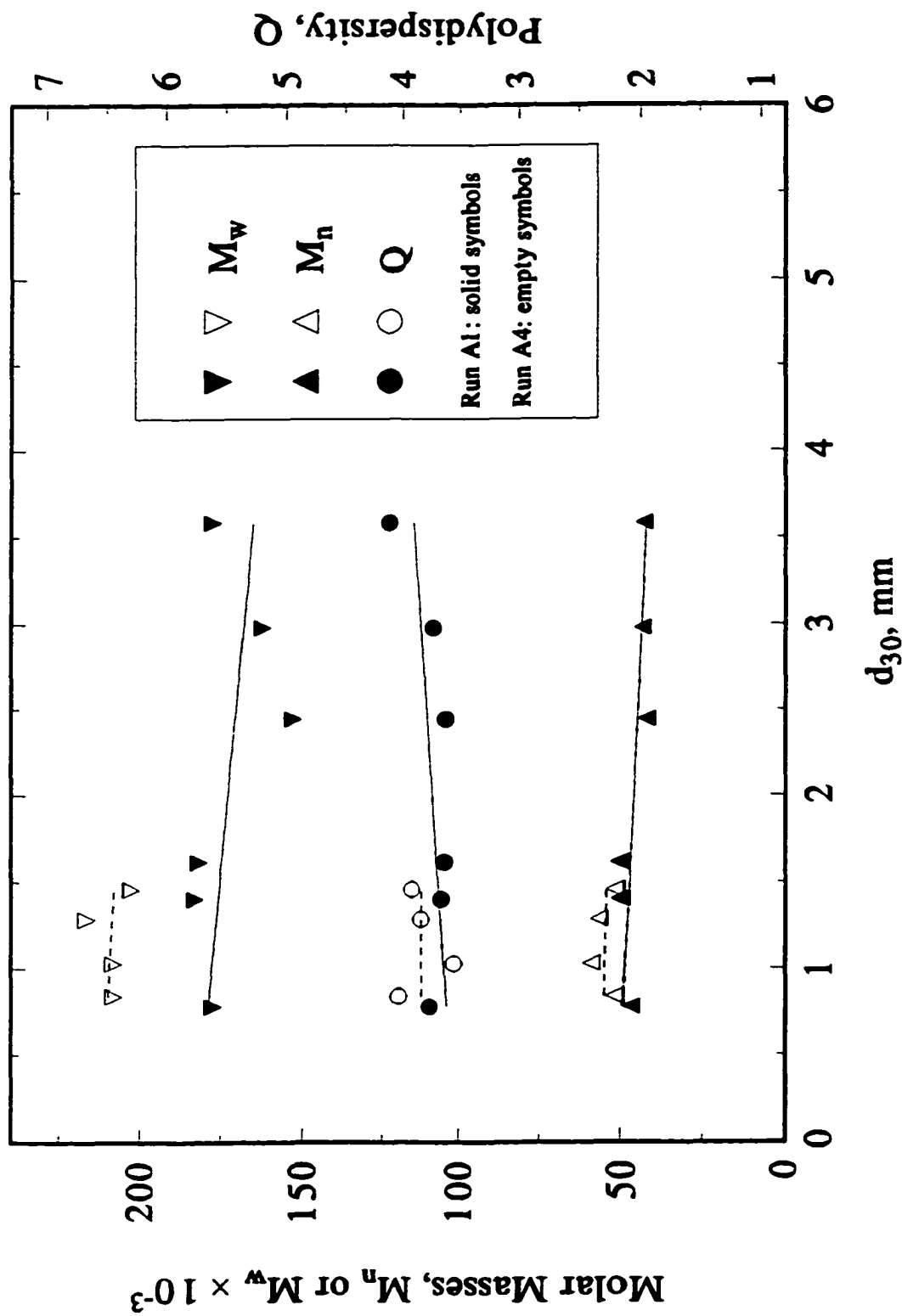
Figure 7.17   Effects of polymerization time on M_n, M_w, and Q in gas-phase operation ($t=2.0$ h for Run A1, $t=7.8$ h for Run A4).

In summary, molar masses decrease and polydispersity increases, to a lesser degree, with increasing granule size for nascent polyethylene granules made from slurry polymerization, while both molar masses and polydispersity are essentially independent of granule size in all the gas-phase operations. The size dependencies of molar masses and polydispersity in the slurry operations are probably caused by the presence of mass transfer limitations. Molar masses and polydispersity of polyethylene made in both slurry and gas-phase polymerization are affected by reactor operation conditions with the catalyst used in this study; molar masses are more sensitive to the reactor operation conditions than polydispersity. Among the operation conditions, ethylene pressure, reaction temperature and reactor operation mode have larger effects on molar masses and polydispersity than other operation conditions, such as the catalyst amount and polymerization time (besides hydrogen effects, which were not investigated in this study). With increasing ethylene pressure, molar masses increase and polydispersity decreases. The increase of molar masses with ethylene pressure (*i.e.*, ethylene concentration) is also reflected by the reactor operation mode, *i.e.*, with similar polymerization conditions, higher molar masses are obtained in slurry experiments due to the higher concentration of ethylene in the liquid than in the gas phase. The decrease of molar masses with increasing reaction temperature observed in this study indicates that the activation energy for chain termination is higher than that for chain propagation process; the increase of polydispersity with increasing reaction temperature suggests the presence of different catalytic sites which deactivate more pronouncedly with increasing polymerization temperature. This suggestion was supported by the more pronounced rate decay and the appearance of two maxima in the rate profiles observed in this study.

8. Kinetic Modeling of Gas-Phase Ethylene Homopolymerization

Modeling, including empirical modeling and kinetic modeling, is required for optimization of operation conditions and industrial process design. Empirical modeling may be more generally applicable than kinetic modeling, but kinetic theory-based modeling can provide more valuable information to understand reaction kinetics, to modify the performance of catalysts, and to predict the quality of final products.

In the previous chapters, it has been demonstrated that the multigrain model, a well-defined transport resistance model based on the first order kinetics and mass transfer limitations, cannot be used to model the rate profiles of gas-phase homopolymerization of ethylene in this study (see Chapter 5); effects of mass and heat transfers are negligible, *i.e.*, the polymerization rates measured are intrinsic rates, for the polymerization conditions used in the present study (see Chapter 6). Numerous kinetic models have been proposed for Ziegler-Natta polymerization in the absence of mass transfer limitations (reviewed in Chapter 2); none of them can describe the kinetic behavior reported in this study.

In Section 8.1 of this chapter, a model, according to the reaction kinetics, is proposed for gas-phase homopolymerization of ethylene, then a set of rate equations governed by the model are solved to yield the evolution of catalytic site concentrations. In Section 8.2, the model predictions are compared with the experimental results reported in Chapters 5 and 6. The limitations and improvement of this model is further discussed in Section 8.3. The objective of the kinetic modeling in this study is to determine whether the model can predict the characteristics of the kinetic behavior observed in experiments. No

attempts are made to fit parameters to the experimental data since experiments on absolute rate can vary by up to 60% as reported in Chapter 5.

8.1 Development of Reaction-Kinetic Model

The kinetics of catalytic reaction systems are usually described by overall reaction rate of a proposed scheme in which each reaction step may not be necessarily an elementary step. The reaction-kinetic scheme proposed in this study is mainly based on the results and the reaction-kinetic interpretations of the rate profiles in the gas-phase experiments (see Chapter 5). The characteristic features of the rate profiles presented in Chapter 5 include: the decrease of the polymerization rates started either after an acceleration period such as those at polymerization temperatures below 70°C or early in the beginning of polymerization such as those at polymerization temperatures above 70°C, which indicated that the catalyst deactivated more rapidly with increasing polymerization temperature; at low ethylene pressures and polymerization temperatures, the initial acceleration period appear to be S-shaped; the distinguishable two maxima were observed in the rate profiles at polymerization temperatures above 40°C; and the second peak is broader than the first peak. It was also shown in Chapters 5 and 6 that the rate profiles are insensitive to catalyst amounts at a fixed amount of cocatalyst, and mass and heat transfer limitations are negligible during polymerization. The insensitivity of catalyst amount on the rate profiles at fixed amount of cocatalyst also indicates that variation in the amount of cocatalyst has negligible effect on the rate profiles under the polymerization conditions used in this study. However, the experiments in this study (Chapters 5 and 6) did not provide information on the deactivation kinetics.

182

As reviewed in Chapter 2, the S-shaped acceleration period in the initial polymerization rate can be kinetically described well by a two-step initiation reaction of the catalytic sites, in which monomer participates in the second step with the first-order dependence (Kissin, 1985). However, the chemical detail of catalyst deactivation is not known. Since the catalyst deactivation is usually insensitive to the amount of polymer formed (*e.g.*, Keii, 1972; Kissin, 1985), the catalyst deactivation can be regarded, to a first approximation, as a kinetic phenomenon which is independent of the polymerization process (Kissin, 1985). Attempts to fit the rate decay profiles by the power-law rate functions indicated that the deactivation process depends on the catalyst used (reviewed in Chapter 2). The rate decay can be reasonably described well by a first order reaction, a second order, or a mixed first and second order reactions with respect to the concentration of the catalytic site. However, change of deactivation order with polymerization time (Keii *et al.*, 1982; Brockmeier and Rogan, 1985) and monomer-assisted deactivation (Chien and Kuo, 1986) were also reported for Ziegler-Natta polymerization.

The distinguishable two maxima in the rate profiles observed in Chapter 5 have been explained by the presence of at least two different types of catalytic sites, Site 1 and Site 2, in the prepolymerized catalyst. Each catalytic site has its own concentration and temperature dependencies on the activation and deactivation kinetics. In the analysis of polymerization kinetics by the new method presented in Chapter 6, the reaction orders with respect to ethylene concentration in the power-law rate function vary with temperature and are a strong function of time-on-stream. The power-law order decreases from about 1.5 to about 1 after 1 to 4 hours of polymerization. The power-law orders after 4 hours on stream

183

tend to be slightly less than 1 at 30°C, and slightly greater than 1 at higher temperatures. These results suggest that for the presence of at least two different types of catalytic sites in the catalyst, Site 1 activates and deactivates faster than Site 2 (see Chapter 6).

Literature reports on catalyst, kinetics and product characterization of Ziegler-Natta polymerization, in addition to deactivation studies (reviewed in Section 2.5.5), provide additional evidence that at least two different types of catalytic sites exist in the heterogeneous Ziegler-Natta catalysts. The study of energy distribution of active sites by temperature programming deposition / mass spectroscopy (TPD/MS) showed that there are at least two types of active sites with different activation energies for a thermal destruction of Ti-C bonds in ethylene polymerization over $SiO_2/TiCl_4/AlEt_2Cl$ catalysts; each type of sites has its own distribution of activation energies (Novokshonova *et al.*, 1997).

The heterogeneity of polymerization active sites was mathematically developed by Clark and Bailly (1963) according to a Langmuir-Hinshelwood mechanism. Clark and Bailly (1963) found that variations of adsorption energies among the sites were required to fit the experimental data closely and to fit the broadness of MMD of polyethylene made on chromium oxide-silica-alumina catalysts. A combination of at least two Langmuir-Hinshelwood rate functions with different ethylene concentration dependencies was found by Bu *et al.* (1995) to be the only explanation for the observed rate behavior in the gas-phase homopolymerization of ethylene over $SiO_2/MgCl_2$-supported $TiCl_4$ catalysts.

By applying TREF, SEC, ^{13}C NMR, DSC and FTIR to characterize LLDPE made by different processes and HP-LDPE blend, Usami *et al.* (1986) reported that at least two different kinds of active sites are present in Ti based heterogeneous Ziegler catalysts. The

184

quantitative results of the PTREF-SEC cross-fractionation of LLDPE produced by systematic experiments showed that the different catalytic sites have different functional forms for chain termination by transfer to hydrogen (Huang *et al.*, 1997).

The experimental results observed in this study and in the literature are further discussed after the modeling. The results that are of particular interest to the formulation of the present model are summarized:

1. Effects of catalyst (or cocatalyst) amounts on the rate profiles are negligible.

2. Effects of mass and heat transfer limitations are negligible.

3. At low temperatures, the initial acceleration period appears to be S-shaped.

4. Two different types of catalytic sites, *i.e.*, Site 1 and Site 2, are present in the catalyst.

5. Different types of catalytic sites have different activation and deactivation behavior; Site 1 activates and deactivates faster than Site 2.

6. Different types of catalytic sites have different ethylene concentration and temperature dependencies on their activation and deactivation kinetics.

No real modeling can be done without any assumptions. For this model, significant simplification can be achieved mathematically with the following assumptions. Some of the assumptions (*e.g.*, the equal reactivity assumption) are common for general polymerization.

1. The two types of catalytic sites, Site 1 and Site 2 present in the catalyst, are initiated (activated) in parallel. This is based on the insensitivity of catalyst or cocatalyst amount on rate profiles observed in this study.

2. Site 1 and Site 2 are evenly dispersed in the catalyst particles, and the specific activity of the catalyst is independent of catalyst particle size.

185

3. The ratio of Ti in Site 1 to Ti in Site 2 was assumed to be constant since effects of cocatalyst/catalyst ratio on rate profiles are negligible in this study (see Chapter 5). This constant ratio was assumed to 7 to 3 according to Chien *et al.* (1989).

4. Gases in the reactor obey the ideal gas law, and gas-phase ethylene concentration is calculated by the ideal gas law, *i.e.*, $[M]_{C_2H_4} = P_{C_2H_4} / RT$.

5. Effects of ethylene sorption in polyethylene are ignored; thus, the gas-phase ethylene concentration will be used as the ethylene concentration at the catalytic site; this is the same as assuming that the absorption of ethylene in the polyethylene obeys Henry's law.

6. The initiation of Site 1 is a two-step reaction with a first-order monomer dependence on the second step reaction to account for the S-shaped initial rate profiles at low temperature. Due to the participation of monomer in the initiation, it is not unreasonable to assume that the first-order monomer dependence is also required for the deactivation of Site 1. Monomer does not participate in the initiation and deactivation for Site 2.

7. The first order deactivation with respect to the concentration of catalytic site is applied to each type of site.

8. The chain propagation rate constant for each type of active site is independent of polymerization degree (equal reactivity assumption). The propagation rate for each type of site is first order with respect to concentrations of ethylene and active site.

9. The average values of various rate constants will be used although a broad distribution of activation energies for each type of catalytic site may be present in the heterogeneous Ziegler-Natta catalysts.

10. Consumption of ethylene by chain propagation is the only contribution to the overall polymerization rate because the initiation and deactivation consume only small amount of ethylene relative to the chain propagation.

186

According to the above summaries and assumptions, the following reaction steps, including initiation, propagation and deactivation, are proposed for Site 1 and Site 2:

Initiation

for Site 1 $S_1 \xrightarrow{k_{i1}} S_{a1}$ (8.1a)

$S_{a1} + M \xrightarrow{k_{s1}} C_{p1} (x = 1)$,   where: $C_{p1}(x=1) = S_{a1}\text{-}M$ (8.1b)

for Site 2 $S_2 \xrightarrow{k_{i2}} C_{p2}(x = 0)$ (8.2)

Propagation

for Site 1 $C_{p1}(x) + M \xrightarrow{k_{p1}} C_{p1}(x + 1)$, where: $C_{p1}(x) = S_{a1}M\text{-}M_{x-1}$ (8.3)

$C_{p1}(x+1) = S_{a1}M\text{-}M_x$

for Site 2 $C_{p2}(x) + M \xrightarrow{k_{p2}} C_{p2}(x + 1)$, where: $C_{p2}(x) = S_1M_x$ (8.4)
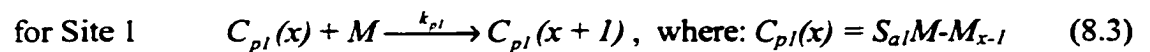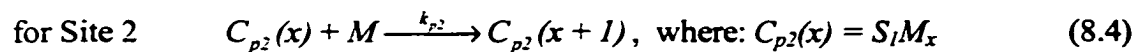
$C_{p2}(x+1) = S_2M_{x+1}$

Deactivation

for Site 1 $S_{a1} \xrightarrow{k_{d1}} S_{d1}$ (8.5)

$C_{p1}(x) + M \xrightarrow{k_{d m1}} S_{d1} + polymer(x)$ (8.6)

for Site 2 $S_2 \xrightarrow{k_{t2}} S_{d2}$ (8.7)

$C_{p2}(x) \xrightarrow{k_{d2}} S_{d2} + polymer(x)$ (8.8)

187

where: subscripts 1 and 2 denote two different types of catalytic sites; S_1 and S_2 are the potential active sites for polymerization, S_{a1} is an active site for Site 1, $C_{p1}(x)$ (*i.e.*, $S_{a1}M$-M_{x-1}) and $C_{p2}(x)$ (*i.e.*, S_2M_x) are active chains or propagation sites for Site 1 (monomer-complexed) and Site 2 with a polymerization degree of x, S_{d1} and S_{d2} are catalytically inactive sites; k_{f1} and k_{f2} are the rate constants for formation of active sites, k_{i1} is the initiation rate constants for Site 1, k_{p1} and k_{p2} are rate constants of chain propagation, k_{d1}, and k_{d2} are rate constants of spontaneous deactivation for Site 1 and Site 2, and k_{dm1} is rate constant for monomer-assisted deactivation of propagation Site 1; M is ethylene monomer.

Note that difference between Site 1 and Site 2 in the above reaction model lies in the initiation (see Equations 8.1 and 8.2) and deactivation steps (see Equations 8.6 and 8.8). The initiation for Site 1 consists of two consecutive steps: an active site generating step without monomer participation (Equation 8.1a) and an initiation step with first monomer (Equation 8.1b). The initiation for Site 2 has only one step: an active site generating step without monomer participation (Equation 8.2). In other words, the reaction of the first monomer with active site is different from the reaction of the second monomer with active site for Site 1, while there is no difference between these two reactions for Site 2. As a result, the active site for the chain propagation of Site 1 can be considered as a complex of a catalytic site and a monomer (Ti-M); the active site for the chain propagation of Site 2 is the catalytic site (Ti) only. The propagation Site 1 deactivates with monomer assistance, but the propagation Site 2 deactivates spontaneously without monomer assistance.

Based on the reaction steps proposed above, the change of potential active sites, the initiation sites, and the active sites with time t for Site 1 and Site 2 can be written:

188

for Site 1

$$\frac{d[S_1]}{dt} = -k_{f1}[S_1]$$

(8.9)

$$\frac{d[S_{a1}]}{dt} = k_{f1}[S_1] - k_{i1}[S_{a1}][M] - k_{d1}[S_{a1}]$$

(8.10)

$$\frac{d[C_{p1}]}{dt} = k_{i1}[S_{a1}][M] - k_{dm1}[C_{p1}][M]$$

(8.11)

for Site 2

$$\frac{d[S_2]}{dt} = -k_{f2}[S_2] - k_{d2}[S_2]$$

(8.12)

$$\frac{d[C_{p2}]}{dt} = k_{f2}[S_2] - k_{d2}[C_{p2}]$$

(8.13)

The above differential Equations 8.9 to 8.11 and Equations 8.12 and 8.13 can be solved analytically to give the dependence of propagation sites on time for Site 1 and Site 2, respectively. Solving Equations 8.9 to 8.11 for Site 1 yields:

$$[C_{p1}] = \frac{k_{i1}k_{f1}[M][S_{10}]}{k_{i1}[M] + k_{d1} - k_{f1}} e^{-k_{dm1}[M]t} \left(\frac{1 - e^{-(k_{f1} - k_{dm1}[M])t}}{k_{f1} - k_{dm1}[M]} - \frac{1 - e^{-(k_{i1}[M] - k_{d1} - k_{dm1}[M])t}}{k_{i1}[M] + k_{d1} - k_{dm1}[M]} \right)$$

(8.14)

Solving Equations 8.12 and 8.13 for Site 2 yields:

$$[C_{p2}] = [S_{2,0}](e^{-k_{d2}t} - e^{-(k_{f2} + k_{d2})t})$$

(8.15)

where $[S_{1,0}]$ and $[S_{2,0}]$ in Equations 8.14 and 8.15 are the initial concentrations of potential active sites for Site 1 and Site 2, respectively.

189

The polymerization rates for Site 1 and Site 2, R_{p1} and R_{p2}, are expressed as:

$$R_{p1} = k_{p1}[C_{p1}][M] \qquad (8.16)$$

$$R_{p2} = k_{p2}[C_{p2}][M] \qquad (8.17)$$

Substitution of Equations 8.14 and 8.15 into Equations 8.16 and 8.17, respectively, yields:

$$R_{p1} = k_{p1}[S_{1,0}] \frac{k_{i1}k_{f1}[M]^2}{k_{i1}[M] + k_{d1} - k_{f1}} e^{-k_{dm1}[M]t} \left(\frac{1 - e^{-(k_{f1}-k_{dm1}[M])t}}{k_{f1} - k_{dm1}[M]} - \frac{1 - e^{-(k_{i1}[M]+k_{d1}-k_{dm1}[M])t}}{k_{i1}[M] + k_{d1} - k_{dm1}[M]} \right) \qquad (8.18)$$

$$R_{p2} = k_{p2}[S_{2,0}][M](e^{-k_{a2}t} - e^{-(k_{a2}+k_{f2})t}) \qquad (8.19)$$

Equations 8.18 and 8.19 show that the two types of catalytic sites with different activation and deactivation kinetics have different monomer concentration and different temperature dependencies on their polymerization rates although both types of sites have similar propagation kinetics.

The simplest form of overall polymerization rate, R_p, is the simple summation of polymerization rates for Site 1 and Site 2:

$$
\begin{aligned}
R_p &= R_{p1} + R_{p2} \\
&= k_{p1}[S_{1,0}] \frac{k_{i1}k_{f1}[M]^2}{k_{i1}[M] + k_{d1} - k_{f1}} e^{-k_{dm1}[M]t} \left(\frac{1 - e^{-(k_{f1}-k_{dm1}[M])t}}{k_{f1} - k_{dm1}[M]} - \frac{1 - e^{-(k_{i1}[M]+k_{d1}-k_{dm1}[M])t}}{k_{i1}[M] + k_{d1} - k_{dm1}[M]} \right) \\
&\quad + k_{p2}[S_{2,0}][M](e^{-k_{a2}t} - e^{-(k_{a2}+k_{f2})t})
\end{aligned}
$$

$$(8.20)$$

Since the effects of catalyst amounts on the rate profiles are negligible (see Chapter 5), a fixed amount of catalyst (*i.e.*, 0.1 g of prepolymerized catalyst) was used for all the simulation runs. The complete set of parameters used for simulation is listed in Table 8.1.

Table 8.1   Parameters Used for Equation 8.20 (the universal gas constant $R=8.314$ $J/mol \cdot K$)

Parameters	Values at T=323.15 K	Units
$k_{f1} = 1.2 \times 10^7 exp(- 40000/RT)$	4.105	h^{-1}
$k_{i1} = 1.5 \times 10^2 exp(- 40000/RT)$	5.131×10^{-5}	$m^3 \cdot mol^{-1} \cdot h^{-1}$
$k_{p1} = 2.5 \times 10^{14} exp(- 40000/RT)$	8.551×10^7	$kgPE \cdot m^3 \cdot mol^{-1} \cdot (mol\ Ti)^{-1} \cdot h^{-1}$
$k_{d1} = 3.6 \times 10^5 exp(- 32000/RT)$	2.419	h^{-1}
$k_{dm1} = 9.6 \times 10^2 exp(- 32000/RT)$	6.450×10^{-3}	$m^3 \cdot mol^{-1} \cdot h^{-1}$
$k_{i2} = 1.2 \times 10^3 exp(- 32000/RT)$	8.062×10^{-3}	h^{-1}
$k_{p2} = 1.07 \times 10^{13} exp(- 32000/RT)$	7.189×10^7	$kgPE \cdot m^3 \cdot mol^{-1} \cdot (mol\ Ti)^{-1} \cdot h^{-1}$
$k_{d2} = 4.2 \times 10^2 exp(- 20000/RT)$	0.2456	h^{-1}
$[S_{1,0}] = 70\%\ of\ Ti\ in\ catalyst$	5.95×10^{-8}	$mol\ Ti \cdot (0.1\ gCat)^{-1}$
$[S_{2,0}] = 30\%\ of\ Ti\ in\ catalyst$	2.55×10^{-8}	$mol\ Ti \cdot (0.1\ gCat)^{-1}$

In Table 8.1, the values of the activation energies of initiation and propagation for Site 1 and Site 2 were assumed to be 40,000 and 32,000 J/mol, respectively. These values are in the range of 30,000 to 50,000 J/mol which is typical for supported Ziegler-Natta catalysts (*e.g.*, Kim *et al.*, 1990; Jejelowo *et al.*, 1991). The activation energies for deactivation of catalytic sites have not been frequently reported in the literature and the experiments in this study did not provide information on the deactivation kinetics. Thus, the

lower activation energies for deactivation than for propagation of two sites and the pre-exponential factors were chosen to get approximately correct magnitudes of polymerization rates. The adjustment of the pre-exponential factors for propagation rate constants can also accommodate the change in the ratio of the initial Ti contents in Site 1 and Site 2 (*i.e.*, the ratio of 7 to 3 was assumed in this model).

With parameters listed in Table 8.1, polymerization rates for Site 1 and Site 2, and the overall polymerization rate can be calculated for a given polymerization condition, *i.e.*, ethylene concentration and temperature, as a function of time. The overall polymerization rate, according to Equation 8.20, is of most interest to the present modeling because the overall polymerization rate can be measured experimentally, which allows direct comparison of model predictions with experimental results. These comparisons on the rate profiles reported in Chapters 5 and on the reaction orders reported in Chapters 6 are presented in Section 8.2. No adjustments of the parameter values were made in obtaining the rates predicted by Equation 8.20.

8.2 Comparison of Model Predictions with Experimental Results

For model predictions of the rate profiles of Type B experiments reported in Chapter 5, ethylene pressures used were 0.69, 1.38, and 2.07 MPa, and polymerization temperatures used were 30, 40, 50, 60, and 70°C. The same values of ethylene pressure and polymerization temperature were chosen in order to compare the effects of ethylene pressure on the rate profiles at each polymerization temperature predicted by the model. The ethylene concentrations were calculated from the ethylene pressure and polymerization

temperature according to the ideal gas law. The model predictions by Equation 8.20 and experimental results are compared in Figures 8.1 to 8.5, for the effects of ethylene pressures on the rate profiles, at polymerization temperatures of 30, 40, 50, 60, and 70°C, respectively. In Figures 8.1 to 8.5, the bottom panels are the experimental results, and the top panels are the model predictions.

It can be seen from Figures 8.1 to 8.5 that the characteristics of the model predictions (Equation 8.20) show similarities to the experimental observations on the rate profiles. The model predicts most of the trends observed experimentally (see Chapter 5). These trends include: there is a single maximum at low polymerization temperatures and double maxima at higher temperatures; the S-shaped initial acceleration period at low polymerization temperatures and ethylene pressures which can be explained by the two-step fast initiation of Site 1 and one-step slow initiation of Site 2; and the broader second peaks than the first peaks which is due to the slower initiation and deactivation rates for Site 2 than for Site 1 (see Table 8.1 for parameter values).

The results presented in Figures 8.1 to 8.5 also indicate that the initiation steps in the model can account for the shift of the first peak form longer times to shorter times with increasing ethylene pressure and polymerization temperature. The shift of the maximum position of the first peak as function of ethylene pressure and polymerization temperature are illustrated in Table 8.2 for the model predictions. The experimental data listed in Table 5.4 are also included in Table 8.2 for comparison.
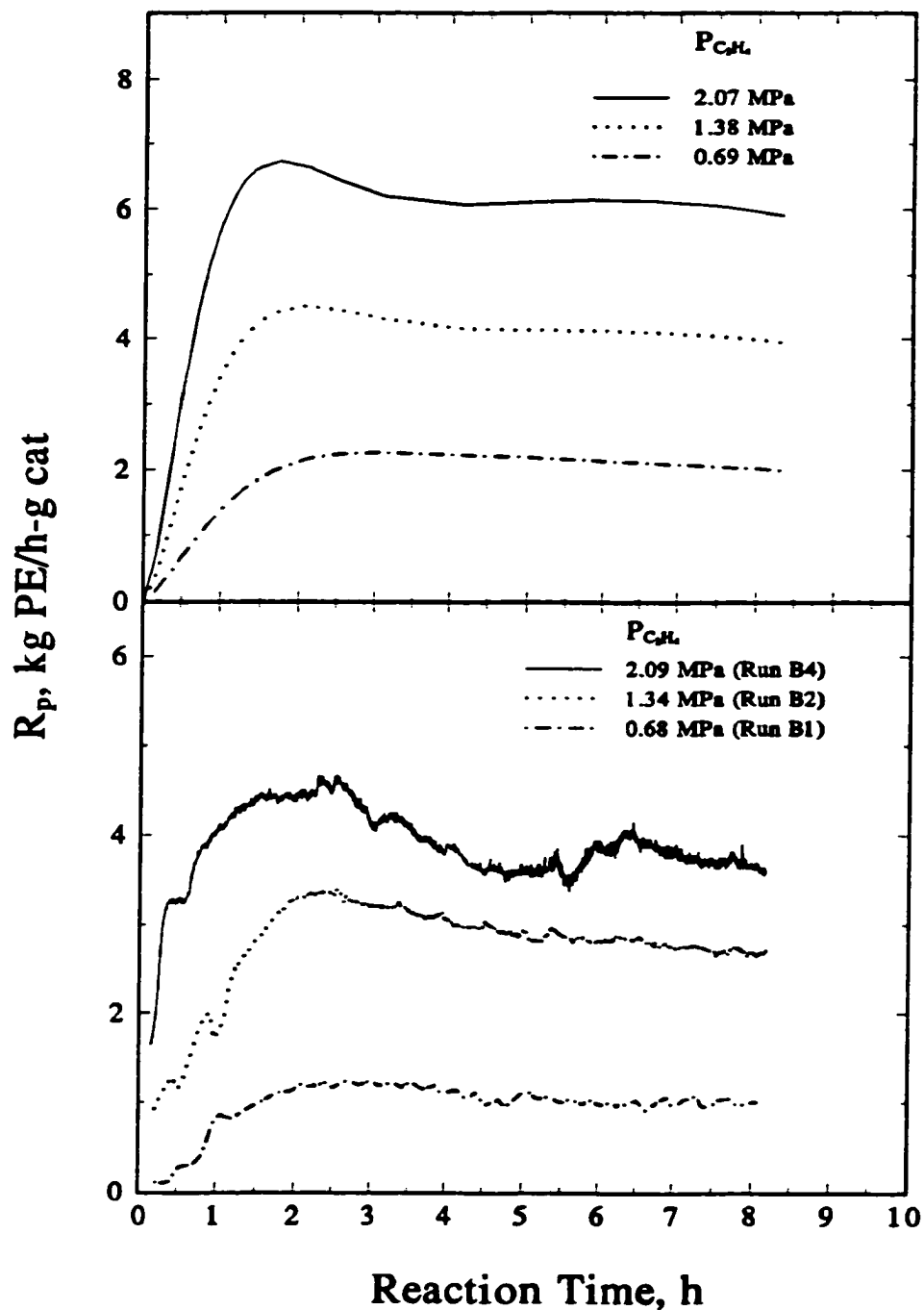
Figure 8.1 Comparison of model predictions (top panel) of rate profiles with experimental results (bottom panel) at 30°C.
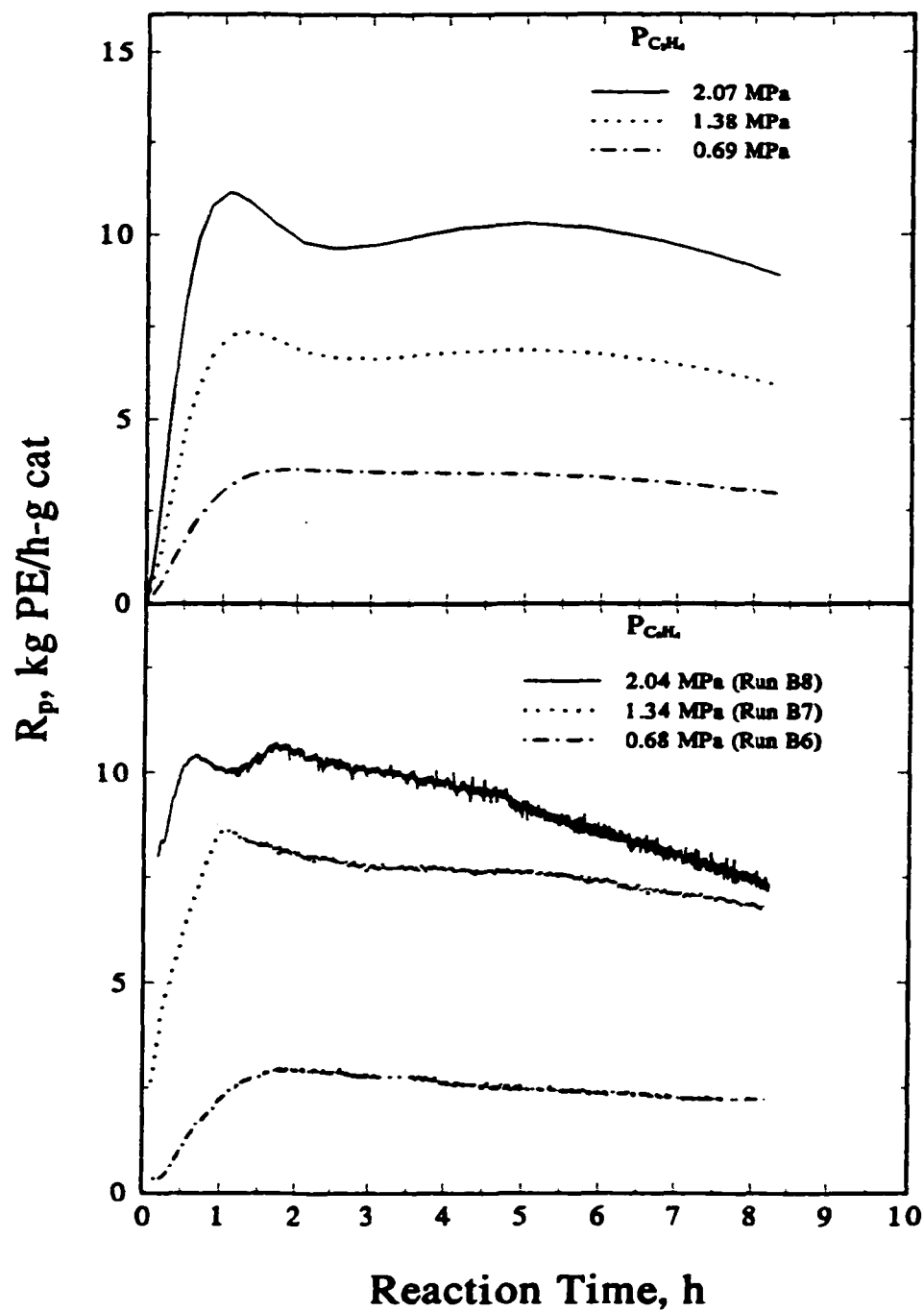
Figure 8.2 Comparison of model predictions (top panel) of rate profiles with experimental results (bottom panel) at 40°C.
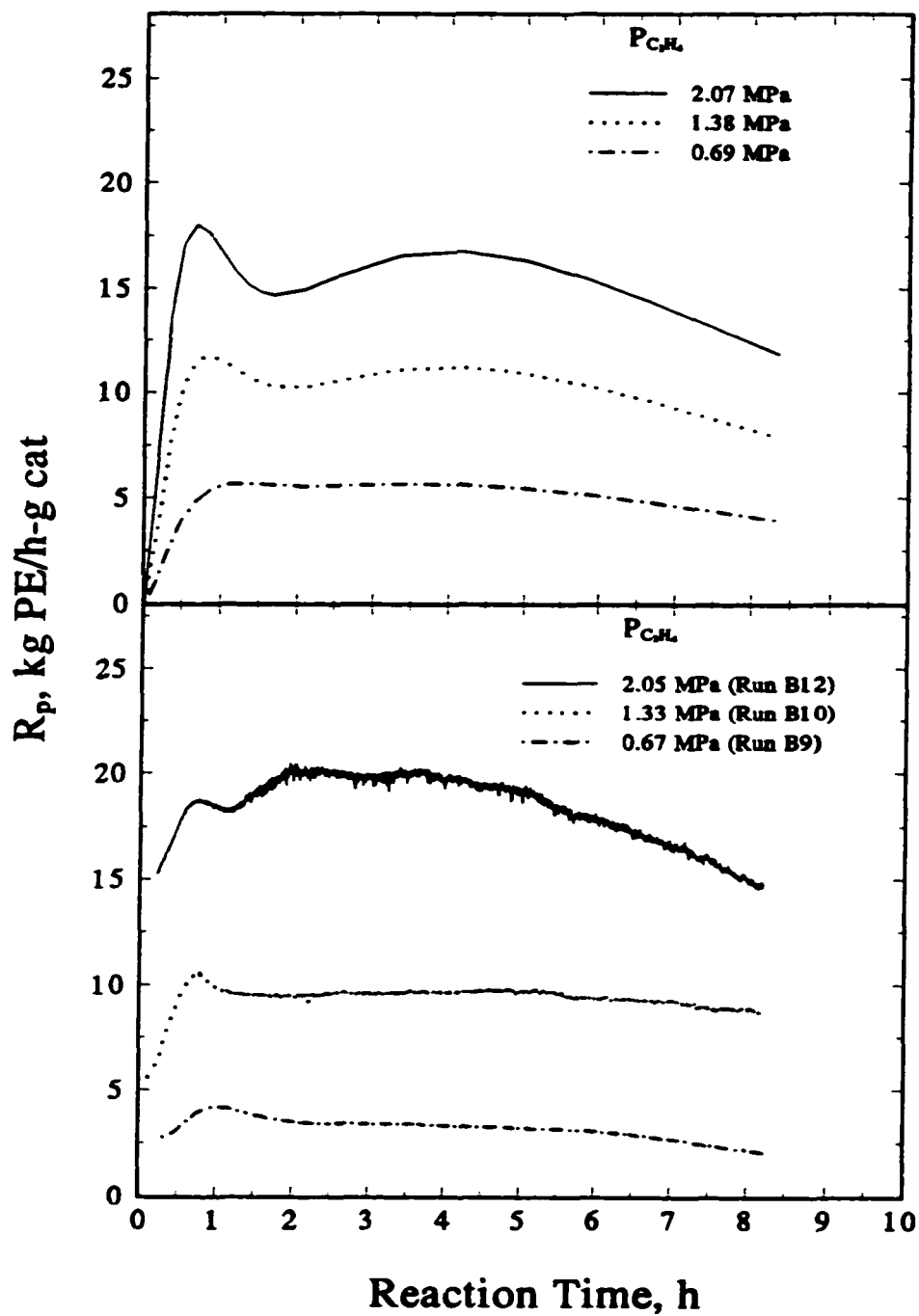
Figure 8.3 Comparison of model predictions (top panel) of rate profiles with experimental results (bottom panel) at 50°C.

196
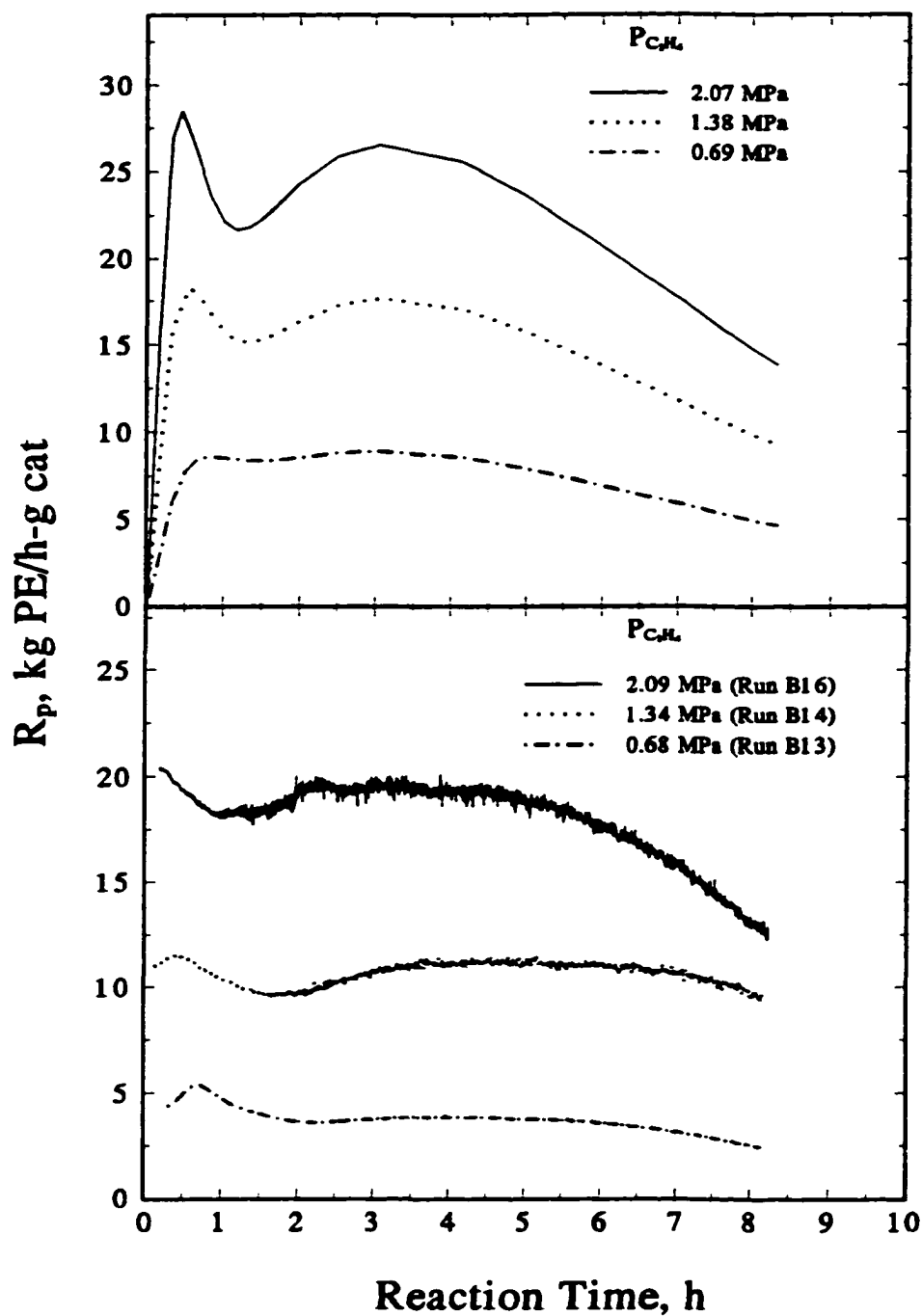
Figure 8.4   Comparison of model predictions (top panel) of rate profiles with experimental results (bottom panel) at 60°C.

197
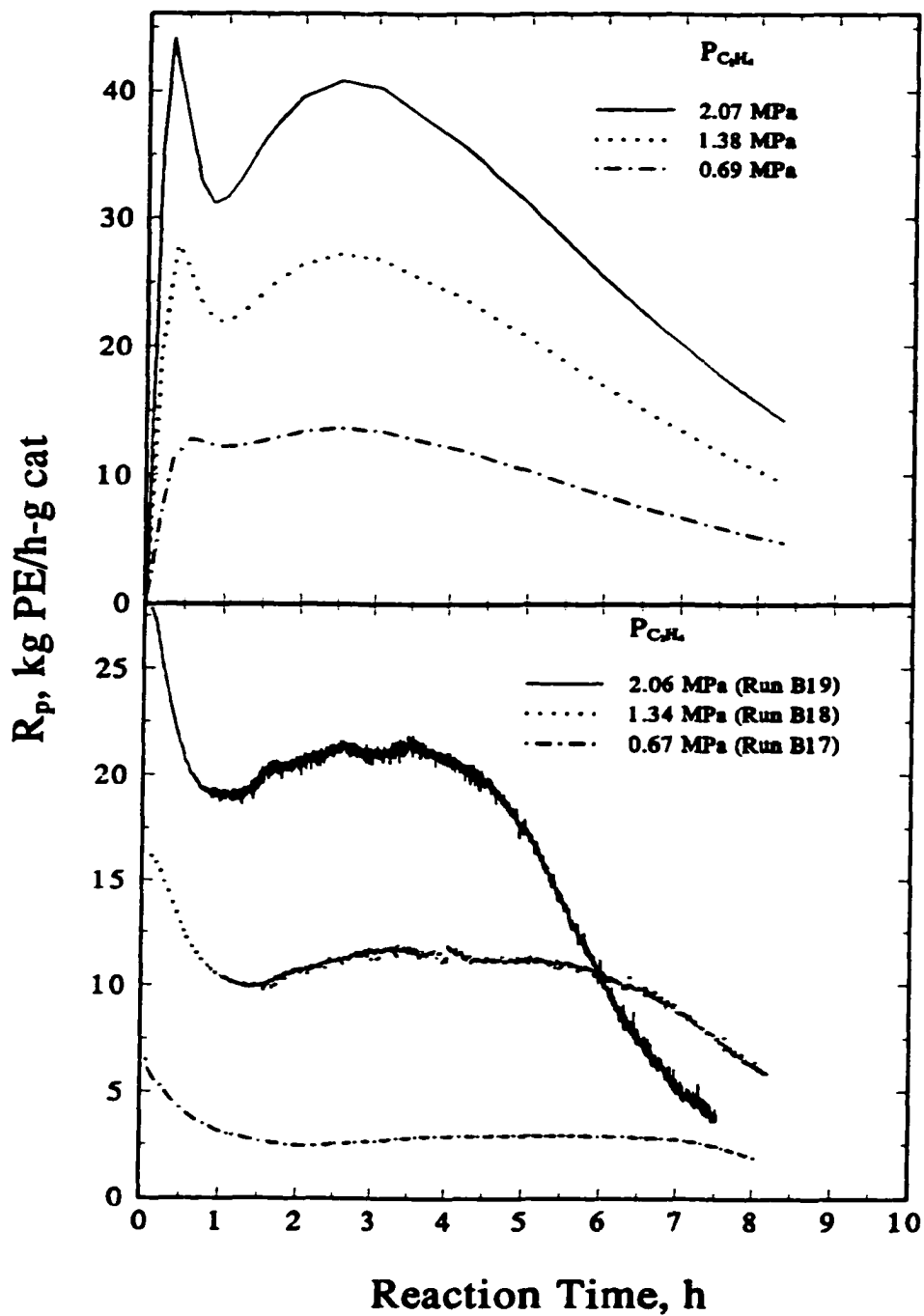
Figure 8.5 Comparison of model predictions (top panel) of rate profiles with experimental results (bottom panel) at 70°C.

Table 8.2   Comparison of Simulation Results (Equation 8.20) with Experiments on the Position of the Maximum of the First Peak

	$P_{C_2H_4}$, MPa	t_{max}, h				
		30°C	40°C	50°C	60°C	70°C
	0.69	3.05	1.98	1.28	0.83	0.55
Simulation	1.38	2.07	1.28	0.82	0.53	0.37
	2.07	1.73	1.07	0.67	0.45	0.30
	0.68	2.73	1.59	1.09	0.73	N/D[1]
Experiment[2]	1.34	2.42	1.12	0.74	0.49	N/D
	2.06	1.59	0.65	0.66	0.23	N/D

Notes:
1. N/D = not detectable.
2. See Table 5.3 for polymerization conditions.

The reaction-kinetic model with two types of catalytic sites gives reasonable agreement with the two-peak rate profiles observed experimentally. However, the absolute values of simulation results, such as the overall polymerization rate (see Figures 8.1 to 8.5) and the first peak maximum (see Table 8.2), deviate from experimental results. The deviation of the first peak maximum is probably due to the deviation of the overall polymerization rate. These deviations are not surprising when one set of parameters was used to model polymerization rates at different ethylene pressures and different temperatures.

Reaction orders obtained by Type C experiments reported in Chapter 6 can also be simulated by the model (Equation 8.20). The comparisons of model predictions with experimental results of the reaction orders are shown in Figures 8.6 to 8.10 for one run at
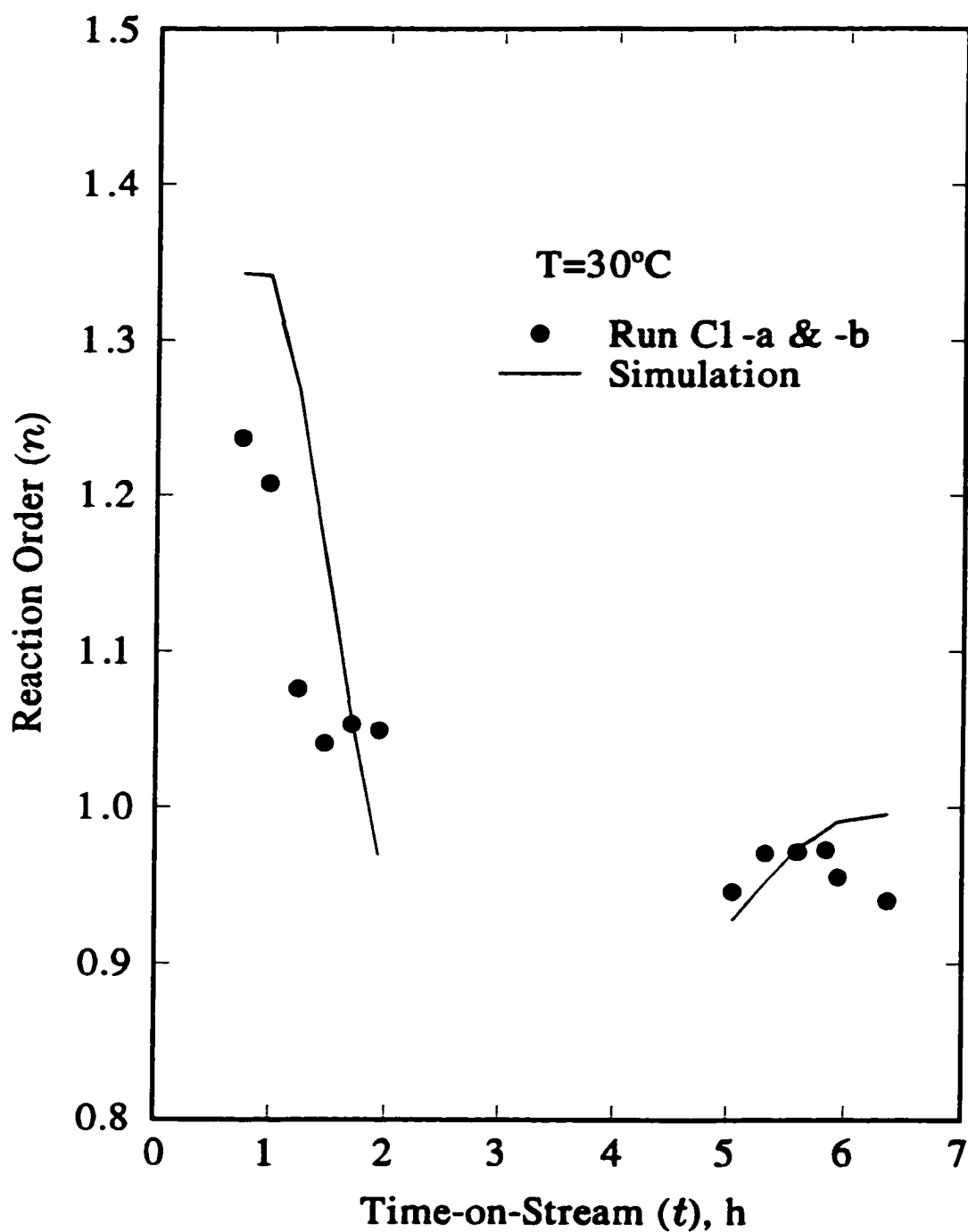
Figure 8.6 Comparison of experimental and simulated power-law orders as a function of time at 30°C (Run C1).
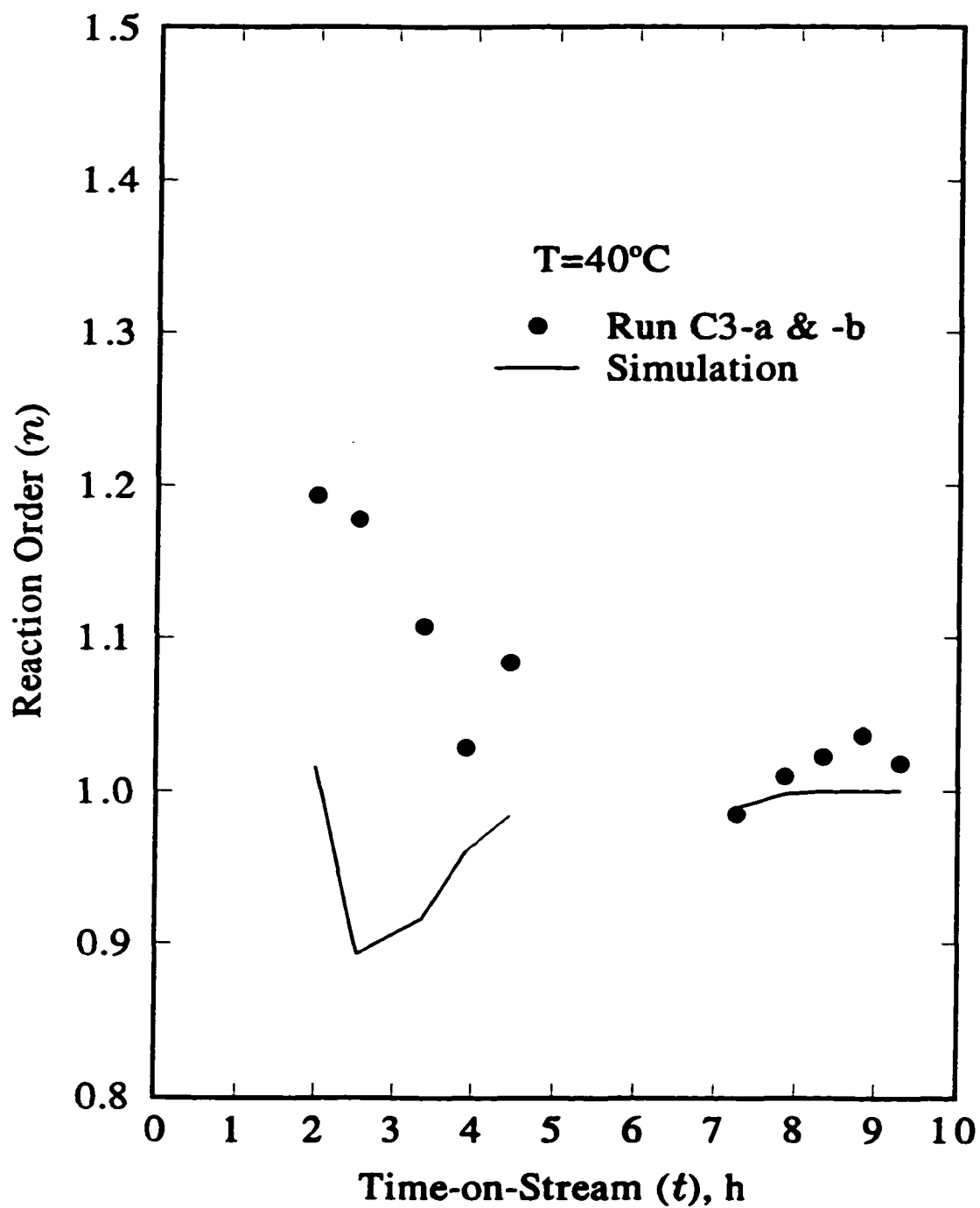
Figure 8.7 Comparison of experimental and simulated power-law orders as a function of time at 40°C (Run C3).

201
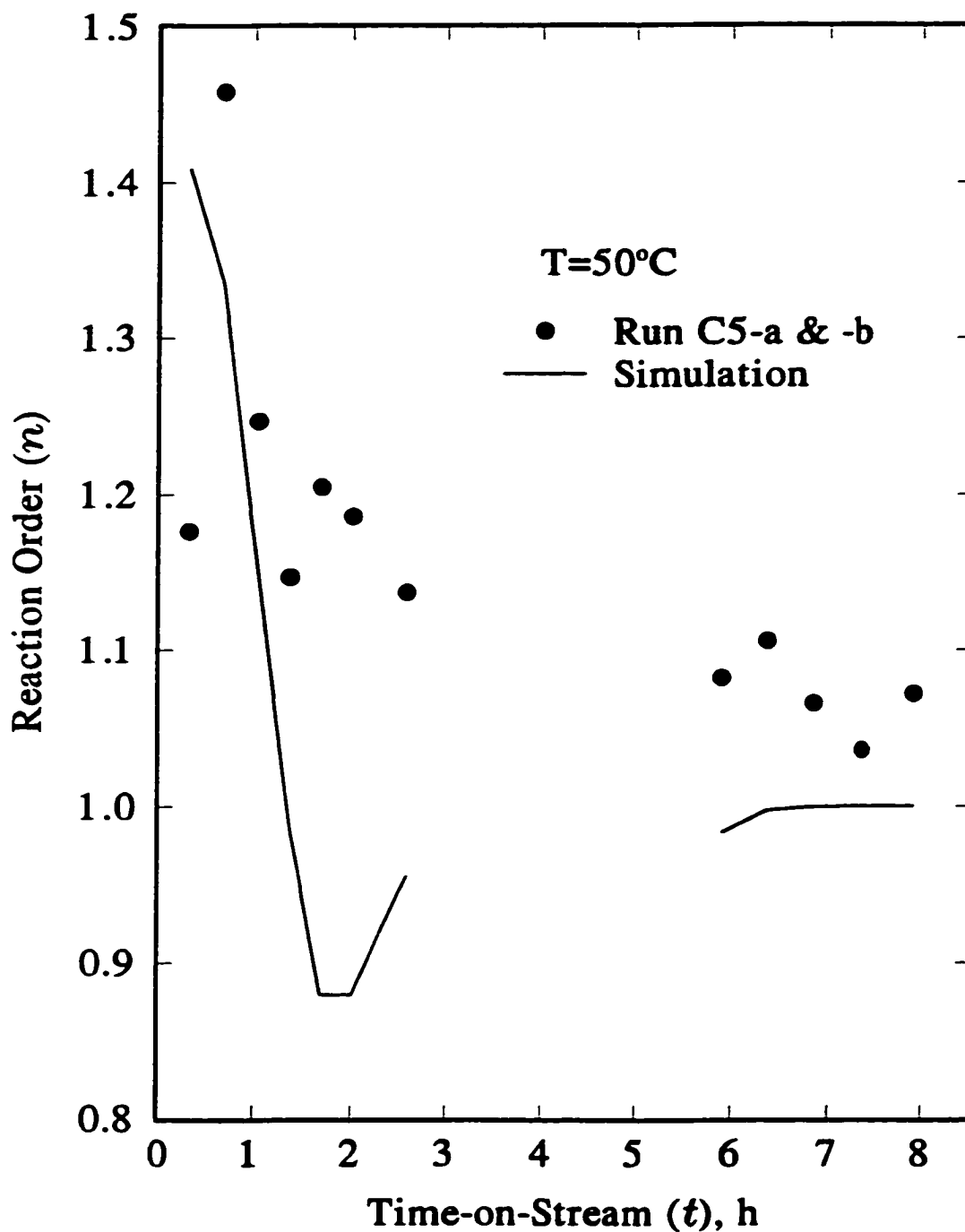
Figure 8.8 Comparison of experimental and simulated power-law orders as a function of time at 50°C (Run C5).
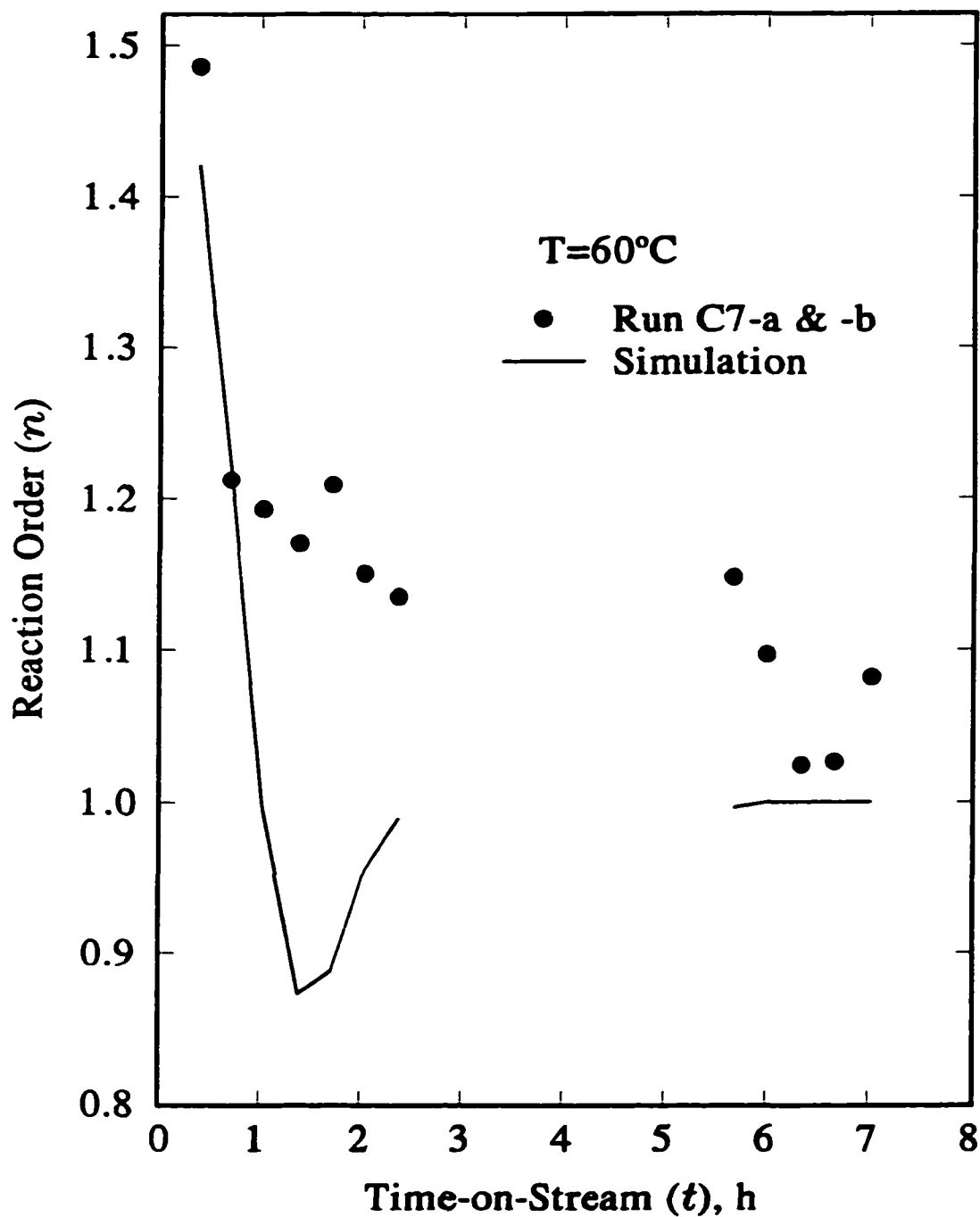
Figure 8.9 Comparison of experimental and simulated power-law orders as a function of time at 60°C (Run C7).
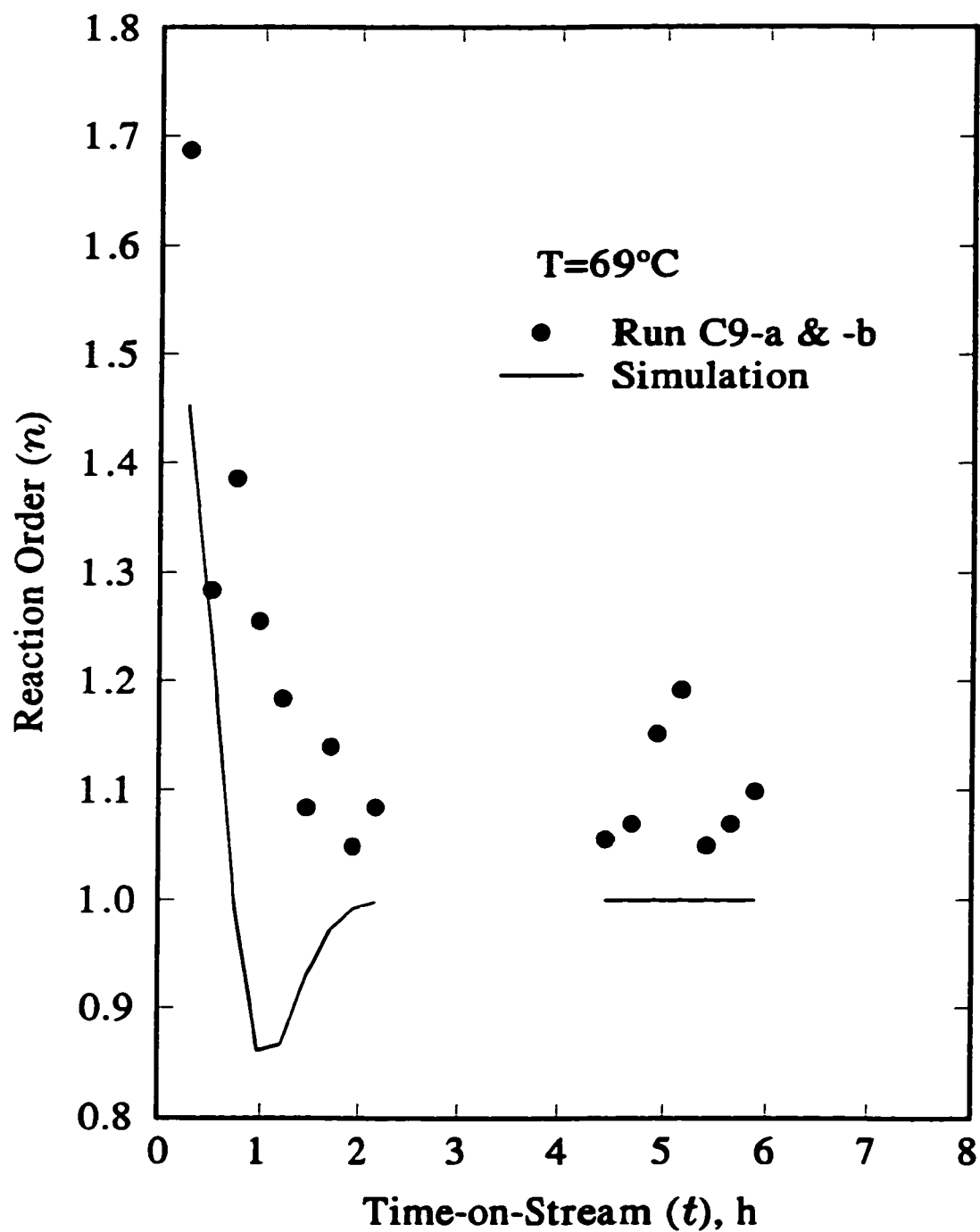
Figure 8.10 Comparison of experimental and simulated power-law orders as a function of time at 69°C (Run C9).

204

each temperature of 30, 40, 50, 60, and 69°C for Type C experiments. For the simulation of the reaction orders with the parameters listed in Table 8.1, temperatures and ethylene concentrations under experimental conditions were used. It can be seen from Figures 8.6 to 8.10 that the model predicts the reaction orders of greater than 1 at shorter times; it also predicts the reaction orders of less than 1 at low polymerization temperatures and longer times. However, at temperatures $\geq$ 40°C, the predicted reaction orders are lower than the experimental results at both shorter and longer times. This is due to the oversimplified deactivation of catalytic sites proposed in the model, *i.e.*, a simple dependence of deactivation rate on monomer concentration for propagation Site 1 (first-order) and for Site 2 (zero-order). The former causes lower values of reaction orders at shorter times, and the later results in insensitivity of the reaction order with temperature (essentially equal to 1) due to the complete deactivation of Site 1 at longer times. The complete deactivation of Site 1 is caused by its higher deactivation rate constant (see Table 8.1 for the values of deactivation rate constants for Site 1 and Site 2). At higher temperatures and longer times, the rate profile of complete deactivation of Site 1, according to the model (Equation 8.18), is illustrated in Figure 8.11 at a temperature of 50°C. Model predictions of rate profiles according to Equations 8.19 and 8.20 are also shown in Figure 8.11 for comparison.

It can also be seen in Figure 8.11 that the model (Equation 8.20) can also be used to predict various types of one-peak rate profiles if the relative amount of Site 1 and Site 2 in catalyst is adjusted in the model. For example, if Site 1 is the major type of catalytic site in catalyst, the model (Equation 8.18) will describe rate profiles of decay- or hybrid-types; if

205
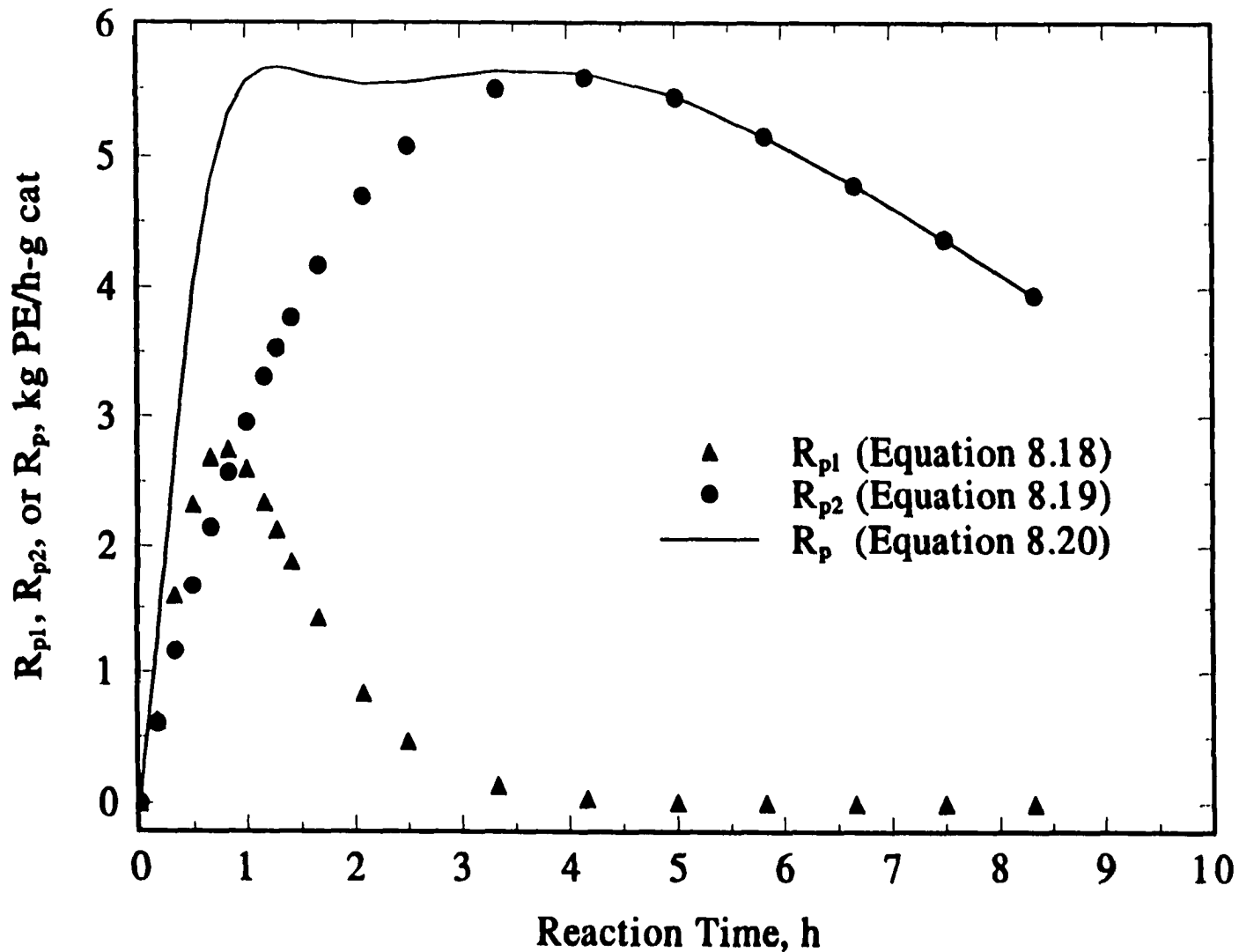
Figure 8.11   Model prediction of rate profiles for Site 1 (Equation 8.18), Site 2 (Equation 8.19), and overall rate (Equation 8.20) at $P_{C_2H_4}$=0.69 MPa and T=50°C (see Table 8.1 for parameters used in Equations 8.18, 8.19 and 8.20).

Site 2 is the major type of catalytic site, the model (Equation 8.19) will describe rate profiles of acceleration-type (see Section 2.4 for the description of different types of rate profiles).

The predicted rate profiles shown in Figure 8.11 can provide guidance to the catalyst preparation if the proposed model can be verified (see Chapter 9). It is known that the presence of Lewis base in $MgCl_2$-supported $TiCl_4$ catalysts can enhance the copolymerization ability and affect catalyst activity and polymer properties although the mechanism is not well understood (Zucchini and Cecchin, 1983; Soga *et al.*, 1989a). If the relative amount of Site 1 and Site 2 in a catalyst is related to the amount and type of Lewis base (*e.g.*, dibutyl phthalate in the current catalyst), then modification of catalyst can give different rate profiles and polymer properties. Suggestions on catalyst preparation and ethylene polymerization are given in Chapter 9.

8.3 Limitations and Discussions of the Reaction-Kinetic Model

The reaction-kinetic model, *i.e.*, Equation 8.20, which is based on the experimental results and simple kinetics, can generally describe the characteristic features of the kinetic behavior reported in Chapters 5 and 6. The disagreement of model predictions with experimental results exists in the absolute rates and the power-law reaction orders.

Since the reaction order measurement was very reliable (see Section 6.2), modification of the model in the kinetic-reaction scheme is required in order to increase the low predicted values of reaction orders at polymerization temperatures $\geq 40°C$. At shorter times, the simulated reaction order can be increased, *e.g.*, by assuming that the functional form of catalyst deactivation rate depends on polymerization temperature. For example, at

207

polymerization temperature of 40°C, a spontaneous deactivation, *i.e.*, Equation 8.21, may be assumed applicable for propagation Site 1, *i.e.*:

$$C_{pl}(x) \xrightarrow{k_{dl}} S_{dl} + polymer(x) \tag{8.21}$$

Writing differential equations for the model presented in Section 8.1 by replacing Equation 8.6 with Equation 8.21 (*i.e.*, Equations 8.1 to 8.5, 8.21, 8.7 and 8.8) and solving them yield:

$$
\begin{aligned}
R_p &= R_{pl} + R_{p2} \\
&= k_{pl}[S_{1,0}] \frac{k_{il}k_{fl}[M]^2}{k_{il}[M] + k_{dl} - k_{fl}} e^{-k_{dl}t} \left(\frac{1 - e^{-(k_{fl} - k_{dl})t}}{k_{fl} - k_{dl}} - \frac{1 - e^{-k_{il}[M]t}}{k_{il}[M]} \right) \\
&\quad + k_{p2}[S_{2,0}][M] (e^{-k_{d2}t} - e^{-(k_{d2} - k_{f2})t})
\end{aligned}
\tag{8.22}
$$

The improvement of the predicted reaction orders, according to Equation 8.22, is illustrated in Figure 8.12 for Run C3 at polymerization temperature of 40°C.

It can be seen in Figure 8.12 that the reaction orders at 40°C predicted by Equation 8.22 at shorter times have been significantly increased comparing with the simulation results of Equation 8.20 shown in Figure 8.7 (same values of parameters listed in Table 8.1 were used for Equation 8.22 in the simulation result illustrated in Figure 8.12). Note that rate profiles predicted by Equation 8.22 are slightly different from those predicted by Equation 8.20 at polymerization temperature of 40°C with the same values of parameters listed in Table 8.1, but their characteristic features are similar.

At longer times, the predicted reaction order at higher temperatures can also be increased, *e.g.*, by using a more complicated rate function, Equation 8.23, instead of first-order rate function (Equation 8.17), with respect to monomer concentration for the propagation rate of Site 2.
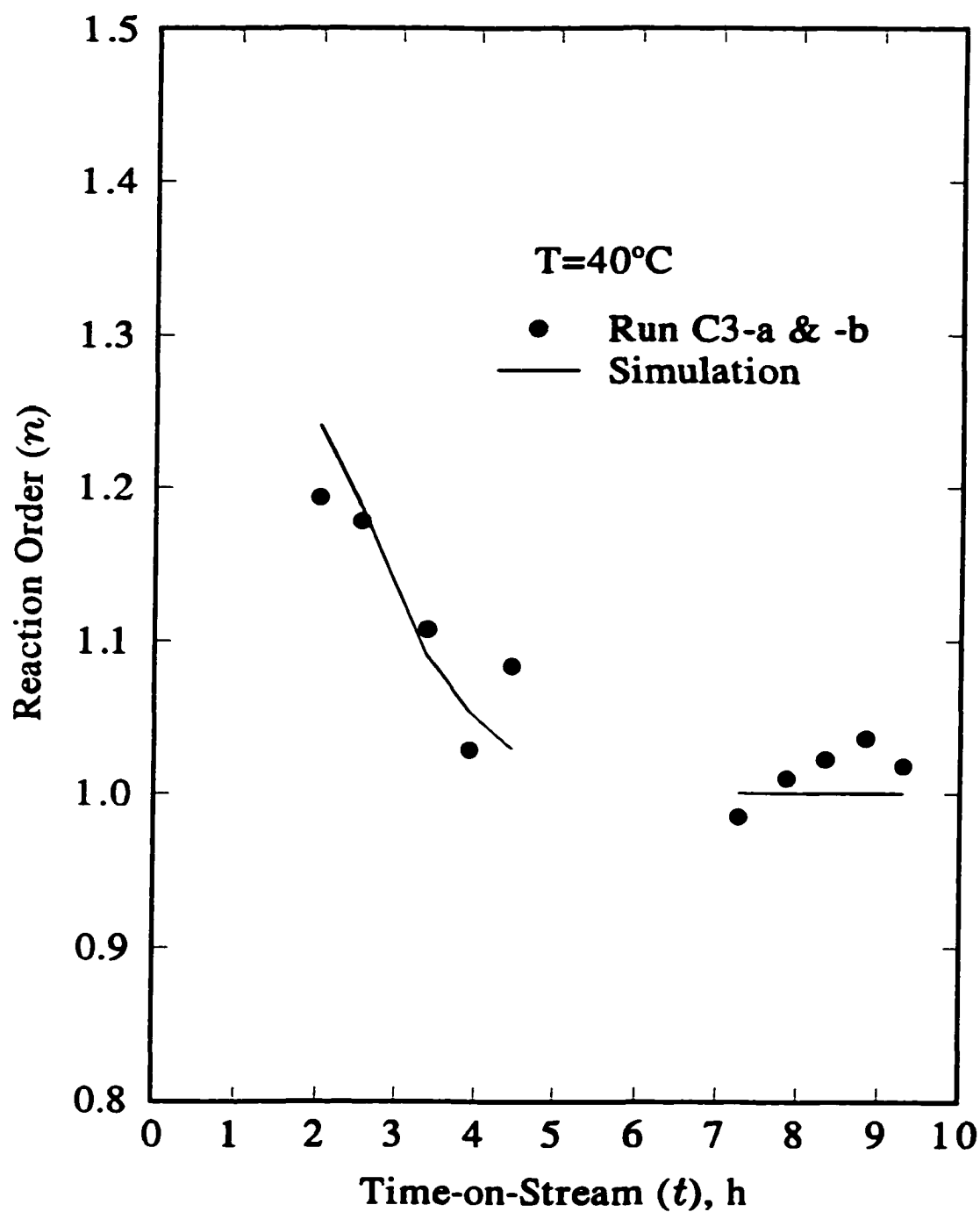
Figure 8.12   Comparison of the experimental power-law orders with model prediction by Equation 8.22 for Run C3 at 40°C.

$$R_{p2} = k_{p2} [C_{p2}] [M] \frac{K[M]}{1 + K[M]} \qquad (8.23)$$

Inconsistency of the rate profiles between the model predictions and experimental results could be reduced by simply adjusting the parameters in the model if the reproducibility of experiments is reliable. Adjustment of the parameters can be achieved, *e.g.*, by fitting one parameter in Equation 8.20 to each rate profile to yield a distribution of parameter values while keeping other parameters fixed. However, it was not the objective of this modeling to fit parameters with experimental data, as stated early in this chapter. As pointed out by Bu *et al.* (1995), one should not attach too much mechanistic significance to the functional form and numerical values of parameters.

It should be mentioned that the second-order deactivation with respect to the catalytic site concentration was not examined in the model simulation because the second-order deactivation imply the clustering the catalytic sites, and it is unlikely for solid catalytic sites covered with polymer to migrate and react with each other. In addition, the site which has second-order deactivation with respect to site concentration are likely to require similar dependence of chain propagation on catalytic site, which was never reported in Ziegler-Natta polymerization.

9. Summary and Future Work

The summary of the current work and recommendation for future studies in the areas of the catalyst preparation, ethylene polymerization and characterization of resulting polyethylene are presented in this chapter. Suggestion for the future work on ethylene copolymerization with α-olefins is also given.

9.1 Summary

Equipment for melt quenching of magnesium chloride ($MgCl_2$)-ethanol in Vaseline emulsions, which is an effective method for preparing spherical $MgCl_2$ particles, was designed and constructed. The spherical $MgCl_2$ support made by melt quenching was used for preparing the morphology-controlled $TiCl_4$ catalyst; the diameters of the catalyst particles prepared were about 30 to 150 μm. This morphology-controlled catalyst was very active for polymerizing ethylene, and it was observed that the morphology of the catalyst particles was replicated into the morphology of polymer in a two-stage polymerization, *i.e.*, prepolymerization followed by homopolymerization.

The first stage of polymerization was ethylene prepolymerization over morphology-controlled $TiCl_4$ catalyst prepared in this study; the optimal prepolymerization conditions are determined to be slurry operations at low ethylene pressure and low temperature. The optimal prepolymerization conditions were essential in replicating the shape of catalyst particles in polymer particles. The second stage of polymerization was ethylene homopolymerization using the prepolymer particles produced in the first stage as the

211

catalyst. Spherical polyethylene granules produced in the second stage had a bulk density of up to 0.45 g/cm^3 in gas-phase operation and of up to 0.4 g/cm^3 in slurry operation.

Under the conditions used in ethylene prepolymerization and homopolymerization of this study, the results of analyzing rate profiles systematically and characterizing prepolymer and polymer by size exclusion chromatography and scanning electron microscopy indicated that mass transfer effects were negligible in the gas-phase operation, but were probably present during slurry operation; heat transfer effects were generally negligible in the slurry and gas-phase operations, but it is likely that heat transfer effects were present at the very initial stage of gas-phase polymerization at high temperatures due to the high initial activity. Thus, a transport resistance model is not required for modeling the reaction behavior at conditions used in this study for gas-phase polymerization of ethylene.

For ethylene homopolymerization in the gas phase, polymerization rates changed dramatically with polymerization time and temperature, and many of the rate profiles had two maxima; these maxima were especially pronounced at high polymerization temperatures. A new experimental method was proposed for determining intrinsic reaction orders in the power-law rate function. Power-law reaction orders with respect to ethylene concentration, obtained according to the new method, varied with polymerization temperature and were a strong function of polymerization time-on-stream for ethylene homopolymerization in gas-phase operation. This new method for determining overall reaction orders is applicable to reaction systems with time-varying activities in which the response of reaction rate to changes in reactant concentration is rapid, such as gas-phase

212

polymerization. The overall reaction orders determined by this new method were significantly different from those obtained by direct fitting of the rate data to the overall power-law rate function.

The rate profiles with two maxima and the change of reaction orders with time-on-stream observed in the systematic gas-phase experiments provided very convincing kinetic evidence for the presence of at least two different types of catalytic sites in the catalyst used in the current study. The presence of two different types of catalytic sites was also suggested by the two different globules observed by SEM on the fractured surface of nascent polyethylene granules. It can be further concluded from the rate profiles that one type of the catalytic site activates and deactivates faster than the other.

The rate profiles of gas-phase and slurry operations were different under similar conditions of ethylene homopolymerization; there was only one maximum in the rate profile for slurry operation while two maxima were observed for gas-phase operation. This difference in the rate profiles provided evidence which indicates that rates in slurry reactors cannot be used directly for the modeling of ethylene polymerization in gas-phase reactors.

The reaction-kinetic model with two types of catalytic sites was proposed for the gas-phase ethylene polymerization process. The model predictions agreed reasonably with the experimental results. The most likely cause for deviations of the model predictions from the experimental observation is the oversimplification of assumed catalyst deactivation kinetics. Modifications of the model are suggested for improving the model predictions, specifically for increasing the predicted values of reaction orders by the model.

213

9.2 Future Work

Catalysts with a rather broad size distribution were used in the current study. Valuable insight into the heat and mass transfer behavior could be obtained with the use of catalyst with narrow size distributions. Catalysts with narrow size distributions could be obtained by separation of catalysts with broad size distributions into narrow size distribution fractions. Such classification of catalysts from the same batch would also provide evidence on whether the specific activity of catalyst, *i.e.*, the activity per unit mass, is independent of particle size. This was one of the assumptions made in the current study. Investigations on heat and mass transfer effects, which must come into effect for large catalyst particles, also become possible if large catalyst particles with a narrow size distribution are available.

The classification of catalyst particles is not a simple matter because rapid deactivation occurs during exposure to oxygen or moisture. The use of gas fluidization (entrainment) for size classification is difficult due to the sensitivity of the catalyst to oxygen and moisture. The presence of static forces also limits the use of gas fluidization. The use of a catalyst particle-hydrocarbon slurry is suggested for the size classification of catalyst particles. For separating a small quantities of $MgCl_2$-supported $TiCl_4$ catalyst particles on a laboratory scale, simplest method would be the slurry screening. Once the particles are classified, particle size distributions can be measured by optical microscopy. With the help of digital processing image software, the microscopic examination is reliable with the limit of an accuracy of 0.5 μm (McCrone *et al.*, 1967). The slurry screening and optical microscopic methods can also be applied for classifying prepolymerized catalyst.

214

The new method proposed in Chapter 6 for determining intrinsic reaction orders in the power-law rate function (Equation 6.4) does not provide information on activation energy of the apparent rate constant k (Equation 6.4). The activation energy can be obtained by changing reaction temperature at constant ethylene concentration; this is similar to changing ethylene pressure at constant reaction temperature described in Chapter 6. However, a rapid response of reaction temperature is required; this can be achieved by improving the heat transfer in the reactor system. The heat transfer in the reactor system can be improved by increasing inside and outside heat transfer coefficients of the reactor. For example, decreasing the reactor diameter and increasing stirring speed can increase the inside heat transfer coefficient, and increasing the oil flow rate in the oil bath outside the reactor can increase the outside heat transfer coefficient.

It was speculated that relative amounts of Site 1 and Site 2 in the catalyst are related to the amount and type of the Lewis bases from the modeling results (see Chapter 8). To verify this speculation, the kinetic behavior of catalysts with varying amounts of the Lewis base (*e.g.*, dibutyl phthalate) in the catalyst should be determined. Ethylene prepolymerization and homopolymerization should be carried out under similar conditions used in the current work. The comparison of rate profiles of ethylene homopolymerization over catalysts with systematic variation in the amount of the Lewis base can quantify the effects of the Lewis base on the kinetic behavior of different types of catalytic sites in the catalyst. This is also of significance for ethylene copolymerization with α-olefins if the copolymerization ability of different types of catalytic sites are different. Polyethylene with different copolymer content can be produced by modifying the catalyst if the different types

215

of catalytic sites would be differentiated in the catalyst. If the different types of catalytic sites have different α-olefin incorporation rates as well as different activity profiles, then the comonomer content of the polymer should be a function of reaction time. Hence, it is recommended that copolymerization runs of various lengths (e.g., 0.5 to 8 h) be done and that the comonomer content be determined as a function of reaction time.

216

References

Bailly, J.-C. A., Process for Preparing a Vanadium-Based Catalyst Suitable for Olefin Polymerization, *U. S. Patent 5 208 303*, issued May 4, 1993 (filed July 29, 1991).

Bailly, J.-C. A. and P. Behue, Process for Preparing a Ziegler-Natta Type Catalyst, *U.S. Patent 5 106 805*, issued April 21, 1992 (filed December 17, 1990).

Bailly, J.-C. A. and P. Behue, Process for Preparing a Ziegler-Natta Type Catalyst, *U. S. Patent 5 252 688*, issued October 12, 1993 (filed December 23, 1991).

Baker, R. T. K., P. S. Harris, R. J. Waite and A. N. Roper, Continuous Electron Microscopic Observation of the Behavior of Ziegler-Natta Catalysts, *Journal of Polymer Science, Polymer Letters Edition*, 11, 45-53 (1973).

Blais, P. and R. St. John Manley, Morphology of Nascent Polyolefins Prepared by Ziegler-Natta Catalysis, *Journal of Polymer Science: Part A-1*, 6, 291-334 (1968).

Böhm, L. L., Ethylene Polymerization Process with a Highly Active Ziegler-Natta Catalyst: 1. Kinetics, *Polymer*, 19, 553-561 (1978c).

Böhm, L. L., Ethylene Polymerization Process with a Highly Active Ziegler-Natta Catalyst: 2. Molecular weight regulation, *Polymer*, 19, 562-566 (1978d).

Böhm, L. L., Homo- and Copolymerization with a Highly Active Ziegler-Natta Catalyst, *Journal of Applied Polymer Science*, 29, 279-289 (1978a).

Böhm, L. L., Reaction Model for Ziegler-Natta Polymerization Processes, *Polymer*, 19, 545-552 (1978b).

Boor, J., Jr., *Ziegler-Natta Catalysts and Polymerization*, Academic Press, New York (1979).

Brockmeier, N. F. and J. B. Rogan, Propylene Polymerization Kinetics in a Semibatch Reactor by Use of a Supported Catalyst, *Industrial and Engineering Product Research and Development*, 24, 278-283 (1985).

Bu, N., D. T. Lynch and S. E. Wanke, Kinetics of Catalytic Gas-Phase Homopolymerization of Ethylene over $SiO_2/MgCl_2$-Supported $TiCl_4$ Catalysts, *Polymer Reaction Engineering*, 3, 1-22 (1995).

Bulls, V. W. and T. L. Higgins, A Particle Growth Theory for Heterogeneous Ziegler Polymerization, *Journal of Polymer Science: Part A-1*, 8, 1037-1053 (1970).

Burfield, D. R., I. D. McKenzie and P. J. T. Tait, Ziegler-Natta Catalysis: 7. The settling period, *Polymer*, 17, 130-136 (1976).

217

Busico, V., P. Corradini, A. Ferraro and A. Proto, Polymerization of Propene in the Presence of MgCl₂-Supported Ziegler-Natta Catalysts. 3. Catalyst deactivation, *Makromolekulare Chemie*, **187**, 1125-1130 (1986).

Busico, V., P. Corradini, L. De Martino, A. Proto and V. Savino, Polymerization of Propene in the Presence of MgCl₂-Supported Ziegler-Natta Catalysts. 1. The role of ethyl benzoate as 'internal' base, *Makromolekulare Chemie*, **186**, 1279-1288 (1985).

Busico, V., R. Cipullo and P. Corradini, Hydrooligomerization of Propene: A "fingerprint" of a Ziegler-Natta Catalyst. 1. Preliminary results for MgCl₂-supported systems, *Makromolekulare Chemie, Rapid Communications*, **13**, 15-20 (1992).

Butts, R., ,M.Sc. Thesis, Department of Chemical Engineering, University of Alberta, Edmonton, Alberta, Canada (1999).

Buzina, N. A., L. S. Bresler and I. V. Ikonitskii, Use of IR Spectroscopy in Studying Carbon monoxide as a Ti-C Bond Ziegler-Natta Catalyst Activity Indicator, *Polymer Science U. S. S. R.*, **30**, 533-539 (1988).

Campbell, R., Jr., T. H. Newman and M. T. Malanga, MAO Based Catalysts for Syndiotactic Polystyrene(s-PS), *Macromolecular Symposia*, **97**, 151-160 (1995).

Carberry, J. J., *Chemical and Catalytic Reaction Engineering*, McGraw Hill, Inc., New York, p. 410 (1976).

Carson, I. G., Particle Size Distribution of Polypropylene Produced in Continuous Polymerisation, *Die Angewandte Makromolekulare Chemie*, **16**, 145-156 (1988).

Cavallo, L., G. Guerra, M. Vacatello and P. Corradini, A Possible Model for the Stereospecificity in the Syndiospecific Polymerization of Propene with Group 4A Metallocenes, *Macromolecules*, **24**, 1784-1790 (1991).

Chien, J. C. W., Criteria for Diffusion Limitation in Coordination Polymerization, *Journal of Polymer Science: Polymer Chemistry Edition*, **17**, 2555-2565 (1979).

Chien, J. C. W. and P. Bres, Magnesium Chloride Supported High-Mileage Catalysts for Olefin Polymerization. XIII. Effect of External Lewis Base on Ethylene Polymerization, *Journal of Polymer Science: Part A: Polymer Chemistry*, **24**, 1967-1988 (1986).

Chien, J. C. W. and Y. Hu, Magnesium Chloride Supported High-Mileage Catalysts for Olefin Polymerization. XVII. Effect of Lewis base on propylene polymerization, *Journal of Polymer Science: Part A: Polymer Chemistry*, **25**, 2847-2870 (1987).

Chien, J. C. W. and Y. Hu, Superactive and Stereospecific Catalysts. III. Definitive identification of active sites by electron paramagnetic resonance, *Journal of Polymer Science: Part A: Polymer Chemistry*, **27**, 897-913 (1989).

218

Chien, J. C. W. and C.-I. Kuo, Magnesium Chloride Supported High-Mileage Catalysts for Olefin Polymerization. X. Effect of Hydrogen and Catalytic Site Deactivation, *Journal of Polymer Science: Part A: Polymer Chemistry*, **24**, 2707-2727 (1986).

Chien, J. C. W. and B.-P. Wang, Metallocene-Methylaluminoxane Catalysts for Olefin Polymerization. I. Trimethylaluminum As Coactivator, *Journal of Polymer Science: Part A: Polymer Chemistry*, **26**, 3089-3102 (1988).

Chien, J. C. W., S. Weber and Y. Hu, Magnesium Chloride Supported Catalysts for Olefin Polymerization. XIX. Titanium oxidation states, catalyst deactivation, and active site structure, *Journal of Polymer Science: Part A: Polymer Chemistry*, **27**, 1499-1514 (1989).

Clark, A and G. C. Bailey, Formation of High Polymers on Solid Surfaces. II. Polymerization of ethylene on chromium oxide-silica-alumina catalysts, *Journal of Catalysis*, **2**, 241-247 (1963).

Conner, W. C., M. Ferrero, S. Webb, R. Sommer, M. Chiovetta, K. Jones and P. Spanne, New Insight into the Changing Catalyst/Polymer Morphology during Olefin Polymerization: The application of Tomography, *Studies in Surface Science and Catalysis*, **75, Part B**, 1827-1830 (1993).

Covezzi, M., The Spherilene Process: Linear polyethylenes, *Macromolecular Symposia*, **89**, 577-586 (1995).

Di Drusco, G. and R. Rinaldi, Polypropylene - Process selection criteria, *Hydrocarbon Processing*, **11**, 113-117 (1984).

Doi, Y., M. Murata, K. Yano and T. Keii, Gas-Phase Polymerization of Propene with the Supported Ziegler Catalyst: $TiCl_4/MgCl_2/C_6H_5COOC_2H_5/Al(C_2H_5)_3$, *Industrial & Engineering Chemistry Production Research and Development*, **21**, 580-585 (1982).

Dumas, C. and C. C. Hsu, Propylene Polymerization in a Semibatch Slurry Reactor over Supported $TiCl_4/MgCl_2$/Ethyl Benzoate/Triethyl Aluminum Catalyst. II. A kinetic study based on a multisite model, *Journal of Applied Polymer Science*, **37**, 1625-1644 (1989).

Dumas, C. and C. C. Hsu, Supported Propylene Polymerization Catalyst, *Journal of Macromolecular Chemistry and Physics*, **C24(3)**, 355-386 (1984).

Dusseault, J. J. and C. C. Hsu, Gas-Phase Polymerization of Ethylene Using $MgCl_2$/Ethylene Benzoate/$TiCl_4$ + Triethylaluminum Catalyst: Effects of Triethylaluminum and temperature, *Journal of Applied Polymer Science*, **50**, 431-447 (1993).

Dyer, G., L. Manuel and D. Robinson, The SCLAIR Story, *Canadian Chemical News*, **49(1)**, 24-25 (1997).

219

Ferraris, M., F. Rosati, S. Parodi, E. Giannetti, and E. Albizzati, Catalyst Components and Catalysts for the Polymrization of Alpha-Olefins, *U.S. Patent 4,339,054*, issued August 16, 1983 (filed January 21, 1981).

Fisa, B., J. F. Revol and R. H. Marchessault, Crystallization during Polymerization of Ethylene: Successive Events, *Journal of Polymer Science: Polymer Physics Edition,* **12**, 2309-2317 (1974).

Floyd, S., K. Y. Choi, T. W. Taylor and W. H. Ray, Polymerization of Olefins through Heterogeneous Catalysis. IV. Modeling of heat and mass transfer resistance in the polymer particle boundary layer, *Journal of Applied Polymer Science,* **31**, 2231-2265 (1986a).

Floyd, S., K. Y. Choi, T. W. Taylor and W. H. Ray, Polymerization of Olefins through Heterogeneous Catalysis. III. Polymer particle modeling with an analysis of intraparticle heat and mass transfer effects, *Journal of Applied Polymer Science,* **32**, 2935-2960 (1986b).

Floyd, S., T. Heiskanen, T. W. Taylor, G. E. Mann, and W. H. Ray, Polymerization of Olefins through Heterogeneous Catalysis. VI. Effect of particle heat and mass transfer on polymerization behavior and polymer properties, *Journal of Applied Polymer Science,* **33**, 1021-1065 (1987).

Galli, P., G. Di Drusco and S. De Bartolo, Catalyst for the Polymerization Process with Spherically Shaped Particles *U.S. Patent 3,953,414*, issued April 27, 1976 (filed Septembr 15, 1974).

Galli, P., The "Spherilene" Process, *Popular Plastics & Packaging,* **5**, 71-80 (1993).

Galli, P., The Reactor Granule Technology: A revolutionary approach to polymer blends and alloys, *Macromolecular Symposia,* **78**, 269-284 (1994).

Galli, P., P. C. Barbè and L. Noristi, High Yield Catalysts in Olefin Polymerization, *Die Angewandte Makromolekulare Chemie,* **120**, 73-90 (1984).

Galli, P. and G. Cecchin, Advances in the Polymerization of Polyolefins with Coordination Catalysts, *Die Angewandte Makromolekulare Chemie,* **94**, 63-89 (1981).

Galli, P. and J. C. Haylock, New Fronties of Polyolefins and Advanced Olefin-Based Alloys, *Proceedings of the Pacific Polymer Conference, 1989,* Edited by B. C. Anderson and Y. Imanishi, pp. 51-65 (1991).

Galvan, R. and M. Tirrell, Molecular Weight Distribution Predictions for Heterogeneous Ziegler-Natta Polymerization Using a Two-Site Model, *Chemical Engineering Science,* **41**, 2385-2393 (1986).

Giannini, U., Polymerization of Olefins with High Activity Catalysts, *Makromolekulare Chemie, Supplements,* **5**, 216-229 (1981).

220

Graff, R. J. L., G. Kortleve and C. G. Vonk, On the Size of the Primary Particles in Ziegler Catalysts, *Journal of Polymer Science, Polymer Letters*, **8**, 735-739 (1970).

Guastalla, G. and U. Giannini, The Influence of Hydrogen on the Polymerization of Propylene and Ethylene with an $MgCl_2$ Supported Catalyst, *Makromolekulare Chemie, Rapid Communications*, **4**, 519-527 (1983).

Hamer, A. D. and F. J. Karol, Spheroidal Polymerization Catalyst, Process for Preparing, and Use for ethylene Polymerization, *U.S. Patent 4,376,062*, issued March 8,1983 (filed March 31, 1981).

Han-Adebekun, G. C., M. Hamba and W. H. Ray, Kinetic Study of Gas Phase Olefin Polymerization with a $TiCl_4/MgCl_2$ Catalyst I. Effect of Polymerization Conditions, *Journal of Polymer Science: Part A: Polymer Chemistry*, **35**, 2063-2074 (1997).

Han-Adebekun, G. C., and W. H. Ray, Polymerization of Olefins through Heterogeneous Catalysis XVII. Experimental Study and model Interpretation of Some Aspects of Olefin Polymerization over $TiCl_4/MgCl_2$ Catalyst, *Journal of Applied Polymer Science*, **65**, 1037-1052 (1997).

Hill, C. G., Jr., *An Introduction to Chemial Engineering Kinetics & Reactor Design*, John Wiley & Sons,Inc., New York/Santa Barbara/Chichester/Brisbane/Toronto, p.64 (1977).

Hock, C. W., How $TiCl_3$ Catalysts control the Texture of As-Polymerized Polypropylene, *Journal of Polymer Science: Part A-1*, **4**, 3055-3064 (1966).

Horns, U., T. Jostmann, K.-D. Kassmann, R. Matthes, and H. Rauleder, Process for the Preparation of Spherical Particles of Magnesium Alkoxide, *U.S. Patent 5,227,542*, issued July 13, 1993 (filed September 1, 1992).

Hu, Y. and J. C. W. Chien, Superactive and Stereospecific Catalysts. 1. Structures and productivity, *Journal of Polymer Science: Part A: Polymer Chemistry*, **26**, 2003-2018 (1988).

Huang, J. C.-K., Y. Lacombe, D. T. Lynch and S. E. Wanke, Effects of Hydrogen and 1-Butene Concentrations on the Molecular Properties of Polyethylene Produced by Catalytic Gas-Phase Polymerization, *Industrial Engineering Chemistry and Research*, **36**, 1136-1143 (1997).

Hutchinson, R. A., C. M. Chen and W. H. Ray, Polymerization of Olefins through Heterogeneous Catalysis. X. Modeling of particle growth and morphology, *Journal of Applied Polymer Science*, **44**, 1389-1414 (1992).

Hutchinson, R. A. and W. H. Ray, Polymerization of Olefins through Heterogeneous Catalysis. VIII. Monomer Sorption Effects, *Journal of Applied Polymer Science*, **41**, 51-81 (1990).

221

Hutchinson, R. A. and W. H. Ray, Polymerization of Olefins through Heterogeneous Catalysis. IX. Experimental study of propylene polymerization over a high activity MgCl$_2$-supported Ti catalyst, *Journal of Applied Polymer Science,* **43**, 1271-1285 (1991).

Iikolan, E. and J. Koskinen, Procedure for Manufacturing Catalyst Components for Polymerizing Olefins, *U.S. Patent 4,829,034,* issued May 9, 1989 (filed June 9, 1987).

Imaoka, K., S. Ikai, M. Tamura, M. Yoshikiyo and T. Yano, Effects of Hydrogen on the Polymerization of Propylene with a Magnesium Chloride Supported Ziegler-Natta Catalyst, *Journal of Molecular Catalysis,* **82**, 37-44 (1993).

Jacobsen, R. T., M. Jahangiri, R. B. Stewart, R. D. McCarty, J. M. H. Levelt Sengers, J. J. White, Jr., J. V. Sengers and G. A. Olchowy, *International Thermodynamic Tables of the Fluid State - 10. Ethylene (Ethene),* Blackwell Scientific Publications, Oxford/London/ Edinburgh/Boston/Melbourne, Table 4 (1988).

Jejelowo, M. O., D. T. Lynch and S. E. Wanke, Comparison of Ethylene Polymerization in Gas-Phase and Slurry Reactors, *Macromolecules,* **24**, 1755-1761 (1991).

Jericó, S., U. Schuchardt, I. Joekes, W. Kaminsky and A. Noll, Chlorinated Organic Polymers as Supports for Ziegler-Natta Catalysts, *Journal of Molecular Catalysis A: chemical,* **99**, 167-173 (1995).

Kakugo, M., H. Sadatoshi, M. Yokoyama and K. Kojima, Transmission Electron Microscopic Observation of Nascent Polypropylene Particles Using a New Staining Method, *Macromolecules,* **22**, 547-551 (1989a).

Kakugo, M., H. Sadatoshi, J. Sakai and M. Yokoyama, Growth of Polypropylene Particles in Ziegler-Natta Polymerization, *Macromolecules,* **22**, 2172-3177 (1989b).

Kang, K.-S., M.-A. OK, and S.-K. Ihm, Effects of Internal Lewis Bases on Recrystallized MgCl$_2$-TiCl$_4$ Catalysts for Polypropylene, *Journal of Applied Polymer Science,* **40**, 1303-1311 (1990).

Kashiwa, N. and J. Yoshitake, The Influence of the Valence State of Titanium in MgCl$_2$-Supported Titanium Catalysts on Olefin Polymerization, *Makromolekulare Chemie,* **185**, 1133-1138 (1984).

Keii, T., *Kinetics of Ziegler-Natta Polymerization,* Kodansha Ltd., Tokyo and Chapman & Hall Limited, London (1972).

Keii, T., Mechanistic Studies on Ziegler-Natta Catalysis - A methodological reconsideration, *Studies in Surface Science and Catalysis,* **25**, 1-27 (1986).

Keii, T., Y. Doi, E. Suzuki, M. Tamura, M. Murata and K. Soga, Propene Polymerization with a Magnesium Chloride-Supported Ziegler Catalyst. 2. Molecular weight distribution, *Macromolecular Chemie,* **185**, 1537-1557 (1984).

Keii, T., E. Suzuki, M. Tamura, M. Murata and Y. Doi, Propene Polymerization with a Magnesium Chloride-Supported Ziegler Catalyst. 1. Principal kinetics, *Macromolecular Chemie*, **183**, 2285-2304 (1982).

Kim, I., J. H. Kim and S. I. Woo, Kinetic Study of Ethylene Polymerization by Highly Active Silica Supported TiCl₄/MgCl₂ Catalysts, *Journal of Applied Polymer Science*, **39**, 837-854 (1990).

Kissin, Y. V., Mechanical Termination in Stereospecific Polymerization with Heterogeneous Complex Catalysts, *Polymer Science U. S. S. R.*, **11**, 1779-1789 (1969).

Kissin, Y. V., *Isospecific Polymerization of Olefins with Heterogeneous Ziegler-Natta Catalysts*, Springer-Verlag New York Inc. (1985).

Kissin, Y. V., 'Homogeneous' Interpretation of Ethylene Polymerization Kinetics with Supported Ziegler-Natta Catalysts, *Journal of Molecular Catalysis*, **56**, 220-236 (1989).

Laurence, R. L. and M. G. Chiovetta, Heat and Mass Transfer During Olefin Polymerization from the Gas Phase, *Polymer Reaction Engineering: Influence of reaction engineering on polymer properties*, Edited by K. H. Teichert and W. Geiseler, Hanser Publishers, Munich, pp. 73-112 (1983).

Lee, S. S. and N. M. Karayannis, Olefin Polymerization and Copolymerization Catalyst, *U.S. Patent 5,223,446*, issued June 29, 1993 (filed March 20, 1992).

Luciani, L., F. Milani, R. Invernizzi, I. Borghi and A. Labianco, Catalyst for the Polymerization of Olefins, *Canadian Patent 2,073,723*, issued January 26, 1993 (filed July 13, 1992).

Luciani, L., F. Milani and R. Zannetti, Some Peculiar Aspects of a New Catalyst for Propene Polymerization, *Macromolecular Symposia*, **89**, 139-149 (1995).

Lynch, D. T. and S. E. Wanke, Reactor Design and Operation for Gas-Phase Ethylene Polymerization Using Ziegler-Natta Catalysts, *The Canadian Journal of Chemical Engineering*, **69**, 332-339 (1991).

Marques, M. M. V., C. P. Nunes, P. J. T. Tait and A. R. Dias, Polymerization of Ethylene Using a High-Activity Ziegler-Natta Catalyst. I. Kinetic Studies, *Journal of Polymer Science: Part A: Polymer Chemistry*, **31**, 209-218 (1993).

Marques, M. M., P. J. T. Tait, J. Mejzlik and A. R. Dias, Polymerization of Ethylene Using High Activity Ziegler-Type Catalysts: Active center determination, *Journal of Polymer Science: Part A: Polymer Chemistry*, **36**, 573-585 (1998).

Masi, F., A. Moalli, R. Invernizzi, S. Malquori, L. Aarazzoni, and M. Polesello, Catalyst Component and Catalyst for the Production of Very High Molecular Weight Polyolefins, *U.S. Patent 5,070,051*, issued December 3, 1991 (filed February 22, 1991).

223

McCrone, W. C., R. G. Draftz and J. G. Delly, *The Particle Atlas*, Ann Arbor Science Publications, Ann Arbor, Michigan (1967).

McKenna, T. F., F. Barbotin and R. Spitz, Modeling of Transfer Phenomena on Heterogeneous Ziegler Catalysts. II. Experimental investigation of intraparticle mass transfer resistance during the polymerization of ethylene in slurry, *Journal of Applied Polymer Science*, 62, 1835-1841 (1996).

McKenna, T. F., J. DuPuy and R. Spitz, Modeling of Transfer Phenomena on Heterogeneous Ziegler Catalysts: Differences between theory and experiment in olefin polymerization (An Introduction), *Journal of Applied Polymer Science*, 57, 371-384 (1995).

Mei, G. and G. Cecchin, Polypropylene Particle Growth Study, *La Chimica e l'Industria*, 78, 437-442 (1996).

Miya, S., M. Tachibana and Y. Karasawa, Process for Producing a Catalyst for Olefin Polymerization, *U.S. Patent 5,100,849*, issued May 21, 1992 (filed August 28, 1990).

Mkrtchyan, S. A., B. A. Uvarov, V. I. Tsvetkova, Y. M. Tovmasyan, S. O. Chistyakov, G. F. Rachinskii and F. S. D'Yachkovskii, Formation and Growth of Polypropylene and Polyethylene Particles during the Polymerization of Olefins on Deposited Catalysts, *Polymer Science U. S. S. R.*, 28, 2343-2350 (1986).

Mori, H., H. Iguchi, K. Hasebe and M. Terano, Kinetic Study of Isospecific Active Sites Formed by various Alkylaluminums on MgCl2-Supported Ziegler Catalyst at the Initial Stage of Propene Polymerization, *Macromolecular Chemistry and Physics*, 198, 1249-1255 (1997).

Morse, P. M., New Catalysts Renew Polyolefins, *Chemical and Engineering News*, pp. 11-16 (July 6, 1998).

Muñoz-Escalona, A. and A. Parada, Factors Affecting the Nascent Structure and Morphology of Polyethylene Obtained by Heterogeneous Ziegler-Natta Catalysts, *Journal of Crystal Growth,*, 48, 250-258 (1980).

Muñoz-Escalona, A., C. Villamizar and P. Frias, Structure and Morphology of Nascent Polyethylenes Obtained by TiCl₃ Heterogeneous Ziegler-Natta Catalyst, *Polymer Science and Technology*, 22, 95-113 (1983).

Murachev, V. B., M. V. Terganova, I. F. Kuz'kina, I. G. Makarov, Y. F. Shashkina, N. N. Byrikhina, V. M. Kazakova and V. I. Aksenov, Study of the Deactivation of a Titanium Catalytic System of the Ziegler Type, *Polymer Science U.S.S.R.*, 31, 560-565 (1989).

Nagasawa, T. and Y. Shimomura, Mechanism of Formation of Shish Kebab Structures, *Journal of Polymer Science: Polymer Physics Edition*, 12, 2291-2308 (1974).

Nagel, E. J., V. A. Kirillov and W. H. Ray, Prediction of Molecular Weight Distributions for High-Density Polyolefins, *Industrial & Engineering Chemistry Product Research and Development,* **19,** 372-379 (1980).

Natta, G., P. Pino and G. Mazzanti, *U.S. Patent 3,112,300,* issued November 26, 1963 (filed June 8, 1954).

Natta, G., P. Pino, P. Corradini, F. Danusso, E. Mantica, G. Mazzanti and G. Moraglio, Crystalline High Polyerms of α-olefins, *Journal of the American Chemical Society,* **77,** 1708-1701 (1955).

Neckers, D. C., D. A. Kooistra and G. W. Green, Polymer-Protected Reagents. Polystyrene-Aluminum Chloride, *Journal of the American Chemical Society,* **94:26,** 9284-9285 (1971).

Noristi, L., E. Marchetti, G. Baruzzi and P. Sgarzi, Investigation on the Particle Growth Mechanism in Propylene Polymerization with MgCl2-Supported Ziegler-Natta Catalysts, *Journal of Polymer Science: Part A: Polymer Chemistry,* **32,** 3047-3059 (1994).

Novokshonova, L. A., N. Y. Kovaleva, Y. A. Gavrilov, V. G. Krasheninnikov, I. O. Leipunskii, A. N. Zhigach, M. N. Larichev, M. V. Chebunin, Study of Energy Distribution of Active Sites in Hetereogeneous Ziegler-Natta Catalysts, *Polymer Bulletin,* **39,** 59-65 (1997).

Park, H. M. and W. Y. Lee, The Effect of Triethylaluminium Treatment on a Ziegler-Natta Catalyst Supported on Magnesium Chloride Prepared by a Recrystrallization method for Propylene polymerization, *European Polymer Journal,* **28,** 1417-1422 (1992).

Peng, D.-Y. and D. B. Robinson, A New Two-Constant Equation of State, *Industrial and Engineering Chemistry, Fundamentals,* **15,** 59-64 (1976).

Pentti, I. and P. Leskinen, A Prepolymerized Catalyst Composition, a Process for the Preparation thereof, and a Process for Polymerizing Alpha-olefins, *European Patent 607,703,* (date of filing December 29 1993).

Pieters, W. J. M. and A. F. Venero, A Novel Automated High Resolution BET Apparatus, *Studies in Surface Science and Catalysis,* **19,** 155-163 (1984).

Pino, P., B. Rotzinger and E. von Achenbach, The Role of Some Bases in the Stereospecific Polymerization of Propylene with Titanium Catalysts Supported on Magnesium Chloride, *Makromolekulare Chemie, Supplements,* **13,** 105-122 (1985).

Putanov, P., E. Kiš, L. Fekete and E. Dingova, The Efficts of the Architecture of the Ziegler-Natta Catalyst on the Morphology of Polypropylene, *Polyhedron,* **8,** 1867-1869 (1989).

225

Ray, W. H., Modelling of Addition Polymerization Process - Free Radical, Ionic, Group Transfer, and Ziegler-Natta Kinetics, *The Canadian Journal of Chemical Engineering*, **69**, 626-629 (1991).

Ran, R., Polymer-Supported Ziegler-Natta Catalyst for the Polymerization of Isoprene, *Journal of Polymer Science: Part A: Polymer Chemistry*, **31**, 1561-1569 (1993).

Revol, J.-F., W. Luk and R. H. Marchessault, Electron Microscope Investigation on Nascent Polyethylene, *Journal of Crystal Growth*, **48**, 240-249 (1980).

Rishina, L. A., E. I. Vizen, L. N. Sosnovskaja and F. S. Dyachkovsky, Study of the Effect of Hydrogen in Propylene Polymerization with the MgCl2-Supported Ziegler-Natta Catalyst - Part I. Kinetics of polymerization, *European Polymer Journal*, **30**, 1309-1313 (1994).

Sacchetti, M., G. Govoni and A. Clarrocchi, Component and Catalysts for the Polymerizatin of olefins, *U.S. Patent 5,221,651*, issued June 22, 1993 (filed November 16, 1992).

Sacchi, M. C., F. Forlini, I. Tritto, P. Locattelli, G. Morini, G. Baruzzi, and E. Albizzati, *Macromolecular Symposia*, **89**, 91-100(1995).

Salajka, Z., J. Kratochvila, P. Hudec and P. Vecorek, One-Phase Supported Titanium-Based Catalysts for Polymerization of Ethylene. II. Effect of Hydrogen, *Journal of Polymer Science: Part A: Polymer Chemistry*, **31**, 1493-1498 (1993).

Schindler, A., Kinetic Studies in Ethylene Polymerization with Ziegler-Type Catalysts, *Journal of Polymer Science: Part C: Polymer Symposium*, **4**, 81-96 (1963).

Schmeal, W. R. and J. R. Street, Polymerization in Expanding Catalyst Particles, *AIChE Journal*, **17**, 1188-1197 (1971).

Schnauβ, A and K.-H. Reichert, Modelling the Kinetics of Ethylene Polymerization with Ziegler-Natta Catalysts, *Makromolekulare Chemie, Rapid Communications*, **11**, 315-320 (1990).

Shanbhag, K. N., Thermal Behavior of Gas-Phase Ethylene Polymerization Reactor, M.Sc. Thesis, Department of Chemical Engineering, University of Alberta, Edmonton, Alberta, Canada (1992).

Shiono, T., M. Ohgizawa and K. Soga, Reaction between Carbon Monoxide and a Ti-Polyethylene Bond with a MgCl2-Supported TiCl4 Catalyst System, *Makromolekulare Chemie*, **194**, 2075-2085 (1993).

Singh, D. and R. P. Merrill, Molecular Weight Distribution of Polyethylene Produced by Ziegler-Natta Catalysts, *Macromolecules*, **4(5)**, 599-604 (1971).

Smith, P, H. D. Chanzy and B. P. Rotzinger, Drawing of Virgin Ultrahigh Molecular Weight Polyethylene: An Alternative Route to High Strength/High Modulus Materials. Part

2. Influence of polymerization temperature, *Journal of Materials Science*, **22**, 523-531 (1987).

Soga, K., R. Ohnishi and T. Sano, Copolymerization of Ethylene and Propylene over the SiO_2-Supported $MgCl_2/TiCl_3$ Catalyst, *Polymer Bulletin*, **7**, 547-552 (1982).

Soga, K., J. R. Park, H. Uchino, T. Uozumi and T. Shino, Perfect Conversion of Aspecific Sites into Isospecific Sites in Ziegler-Natta Catalysts, *Macromolecules*, **22**, 3834-3826 (1989a).

Soga, K., H. Yanagihara and D.-h. Lee, Effect of Monomer Diffusion in the Polymerization of Olefins over Ziegler-Natta Catalysts, *Makromolekulare Chemie*, **190**, 995-1006 (1989b).

Standke, B., J., Rauleder, H.-J. Biangardi and H.-J. Koetzsch, Process for the Preparation of Alkaline Earth Metal Alcoholates Having a Shperical Particle Habitus, *Canadian Patent 2,057,582*, issued June 6, 1992 (filed December 13, 1991).

Stern, S. A., J. T. Mullhaupt and P. J. Gareis, The Effect of Pressure on the Permeation of Gases and Vapors through Polyethylene. Usefulness of the Corresponding States Principle, *AIChE Journal*, **15**, 64-73 (1969).

Sun, L., C. C. Hsu and D. W. Bacon, Polymer-Supported Ziegler-Natta Catalysts. I. A preliminary study of catalyst synthesis, *Journal of Polymer Science: Part A: Polymer chemistry*, **32**, 2127-2134 (1994a).

Sun, L., C. C. Hsu and D. W. Bacon, Polymer-Supported Ziegler-Natta Catalysts. II. Ethylene homo- and copolymerization with $TiCl_4/MgR_2/poly(ethylene$-*co*-acrylic acid) catalyst, *Journal of Polymer Science: Part A: Polymer chemistry*, **32**, 2135-2145 (1994b).

Tait, P. J. T., Kinetic Considerations and Active Centre Determination in Ziegler-Natta Polymerization, *Preparation and Properties of Stereoregular Polymers*, NATO Advanced Study Institute Series: Series C, Mathematical and Physical Series, **51**, pp. 85-112, 1978.

Tang, S. P., Studies on Olefin Polymerization, *Studies in Surface Science and Catalysis*, **25**, 165-179 (1986).

Usami, T., Y. Gotoh and S. Takayama, Generation Mechanism of Short-Chain Branching Distribution in Linear Low-Density Polyethylene, *Macromolecules*, **19**, 2722-2726 (1986).

Ushida, Y., Y. Amimoto, A. Toyota, and N. Kashiwa, Process for the Production of Spherical Carrier Partilces for Olefin Polymerization Catalysts, *U.S. Patent 4,315,847*, issued February 16, 1982 (filed April 7, 1980).

Vermel', Y. Y., V. A. Zakharov, Z. K. Bukatova, G. P. Shkurina, L. G. Yechevskaya, E. M. Moroz and S. V. Sudakova, Polymerization of Propylene with Highly Active Titanium-Magresium Catalysts, *Polymer Science U. S. S. R.*, **22**, 23-30 (1980).

227

Vizen, E. I., L. A. Rishina, L. N. Sosnovskaja, F. S. Dyachkovsky, I. L. Dubnikova and T. A. Ladygina, Study of the Effect of Hydrogen in Propylene Polymerization with the MgCl2-Supported Ziegler-Natta Catalyst - Part 2. Effect of CS_2 on polymerization centres, *European Polymer Journal*, **30**, 1315-1318 (1994).

Vizzini, J. C., J.-F. Shi and J. C. W. Chien, Solid-State NMR Characterization of a Superactive Supported Ziegler-Natta Catalyst, *Journal of Applied Polymer Science*, **48**, 2173-2179 (1993).

Vogel, A. I., A Text-Book of Quantitative Inorganic Analysis including Elementary Instrumental Analysis, 3rd edition, Longmans, Green and Co. Ltd., London, pp. 788-790 (1961).

Wristers, J., Nascent Polypropylene Morphology: Polymer fiber, *Journal of Polymer Science: Polymer Physics Edition*, **11**, 1601-1617 (1973a).

Wristers, J., Direct Examination of Polymerization Catalyst by Electron Scanning Microscopy, *Journal of Polymer Science: Polymer Physics Edition*, **11**, 1619-1629 (1973b).

Zakharov, V. A., S. I. Makhtarulin, D. V. Perkovets, E. M. Moroz, T. B. Mikenas and G. D. Bukatov, Structure, Composition and Activity of Supported Titanium-Magnesium Catalysts for Ethylene Polymerization, *Studies in Surface Science and Catalysis*, **25**, 71-89 (1986).

Zhou, G., Characteristics of Turbulence Energy Dissipation and Liquid-Liquid Dispersions in an Agitated Tank, Ph. D. Thesis, Department of Chemical Engineering, University of Alberta (1997).

Ziegler, K., H. Breil, H. Martin, and E. Holzkamp, *German Patent 973,626*, issued April 14, 1960 (filed November 17, 1953). [See also *U.S. Patent 3,257,332*, issued June 21, 1966 (filed November 15, 1954).]

Zlotnikov, L. M., Y. L. Ponomareva, S. Y. Khaikin, S. I. Korotkov, V. A. Grigor'ev, V. P. Budtov and S. S. Ivanchev, Determination of the Concentration of Active Centres and the Propagation Reaction Rate Constants of the Macrochain on Polymerization of Ethylene on Highly Active Catalysts, *Polymer Science U.S.S.R.*, **30**, 16-22 (1988).

Zucchini, U. and G. Cecchin, Control of Molecular-Weight Distribution in Polyolefins Synthesized with Ziegler-Natta Catalytic Systems, *Advances in Polymer Science*, **51**, 101-154 (1983).

Appendix A

Experiments on Chemical Reaction Precipitation

The catalyst shown in the SEM micrograph in Figure 7.2 (Chapter 7) was a $MgCl_2$-supported $TiCl_4$ catalyst in which $MgCl_2$ support was prepared by chemical reaction precipitation. The method of chemical reaction precipitation was similar to that described by Bailly and Behue (1990; 1991) and Bailly (1991). Experiments presented in this appendix include preparation methods of $MgCl_2$ and catalyst. The semibatch reactor system with the Pyrex reactor described in Section 3.3 was used for prepolymerization and homopolymerization of ethylene in slurry operations. The prepolymerization method was similar to that described in Section 3.4, and the homopolymerization method was Type D operation (see Section 3.5). The results on ethylene polymerizations and the resulting polymer morphology are briefly reported.

Preparation of $MgCl_2$ support

A one-litre, jacketed Pyrex reactor, which was equipped with a thermocouple and a stirrer, was used for preparing $MgCl_2$, as catalyst support. The temperature in the reactor was controlled by a heating/cooling circulating bath. The stirring speed in the reactor was kept at 500 rpm during the $MgCl_2$ precipitation.

Reagents, 200 mL of heptane, 16.9 mL of dibutyl ether, and 97 mL of dibutyl magnesium, were introduced into the Pyrex reactor at room temperature and under a nitrogen atmosphere. After the temperature in the reactor was increased to 50°C, a solution of 24 mL of *tert*-butyl chloride in 80 mL of heptane was added into reactor in 10 hours. The

229

temperature in the reactor was kept at 50°C for additional 2 hours. The solid MgCl₂ precipitated was washed 4 times at room temperature; 100 mL of heptane was used for each wash.

Preparation of MgCl₂-Supported TiCl₄ Catalyst

The Pyrex reactor used for the precipitation of MgCl₂ was also used for the catalyst preparation, and the stirring speed in the reactor was kept at 500 rpm. The MgCl₂ particles were suspended in heptane of 200 mL at 30°C in the Pyrex reactor. The solution of 9.15 mL of n-butanol in 20 mL of heptane was added into the MgCl₂-heptane suspension in 1 hour. After the addition of n-butanol, the reaction mixture in the Pyrex reactor was kept 30°C for additional 0.5 hour. The solid particles were washed at 30°C with 100 mL of heptane; the wash was repeated twice, then the solid particles were suspended in 200 mL of heptane. At 50°C, 100 mL of triethylaluminum was added into the suspension in 1 hour. The temperature of the mixture in the reactor was increased to 80°C, and kept at 80°C for 1 hour. The resulting solid particles were washed with 100 mL of heptane at 50°C, and the wash was repeated twice.

At 30°C, 1.5 mL of TiCl₄ in 50 mL of heptane was added into 200 mL of a suspension of the solid particles and heptane in 2 hours. The temperature of the mixture in the reactor was increased to 80°C and kept at 80°C for 1 hour. The solid particles were then washed at 50°C with 100 mL of hexane, and the wash was repeated twice. The particles obtained were dried in vacuum at room temperature for 2 hours. The concentration of Ti in the dry solid catalyst was determined to be 1.2 wt % by a colorimetric analysis.

Results and Discussion

One prepolymerization run and two homopolymerization runs are reported in this appendix. The reaction conditions for these runs are listed in Table A.1.

Table A.1   Run Conditions[1] for Prepolymerization and Homopolymerization

Run No.	TEAL, mL	Catalyst[2], mg	T, °C	P_{H2}, kPa	P_{C2H4}, kPa	Time, h	Yield[3], g PE/g Cat	Bulk Density, g/cm³
			Prepolymerization					
Pre-A1	0.25	250	31	88	124	4.4	28.4	N/M[4]
			Homopolymerization					
DA1	0.15	500	63	92	433	7.5	2,891	0.37
DA2	0.20	290	61	92	459	18.8	4,615	0.33

Notes:

1. The stirring speed of the reactor was 720 rpm, and heptane was 300 mL for all three runs.

2. Catalyst for Run Pre-A1 was the $MgCl_2$-supported $TiCl_4$ catalyst; catalyst for Runs DA1 and DA2 was the product of Run Pre-A1 (the prepolymerized catalyst).

3. Yield was based on the $MgCl_2$-supported $TiCl_4$ catalyst for all three runs.

4. N/M = not measured.

The rate profile for Run Pre-A1 is shown in Figure A.1, which shows an acceleration type. The rate profiles for Runs DA1 and DA2 are shown in Figure A.2, which show a slow activation and deactivation with one broad peak.

In addition to the shape replication observed from Figure 7.2 in Section 7.1, the $MgCl_2$-supported $TiCl_4$ catalyst prepared by the chemical reaction precipitation method had

231
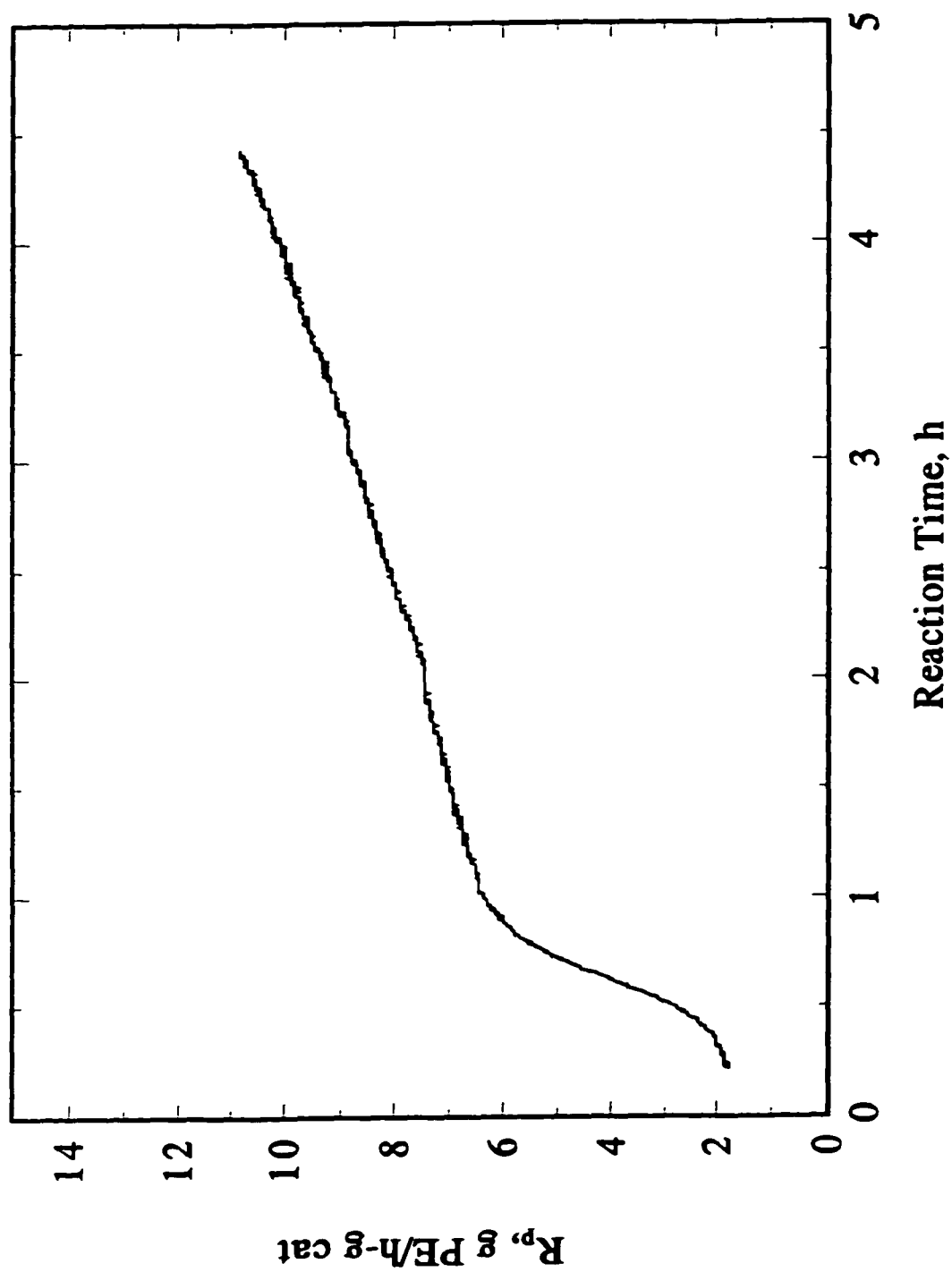
Figure A.1   Rate profile of ethylene prepolymerization for Run Pre-A1.

232
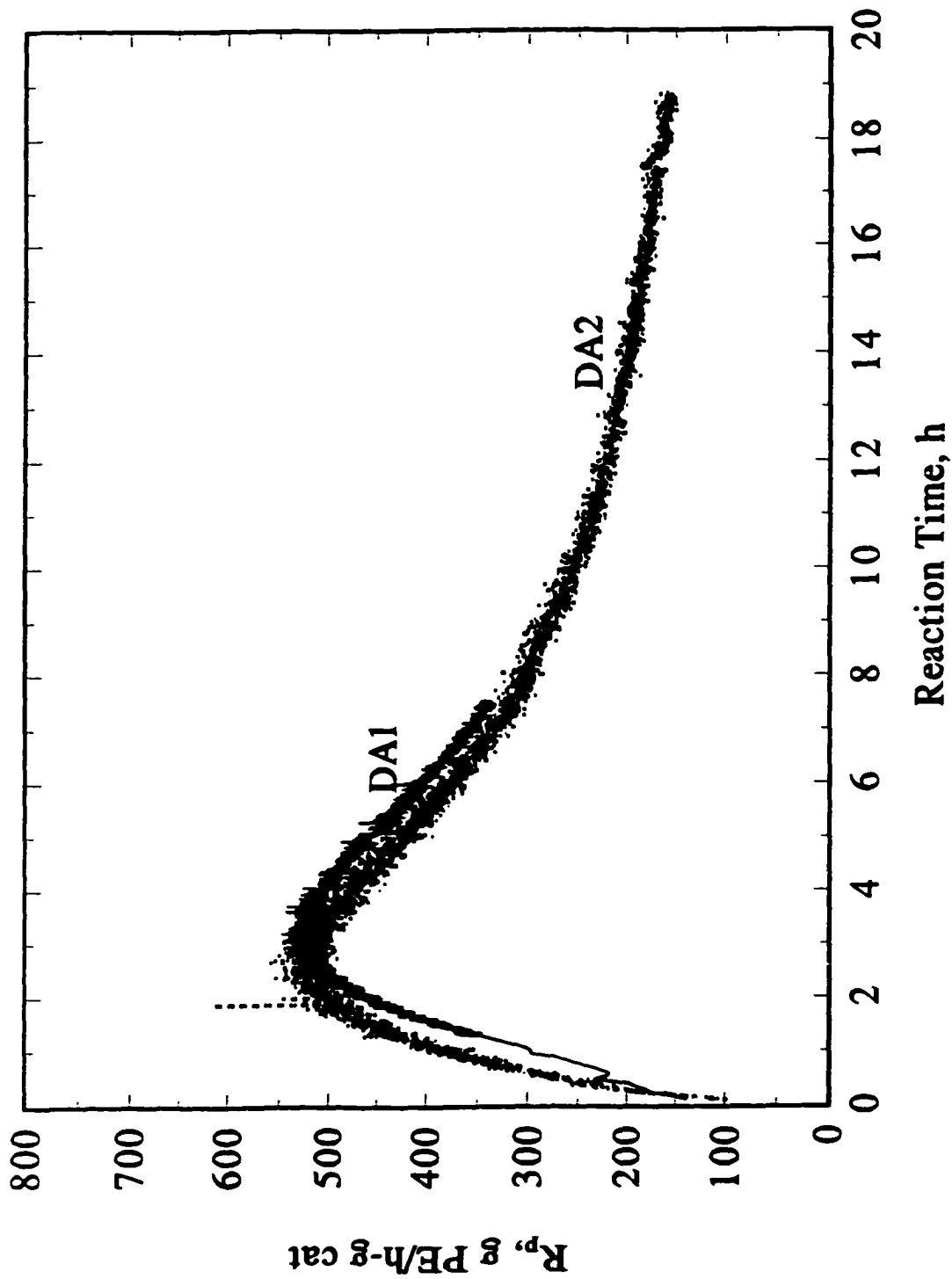
Figure A.2 Rate profiles of ethylene homopolymerization for Runs DA1 and DA2.

a narrow size distribution, and the narrow size distribution of the catalyst was replicated to the prepolymer and polymer. The narrow size distribution of the prepolymer from Run Pre-A1 can be clearly seen from the SEM micrograph at a low magnification shown in Figure A.3.

The typical cobweb structures on the surface of prepolymer and polymer are shown in Figure A.4, in which Figures A.4 a & b are prepolymer from Run Pre-A1, Figures A.4 c & d are polymer from Run DA1, and Figures A.4 e & f are polymer from Run DA2. It can be seen in Figure A.4 that as polymerization yield increases (see Table A.1) from Run Pre-A1 (prepolymer) to Run DA1 and Run DA2 (polymer), the fibrils are getting longer and the globules are getting bigger. The longer fibrils will result in a lower bulk density of polymer (see Table A.1 for the lower bulk density of polymer produced from Run DA2 than from Run DA1).
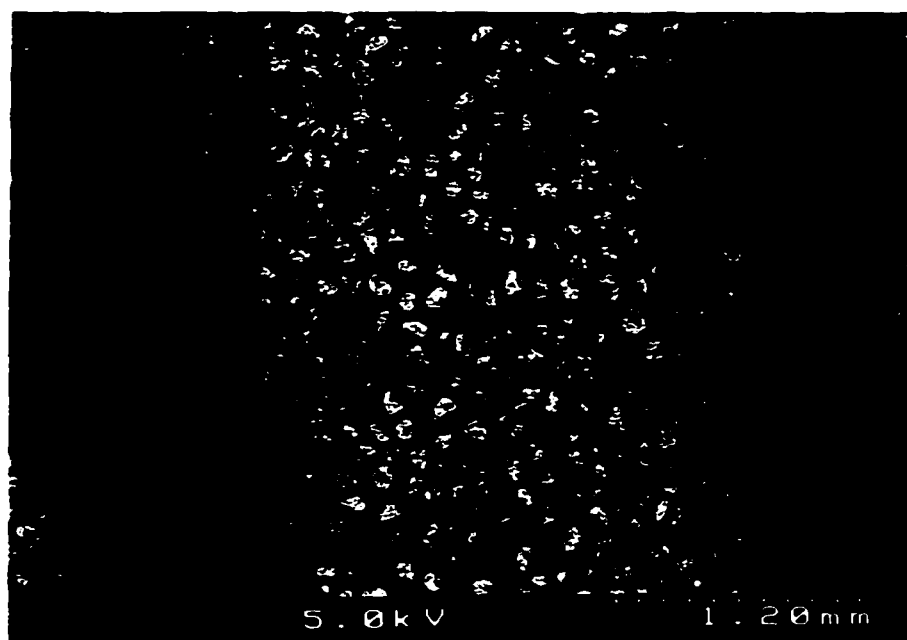
Figure A.3 Narrow size distribution of prepolymer particles from Run Pre-A1.
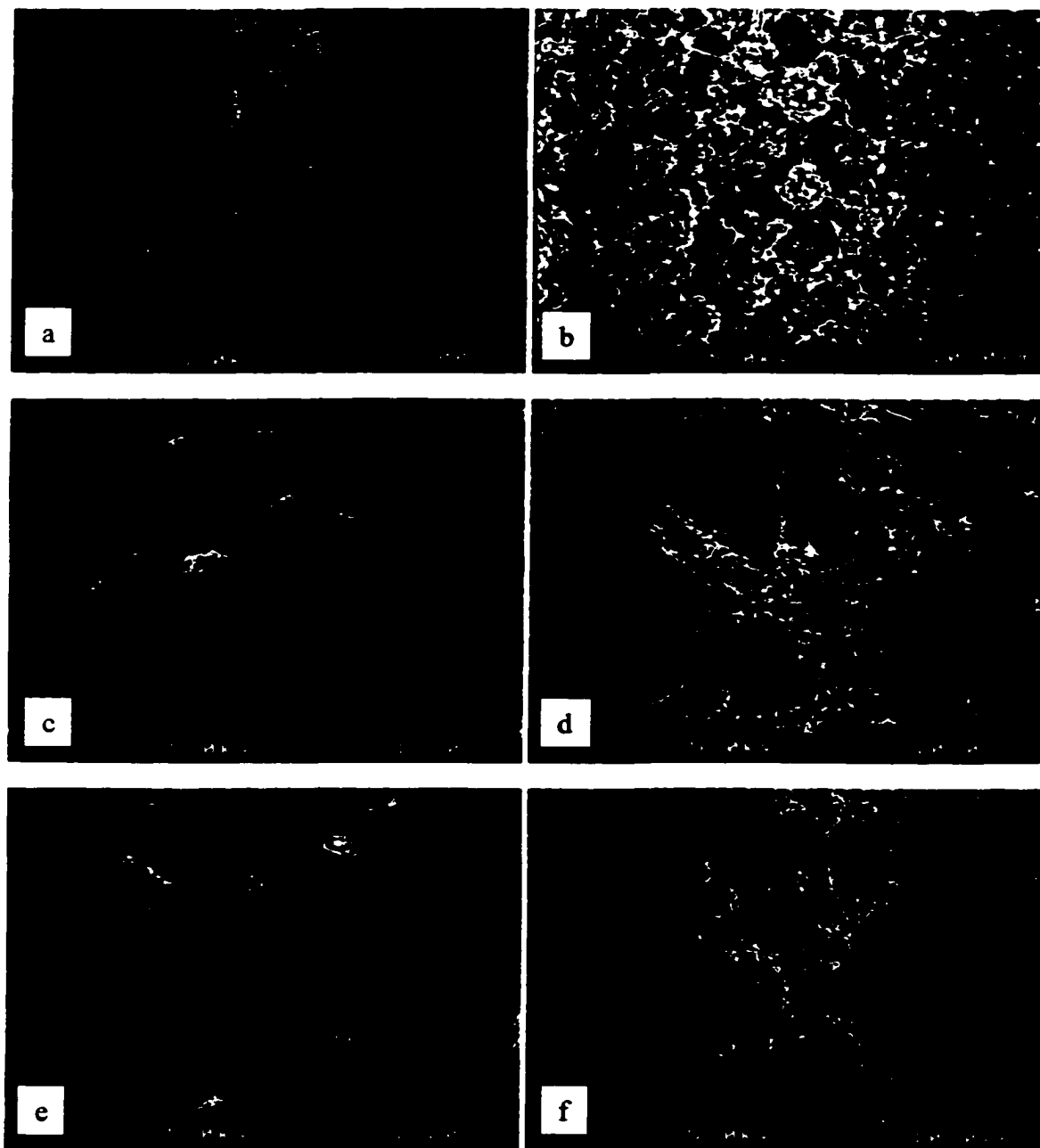
Figure A.4 Surface structures of prepolymer from Run Pre-1 (a & b) and polymer from Runs DA1 (c & d) and DA2 (e & f).

236

Appendix B

Reaction Conditions and Rate Profiles of Ethylene Prepolymerization

The reaction conditions for all the prepolymerization runs are listed in Table B.1.

The rate profiles of Runs Pre-1 and Pre-3 are shown in Figure B.1; the rate profiles of Runs

Pre-4 and Pre-5 are shown in Figure B.2. The polymerization rates for Runs Pre-2 and Pre-6

exceeded the maximum range that the mass flow transducer can measure, and are not

shown.

Table B.1   Run Conditions[1] for Ethylene Prepolymerization

Run No.	Reactor Type	Catalyst, mg	T, °C	P_{H_2}, kPa	$P_{C_2H_4}$, kPa	Time, h
Pre-1	Gas phase	30	30.0	89.8	36.2	2.43
Pre-2	Gas phase	30	91.6	351.7	1,387.9	0.24
Pre-3	Slurry	110	29.6	86.2	61.6	2.64
Pre-4	Slurry	50	30.6	83.6	342.2	1.11
Pre-5	Slurry	35	72.6	85.4	342.9	0.33
Pre-6	Slurry	30	78.4	356.8	1,411.0	0.30

Note:

1. For all the prepolymerization runs, catalyst used was as shown in Figure 3.1, cocatalyst used was 0.25 mL of triethylaluminum; 300 mL of heptane was used as a diluent in slurry reactor while 35 g of Rulon LR particles were used as seed beds in gas phase reactor.

237
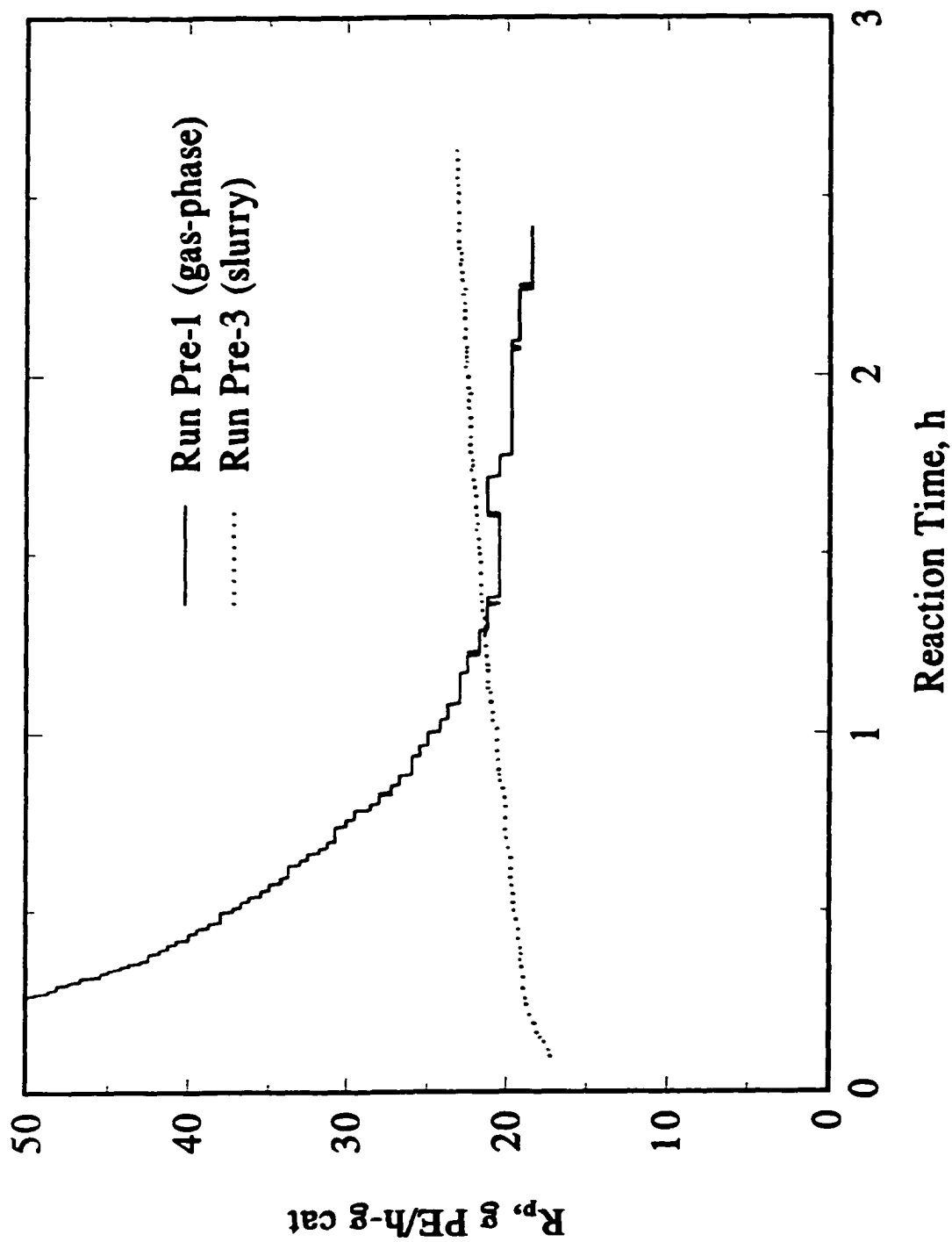
Figure B.1   Rate profiles of ethylene prepolymerization for Runs Pre-1 and Pre-3.

238
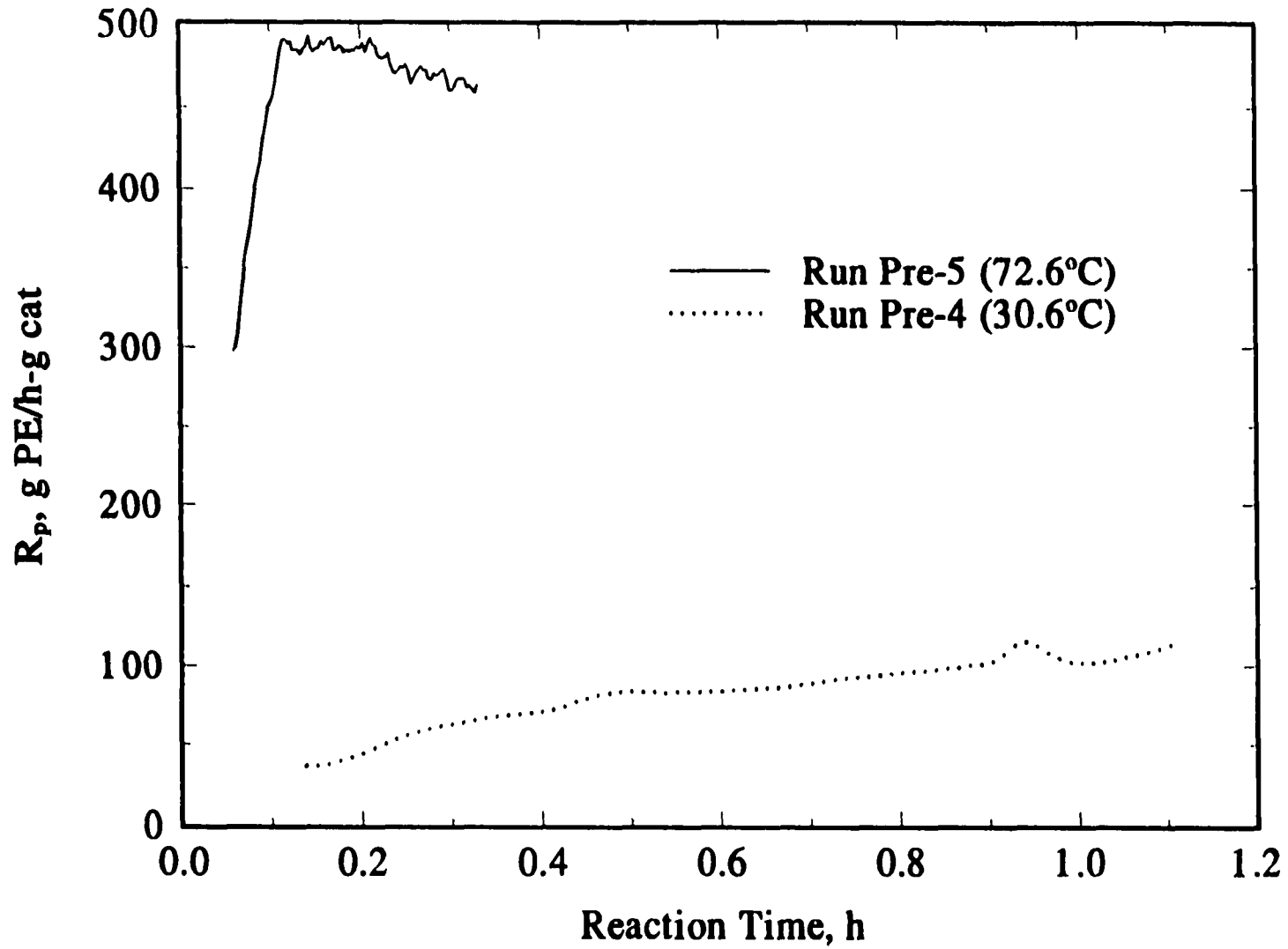
Figure B.2   Rate profiles of ethylene prepolymerization for Runs Pre-4 and Pre-5.

Appendix C

Reaction Conditions and Rate Profiles of Ethylene Homopolymerization

The run conditions for all the homopolymerization described in Section 3.5, Chapter 3 are listed in Table C.1. The rate profiles of Runs A1 and A2 are shown in Figure C.1.

Table C.1   Reaction Conditions[1] for All the Runs of Ethylene Homopolymerization

Run No.	Amount of TEAL, mL	Prepolymerized Catalyst, mg	T, °C	P_{H2}, MPa	P_{C2H4}, MPa	Time, h	Rate Profiles in Figure #
Type A Experiment (Gas-Phase)							
A1	0.25	45	68.1	0.36	1.39	2.00	C.1
A2[2]	0.25	200	70.5	0.31	1.37	2.02	C.1
A3	0.25	63	67.9	0.35	0.69	2.01	7.12; 7.16
A4[3]	0.25	50	68.4	0.35	1.41	7.79	7.12
A5	0.25	36	28.7	0.34	0.71	2.03	7.16
Type B Experiment[4] (Gas-Phase)							
B1	0.30	95	30.1	0	0.68	8.08	5.6
B2	0.30	98	32.0	0	1.34	8.22	5.7
B3	0.30	51	30.1	0	2.06	8.17	5.1
B4	0.30	48	30.0	0	2.09	8.18	5.1; 5.8
B5	0.30	85	40.5	0	0.67	8.46	5.2
B6	0.30	30	41.9	0	0.68	8.20	5.2; 5.6
B7	0.30	99	41.6	0	1.34	8.18	5.7
B8	0.30	97	42.2	0	2.04	8.24	5.8
B9	0.30	85	50.1	0	0.67	8.23	5.6
B10	0.30	90	49.5	0	1.33	8.22	5.7
B11[5]	0.30	85	52.1	0	2.07	7.29	5.3
B12	0.30	50	50.0	0	2.05	8.20	5.3; 5.8
B13	0.30	88	59.9	0	0.68	8.14	5.6; 5.10
B14	0.30	46	59.2	0	1.34	8.16	5.7; 5.10
B15	0.25	47	60.1	0	2.07	7.21	5.4
B16	0.25	40	59.9	0	2.09	8.22	5.4; 5.8; 5.10
B17	0.30	63	68.7	0	0.67	8.07	5.6
B18	0.30	50	69.7	0	1.34	8.19	5.7
B19	0.30	50	69.8	0	2.06	7.52	5.5; 5.8
B20	0.30	40	69.8	0	2.08	8.19	5.5

240

Run No.	Amount of TEAL, mL	Prepolymerized Catalyst, mg	T, °C	P$_{H_2}$, MPa	P$_{C_2H_4}$, MPa	Time, h	Rate Profiles in Figure #
Type C Experiment[4] (Gas-Phase)							
C1-a	0.30	94	31.5	0	0.38 - 1.59		
C1-b			31.3		0.86 - 1.99		
C2-a	0.30	108	29.9	0	0.35 - 1.77		
C2-b			30.2		0.97 - 1.98		
C3-a	0.30	103	39.2	0	0.53 - 1.39		
C3-b			39.6		0.55 - 1.37		
C4-a	0.30	90	40.2	0	0.34 - 1.55		
C4-b			40.6		0.55 - 1.55		
C5-a	0.30	95	49.8	0	0.35 - 1.36		
C5-b			50.2		0.37 - 1.35		
C6-a	0.30	84	50.0	0	0.34 - 1.35		
C6-b			50.4		0.39 - 1.35		
C7-a	0.30	96	59.5	0	0.35 - 1.35		
C7-b			60.2		0.36 - 1.36		
C8-a	0.30	90	59.8	0	0.33 - 1.35		
C8-b			60.1		0.34 - 1.35		
C9-a[6]	0.35	80	69.3	0	0.34 - 1.27		
C9-b			69.6		0.54 - 1.28		
C10-a	0.30	94	68.4	0	0.34 - 1.36		6.1; 6.4
C10-b			68.7		0.55 - 1.56		
Type D Experiment (Slurry)							
D1	0.25	65	68.9	0.35	0.66	2.03	7.12
D2	0.25	100	68.3	0.33	1.38	5.15	7.12

Notes:

1. For all the runs unless specified, prepolymer produced from Pre-3 was used as the catalyst, and the stirring speed of the reactor was 204 rpm. Unless specified, 100 g of NaCl was used as a seed bed for gas-phase experiments; 300 mL of heptane was used as a reaction medium for slurry experiments.

2. For this run, 35 g of Rulon LR particles (2×2×2 mm by length) were used as seed bed.

3. For this run, the majority of polyethylene granules were broken in the reactor.

4. For Types B and C experiments, the majority of polyethylene granules were broken in the reactor.

5. The temperature in this run was increased by 4°C at the end of the run.

6. For Run C9, 200 g of NaCl was used as a seed bed.

241
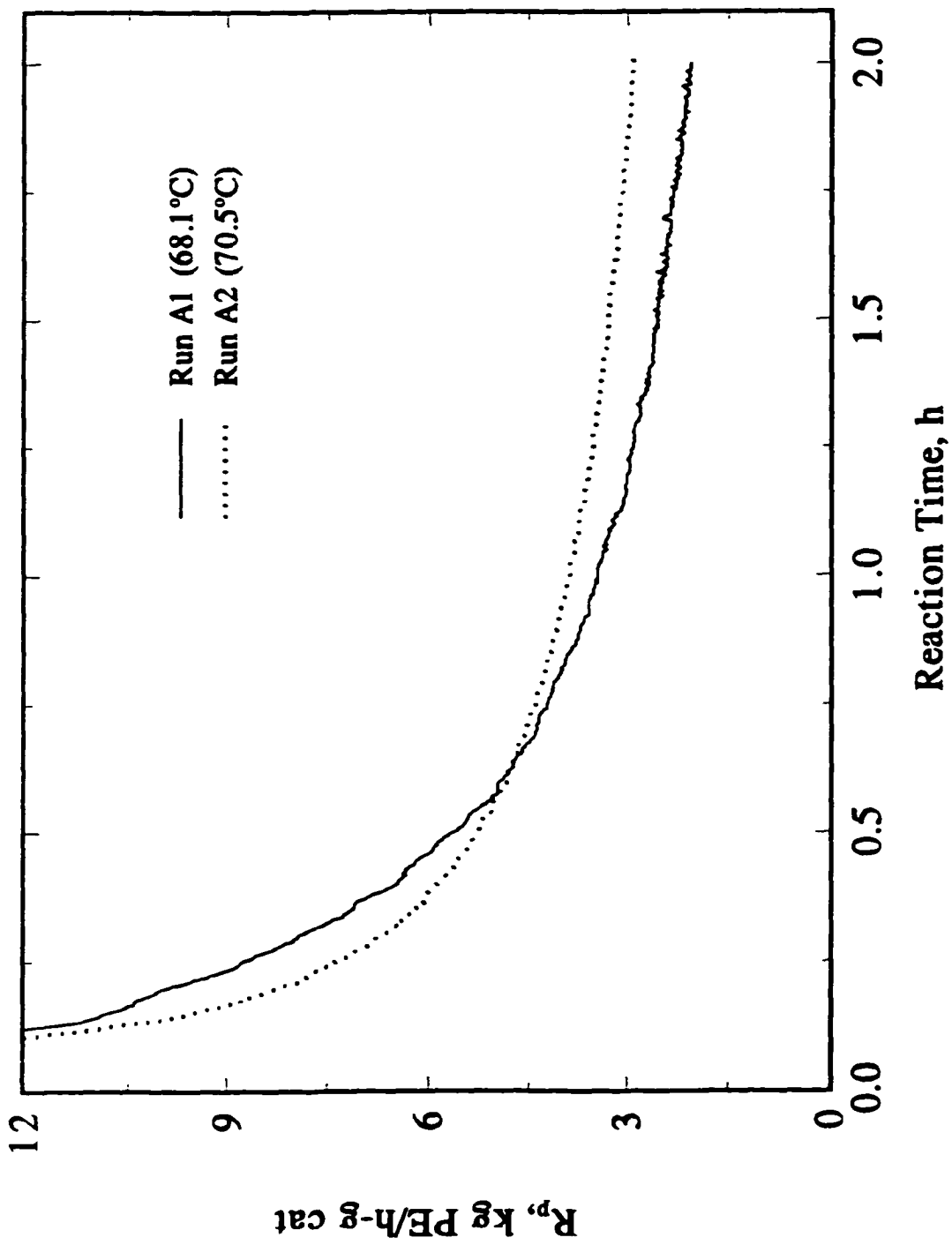
Figure C.1 Rate profiles of Runs A1 and A2.

242